

NASA Technical Memorandum

100476

REDESIGN OF SOLID ROCKET BOOSTER/EXTERNAL TANK ATTACHMENT RING FOR THE SPACE TRANSPORTATION SYSTEM

**{NASA-TM-100476} REDESIGN OF SOLID ROCKET
BOOSTER/EXTERNAL TANK ATTACHMENT RING FOR
THE SPACE TRANSPORTATION SYSTEM {NASA} 254
p Avail: NTIS HC A12/MF A01 CSCL 22B**

N88-10101

**Unclas
G3/18 0104542**

Harvey G. McComb, Jr., Compiler

October 1987



**National Aeronautics and
Space Administration**

**Langley Research Center
Hampton, Virginia 23665**

REDESIGN OF SOLID ROCKET BOOSTER / EXTERNAL TANK ATTACHMENT RING
FOR THE SPACE TRANSPORTATION SYSTEM

Harvey G. McComb, Jr., Compiler
Analytical Services and Materials, Inc.
Hampton, Virginia 23665

ABSTRACT

An improved design concept is presented for the Space Shuttle solid rocket booster (SRB)/external tank (ET) attachment ring structural component. This component picks up three struts which attach the aft end of each SRB to the ET. The concept is a partial ring with carefully tapered ends to distribute fastener loads safely into the SRB. Extensive design studies and analyses were performed to arrive at the concept. Experiments on structural elements were performed to determine material strength and stiffness characteristics. Materials and fabrication studies were conducted to determine acceptable tolerances for the design concept. The text of the report provides an overview of the work, conclusions and major recommendations. Supporting technical details are contained in ten appendices.

TABLE OF CONTENTS

| TITLE | PAGE |
|--|------|
| 1.0 INTRODUCTION..... | 1 |
| 2.0 DESIGN REQUIREMENTS..... | 2 |
| 3.0 DESIGN ASSUMPTIONS..... | 3 |
| 4.0 DESIGN CONCEPT..... | 4 |
| 4.1 Attachment Ring..... | 4 |
| 4.2 Transition Tunnel..... | 4 |
| 4.3 Concept Verification..... | 5 |
| 5.0 STRUCTURAL ANALYSIS..... | 5 |
| 5.1 SRB Analysis..... | 5 |
| 5.2 Ring Analysis..... | 7 |
| 5.2.1 Simplified Analysis for Sizing..... | 7 |
| 5.2.2 Planar Finite Element Models..... | 7 |
| 5.2.3 Sensitivity to Bolt Shear Stiffness..... | 8 |
| 5.2.4 Single Bolt Failure..... | 8 |
| 5.2.5 Out-of-Round Motor Case..... | 9 |
| 5.2.6 Certification Model Analysis..... | 9 |
| 5.2.7 Other Analyses..... | 9 |
| 6.0 EXPERIMENTS..... | 10 |
| 7.0 MATERIALS AND FABRICATION..... | 10 |
| 7.1 Materials..... | 11 |
| 7.1.1 Material Strength..... | 11 |
| 7.1.2 Material Cleanliness..... | 11 |
| 7.1.3 Material Uniformity..... | 11 |

| | | |
|-------------|---|-----|
| 7.1.4 | Material Tolerances..... | 12 |
| 7.1.5 | Effects of Existing Material on LaRC Design Concept.. | 12 |
| 7.1.6 | Effects of Improved Material Cleanliness..... | 12 |
| 7.2 | Fabrication..... | 12 |
| 7.2.1 | Fabrication Tolerance Effects..... | 12 |
| 7.2.2 | Test Sample Fabrication Experience..... | 15 |
| 7.3 | Recommendations..... | 16 |
| 8.0 | CONCLUSIONS AND RECOMMENDATIONS..... | 17 |
| 9.0 | REFERENCES..... | 18 |
| APPENDIX A: | LOADS..... | 81 |
| APPENDIX B: | GLOBAL LINEAR AND NONLINEAR STRUCTURAL ANALYSIS..... | 97 |
| APPENDIX C: | RING AREA TAPERING ANALYSIS..... | 115 |
| APPENDIX D: | SPLICE ANALYSIS..... | 131 |
| APPENDIX E: | ET/SRB ATTACH RING SYSTEMS COVER ANALYSIS..... | 155 |
| APPENDIX F: | MARGINS OF SAFETY..... | 177 |
| APPENDIX G: | INELASTIC ANALYSIS..... | 195 |
| APPENDIX H: | FRACTURE MECHANICS ANALYSIS..... | 209 |
| APPENDIX I: | EXPERIMENTS..... | 225 |
| APPENDIX J: | WEIGHT STATEMENT..... | 253 |

REDESIGN OF SOLID ROCKET BOOSTER / EXTERNAL TANK ATTACHMENT RING FOR THE SPACE TRANSPORTATION SYSTEM

Harvey G. McComb, Jr., Compiler
Analytical Services and Materials, Inc.
Hampton, Virginia 23665

1.0 INTRODUCTION

The aft ends of the Space Transportation System Solid Rocket Boosters (SRBs) are attached to the External Tank (ET) through a partial ring structural component mounted on the outside of each SRB. The approximate location of these rings is indicated on figure 1. Each ring extends about 270° around the circumference of the SRB shell and supports fittings which mount three struts providing the aft attachment for each SRB to the ET. A sketch of one of these attachment rings including the three struts is shown in figure 2. A more detailed drawing of the ring is in figure 3. The cross-section of the ring is a rectangular box configuration as shown in figure 4.

Two problems are associated with the existing attachment ring design: (1) negative margins of safety are calculated at four locations indicated on figure 5, and (2) sheared fasteners have been experienced on a substantial number of SRBs recovered from flight as listed in Table 1. Sheared fasteners on the recovered units are at locations A and B in figure 6. The end of the ring at location A is termed the "long end", and the end at location B is termed the "short end". Specifically, sheared fasteners occurred in the ring component as follows:

- (1) web/cap fasteners at both ends
- (2) web/tang fasteners at the long end

The shear failures in the articles recovered from flight were thought to be the result of water impact loading and were considered benign. Post-test inspection of the attachment ring used in the JES 3B test in December 1986, however, revealed deformed fasteners in the same locations identified above. Furthermore, the loading conditions imposed in both the JES 3B test and in the earlier STA certification testing were not critical conditions for the attachment ring. The axial SRB tension load imposed was that developed by internal pressure alone. In flight, the axial load at the attachment ring is reduced from that caused by internal pressure because of nozzle thrust on the SRB. This reduced axial load increases the tension load in the ring because of the Poisson effect in the shell wall. A more realistic loading situation could have caused even more shear damage in these tests. It is clear that the existing ring does not meet the requirement of no yielding at $1.1 \times$ limit load. It is necessary, therefore, to redesign the ring and eliminate negative margins of safety. United Space Boosters, Inc. (USBI) is developing a full 360-degree ring design, and Langley Research Center (LaRC) was asked to supply an alternate concept for a partial ring.

The purpose of this report is to discuss the LaRC redesign activity which is a cooperative effort by Systems Engineering Division, Structures and Dynamics Division, and Materials Division at LaRC and Systems Dynamics

Laboratory and Structures and Propulsion Laboratory at MSFC. The following personnel are performing the technical work:

Langley Research Center

Systems Engineering Division

David H. Butler
Thomas C. Jones
John C. Gustafson
Obie H. Bradley, Jr.
Phillip J. Klich
David C. Beals
Robert B. Davis
Donald C. Athearn
Phillip L. Brown

Structures and Dynamics Division

Martin M. Mikulas, Jr.
Mark S. Lake
John T. Dorsey
Harold G. Bush
L. David Wall
Wilbur B. Fichter

Materials Division

James C. Newman, Jr.

Marshall Space Flight Center

Systems Dynamics Laboratory

Jan D. Dozier
Richard E. Dotson
David A. Herda
Robert E. Garrett
Tulon Bullock
Joseph A. Brunty
W. Richard Bell

Structures and Propulsion Laboratory

Sidney E. Rowe
Richard M. Jones, Jr.

2.0 DESIGN REQUIREMENTS

The overall goals of the redesign activity are to develop an alternate design of a partial ring having a safe life of forty missions, and, as much as possible, using existing hardware. Major detailed design requirements are:

- Maintain positive margins of safety with the following factors of safety:
 - 1.1 on limit load or yield
 - 1.4 on ultimate load
- Combine worst loads with appropriate uncertainty factors
- Use internal loads from United Space Boosters, Inc. NASTRAN model instead of Interface Requirements Document model
- Fail-safe design for tang bolts
- Provide thermal protection similar to existing design
- Interface with full 360° ring at 154.48° and 341.30° splices
- Design to 26 psid crush and burst
- Conform to requirements contained in reference 1

Design loads used at LaRC are generated by the roll maneuver and are worst case loads. The following loads from reference 2 are used in the redesign effort and include appropriate uncertainty factors:

- SRB loads

| | |
|-----------------------|-------------------------|
| Internal pressure | 912 psia |
| Axial thrust, tension | Fx = 12,400,000 lb |
| Y-shear | Fy = -121,000 lb |
| Z-shear | Fz = - 99,000 lb |
| Torque | Mx = 300,000 in.-lb |
| Y-moment | My = 32,000,000 in.-lb |
| Z-moment | Mz = -38,000,000 in.-lb |

-Strut loads

| | |
|--------------------|------------|
| P(10), compression | 117,000 lb |
| P(8), tension | 112,000 lb |
| P(9), tension | 147,000 lb |

The SRB loads apply at station X-1550. The axial load is larger farther forward on the SRB. The axial load shown above is critical for this design, however, because larger axial tension reduces circumferential tension in the ring due to the Poisson ratio effect. Detailed discussion of loads is contained in Appendix A.

Material and fastener mechanical properties are as follows:

| | |
|---|-------------|
| 4340 steel, tensile modulus | 30,000 ksi |
| 4340 steel, ultimate tensile strength | 180-200 ksi |
| 4340 steel, yield strength, tension | 160 ksi |
| MP35N steel, 3/8 in. bolts, ultimate shear strength | 16,000 lb |
| MP35N steel, 1/2 in. bolts, ultimate shear strength | 28,000 lb |

These material properties are "A" values from reference 3. Fastener properties are from references 4 and 5. Therefore, allowables are taken as:

| |
|--|
| 180 ksi/1.4 = 128 ksi tension in 4340 steel |
| 16,000 lb/1.4 = 11,430 lb shear in 3/8 in. bolts |
| 28,000 lb/1.4 = 20,000 lb shear in 1/2 in. bolts |

The design is required to pass a final certification analysis provided by MSFC with a NASTRAN certification finite element structural analysis model. MSFC will verify that the redesigned ring and motor case stresses are acceptable under all appropriate loading conditions.

3.0 DESIGN ASSUMPTIONS

Two assumptions made in the design process are: (1) clamped metal-to-metal sealing surfaces are acceptable to prevent hot gas intrusion, and (2) classical stress concentration factors are not appropriate in calculating margins of safety for static strength. This second assumption is consistent with aerospace industry practice when designing with ductile materials, which is the case here. In addition, the design is verified by testing structural elements. Further support for neglecting stress concentration factors in static strength design with ductile materials is contained in references 6 and 7.

4.0 DESIGN CONCEPT

4.1 Attachment Ring

The existing attachment ring configuration consists of webs, caps and a cover in a box cross-section configuration shown in figure 4. A plan view of the existing web for the ring is shown in figure 7. The basic concept of the existing design is retained as much as possible in the proposed redesign concept. The most significant change is to modify the webs and caps at each end of the ring to distribute fastener loads more evenly. Another important change is to fabricate webs and caps as integral units at the ring ends. This change eliminates the difficult problem of satisfying cap area, bearing stress, and fastener shear load requirements at the cap ends.

The redesigned ring web concept is shown in figure 8. The reconfigured ends are spliced to the ring at 153.48° and 341.30° as shown in figure 8. Splices also exist at these locations on the full 360-degree ring design. More detailed views of the ring web ends are in figure 9. A magnified view of a typical ring end is shown in figure 9(a). Views of the web and cap for the long end and short end, respectively, are shown in figures 9(b) and 9(c). Views of the splices are shown in figures 9(d) and 9(e). Comparisons between the new and old designs for each end of the ring are displayed in figures 10 and 11. The pockets shown between the first seven bolt holes in figures 10 and 11 are covered with a 0.10 in. thick shear web. A 2024-T8 aluminum bushing is located in the first bolt hole on each end of the ring. The bushings are anodized and pressed in place with a coating of wet polysulphide sealant to prevent galvanic corrosion. The bushings reduce the effective stiffness of the first bolt and prevent excessive loadings in these fasteners. They would be replaced after each flight. The bushing diameter of approximately 0.43 in. violates the minimum edge distance requirement of $1.5 \times \text{diameter}$ to the plate edge. Tests were conducted to show that the reduced edge distance is acceptable. Two specimens (four ends) were successfully tested to bolt loads of 16,250 lb with the reduced edge distance and bushings installed.

Beneficial features of the partial SRB/ET attachment ring concept compared to a full ring concept are (1) easier installation on the vehicle and (2) retention of existing vehicle dynamic properties. Specific features of the proposed redesign are as follows:

- stresses insensitive to bolt stiffness
- uses same materials as existing design
- all tang bolt loads are less than 11,430 lb
- carry ultimate load with one bolt removed from each end

4.2 Transition Tunnel

A new design is also proposed for the utility wiring transition tunnel which extends from the long end of the attachment ring to the systems tunnel (see figs. 3 and 5). The proposed transition tunnel is shown in figure 12. The major change is addition of expansion joints to prevent excessive loading of the tang fasteners or the systems tunnel. Calculations indicate a

stress problem if the proposed transition tunnel is attached in the same manner as the current design. The expansion joints introduce a possible leak path for external hot gases which must be sealed. Proposed seals for the expansion joints are illustrated in figure 13.

Each tunnel element extends over seven fastener holes in the tangs. One hole among the seven in each tunnel element is circular, and the remainder of the holes are slotted to allow slippage during pressurization of the SRB shell. Further details on the transition tunnel design are contained in Appendix E.

4.3 Concept Verification

Structural analysis is discussed in the subsequent section and presented in detail in Appendices as follows:

- B. Global Linear and Nonlinear Analysis
- C. Ring Area Tapering Analysis
- D. Splice Analysis
- E. ET/SRB Attach Ring Systems Cover Analysis
- F. Margins of Safety
- G. Inelastic Analysis
- H. Fracture Mechanics Analysis

Two additional appendices are included in this report. Experiments to generate data required for detail design are discussed in Appendix I, and a weight statement is in Appendix J. MSFC is responsible for the following analyses:

- Thermal
- Dynamic
- Venting
- Flutter
- Safety and Hazard

Responsibility for Qualification and Test Program is shared by MSFC and LaRC.

A master schedule for the redesign effort is shown in figure 14. Preliminary drawings will be produced by LaRC. Currently existing LaRC drawings are listed by number and title in Table 2. Final drawings will be produced by MSFC. Hardware will be fabricated by McDonnell Douglas Corporation through contract with United Space Boosters, Inc.

5.0 STRUCTURAL ANALYSIS

5.1 SRB Analysis

Analyses performed in the redesign process include simplified analyses and finite element analyses. Finite element analyses are carried out with the computer programs EAL (ref. 8) and PAL II at LaRC and NASTRAN at MSFC. To give an idea of the relative importance of the loads on the SRB shell, stresses and displacements were calculated from simple membrane shell theory

for a cylindrical shell with approximate dimensions of the motor case.
Results are as follows:

-Dimensions and properties

$R = 72.5 \text{ in.}$
 $t = 0.45 \text{ in.}$
 $I = \pi \times R^3 \times t = 538,737 \text{ in.}^4$
 $J = 2 \times I = 1,077,473 \text{ in.}^4$
 $E = 30,000,000 \text{ lb/in.}^2$
 $G = 11,000,000 \text{ lb/in.}^2$
Material = D6-AC steel

-Stresses

$S1 = \text{Circumferential stress} = (p \times R)/t = 146,933 \text{ psi}$
 $S2 = \text{Axial stress} = F_x/(2 \times \pi \times R \times t) = 60,491 \text{ psi (min.)}$
 $S3 = \text{Average shear stress} = F_y/(2 \times \pi \times R \times t) = 599 \text{ psi (max.)}$
 $S4 = \text{Bending stress} = (M_z \times R)/I = 5,935 \text{ psi (max.)}$
 $S5 = \text{Torsional stress} = (M_x \times R)/J = 279 \text{ psi}$

-Radial displacement

$\Delta R = (E/R) \times (S1 - \nu S2) = 0.3097 \text{ in.}$

To understand how stresses are developed in the ring through pressure loads on the SRB, finite element analyses were performed on a model representing a segment of the SRB including the existing attachment ring component. Details of this work are contained in Appendix B. The finite element model is illustrated in figure 15. The plan view of the ring web for this model is shown in figure 16. The model shown in figure 15 is 34.5 in. long, and the upper end of this model is at the center-line of the attachment ring. In the calculations, symmetry constraints are applied to the model at this location. The model, therefore, simulates a 69-inch long segment of the SRB. The attachment ring center-line is located at SRB X-station 1511.0 and the top and bottom of the model are at SRB X-stations 1476.5 and 1545.5 respectively. The field joint located at about SRB X-station 1491 is not included in this model.

The model displayed in figure 15 contains 2,189 plate elements, 328 beam elements, and about 13,000 degrees of freedom. A typical computer run for a linear analysis requires 30 CPU minutes on a Cyber 175. This analysis was performed for internal pressure loading only. Strut loads were not included. It turns out that strut loads do not influence stresses at the ends of the ring very strongly. Applied loads for this analysis are illustrated in figure 17. Typical linear elastic stresses from these finite element analyses are presented in figure 18 for section A-A and in figure 19 for section B-B (see fig. 16). The analytical solution listed in figure 19 is simply the circumferential stress from membrane theory of shells.

One calculation was performed for the case where a simplified model of the field joint was added to the finite element model. Since this finite element model is symmetric about the attachment ring center-line, the field joint was, in effect, added on both sides of the attachment ring. Results from this calculation are compared in figure 20 with results for the case of no field joint (fig. 18). The effect of the field joint on these stresses is negligible.

Limited nonlinear calculations were made using the finite element model of figures 15 and 16. Results for linear and nonlinear radial displacements are shown in figure 21, and a brief summary of results for linear and nonlinear circumferential stresses is shown in figure 22. Effects of nonlinearity on local bending stresses in the tang at the end of the web on the short end of the attachment ring are shown in figure 23. Additional analysis on a 136 in.-long segment of the SRB including the existing attachment ring at SRB X-station 1511 and the field joint at SRB X-station 1491 are contained in reference 9. In this work, another finite element computer program is used (STAGSC-1), and both linear and nonlinear calculations are performed. Results in reference 9 show high fastener loads at the ends of the ring and also display additional linear/nonlinear comparisons.

All these calculations are for the existing partial attachment ring. They indicate the significance of the axial component of pressure load, show that nonlinear effects are not of major global importance but can be of local importance, and supply data for the simplified analysis discussed in the next section.

5.2 Ring Analysis

5.2.1 Simplified Analysis for Sizing.- A simplified ring bolt load analysis was developed to gain understanding of how load feeds into the ring through the bolts, to provide an efficient and conservative analysis tool for resizing the ring web, and to contribute to certification of the design concept. Details of this work are contained in Appendix C. The basic elements of the method are illustrated in figure 24. Two versions of the method were developed. In the first version, illustrated in figure 25, the bolts are assumed rigid, and the ring webs are assumed rigid in shear. In the second version, illustrated in figure 26, bolt flexibility and shear flexibility (or shear lag) in the webs are accounted for. By using these simplified methods, a cross-section area profile can be calculated for a given bolt load distribution, or bolt loads can be calculated for a given cross-section area profile. Based on the rigid bolt and zero shear lag flexibility assumptions, for a uniform bolt load distribution of 10,000 lb per bolt, the ring cross-section area was calculated. Results are shown as the optimum ring in figure 27. Existing ring area is also shown in figure 27. Calculated bolt loads for these two cases are shown in figure 28. When both bolt and shear lag flexibilities are accounted for, the comparative area profiles are shown in figure 29. A comparison of bolt loads for these two cases is shown in figure 30. These results indicate that drastic reduction in ring cross-section area is required near the ends to keep bolt loads at or less than the 10,000 lb level. The value of 10,000 lb was selected for early calculations. For the final proposed concept, bolt loads were specified to be less than 8,500 lb, as discussed in Appendix C.

5.2.2 Planar Finite Element Models.- For more refined analysis, a series of two-dimensional and three-dimensional planar finite element models of the ring were developed. In these models the curvature of the ring is neglected as in the simplified methods. Examples of these models are shown in figures 31 and 32. The two-dimensional model represents the case wall by a line of bar elements with an effective area and is less demanding of computer resources and turn around time than the three-dimensional model. Therefore, comparisons were made between these two models to determine the best value

of effective shell area and to validate the two-dimensional model for design iterations. In these calculations the bottom of the ring is constrained to remain straight along the length. Results are shown in figure 33 and indicate an effective shell area of 6.5 in.² gives reasonable agreement at the end of the ring where loads are most critical.

Results from the two-dimensional planar model were compared with results from the MSFC NASTRAN certification finite element model, which is similar to but more refined than the shell segment model discussed in the previous section of this report. Comparison is shown in figure 34 where "fixed shell" refers to the planar model in which the ring is constrained to remain straight along the length and "free shell" refers to the planar model in which no such constraint is imposed. These planar models, therefore, bound the NASTRAN results; and the "fixed shell" planar model should lead to designs having bolt loads greater than would be obtained using the MSFC NASTRAN certification model.

The two-dimensional planar finite element model was then refined to represent more accurately the actual proposed redesign concept for the ends of the ring webs. This refined finite element model is compared with an actual design in figure 35. The design shown in figure 35 is not the final proposed concept, however, analysis of the design revealed useful data. Calculations were made with the refined planar model, and results for bolt loads are shown in figure 36. These results are for the so-called "fixed shell" constraints in which the bottom of the model is constrained to remain straight along its length. The curves labelled "tang bolts" and "cap bolts" in figure 36 refer to the refined model. The curve labelled "previous iteration" refers to the original two-dimensional planar model. All these calculations are based on a bolt shear stiffness of 1.3×10^6 lb/in. which was measured in experiments discussed in the next section of this report and in Appendix I. All bolt loads are less than the allowable load of 11,430 lb.

The final proposed concept differs from the design in figure 35 in two major ways. A fastener hole was added between the end hole and the second hole as indicated in figures 9, 10, and 11, and the cap and web were integrated to eliminate cap bolts. This planar finite element model was not updated to the final proposed concept, because detailed analysis was undertaken on the MSFC NASTRAN certification model as discussed in Appendix C.

5.2.3 Sensitivity to Bolt Shear Stiffness.- To obtain an estimate of the sensitivity of these results to bolt shear stiffness, calculations were made for the redesigned ring with bolt shear stiffness of 2.0×10^6 lb/in. Results of these calculations are compared with the previous results for bolt shear stiffness of 1.3×10^6 lb/in. in figure 37. If the shear stiffness of all bolts changes uniformly, then, bolt loads are not strongly influenced by bolt stiffness. Changes in stiffness of individual bolts can influence bolt loads, however, and this fact is exploited by use of bushings in the first fastener hole at each end (see Appendix C).

5.2.4 Single Bolt Failure.- To simulate the single bolt failure condition, calculations were performed for situations in which a single bolt in the

pattern is removed. Results are shown in figure 38 for cases in which the first bolt, the second bolt, and the third bolt have failed. All remaining bolt loads are less than bolt ultimate shear strength of 16,000 lb showing that all these single bolt failure situations are fail-safe.

5.2.5 Out-of-Round Motor Case.- An analysis was made to understand effects of mounting the attachment ring to an out-of-round motor case. A likely shape for out-of-roundness can be represented by the geometry shown on the left-hand side of figure 39. The analysis model consists of the web and cap of the attachment ring and includes the first 40 tang fasteners (counting from the ring tip). The bottom of the ring is modeled as a circular arc, and the piece is assumed to be cantilevered from the right-hand end as shown on the right-hand side in figure 39. Radial displacements are applied at the 40 fasteners according to the formula on the left-hand side of figure 39. These displacements move the circular arc ring into the deformed geometry. The reaction loads to these displacements represent shear loads in the bolt fasteners. For the case of a tip displacement of 0.1 in., the shear loads in the first 38 bolts are plotted in figure 40. The loads in bolts 39 and 40 are not shown in figure 40 because they are thought to be unrealistic--the cantilever boundary condition does not properly model the ring behavior in that region. The response shown in figure 40 is linear with respect to tip displacement, so the data can be used to calculate bolt loads caused by known or estimated out-of-round conditions. Measurements of two SRBs reported in reference 10 indicate that the maximum tip deflection for the model in figure 39 could be as much as 0.2 in.

5.2.6 Certification Model Analysis.- The redesigned partial ring has been incorporated into the MSFC NASTRAN certification model mentioned previously. Analyses with this model account for shell curvature effects and strut load effects. The aluminum bushing in the first fastener hole is accounted for in this model by reducing the effective shear stiffness of the first bolt to 0.6 of the baseline stiffness. This value is consistent with the values obtained from experiment and discussed in Appendix I. Results from these analyses are shown in figures 41 and 42. In figure 41 bolt loads for the redesigned ring are compared with those for the existing ring. Bolt loads for the redesigned ring are less than about 8,500 lb. In figure 42 bolt loads for the redesigned ring are shown for the cases of pressure and strut loads and pressure only. Strut loads have negligible effect on the bolt loads near the ends of the ring. To get some idea of the effect of changing stiffness of the first bolt, results are shown in figure 43 for stiffnesses of 0.4, 0.6, and 0.75 times the baseline bolt stiffness. Only the stiffness of the first bolt is varied in these calculations. Results of all these analyses show bolt shear loads distinctly below the allowable of 11,430 lb.

5.2.7 Other Analyses.- Analysis of the splice joint is presented in Appendix D. Analysis of the transition tunnel is in Appendix E. Margins of safety are presented in Appendix F. A failure analysis accounting for the effects of plasticity is presented in Appendix G, and fracture mechanics analysis is contained in Appendix H.

6.0 EXPERIMENTS

Experiments were performed to measure: (1) stiffness of ring web end component configurations, (2) shear stiffness of bolts, (3) modulus of basic material and (4) behavior of deformable bushing in end hole. Detailed discussion of experiments is contained in Appendix I. The test fixture for the ring web end component stiffness measurements is shown in figure 44. Experiments were performed on dogbone specimens, sculptured thickness or scalloped specimens, and double bar specimens. Dimensions of these specimens were typical of those for the end section (first section) of the ring design. A typical plot of deflection as a function of load is shown in figure 45 (for double bar specimen). Bolt shear stiffness was measured in a single-shear test specimen. Results for extensional stiffnesses for the end configurations and shear stiffnesses for the bolts are presented in figure 46 for the double bar, scalloped, and dogbone specimens. Bolt shear stiffness data are plotted in figure 47.

Average ultimate shear strength of bolts was measured in five tests with four bolts in each test. Result was 17,500 lb, higher than the strength of 16,000 lb which was used in all structural analysis. Young's modulus of 4130 chrome-moly steel was measured as 29,800 ksi, very close to the handbook value of 30,000 ksi used in the structural analysis.

Effect of the deformable bushing in the end hole in the ring web is essentially to reduce the effective shear stiffness of the end bolt. Results of tests using aluminum bushings are shown in figure 48.

7.0 MATERIALS AND FABRICATION

The primary requirement for the ring web runout is that under load it deflects with the SRB tang while limiting the loads generated in the attached bolts to a prescribed level of <11,430 lb. This requirement has driven the design such that the cross sectional area of the web between the last three or four bolts, and the last two bolts, in particular, are the most critical in controlling bolt loads and are the most highly stressed areas.

Prior to incorporation of the deformable bushing in the end bolt hole of the ring, the preferred configuration was a double beam concept with no center shear web as shown in figure 49. With this design there was concern with respect to the fabrication of the ring end. The problem was that the critical cross sectional areas were physically small (0.0417 in.^2) and with a high average stress across the area (120 ksi). The load in the web between the bolts is primarily tensile resulting in a linear relationship between area and stress for a given load. As a result small dimensional variations resulting from either material discrepancies or fabrication process tolerances, which would normally be ignored, have significant effects on the critical cross sectional area.

The web cross section area then becomes the principal item to be addressed in investigating the effects of materials and processes in the production of the part. The goal is to hold the variations due to both materials and fabrication processes to within $\pm 7\%$, with the machining

tolerances held to maintain the cross sectional area to within $\pm 5\%$ of nominal value. This goal results in dimensional tolerances on the order of ± 0.005 in. in the most critical areas.

Incorporation of the deformable bushing in the end hole of the ring web allowed the addition of a shear web between the two tensile beam members and an increase in the total cross sectional area from 0.0834 in.^2 to 0.183 in.^2 . With no change in the $\pm 5\%$ area tolerance criteria, it would be expected that the fabrication tolerances could be increased. Because of the cross section geometry, however, the machining tolerances do not change and have to be maintained at ± 0.005 in. in the most critical areas. This tolerance level, while fairly precise for this size part, can be achieved with reasonable care.

7.1 Materials

The major candidate materials are AISI 4130 and AISI 4340. These choices are based on the fact that both alloys can be heat-treated to adequate strength levels, and both alloys are used as primary structural materials in the existing ring design.

7.1.1 Material Strength.- The existing web uses AISI 4130 procured to MIL-S-18729. The web itself is heat-treated per MIL-H-6875 to 180-200 ksi ultimate strength, with no minimum yield strength specified (ref. 11). Subsequent web drawings for the USBI 360-degree ring improved on the specification by requiring a minimum yield strength for this material of 163 ksi (ref. 12). Other elements in the ring construction, such as splice plates, are also fabricated from 4130 but heat-treated to a lower strength level (ref. 13).

The existing ring cap is fabricated from an AISI 4340 forging and heat-treated per MIL-H-6875. The specified strength after final stress relief is 170-190 ksi ultimate, with a minimum yield of 145 ksi (ref. 14).

7.1.2 Material Cleanliness.- Both materials are classified as "Aircraft Quality Steels" by their appropriate MIL Standards and both Standards call out AMS 2301 as the guiding document for specifying material cleanliness. The parts lists for the existing ring specify the method for magnetic particle inspection and add the limitation that "no crack-like indications are allowed". This limitation tightens the AMS 2301 specification considerably, since flaws up to 1.5 in. long are allowed under the basic requirements. AMS 2301 places a lower limit of $1/16$ in. on the size of indication to be noted in inspection. Therefore, it is assumed that a worst case inclusion of $1/16$ in. in diameter can be considered to exist randomly within the material as currently specified.

7.1.3 Material Uniformity.- All steels, as a result of hot processing, exhibit decarburization of material nearest the surface. Since carbon content is the primary agent that allows the heat treatment for both steels to occur, significant surface decarburization does not allow the desired strength of the material to be achieved across the full section. Specifications on decarburization for the materials are found in two places, the materials specification for "as rolled" stock, and MIL-H-6875 for the

heat treatment of finished material. In the thickness of the 4130 used for the web of the ring the maximum allowable hardness difference between the outer surface and the center of an "as quenched" specimen is 2 points on the Rockwell A scale or 4 points on the Rockwell C scale. In the tempered condition this situation could result in a local variation in tensile strength across the thickness of approximately 15 ksi from the center to the outer surfaces.

Generally, other parts making up the ring assembly are machined down from thick stock, effectively removing the decarburized layer.

7.1.4 Material Tolerances.- "As rolled" material thickness tolerances are generally liberal. In case of 4130 plate specified for the existing web design, the thickness tolerances are found in the Aerospace Material Specification AMS 2252C and are specified as: 0.250 in. +0.016 in., -0.010 in.

7.1.5 Effects of Existing Material on LaRC Design Concept.- Table 3 presents the effects of only material variations on the minimum section area of both the earlier double beam and the final bushed concepts. The data is broken out for each of the sub-areas making up the cross-section (figs. 49 and 50) as well as the total area and reflects the effect of using the materials specified for the existing design in each of the two concepts.

The thickness tolerance column represents the effects of using stock thickness material (where applicable) and holding all machined dimensions at their nominal values. The % Total Variation column represents simply a summing of the worst case conditions.

The conclusion is that the material as specified for the existing design does not support a +/-7% area tolerance criteria for the double beam design but that it might be useable for the bushed design.

The critical values for flaw size on the double beam concept are for the subareas. These areas have no connection with each other except at the bolt pads at the ends of the beams, and there is no capability to redistribute stresses between the areas in the event of a material flaw.

7.1.6 Effects of Improved Material Cleanliness.- Within the Military Specification System there is another quality level of steels called Premium Aircraft-Quality. These steels are consumable electrode remelted or electroslag remelted steels with significantly improved cleanliness requirements as called out in Aerospace Materials Specification AMS 2300F. The minimum size of indication under this specification is 0.015 in. This size is a factor of sixteen improvement over the standard specification and reduces the Total % Variation to levels shown in Table 4.

7.2 Fabrication

7.2.1 Fabrication Tolerance Effects.- Tables 3 and 4 do not include effects of dimensional fabrication tolerances on the critical areas of the various concepts. For these two tables the tolerance of the "as rolled" material was used for the 0.250 in. dimension and all other machined dimensions were assumed to be at their nominal value. A simple analysis was undertaken to

determine the maximum tolerances that could be used and still maintain the critical area for each concept within a given percentage (in this case +/-5% was allocated to fabrication tolerances).

The most sensitive cross section in the LaRC design is shown in section in figure 50. This section can be considered to consist of three areas A_1 , A_2 , and A_3 . For a first order estimate of the allowable tolerance, two simplifying assumptions are made:

- o The area tolerances for each area is held to the same percentage of area as required for the total section.

$$DA_t = DA_1 + DA_2 + DA_3$$

- o The tolerance on a given dimension is held to a constant percentage of that dimension.

For a single rectangular section the equation takes the form

$$A + DA = (h + dh) \times (t + dt)$$

where:

A = nominal area
D = area tolerance
h = nominal height
t = nominal thickness
d = dimension tolerance

Solving for D:

$$D = 2d + d^2$$

For the small percentages under consideration for this problem the second order term can be ignored and

$$d = D/2$$

Therefore, for a 5% allowable area variation the linear dimensions should be held to within 2.5% of the dimension. The results of this analysis for the LaRC concept are presented below.

| Area | Thickness Dimension in. | Tolerance in. | Height Dimension in. | Tolerance in. |
|----------------|-------------------------------|------------------|----------------------------|------------------|
| A ₁ | 0.250 | 0.0062 | 0.210 | 0.0053 |
| A ₂ | 0.250 | 0.0062 | 0.210 | 0.0053 |
| A ₃ | 0.100 | 0.0025 | 0.780 | 0.0195 |

A tolerance of ± 0.005 in. is generally considered to be a reasonable lower limit for conventional machining practice on a part the size of the ring web with a tolerance of ± 0.010 in. or looser being desirable. The thin shear web requires the closest control of thickness because of the constant percentage assumption. All dimensions, except for the shear web height, require careful quality control to assure the areas are within the 5% criteria.

The tight tolerance on shear web thickness was considered unacceptable. Since all other dimensions, except for the height of the shear web, carried tolerances already close to a reasonable limit, an attempt was made to balance the tolerances for the shear web cross sectional area alone. By solving for the case where both the height and thickness tolerances are the same

$$A + DA = (b + d_t) \times (h + d_t)$$

where

$$d_t = \text{absolute dimensional tolerance}$$

Then

$$A + DA = bh + bd_t + hd_t + d_t^2$$

$$= A + d_t(b + h) + d_t^2$$

$$DA = d_t(b + h) + d_t^2$$

By ignoring the second order term and solving for d_t

$$d_t = DA/(b + h) = (0.05 \times 0.078 \text{ in.}^2)/(0.10 \text{ in.} + 0.78 \text{ in.}) = 0.0044 \text{ in.}$$

This result is still lower than desired.

A final case was run where all dimensions making up the total cross sectional area carried the same tolerance. An analysis similar to that shown above resulted in a general tolerance for this cross sectional area of ± 0.005 in. as shown in figure 51 and Table 5.

The tolerance requirement is closer than desired; however, it is only required in the local area near the end of the ring. As the web cross sectional area increases towards the splice area the tolerances are increased up to a relatively loose value of ± 0.020 in. (ref. 15). The relatively close tolerances on the dimensions of the ring ends are achievable in practice but require more precision machining techniques than have been used in fabrication of the existing design and will increase cost. The "as rolled" tolerances are outside of the tolerance necessary to meet the $\pm 5\%$ area requirement, and it is necessary to machine the web thickness from heavier stock.

For purposes of comparison, the results of a similar analysis on the double beam concept is included on Table 5. Table 5 combines the applicable material variations with the fabrication tolerances for a Total % Variation.

The $\pm 5\%$ area tolerance requirement was reexamined to determine if changes made in the design since establishing the criteria would permit the use of a wider tolerance. In figure 52 net section stress along the web is plotted starting at the first bolt. The indication is that in the area around the third bolt and fourth bolt the $\pm 5\%$ tolerance is still required since stresses are still within 90% of the allowable stress of 128 ksi. It is recommended that tolerances be held to support $\pm 5\%$ of nominal cross section area up to bolt 5. Beyond bolt 5 the area tolerance can be increased to $\pm 10\%$.

7.2.2 Test Sample Fabrication Experience - A large number of test specimens replicating various ring and geometry concepts were fabricated at LaRC from AISI 4130. The specimens were full size areas replicating the profile over a two to four bolt spacing on the ring end.

Initially, the material used was 1/4 in. plate similar to that in the existing web. The first parts were machined from annealed stock to the finished dimensions, hardened and tempered to 180-200 ksi ultimate strength. The results were varied, but generally there was significant warpage in the parts. The worst problems occurred on nonsymmetrical sections where 1/4 in. out-of-plane bows over the specimen length of 4.5 in. were noted. Improved circulation in the water quench and other changes such as quench insertion attitude improved the condition but not to an acceptable level. The final solution was to harden and temper thicker plate stock and machine to the final dimension in the heat treated state.

A set of the more symmetrical-configuration samples machined in the annealed state were sent to a local commercial heat treating facility. The warpage on these parts was low enough to be acceptable.

The major cause of warpage appeared to be the water quench necessary to achieve hardness with a shallow-hardening steel such as AISI 4130. An unsuccessful attempt was made to oil quench the material because of a feeling that the 1/4 in. plate thickness would cool rapidly enough to achieve full hardness. Telecons with USBI and McDonnell Douglas personnel who had been involved in the fabrication of the existing ring indicated that similar problems existed during production.

In search for an acceptable solution, P. Nunn, Lockheed Georgia Company, suggested that consideration be given to use of AISI 4340 as a material for the web rather than 4130. The main reason for the suggestion is that 4340 is a much deeper hardening steel than 4130 and can be oil quenched to achieve the necessary hardness. It also lends itself to temper straightening if there is warpage. Another alternative to reduce warpage is to use an intermediate molten salt quench before final quench to room temperature.

An additional advantage to 4340 vacuum remelt is that it is available in plate form. This material is then inspected to the tighter AMS 2300 specification at the raw stock level.

Finally, although there would be a problem with compliance to MSFC-SPEC-522A, AISI 4340 can be heat treated to higher strength levels than AISI 4130 with little loss in ductility. This situation provides an added margin in the web material.

One problem with 4340 is that, because it is such a deep hardening steel, there is a tendency to reform martensite at surfaces machined after hardening due to high tool/workpiece interface temperatures. This situation can be avoided by use of light final machining cuts, sharp tooling, and heavy coolant flow.

LaRC is procuring 4340 plate to fabricate test samples of the proposed configuration and develop the optimum heat treat procedure.

7.3 Recommendations

As a result of the examinations into the materials and processes associated with the attachment ring, the following recommendations are made:

- o Use material inspected to the cleanliness requirement of AMS 2300. This action can be done either by procurement of vacuum remelt plate, electro-slag remelt plate, or by selective inspection of regular plate.
- o Machine the web from heavy plate to the final thickness. This procedure eliminates the potential of a decarburized surface layer and provides tolerance required to maintain the web area profile.
- o Fabricate the new web sections from AISI 4340 rather than AISI 4130.

o Proposed fabrication process:

Finish machine part from normalized plate (except mating tang attachment holes).

Austinitize and oil quench to room temperature.

Snap temper to 400°F.

Temper straighten to 180-200 ksi.

Drill mating tang attachment holes on assembly fixture at McDonnell Douglas.

- o Use fabrication tolerances to support a +/-5K% area variation over the first 5 bolts on each ring end.
- o Use magnetic particle inspection on material between the ring end and the fifth bolt on each end prior to final machining, and after final machining. Magnetic particle inspection of this area should be made as part of the refurbishment procedure after each use of the ring. Indications larger than 0.03 in. should be cause for rejection.

8.0 CONCLUSIONS AND RECOMMENDATIONS

An improved concept for the solid rocket booster/external tank partial attachment ring is presented. Design and analysis studies to support the concept are contained in Appendices. Materials and fabrication studies have been conducted. The ring must be carefully tapered at the ends to distribute bolt loads safely. Stress analysis shows positive margins of safety in the ring, in the solid rocket booster shell wall and tangs, and in all fasteners. Data has been generated from element tests to determine stiffness and strength of tapered ring ends and fasteners. It is recommended that:

- (1) additional element tests be performed to confirm material strength and fatigue behavior
- (2) the concept be subjected to complete NASTRAN certification analysis by MSFC
- (3) hardware implementation of the concept be started as soon as possible
- (4) the ring ends be fabricated of 4340 premium quality aircraft steel and machined out of thick stock
- (5) certification test plans be completed
- (6) certification tests be performed at MSFC
- (7) rings be inspected for cracks after each flight.

REDESIGN OF SOLID ROCKET BOOSTER / EXTERNAL TANK ATTACHMENT RING
FOR THE SPACE TRANSPORTATION SYSTEM

9.0 REFERENCES

1. Marshall Space Flight Center Handbook 505, Revision A
2. Interim IVBC-3 Design Loads for Use in SRB and SRM Steel Case Redesign and Recertification, Marshall Space Flight Center letter from ED01/Dr. McDonough to SA41/Mr. Smith, December 16, 1986.
3. MIL-HDBK-5D, June 1, 1983
4. SPS Technology Part #EWSEM 26-6 and -8
5. Montano, J.: A Mechanical Property and Stress Corrosion Evaluation of MP35N Multiphase Alloy. NASA TMX 64591, 1971.
6. Peery, David J.: Aircraft Structures. McGraw-Hill Book Company, Inc. New York, 1950, p. 303.
7. Osgood, Carl C.: Spacecraft Structures. Prentice-Hall, Inc., Englewood Cliffs, New Jersey, 1966, p.103.
8. Whetstone, W. D.: Engineering Analysis Language Reference Manual. Engineering Information Systems, Inc., San Jose, California. August 1985.
9. Knight, Norman F.: Nonlinear Shell Analysis of the SRB/ET Ring Interface. NASA TM 89164, 1987.
10. Morton Thiokol Document TWR-16307: Photogrammetry, Sinebar, Micrometer, and Pi Tape Measurement Systems Compared. March 18, 1987.
11. USBI Parts List 0170-0032 Note 8
12. USBI Parts List 0170-0250 Notes 8&9
13. USBI Parts List 0170-0016 Note 2
14. USBI Parts List 0179-0170 Note 11
15. LaRC Drawing LE 158039

TABLE 1

ET ATTACH RING FASTENER DAMAGE HISTORY

| LEFT-HAND SRB | | | | | | | | | | RIGHT-HAND SRB | | | | | | | | | |
|-------------------|-----------------------|-----------------------------|-----------------------|----------------|----------------|-------------|----------------|----------------|-----------------------|-----------------------------|-----------------------|----------------|----------------|-------------|----------------|----------------|---|---|--|
| Shuttle Flight | Attach Ring S/N | Paint/ Sealant Cracks | Mo. Sheared Fasteners | | | | | | Attach Ring S/N | Paint/ Sealant Cracks | Mo. Sheared Fasteners | | | | | | | | |
| | | | Ring Fwd | Web/SRB Aft | Cap/Off Loc | Ring Fwd | Web/SRB Aft | Cap/Off Loc | | | Ring Fwd | Web/SRB Aft | Cap/Off Loc | Ring Fwd | Web/SRB Aft | Cap/Off Loc | | | |
| STS-1 | 5 | - | - | - | - | - | - | 6 | - | - | - | - | - | - | - | - | - | - | |
| STS-2 | 7 | - | - | - | - | - | - | 4 | - | - | - | - | - | - | - | - | - | - | |
| STS-3 | 9 | - | - | - | - | - | - | 10 | - | - | - | - | - | - | - | - | - | - | |
| STS-4 (7) | 11 | - | - | - | - | - | - | 12 | - | - | - | - | - | - | - | - | - | - | |
| STS-5 | 13 | - | - | - | - | - | 3 | 14 | - | - | - | - | - | - | 25 bolts (2) | - | - | - | |
| STS-6 | 3 | - | - | - | - | - | - | 2 | - | - | - | - | - | - | - | - | - | - | |
| STS-7 | 5 | - | - | - | - | - | - | 6 | - | - | - | - | - | - | - | - | - | - | |
| STS-8 (6) | 9 | - | - | - | - | - | - | 4 | - | - | - | - | - | - | - | - | - | - | |
| STS-9A | 7 | - | - | - | - | - | 4 | 2 | - | - | - | - | - | - | - | - | - | - | |
| STS-10 | 13 | Yes | - | - | - | - | (3) | 10 | - | - | - | - | - | - | - | - | - | - | |
| STS-11C | 5 | - | - | - | - | - | - | 14 | - | - | - | - | - | - | - | - | - | - | |
| STS-12 (8) | 3 | Yes | - | - | - | - | -30 | 6 | - | - | - | - | - | - | 3 | 14 | - | - | |
| STS-13 | 9 | - | - | - | - | - | - | 2 | - | - | - | - | - | - | - | - | - | - | |
| STS-14 (9) | 7 | Yes | - | - | - | - | - | 10 | - | - | - | - | - | - | - | - | - | - | |
| STS-15A | 13 | Yes | - | - | - | - | - | 14 | - | - | - | - | - | - | - | - | - | - | |
| STS-16 | 15 | - | - | - | - | - | - | 18 | - | - | - | - | - | - | - | - | - | - | |
| STS-17 | 5 | Yes | - | - | - | - | - | 16 | - | - | - | - | - | - | - | - | - | - | |
| STS-18 | 19 | - | - | - | - | - | - | 2 | - | - | - | - | - | - | - | - | - | - | |
| STS-19 | 7 | Yes | - | - | - | - | - | 10 | - | - | - | - | - | - | - | - | - | - | |
| STS-20 (4) | 3 | Yes | - | - | - | - | - | 20 | - | - | - | - | - | - | - | - | - | - | |
| STS-21 | 9 | Yes | - | - | - | - | 27 | 14 | - | - | - | - | - | - | - | - | - | - | |
| STS-22 | 13 | Yes | - | - | - | - | -6 | 6 | - | - | - | - | - | - | - | - | - | - | |
| STS-23 | 17 | Yes | - | - | - | - | -5 | 4 | - | - | - | - | - | - | - | - | - | - | |
| STS-24 | 15 | Yes | - | - | - | - | -5 | 22 | - | - | - | - | - | - | - | - | - | - | |
| STS-25 | 5 | - | - | - | - | - | -5 | 4 | - | - | - | - | - | - | - | - | - | - | |
| STS-26 | 9 | - | - | - | - | - | -5 | 22 | - | - | - | - | - | - | - | - | - | - | |
| STS-27 | 13 | - | - | - | - | - | -5 | 4 | - | - | - | - | - | - | - | - | - | - | |
| STS-28 | 15 | - | - | - | - | - | -5 | 4 | - | - | - | - | - | - | - | - | - | - | |
| STS-29 | 5 | - | - | - | - | - | -5 | 4 | - | - | - | - | - | - | - | - | - | - | |
| STS-30 | 9 | - | - | - | - | - | -5 | 4 | - | - | - | - | - | - | - | - | - | - | |
| STS-31 | 13 | - | - | - | - | - | -5 | 4 | - | - | - | - | - | - | - | - | - | - | |
| STS-32 | 15 | - | - | - | - | - | -5 | 4 | - | - | - | - | - | - | - | - | - | - | |
| STS-33 | 5 | - | - | - | - | - | -5 | 4 | - | - | - | - | - | - | - | - | - | - | |
| STS-34 | 9 | - | - | - | - | - | -5 | 4 | - | - | - | - | - | - | - | - | - | - | |
| STS-35 | 13 | - | - | - | - | - | -5 | 4 | - | - | - | - | - | - | - | - | - | - | |
| STS-36 | 15 | - | - | - | - | - | -5 | 4 | - | - | - | - | - | - | - | - | - | - | |
| STS-37 | 5 | - | - | - | - | - | -5 | 4 | - | - | - | - | - | - | - | - | - | - | |
| STS-38 | 9 | - | - | - | - | - | -5 | 4 | - | - | - | - | - | - | - | - | - | - | |
| STS-39 | 13 | - | - | - | - | - | -5 | 4 | - | - | - | - | - | - | - | - | - | - | |
| STS-40 | 15 | - | - | - | - | - | -5 | 4 | - | - | - | - | - | - | - | - | - | - | |
| STS-41 | 5 | - | - | - | - | - | -5 | 4 | - | - | - | - | - | - | - | - | - | - | |
| STS-42 | 9 | - | - | - | - | - | -5 | 4 | - | - | - | - | - | - | - | - | - | - | |
| STS-43 | 13 | - | - | - | - | - | -5 | 4 | - | - | - | - | - | - | - | - | - | - | |
| STS-44 | 15 | - | - | - | - | - | -5 | 4 | - | - | - | - | - | - | - | - | - | - | |
| STS-45 | 5 | - | - | - | - | - | -5 | 4 | - | - | - | - | - | - | - | - | - | - | |
| STS-46 | 9 | - | - | - | - | - | -5 | 4 | - | - | - | - | - | - | - | - | - | - | |
| STS-47 | 13 | - | - | - | - | - | -5 | 4 | - | - | - | - | - | - | - | - | - | - | |
| STS-48 | 15 | - | - | - | - | - | -5 | 4 | - | - | - | - | - | - | - | - | - | - | |
| STS-49 | 5 | - | - | - | - | - | -5 | 4 | - | - | - | - | - | - | - | - | - | - | |
| STS-50 | 9 | - | - | - | - | - | -5 | 4 | - | - | - | - | - | - | - | - | - | - | |
| STS-51 | 13 | - | - | - | - | - | -5 | 4 | - | - | - | - | - | - | - | - | - | - | |
| STS-52 | 15 | - | - | - | - | - | -5 | 4 | - | - | - | - | - | - | - | - | - | - | |
| STS-53 | 5 | - | - | - | - | - | -5 | 4 | - | - | - | - | - | - | - | - | - | - | |
| STS-54 | 9 | - | - | - | - | - | -5 | 4 | - | - | - | - | - | - | - | - | - | - | |
| STS-55 | 13 | - | - | - | - | - | -5 | 4 | - | - | - | - | - | - | - | - | - | - | |
| STS-56 | 15 | - | - | - | - | - | -5 | 4 | - | - | - | - | - | - | - | - | - | - | |
| STS-57 | 5 | - | - | - | - | - | -5 | 4 | - | - | - | - | - | - | - | - | - | - | |
| STS-58 | 9 | - | - | - | - | - | -5 | 4 | - | - | - | - | - | - | - | - | - | - | |
| STS-59 | 13 | - | - | - | - | - | -5 | 4 | - | - | - | - | - | - | - | - | - | - | |
| STS-60 | 15 | - | - | - | - | - | -5 | 4 | - | - | - | - | - | - | - | - | - | - | |
| STS-61 | 5 | - | - | - | - | - | -5 | 4 | - | - | - | - | - | - | - | - | - | - | |
| STS-62 | 9 | - | - | - | - | - | -5 | 4 | - | - | - | - | - | - | - | - | - | - | |
| STS-63 | 13 | - | - | - | - | - | -5 | 4 | - | - | - | - | - | - | - | - | - | - | |
| STS-64 | 15 | - | - | - | - | - | -5 | 4 | - | - | - | - | - | - | - | - | - | - | |
| STS-65 | 5 | - | - | - | - | - | -5 | 4 | - | - | - | - | - | - | - | - | - | - | |
| STS-66 | 9 | - | - | - | - | - | -5 | 4 | - | - | - | - | - | - | - | - | - | - | |
| STS-67 | 13 | - | - | - | - | - | -5 | 4 | - | - | - | - | - | - | - | - | - | - | |
| STS-68 | 15 | - | - | - | - | - | -5 | 4 | - | - | - | - | - | - | - | - | - | - | |
| STS-69 | 5 | - | - | - | - | - | -5 | 4 | - | - | - | - | - | - | - | - | - | - | |
| STS-70 | 9 | - | - | - | - | - | -5 | 4 | - | - | - | - | - | - | - | - | - | - | |
| STS-71 | 13 | - | - | - | - | - | -5 | 4 | - | - | - | - | - | - | - | - | - | - | |
| STS-72 | 15 | - | - | - | - | - | -5 | 4 | - | - | - | - | - | - | - | - | - | - | |
| STS-73 | 5 | - | - | - | - | - | -5 | 4 | - | - | - | - | - | - | - | - | - | - | |
| STS-74 | 9 | - | - | - | - | - | -5 | 4 | - | - | - | - | - | - | - | - | - | - | |
| STS-75 | 13 | - | - | - | - | - | -5 | 4 | - | - | - | - | - | - | - | - | - | - | |
| STS-76 | 15 | - | - | - | - | - | -5 | 4 | - | - | - | - | - | - | - | - | - | - | |
| STS-77 | 5 | - | - | - | - | - | -5 | 4 | - | - | - | - | - | - | - | - | - | - | |
| STS-78 | 9 | - | - | - | - | - | -5 | 4 | - | - | - | - | - | - | - | - | - | - | |
| STS-79 | 13 | - | - | - | - | - | -5 | 4 | - | - | - | - | - | - | - | - | - | - | |
| STS-80 | 15 | - | - | - | - | - | -5 | 4 | - | - | - | - | - | - | - | - | - | - | |
| STS-81 | 5 | - | - | - | - | - | -5 | 4 | - | - | - | - | - | - | - | - | - | - | |
| STS-82 | 9 | - | - | - | - | - | -5 | 4 | - | - | - | - | - | - | - | - | - | - | |
| STS-83 | 13 | - | - | - | - | - | -5 | 4 | - | - | - | - | - | - | - | - | - | - | |
| STS-84 | 15 | - | - | - | - | - | -5 | 4 | - | - | - | - | - | - | - | - | - | - | |
| STS-85 | 5 | - | - | - | - | - | -5 | 4 | - | - | - | - | - | - | - | - | - | - | |
| STS-86 | 9 | - | - | - | - | - | -5 | 4 | - | - | - | - | - | - | - | - | - | - | |
| STS-87 | 13 | - | - | - | - | - | -5 | 4 | - | - | - | - | - | - | - | - | - | - | |
| STS-88 | 15 | - | - | - | - | - | -5 | 4 | - | - | - | - | - | - | - | - | - | - | |
| STS-89 | 5 | - | - | - | - | - | -5 | 4 | - | - | - | - | - | - | - | - | - | - | |
| STS-90 | 9 | - | - | - | - | - | -5 | 4 | - | - | - | - | - | - | - | - | - | - | |
| STS-91 | 13 | - | - | - | - | - | -5 | 4 | - | - | - | - | - | - | - | - | - | - | |
| STS-92 | 15 | - | - | - | - | - | -5 | 4 | - | - | - | - | - | - | - | - | - | - | |
| STS-93 | 5 | - | - | - | - | - | -5 | 4 | - | - | - | - | - | - | - | - | - | - | |
| STS-94 | 9 | - | - | - | - | - | -5 | 4 | - | - | - | - | - | - | - | - | - | - | |
| STS-95 | 13 | - | - | - | - | - | -5 | 4 | - | - | - | - | - | - | - | - | - | - | |
| STS-96 | 15 | - | - | - | - | - | -5 | 4 | - | - | - | - | - | - | - | - | - | - | |
| STS-97 | 5 | - | - | - | - | - | -5 | 4 | - | - | - | - | - | - | - | - | - | - | |
| STS-98 | 9 | - | - | - | - | - | -5 | 4 | - | - | - | - | - | - | - | - | - | - | |
| STS-99 | 13 | - | - | - | - | - | -5 | 4 | - | - | - | - | - | - | - | - | - | - | |
| STS-100 | 15 | - | - | - | - | - | -5 | 4 | - | - | - | - | - | - | - | - | - | - | |

(1) See attached figure for locations of sheared fasteners

(2) Number of fasteners at each web not available

(3) Unknown quantity of fasteners reported sheared

(4) First flight of cap design

(5) These fasteners sheared at location "A" - (First occurrence at that location)

(6) First flight with high performance motor

(7) SRBs not recovered

(8) First flight of large main chutes on RH SRB
(9) Both SRB with large main chutes

USDI Doosier Production Company, Inc.

TABLE 2

LANGLEY DRAWING NUMBERS AND TITLES

| | |
|-----------|--|
| LB 158045 | BUSHING, TEST CONFIGURATION |
| LE 158047 | WEB/CAP, LONG END, FLIGHT |
| 048 | WEB/CAP, SHORT END, FLIGHT |
| 049 | BUSHING AND INTERCOSTAL, FLIGHT |
| 050 | ASSEMBLY, FLIGHT |
| LE 418086 | TRANSITION TUNNEL ASSEMBLY |
| 087 | CHANNEL ASSEMBLY |
| 088 | LEFT AND RIGHT TERMINAL COVER ANGLE ASSEMBLIES |
| 089 | LEFT AND RIGHT COVER ANGLE ASSEMBLIES |
| 090 | LEFT AND RIGHT TRANSITION ANGLE ASSEMBLIES |
| 091 | COVER PLATES |
| 092 | JOINT MOUNTING ASSEMBLIES |
| 093 | JOINT ASSEMBLY |
| 094 | JOINT DETAILS |
| 095 | TRANSITION CHANNEL ASSEMBLIES |
| 096 | SHIM DETAILS |
| 097 | AIR DAM ASSEMBLIES |
| 118 | TUNNEL CLOSURE ASSEMBLY |
| 119 | LEFT AND RIGHT CLOSURE ANGLE ASSEMBLIES |
| 120 | WEB CAP COVER |
| 121 | CLOSURE CHANNEL ASSEMBLIES |

TABLE 3

EFFECTS OF EXISTING MATERIAL SPECIFICATIONS
ON MINIMUM SECTION AREAS

| Design | Sub-area | Minimum Dimensions in. | Minimum Area in. ² | 0.06 Max. Inclusion % Area | Thickness Tolerance % Area | Total Variation % Area |
|--------------------------------------|-------------------|---------------------------|----------------------------------|-------------------------------|-------------------------------|---------------------------|
| Double Beam With No Shear Web | A1 | 0.25x0.166 | 0.0415 | - 6.8 | - 4.0 + 3.2 | -10.8 + 3.2 |
| | A2 | 0.25x0.166 | 0.0415 | - 6.8 | - 4.0 + 3.2 | -10.8 + 3.2 |
| 2-Bar Bushed With Shear Web | A1 | 0.25x0.21 | 0.0525 | - 5.4 | - 4.0 + 6.4 | - 9.4 + 6.4 |
| | A3 | 0.78x0.10 | 0.0780 | - 3.6 | 0.0 0.0 | - 3.6 0.0 |
| | A2 | 0.25x0.21 | 0.0525 | - 5.4 | - 4.0 + 6.4 | - 9.8 + 6.4 |
| | Total Area 0.1830 | | | - 1.5 | - 2.9 + 4.7 | - 4.4 + 4.7 |

(1) Actual Total Area Is 0.185 in.²
Corner Radii Not Included in Table

TABLE 4

CONSUMABLE ELECTRODE VACUUM REMELT OR ELECTROSLAG REMELT STEELS
TO AMS 2300F CLEANLINESS

| Design | Sub-area | Minimum Dimensions in. | Minimum Area in. ² | 0.016 Max. Inclusion % Area | Thickness Tolerance % Area | Total Variation % Area |
|--------------------------------------|----------|------------------------------|-------------------------------------|-----------------------------------|----------------------------------|------------------------------|
| Double Beam With No Shear Web | A1 | 0.25x0.166 | 0.0415 | - 0.5 | - 4.0 + 3.2 | - 4.5 + 3.2 |
| | A2 | 0.25x0.166 | 0.0415 | - 0.5 | - 4.0 + 3.2 | - 4.5 + 3.2 |
| 2-Bar Bushed With Shear Web | A1 | 0.25x0.21 | 0.0525 | -0.38 | - 4.0 + 6.4 | - 4.4 + 6.4 |
| | A3 | 0.78x0.10 | 0.0780 | -0.26 | 0.0 0.0 | - 0.3 0.0 |
| | A2 | 0.25x0.21 | 0.0525 | -0.38 | - 4.0 + 6.4 | - 4.4 + 6.4 |
| | | Total Area 0.1830 (1) | | | - 0.11 - 2.9 + 4.7 | - 3.0 + 4.7 |

(1) Actual Total Area Is 0.185 in.²
Corner Radii Not Included In Table

TABLE 5

EFFECT OF UNIFORM DIMENSIONAL TOLERANCES
ON MINIMUM SECTION AREAS

Double Beam With No Shear Web

| Area Nominal in. ² | h Nominal in. | h Tolerance | t Nominal in. | t Tolerance | Max/Min Area in. ² | % Nominal Area in. ² |
|-------------------------------------|---------------------|-----------------|---------------------|-----------------|-------------------------------------|---------------------------------------|
| A1=0.0415 | 0.0166 | 0.005 -0.005 | 0.25 | 0.005 -0.005 | 0.0436 0.0394 | 105.07 95.05 |
| A2=0.0415 | 0.166 | 0.005 -0.005 | 0.25 | 0.005 -0.005 | 0.0436 0.0394 | 105.07 95.05 |
| AT=0.083 | | | | | 0.0872 0.0789 | 105.21 95.17 |

2-Bar With Shear Web

| Area Nominal in. ² | h Nominal in. | h Tolerance | t Nominal in. | t Tolerance | Max/Min Area in. ² | % Nominal Area in. ² |
|-------------------------------------|---------------------|-----------------|---------------------|-----------------|-------------------------------------|---------------------------------------|
| A1=0.0525 | 0.21 | 0.005 -0.005 | 0.25 | 0.005 -0.005 | 0.0548 0.0502 | 104.43 95.67 |
| A3=0.0780 | 0.78 | 0.005 -0.005 | 0.10 | 0.005 -0.005 | 0.0824 0.0736 | 105.67 94.39 |
| A2=0.0525 | 0.21 | 0.005 -0.005 | 0.25 | 0.005 -0.005 | 0.0548 0.0502 | 104.43 95.67 |
| AT=0.1830 | (1) | | | | 0.1921 0.1741 | 104.96 95.12 |

(1) Actual Total Area Is 0.185 in.²
Corner Radii Not Included In Table

TABLE 6

VARIATION IN AREA DUE TO MATERIAL CLEANLINESS
AND FABRICATION TOLERANCES

2-Bar Bushed Concept AME 2300 Level Cleanliness

| Area | Nominal Dimension in. | Nominal Area in. ² | 0.016 Max. Inclusion % Area | Fabrication Tolerance % Area | Total Variation % Area |
|------|-----------------------------|-------------------------------------|-----------------------------------|------------------------------------|------------------------------|
| A1 | 0.25x0.21 | 0.0525 | -0.38 | -4.33 4.43 | -4.72 4.43 |
| A3 | 0.78x0.10 | 0.0780 | -0.26 | -5.61 5.67 | -5.87 5.67 |
| A2 | 0.25x0.21 | 0.0525 | -0.38 | -4.33 4.43 | -4.72 4.43 |
| AT | | 0.1830(1) | -0.11 | -4.88 4.96 | -4.99 4.96 |

(1) Actual Total Area Is 0.185 in.²
Corner Radii Not Included In Table

LEFT SIDE VIEW OF THE SPACE SHUTTLE VEHICLE

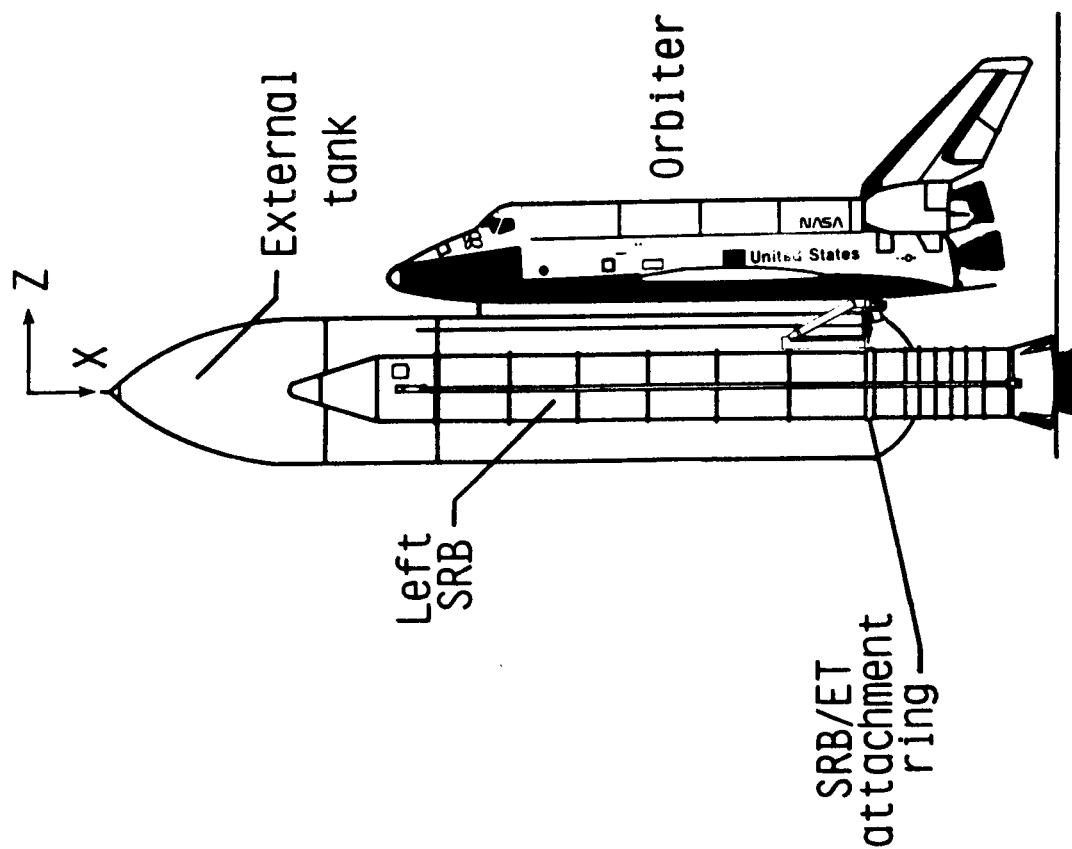


Figure 1.

RING CONFIGURATION/LOCATION ON SRB

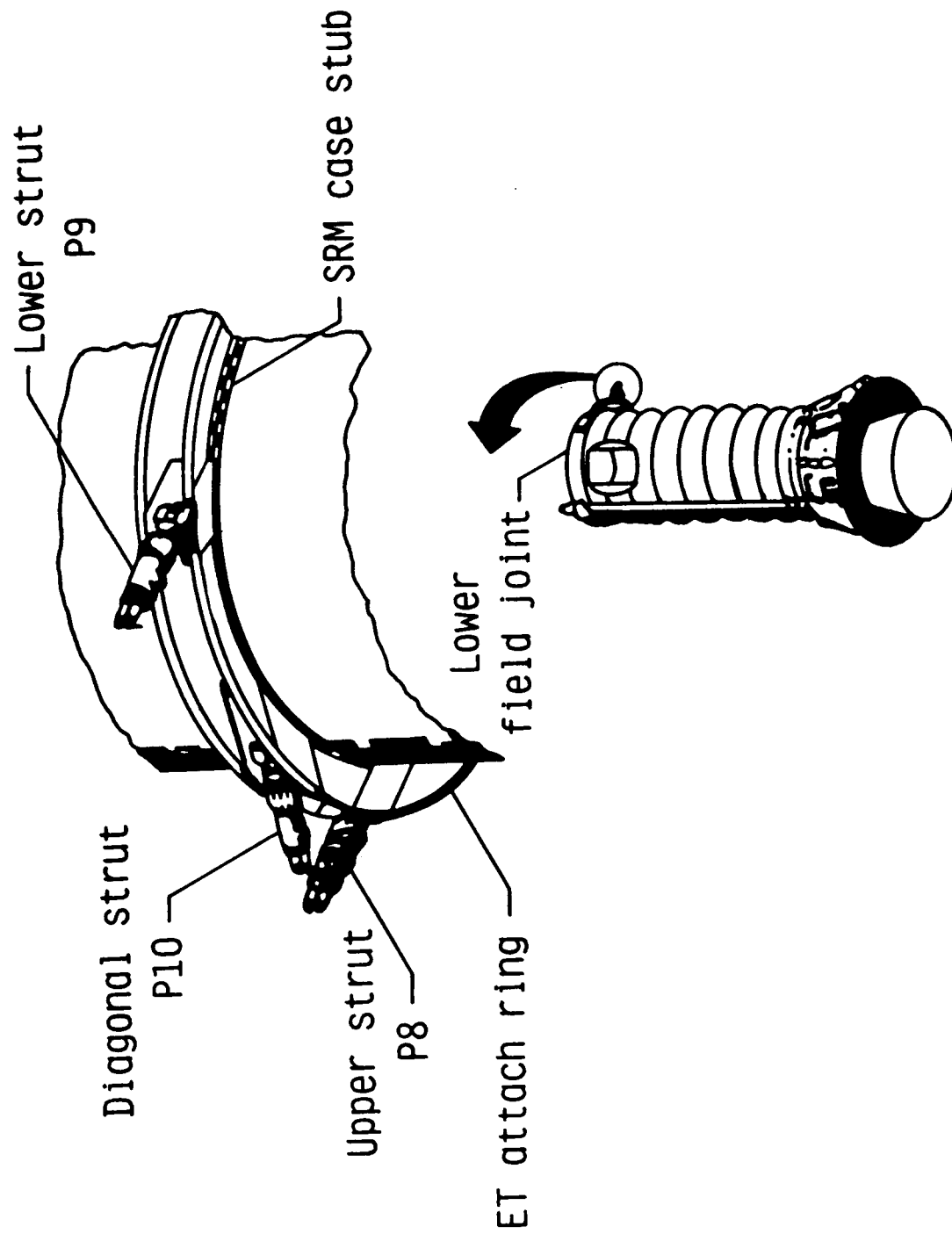


Figure 2.

ETA RING ANALYSIS AND REDESIGN

Left hand SRB/ET attachment ring existing design

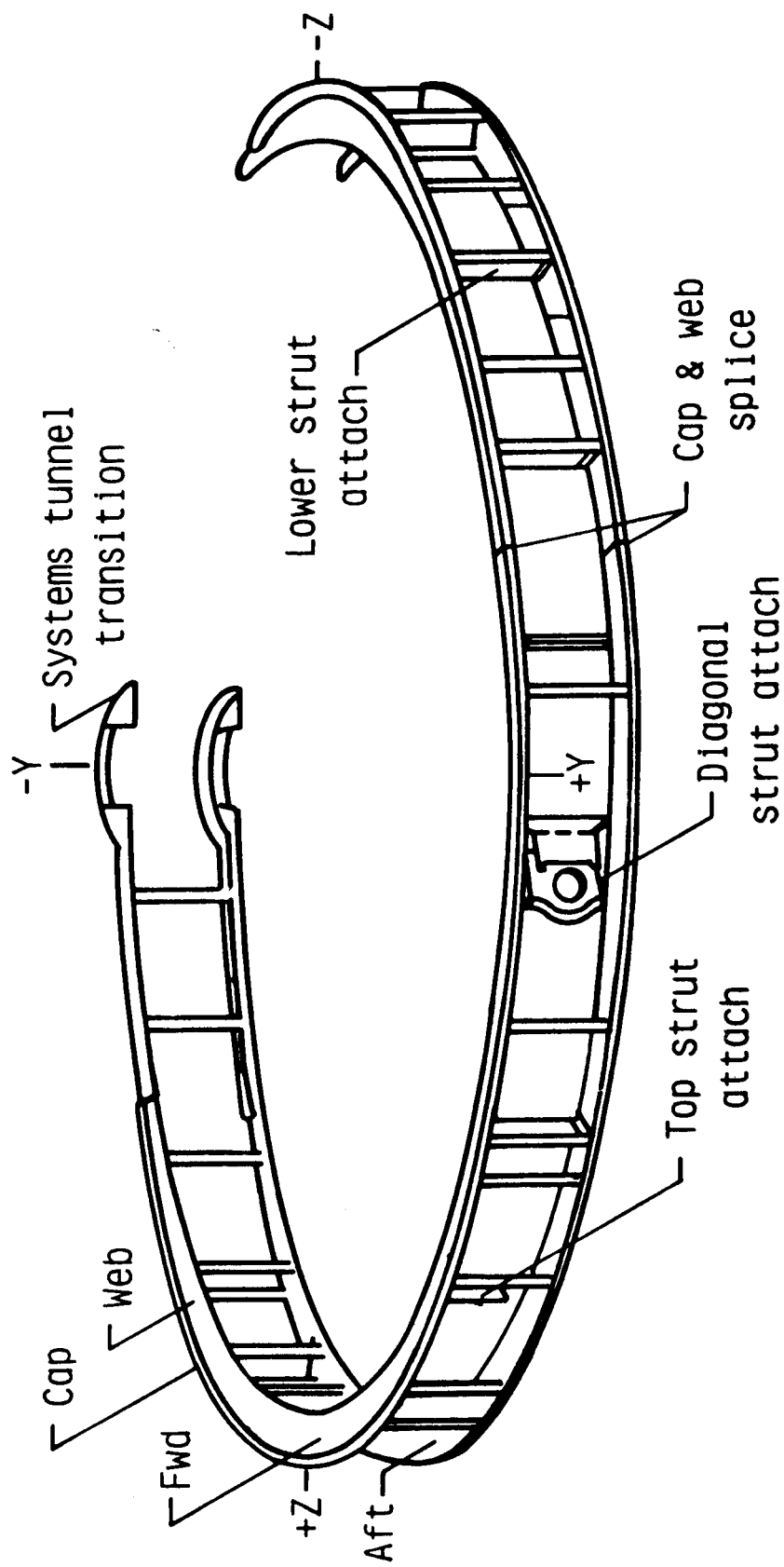


Figure 3.

ETA RING ANALYSIS AND REDESIGN

ETA ring cross section

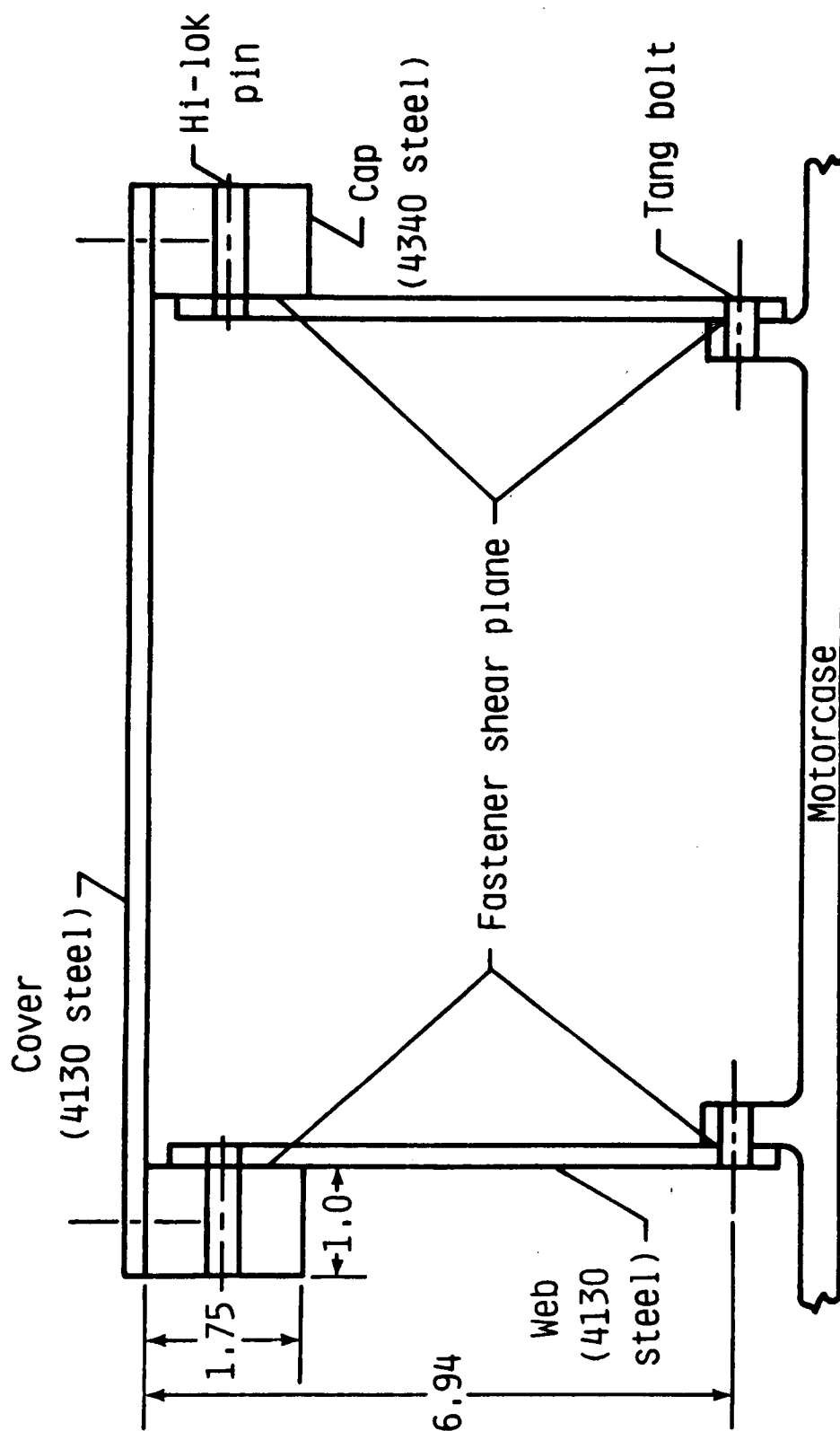


Figure 4.

ETA RING ANALYSIS AND REDESIGN

Right hand ETA ring current configuration

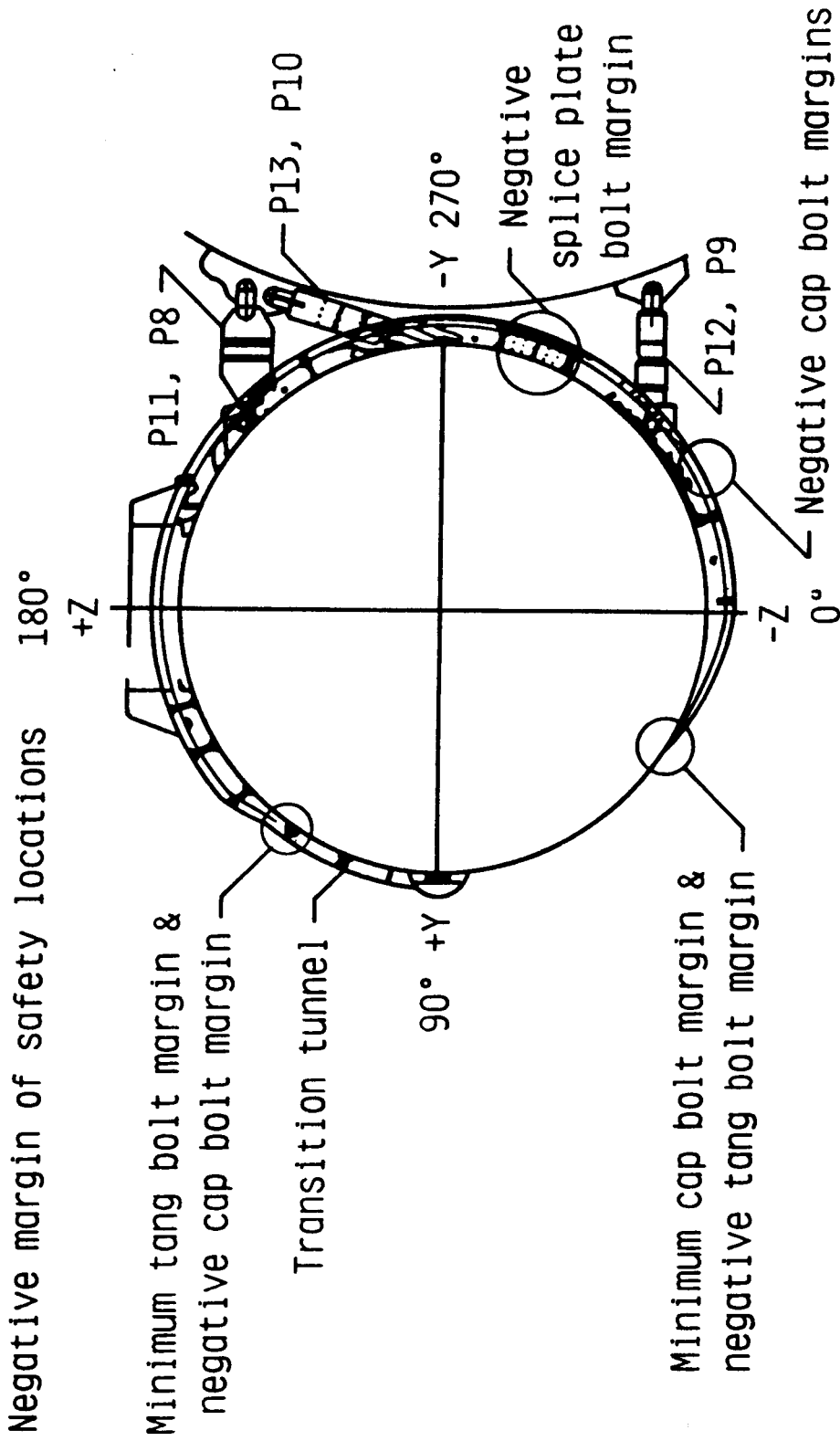
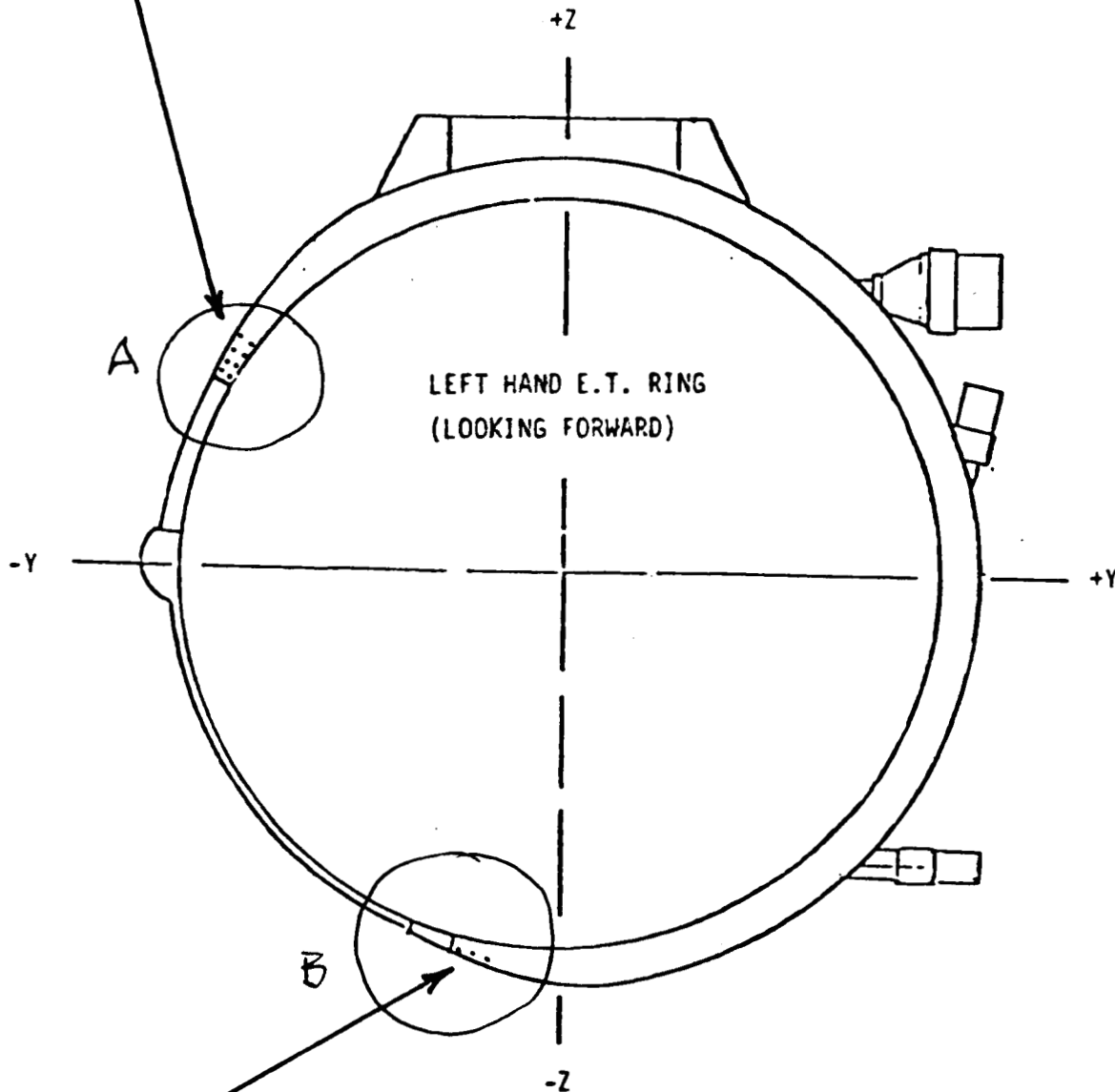


Figure 5.

LEFT HAND SRB/ET RING STRUCTURAL DAMAGE
SHUTTLE FLIGHT 61C

- RING/MOTORCASE BOLTS - ONE (1) SHEARED ON FORWARD, THREE (3) SHEARED ON AFT.
- CAP/WEB BOLTS - SIX (6) SHEARED ON FORWARD (PAINT CRACKED TO 13TH BOLT) ONE (1) SHEARED ON AFT.
(CLOSEOUT ANGLES SHEARED OFF ON BOTH SIDES)
(THIS IS FIRST FLIGHT THAT CAP/WEB BOLTS SHEARED ON THIS END OF THE RING)



- ← CAP TO WEB BOLTS - FORWARD - FIVE (5) SHEARED, PAINT CRACKED TO EIGHTH BOLT
AFT - FIVE (5) SHEARED, PAINT CRACKED TO NINTH BOLT

Figure 6.

SRB ET ATTACH RING

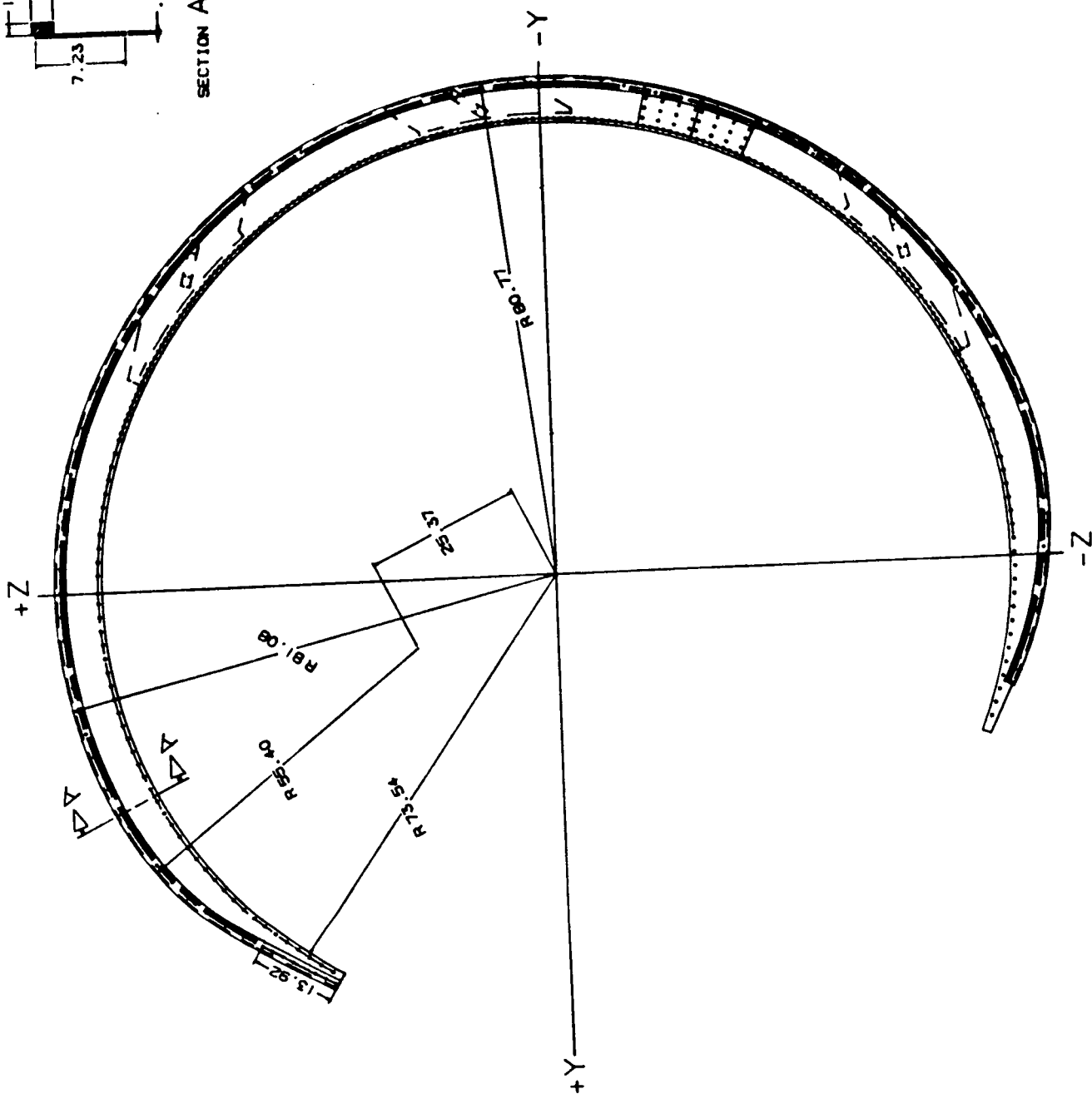
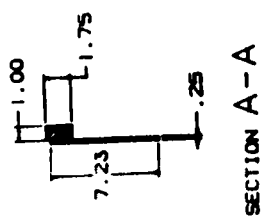


Figure 7.

LARC ET ATTACHMENT RING CONCEPT

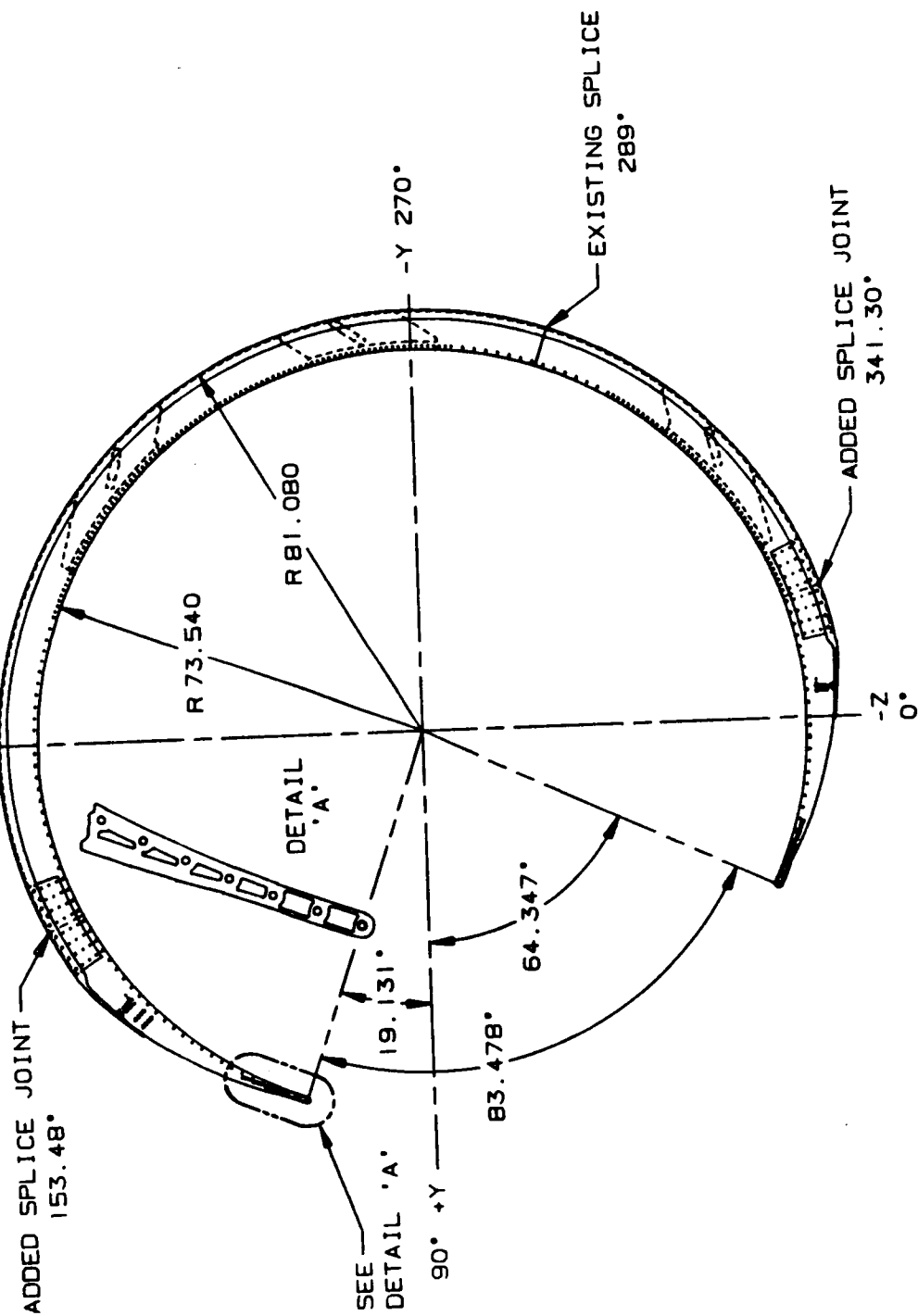


Figure 8.

TYPICAL ETA RING END

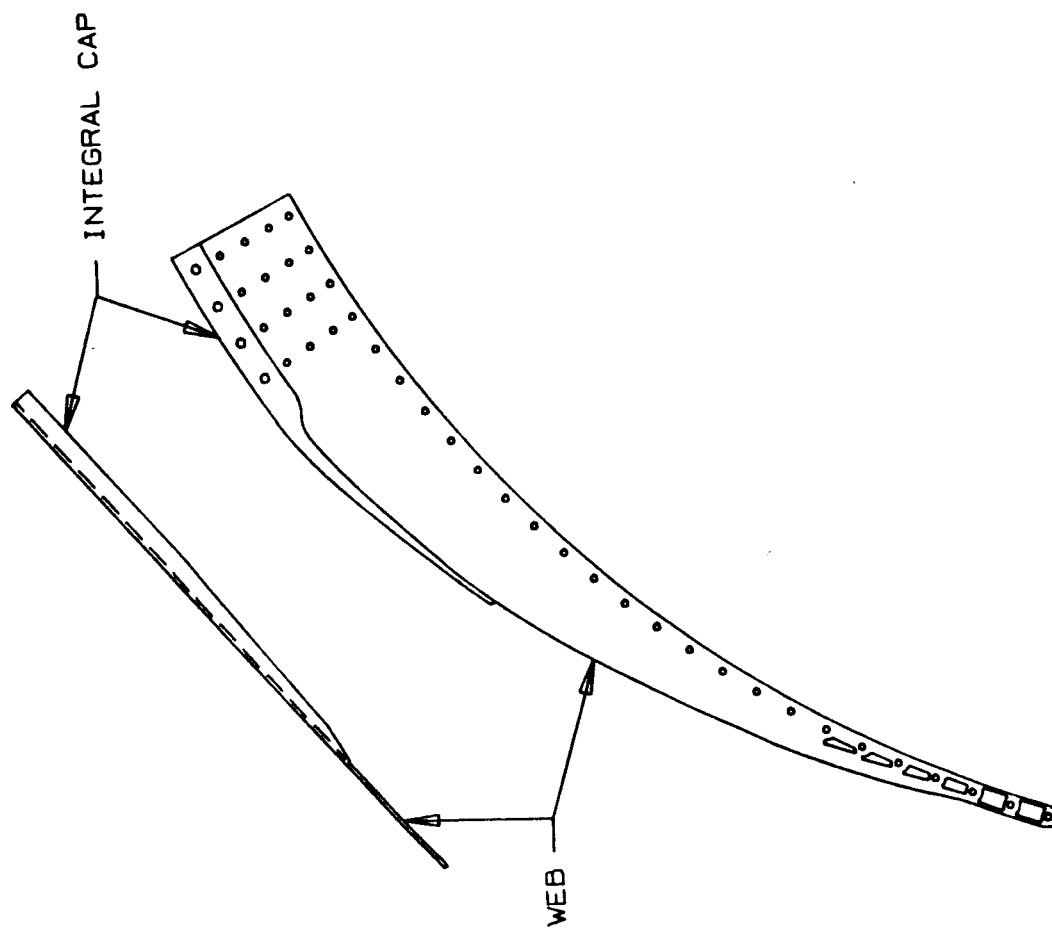


Figure 9(a).

WEB AND CAP (LONG END)

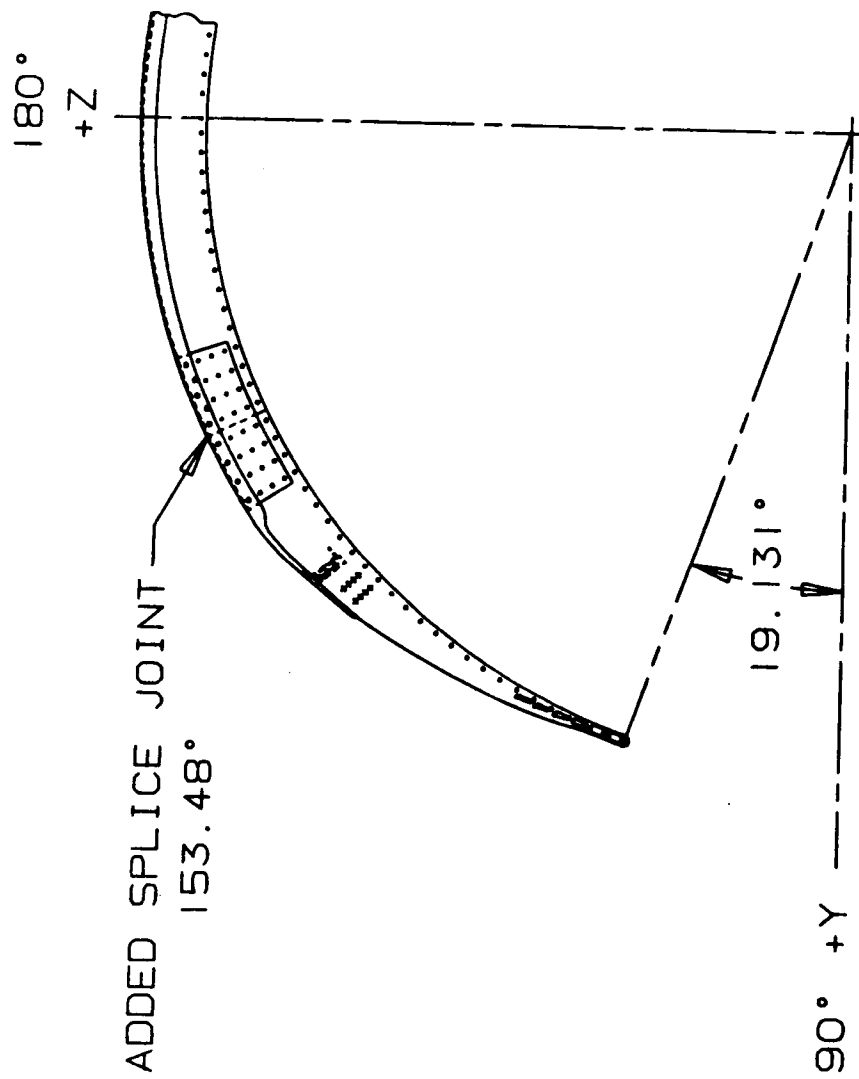


Figure 9(b).

WEB AND CAP (SHORT END)

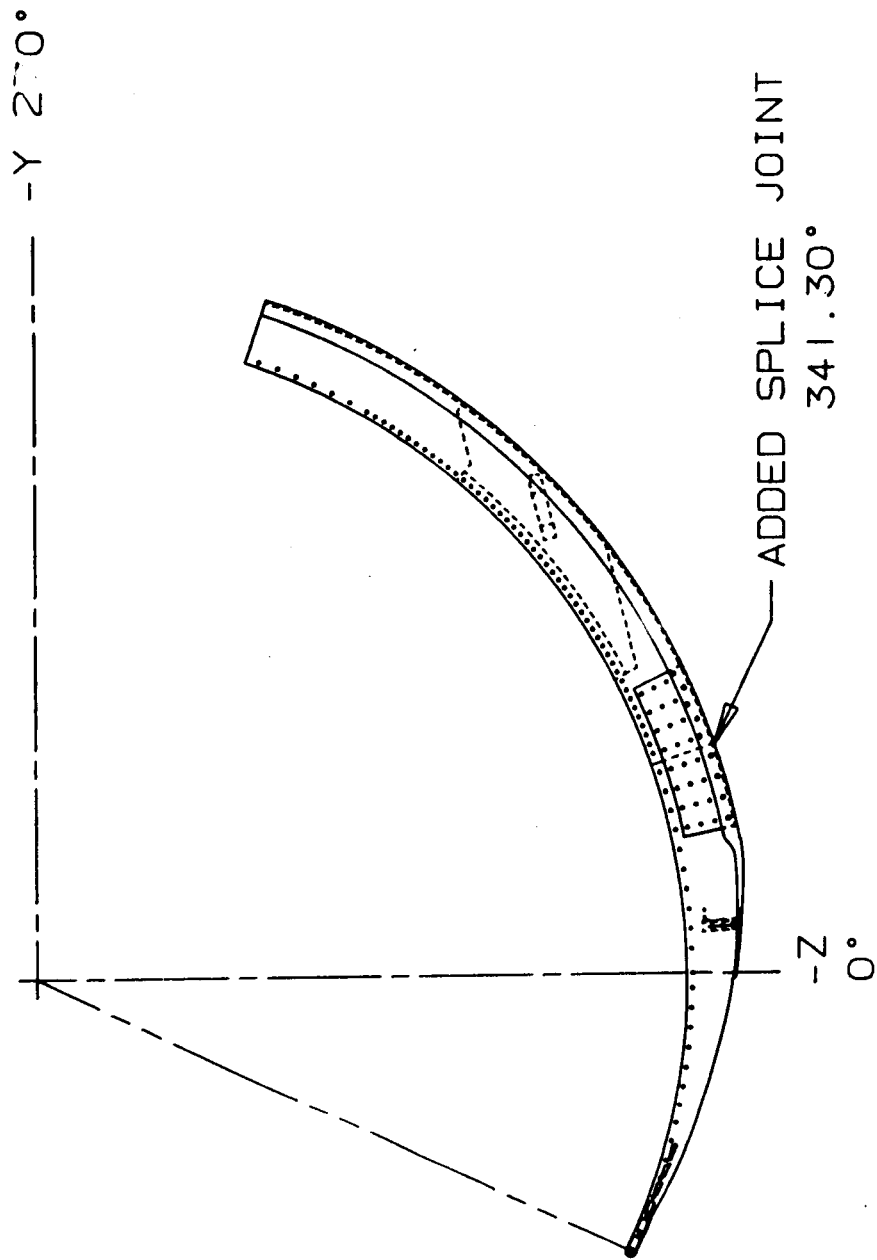


Figure 9(c).

SPLICE PLATE (LONG END)

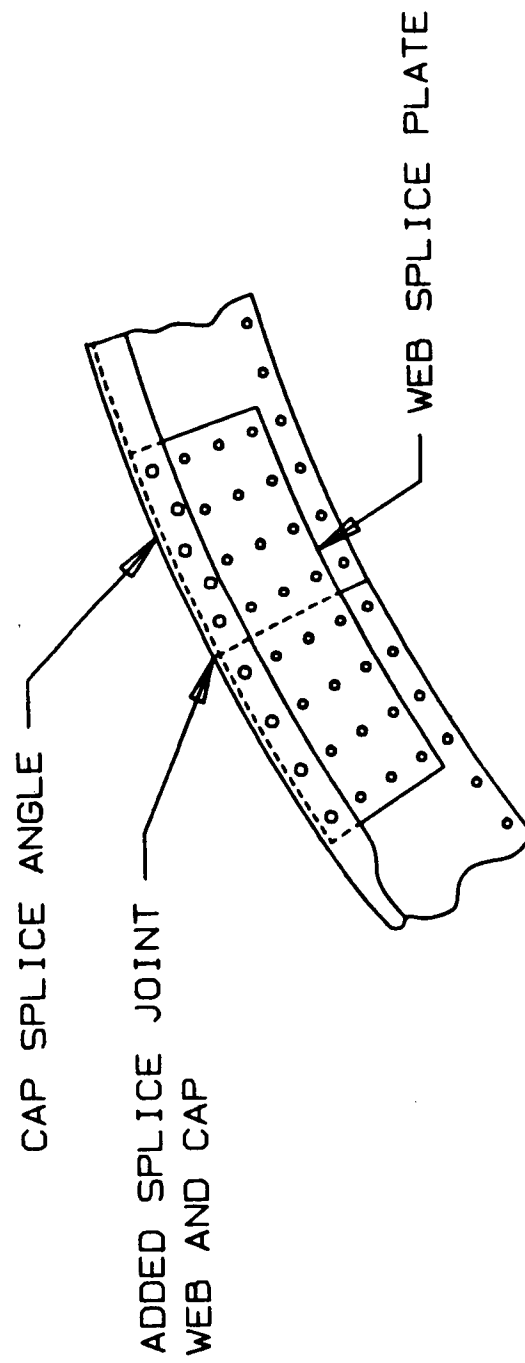


Figure 9(d).

SPLICE PLATE (SHORT END)

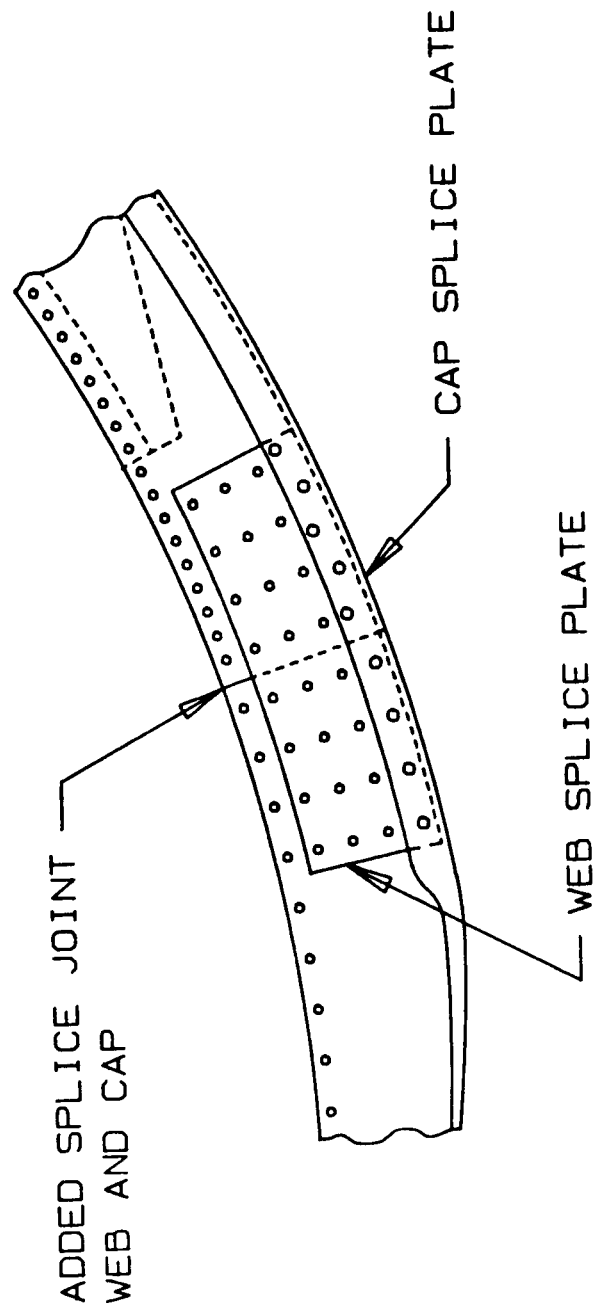
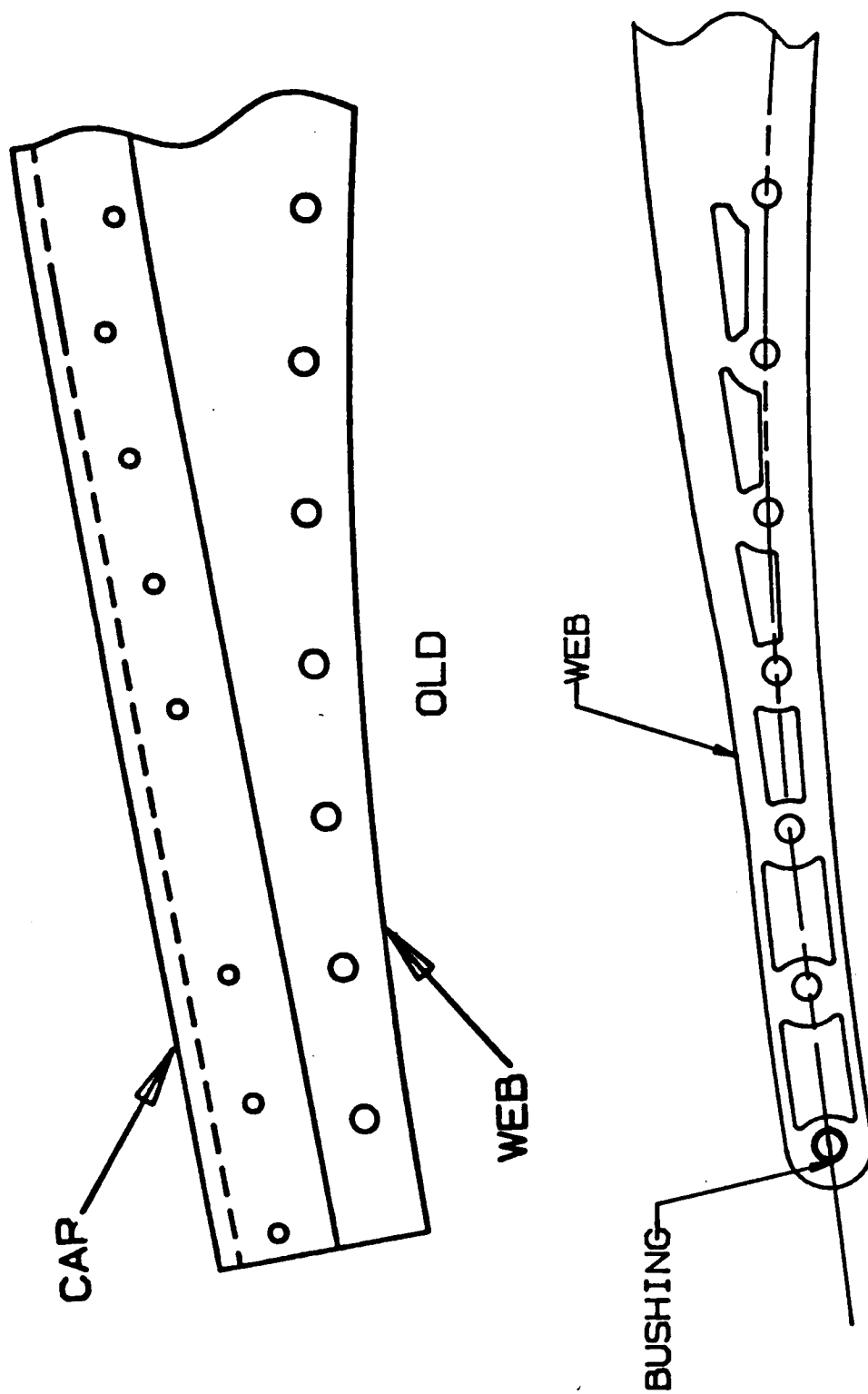


Figure 9(e).

LaRC ET ATTACHMENT RING LONG END COMPARISON



NEW
Figure 10.

LaRC ET ATTACHMENT RING SHORT END COMPARISON

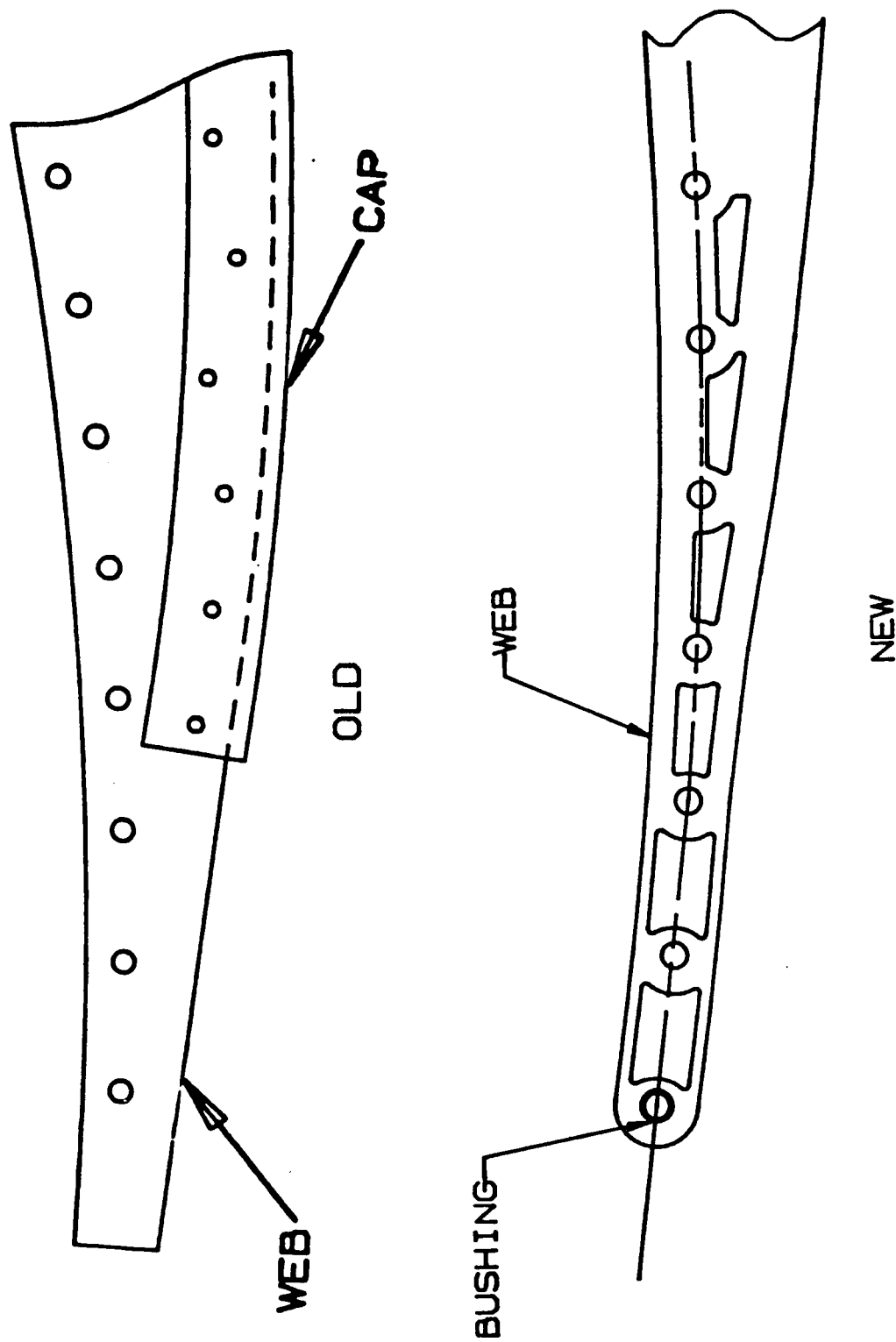


Figure 11.

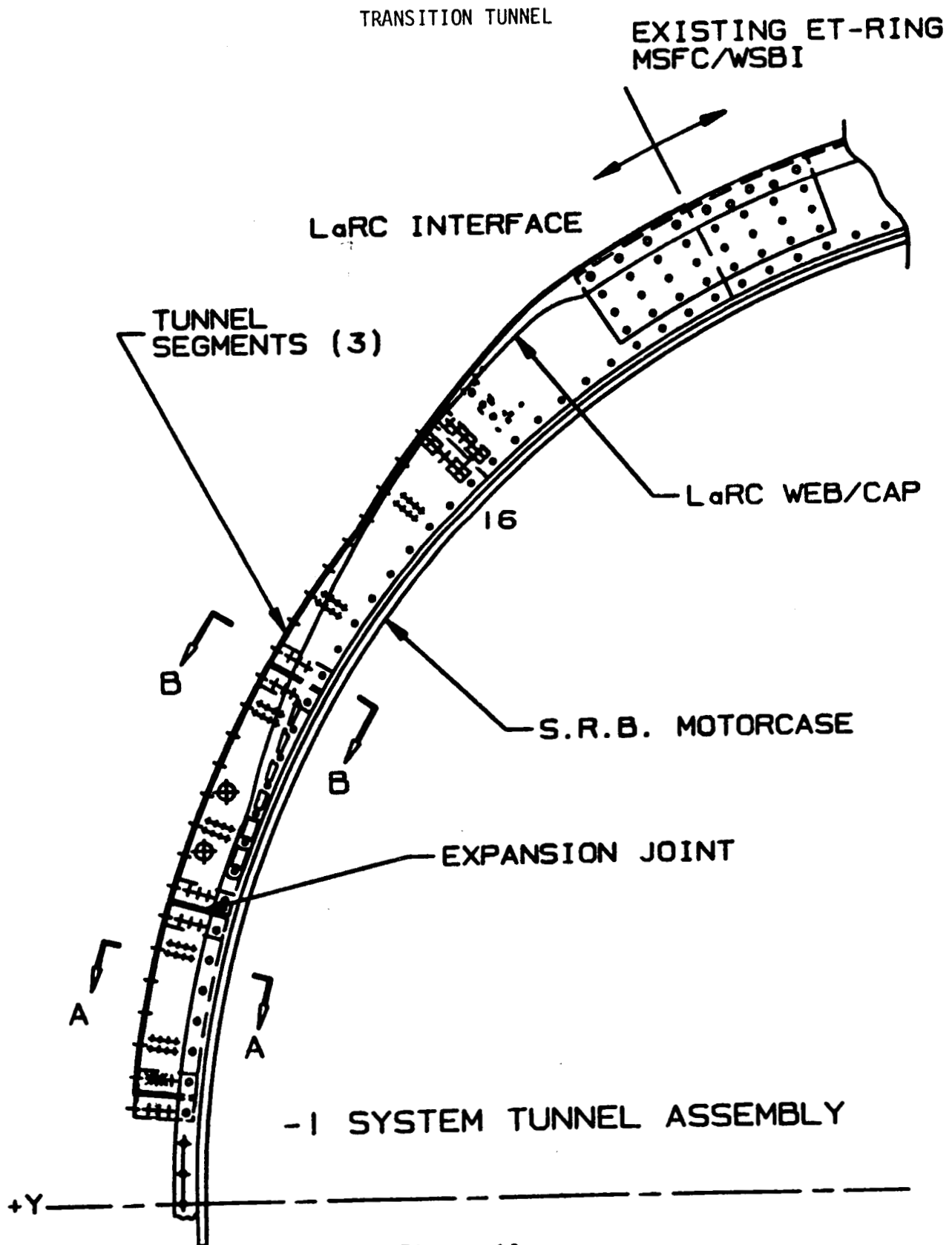
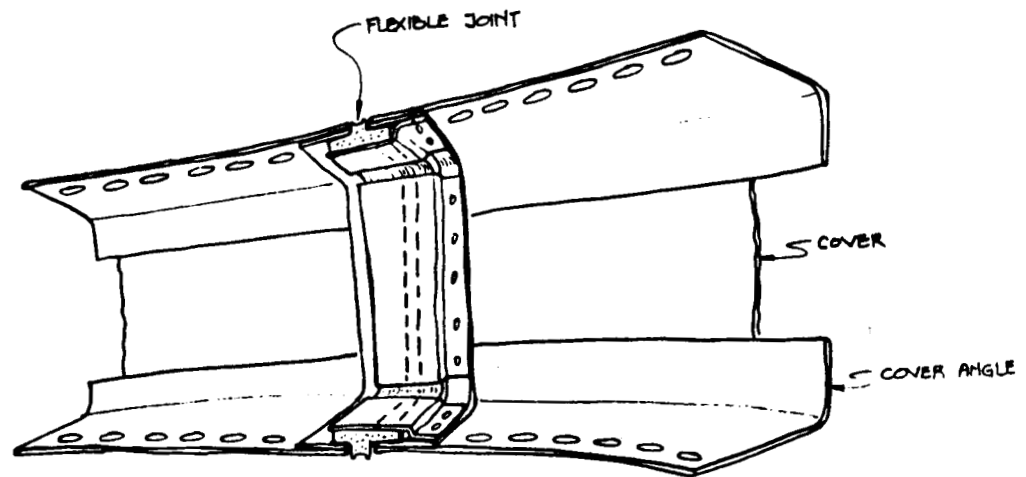
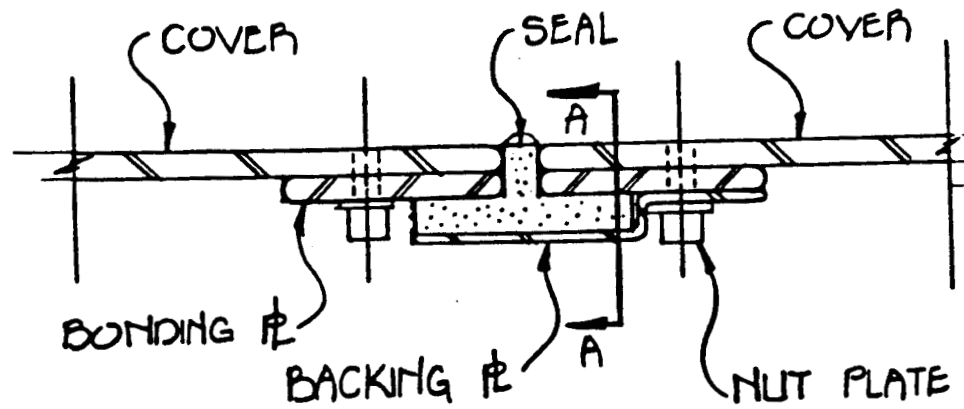


Figure 12.

TRANSITION TUNNEL EXPANSION JOINT AND SEAL

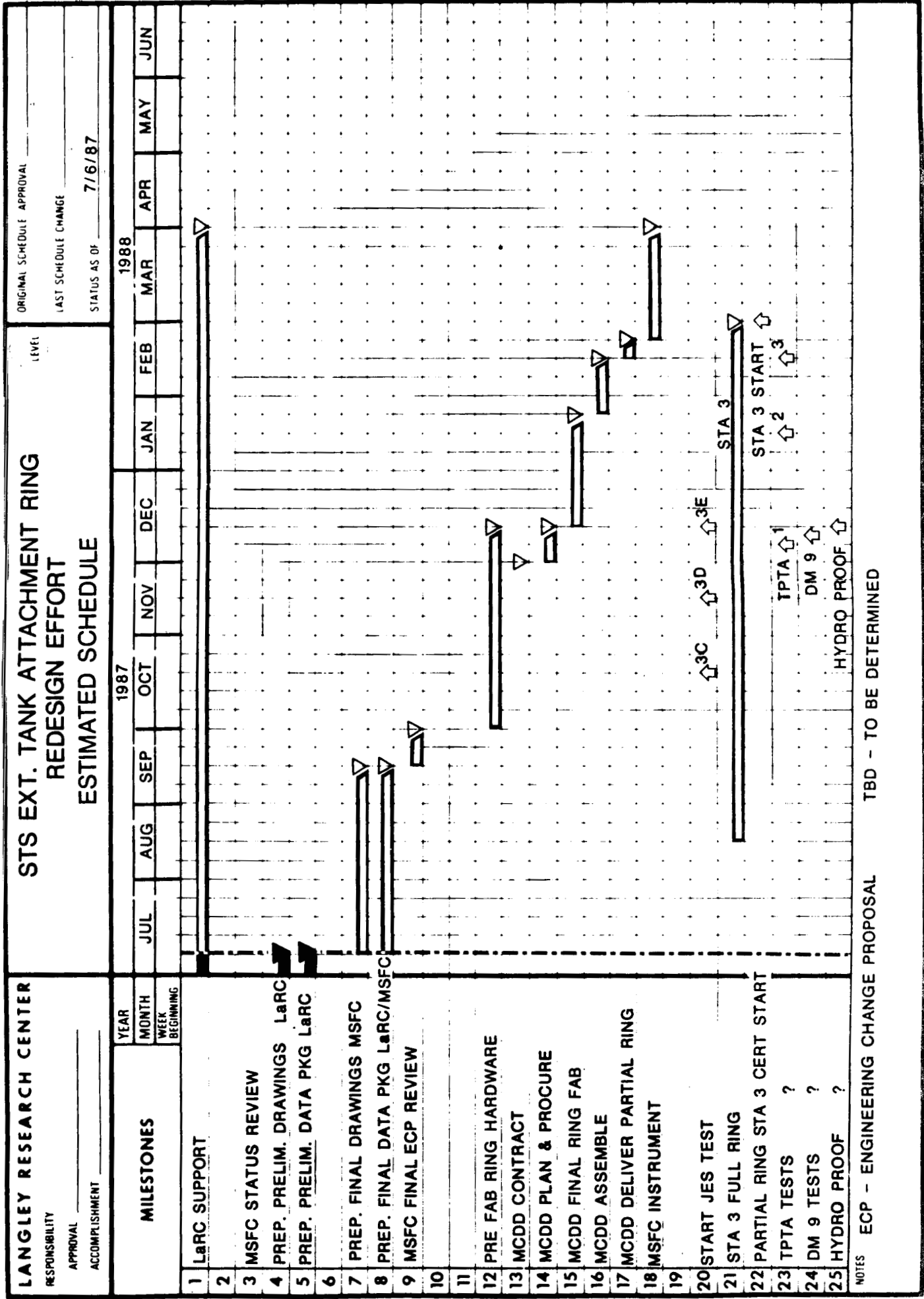


JOINT



SEAL

Figure 13.



NOTES ECP - ENGINEERING CHANGE PROPOSAL TBD - TO BE DETERMINED

Figure 14.

PARTIAL RING FINITE ELEMENT MODEL

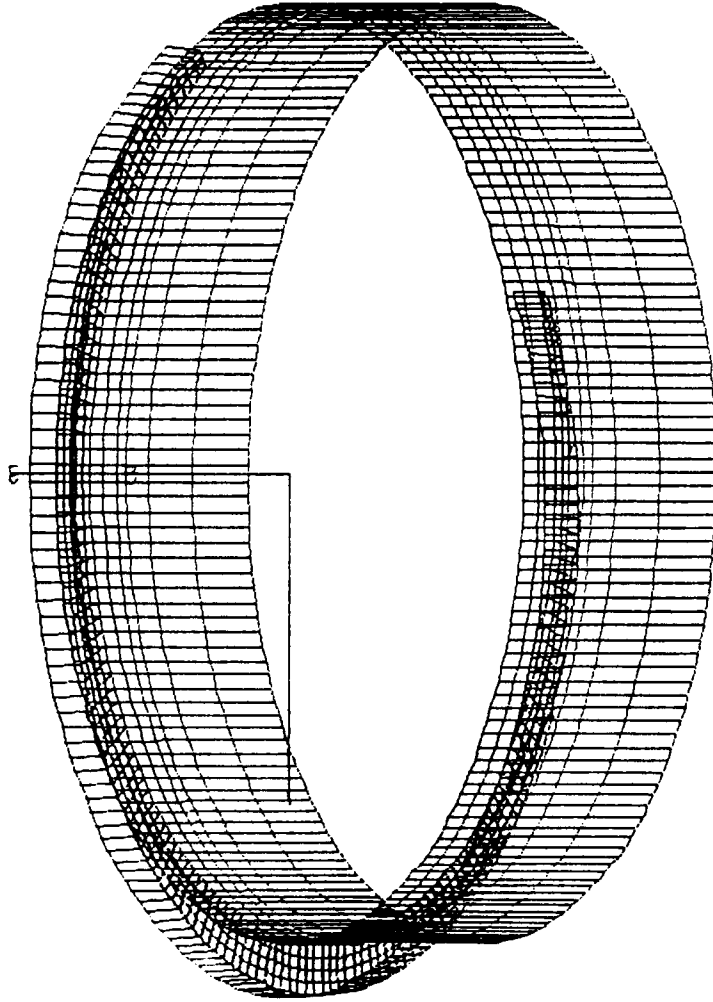


Figure 15.

PARTIAL RING MODEL - WEB PLATFORM

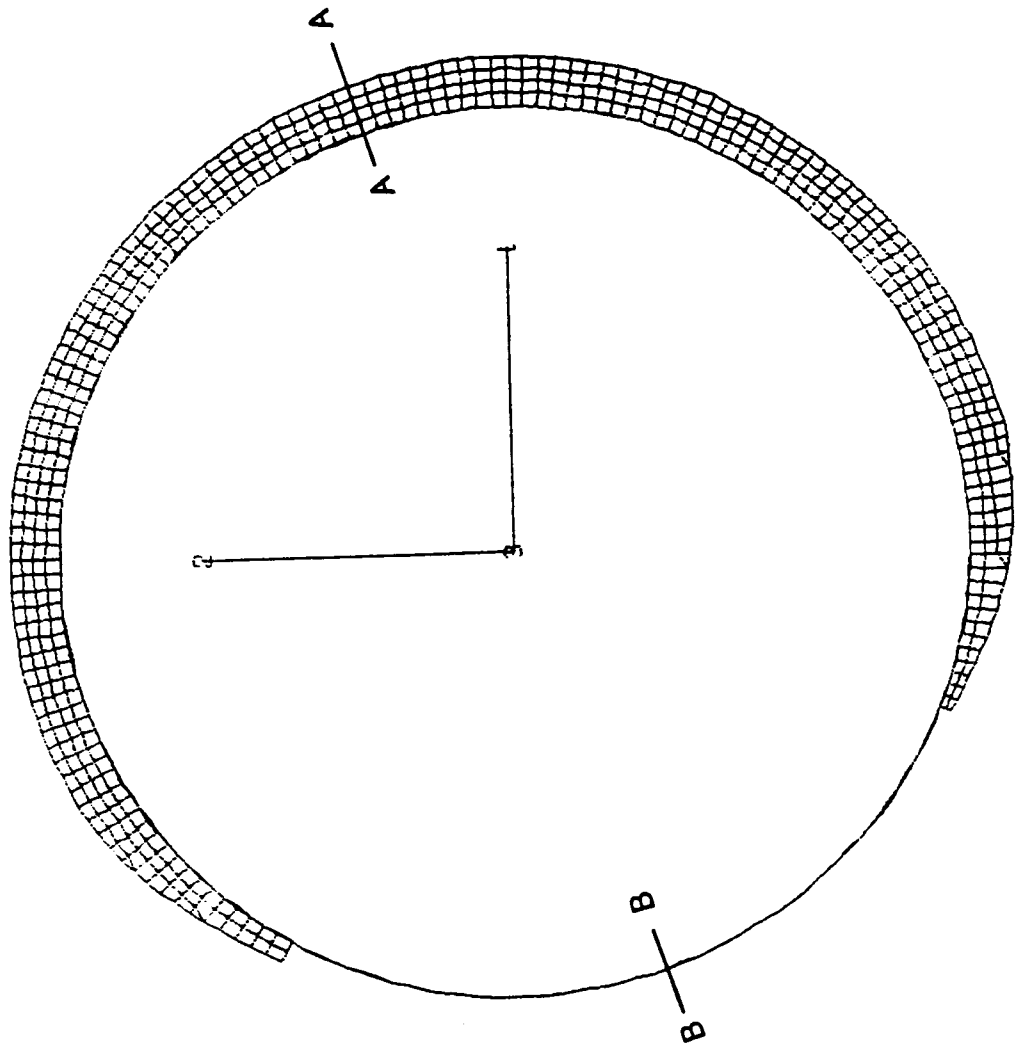


Figure 16.

APPLIED LOADS FOR EXTERNAL TANK ATTACH RING FINITE ELEMENT MODEL

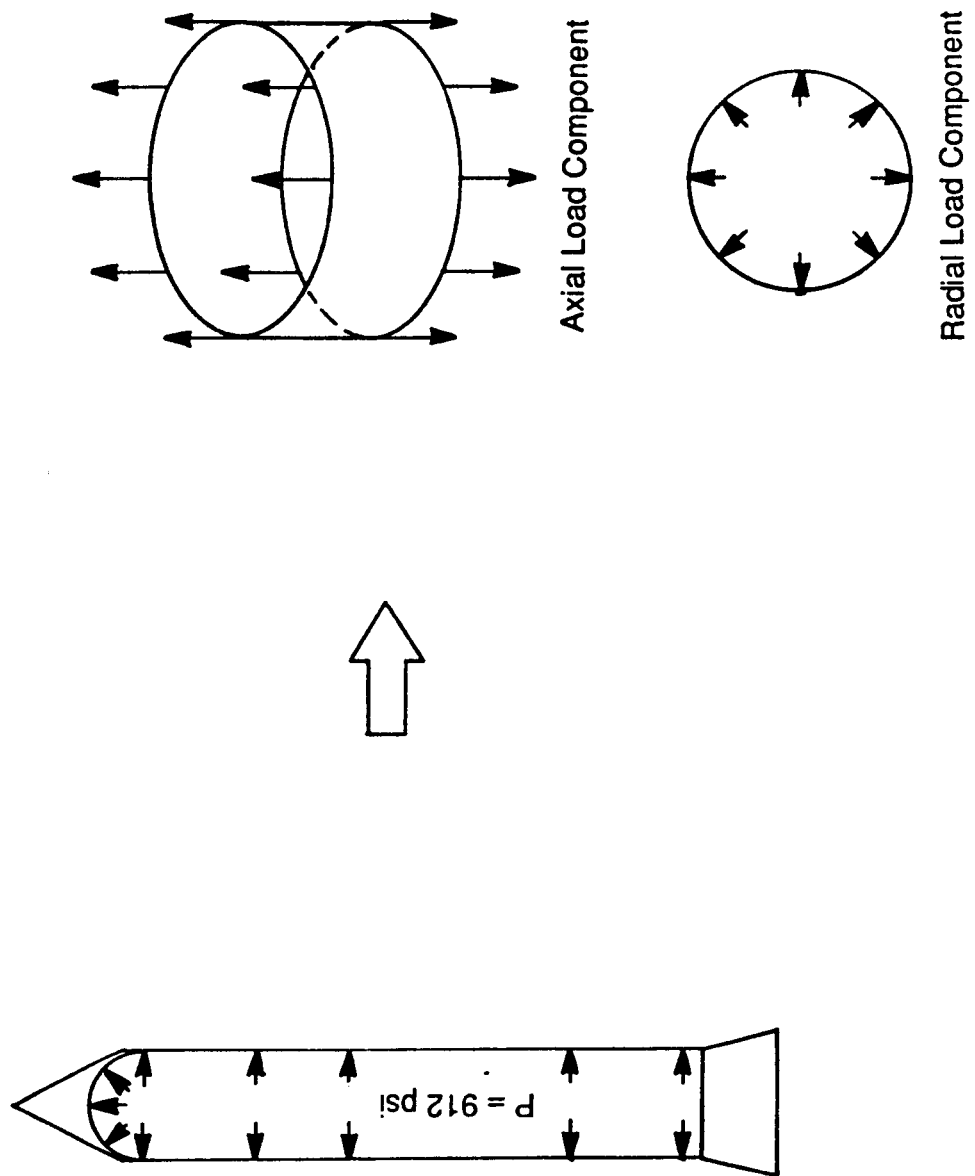
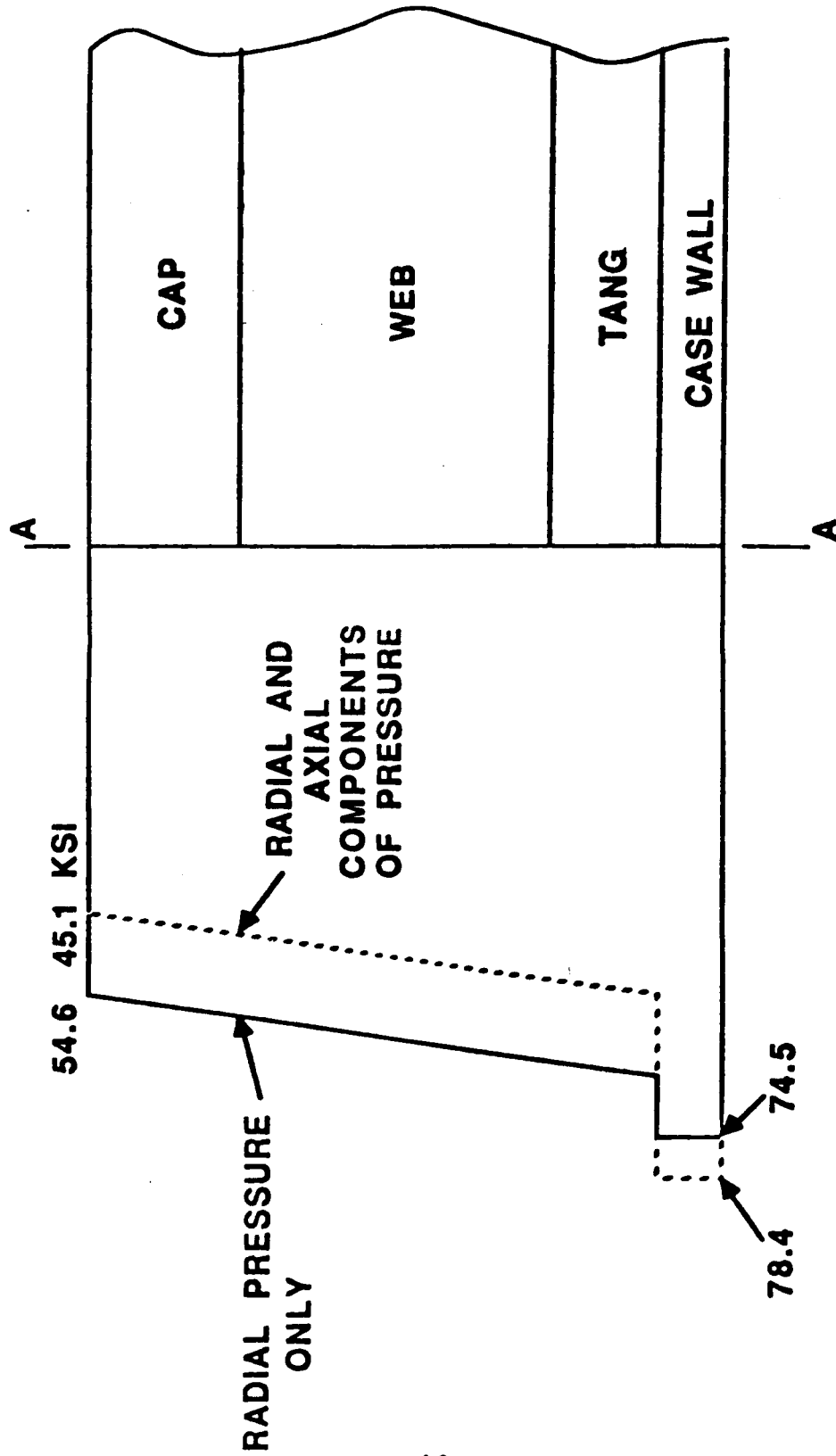


Figure 17.

CIRCUMFERENTIAL STRESSES IN PARTIAL RING

(912PSI)



NOTE: FULL RING STRESSES WITHIN 1% OF THOSE FOR PARTIAL RING

Figure 18.

CIRCUMFERENTIAL STRESSES IN SHELL OF PARTIAL RING MODEL (912 psi Internal Pressure)

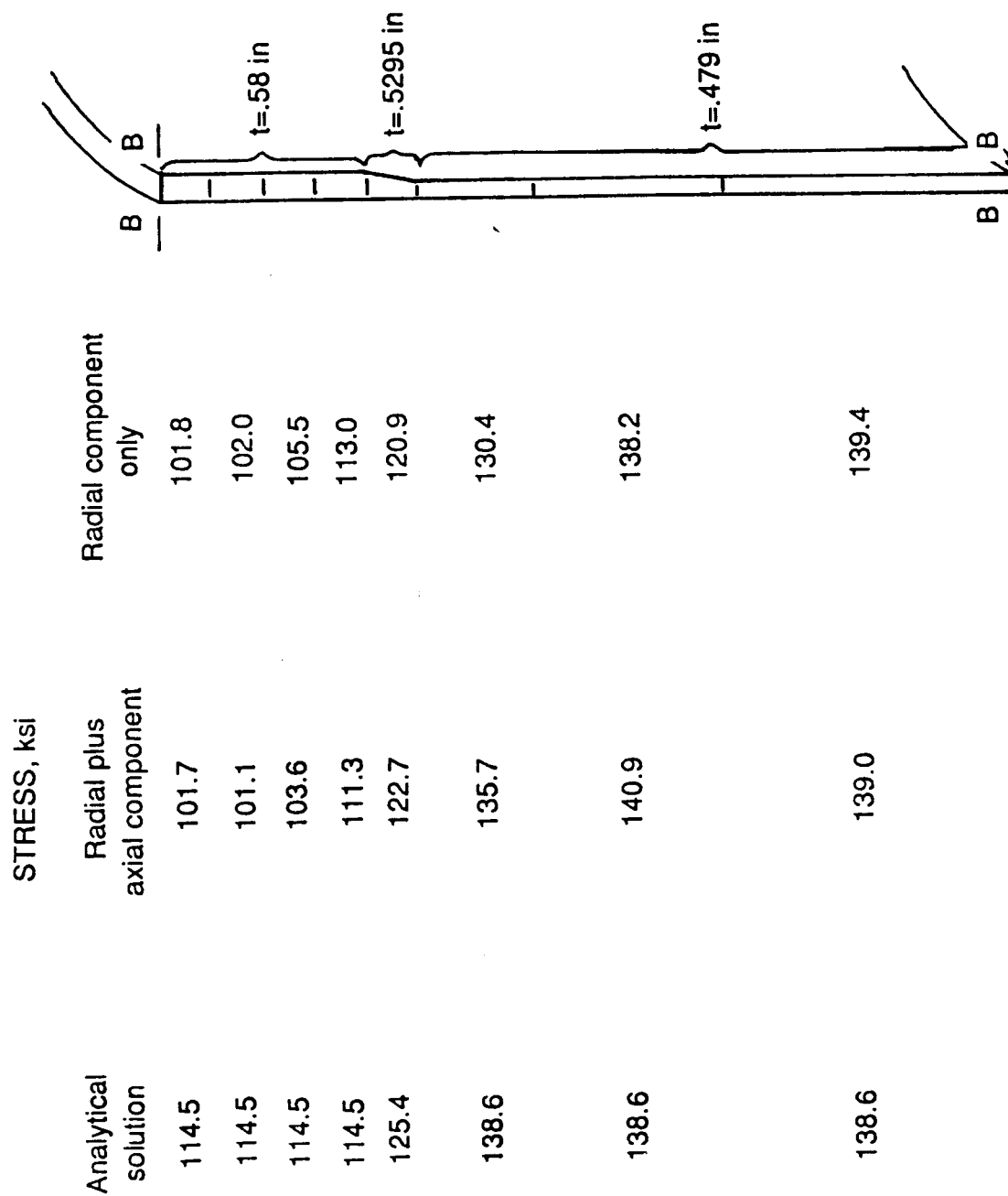


Figure 19.

EFFECT OF FIELD JOINT ON PARTIAL RING STRESSES (912 psi Internal Pressure)

| STRESS, ksi | | $\Delta\%$ | A |
|----------------|------------------|------------|-----------|
| No field joint | With field joint | | |
| 45.1 | 45.8 | +1.6 | CAP |
| 49.3 | 49.7 | +0.8 | |
| 50.8 | 51.2 | +0.8 | WEB |
| 52.4 | 52.8 | +0.8 | |
| 53.5 | 54.4 | +1.7 | |
| 57.2 | 57.5 | +0.5 | TANG |
| 78.4 | 78.2 | -0.3 | CASE WALL |
| WEB MAX: 95.9 | 96.7 | +0.8 | A |

Figure 20.

RADIAL DISPLACEMENTS ON PARTIAL RING MODEL DUE TO INTERNAL PRESSURE (912 psi)

Radial Deflection (in) = Linear/Nonlinear

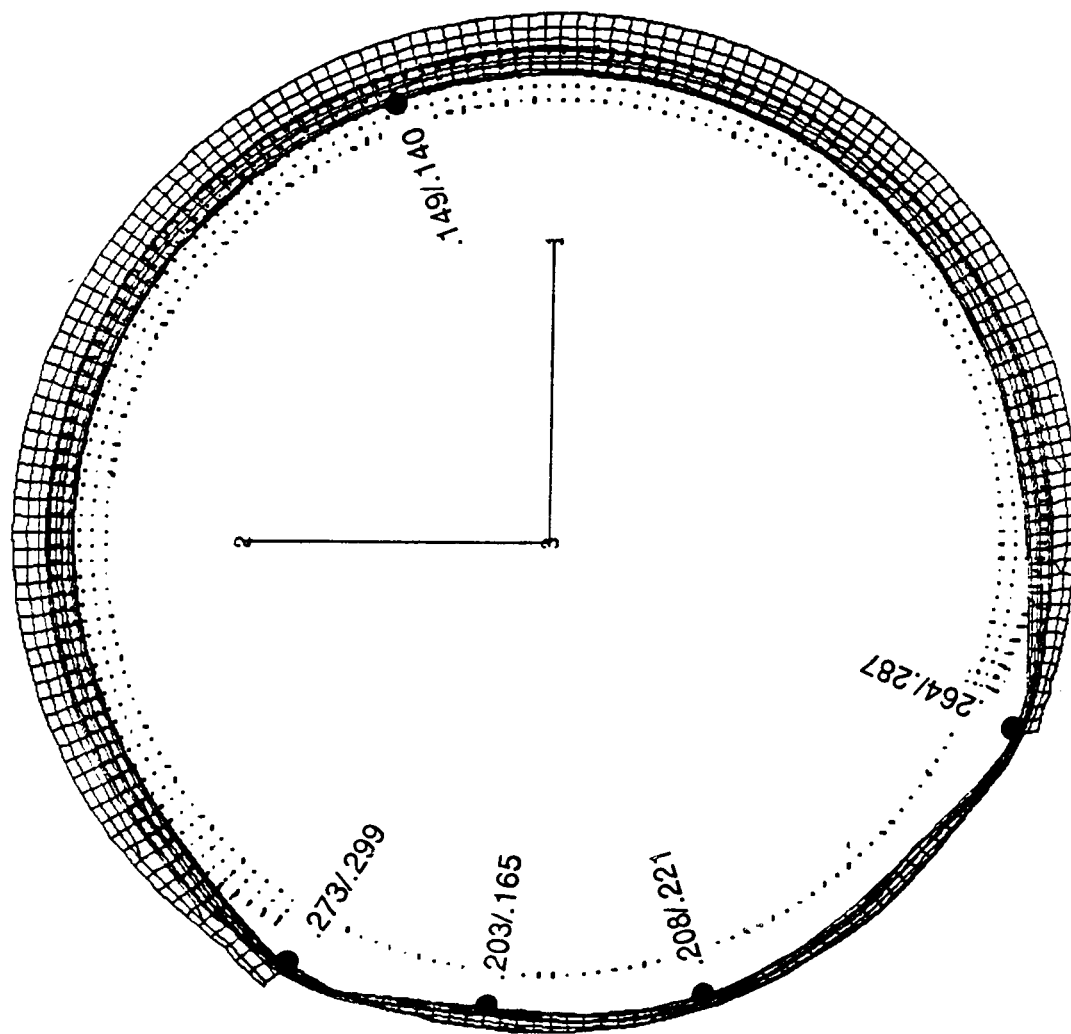


Figure 21.

PARTIAL RING - SUMMARY OF STRESS RESULTS*

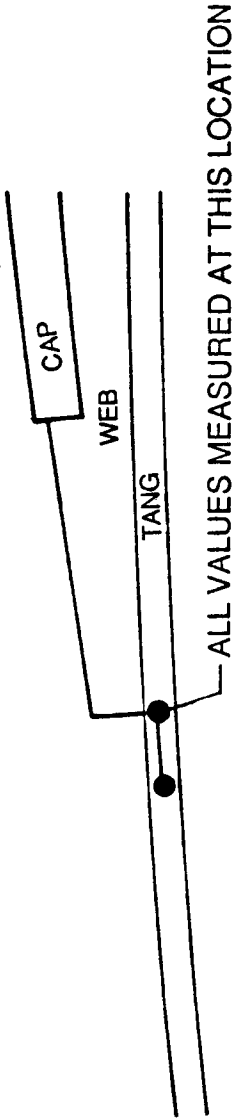
| Component† | STRESS, ksi | | Δ % |
|------------|-------------|-----------|------|
| | Linear | Nonlinear | |
| CAP | 45.1 | 48.0 | +6.4 |
| | 57.2 | 60.9 | +6.5 |
| TANG | 130.0 | 119.9 | -7.8 |
| | | | |
| CASE WALL | | | +4.4 |
| | | | -3.3 |
| WEB | | | |
| | 50.8 | 54.2 | +6.6 |

*912 psi internal pressure, radial and axial components

†Max/Min given for each component

Figure 22.

LOCAL TANG BENDING AT END OF WEB (912 PSI)



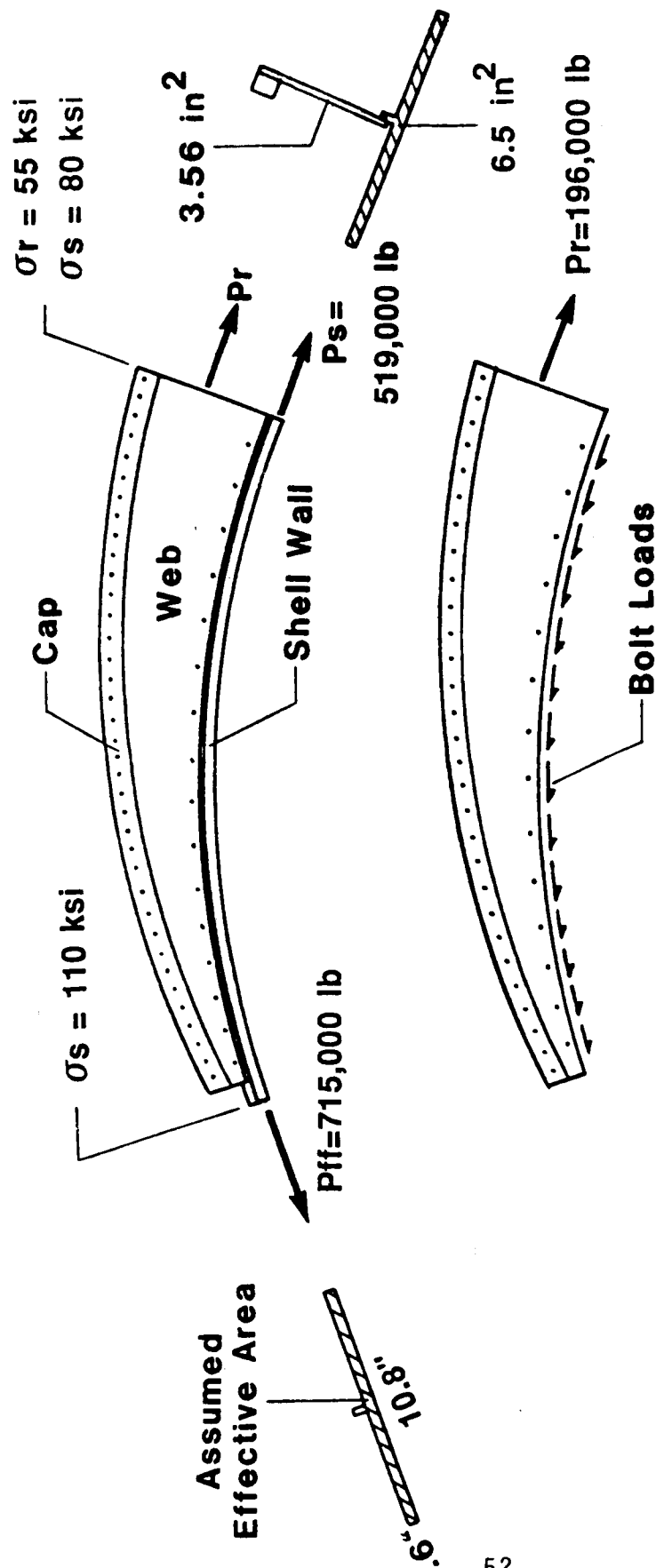
| | LINEAR | NONLINEAR | Δ , % |
|------------------------|--------|-----------|--------------|
| PZ, lbf | 86443. | 79734. | -7.76 |
| MY, in-lbf | 11818. | 9348. | -20.90 |
| σ_{MAX}^* , ksi | 195.5 | 171.8 | -12.12 |

$$\sigma^* = \frac{PZ}{A} + \frac{MY \times Z}{I} : A = .6616 \text{ in}^2 \quad Z = .827 \text{ in} \quad I = .1508 \text{ in}^4$$

Figure 23.

SIMPLIFIED RING TANG BOLT LOAD ANALYSIS

($p=912$ psi)



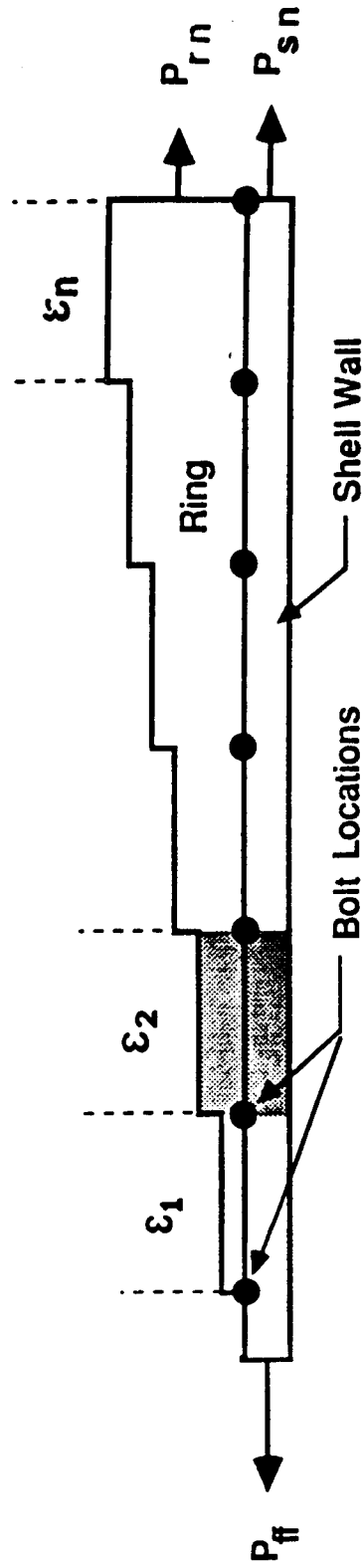
Sum of bolt loads = 196,000
 Assume each bolt carries 10,000
 $N(10,000) = 196,000$
 $N = 20$ bolts

Figure 24.

SIMPLIFIED RING ANALYSIS

ASSUMPTIONS:

- NO BOLT FLEXIBILITY
- NO RING "SHEAR LAG" FLEXIBILITY
- IDEALIZED RING SEGMENT (FLAT)



53

$$\begin{aligned}
 P_{ff} &= P_{ring} + P_{shell} \\
 P_{ff} &= E\epsilon_n(A_{rn} + A_s) \\
 \epsilon_n &= \frac{P_{ff}}{E(A_{rn} + A_s)} \\
 \therefore P_{rn} &= E\epsilon_n A_n = \frac{P_{ff} A_{rn}}{A_{rn} + A_s}
 \end{aligned}$$

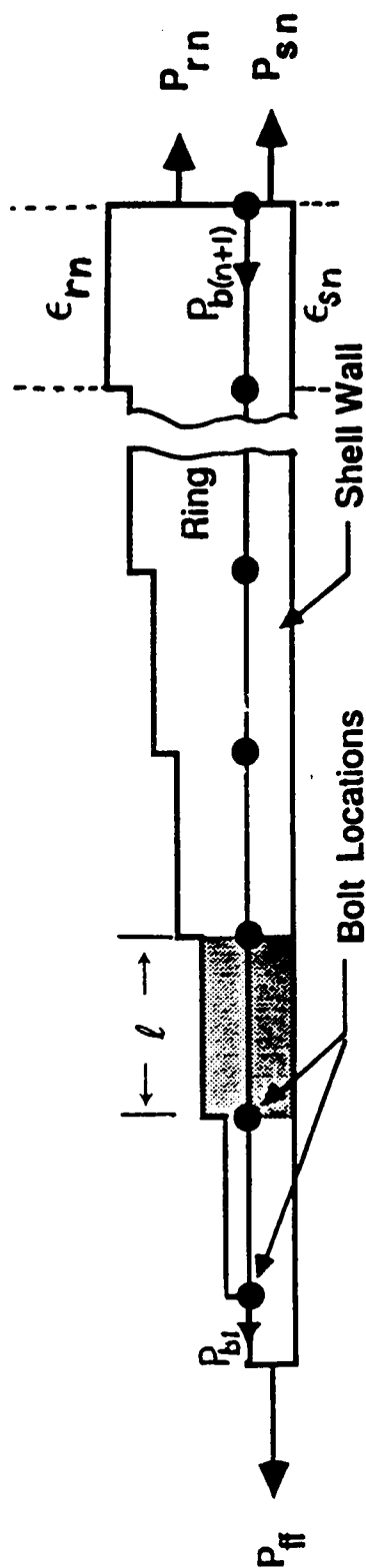
$$(P_{bolt})_n = P_{rn} - P_{rn} - 1 = P_{ff} \left[\frac{A_{rn}}{A_{rn} + A_s} - \frac{A_{rn} - 1}{A_{rn} - 1 + A_s} \right]$$

$$A_{rn} = \frac{A_s \left[\frac{(P_{bolt})_n}{P_{ff}} + \frac{A_{rn} - 1}{A_{rn} - 1 + A_s} \right]}{\left[1 - \frac{(P_{bolt})_n}{P_{ff}} - \frac{A_{rn} - 1}{A_{rn} - 1 + A_s} \right]}$$

Figure 25.

SIMPLIFIED RING ANALYSIS

INCLUDES RING "SHEAR LAG" AND BOLT FLEXIBILITY



$$P_{ff} = P_{rn} + P_{sn}$$

$$K_{bn} = \frac{K_b K_{wn}}{K_b + K_{wn}}$$

$$K_{wn} = G\ell \left(\frac{t_w}{h_w} \right)_n$$

$$\epsilon_{rn} = \frac{P_{rn}}{EA_{rn}}$$

$$\epsilon_{sn} = \frac{P_{sn}}{EA_{sn}}$$

$$\left\{ \frac{P_{ff} - \sum_{i=1}^n P_{bi}}{A_s} - \frac{E}{K_{bn}} P_{bn} + \frac{E}{K_{b(n+1)}} P_{b(n+1)} \right\} = \sum_{i=1}^n P_{bi}$$

and

$$\sum_{i=1}^n P_{bi} = \frac{A_{rn}}{A_{rn} + A_s} P_{ff}$$

Figure 26.

ETA RING AREA TAPER PROFILE

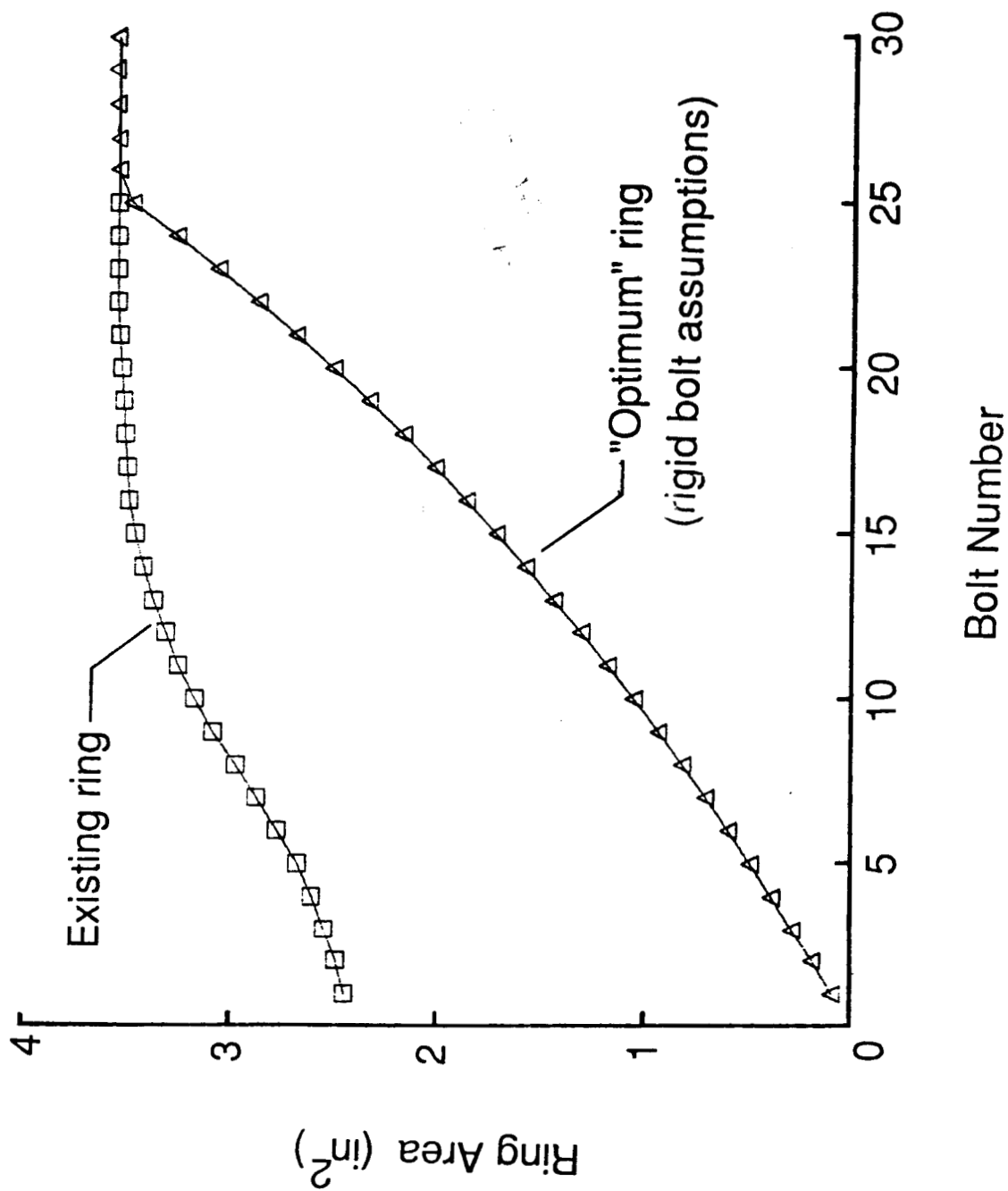


Figure 27.

TANG BOLT LOADS

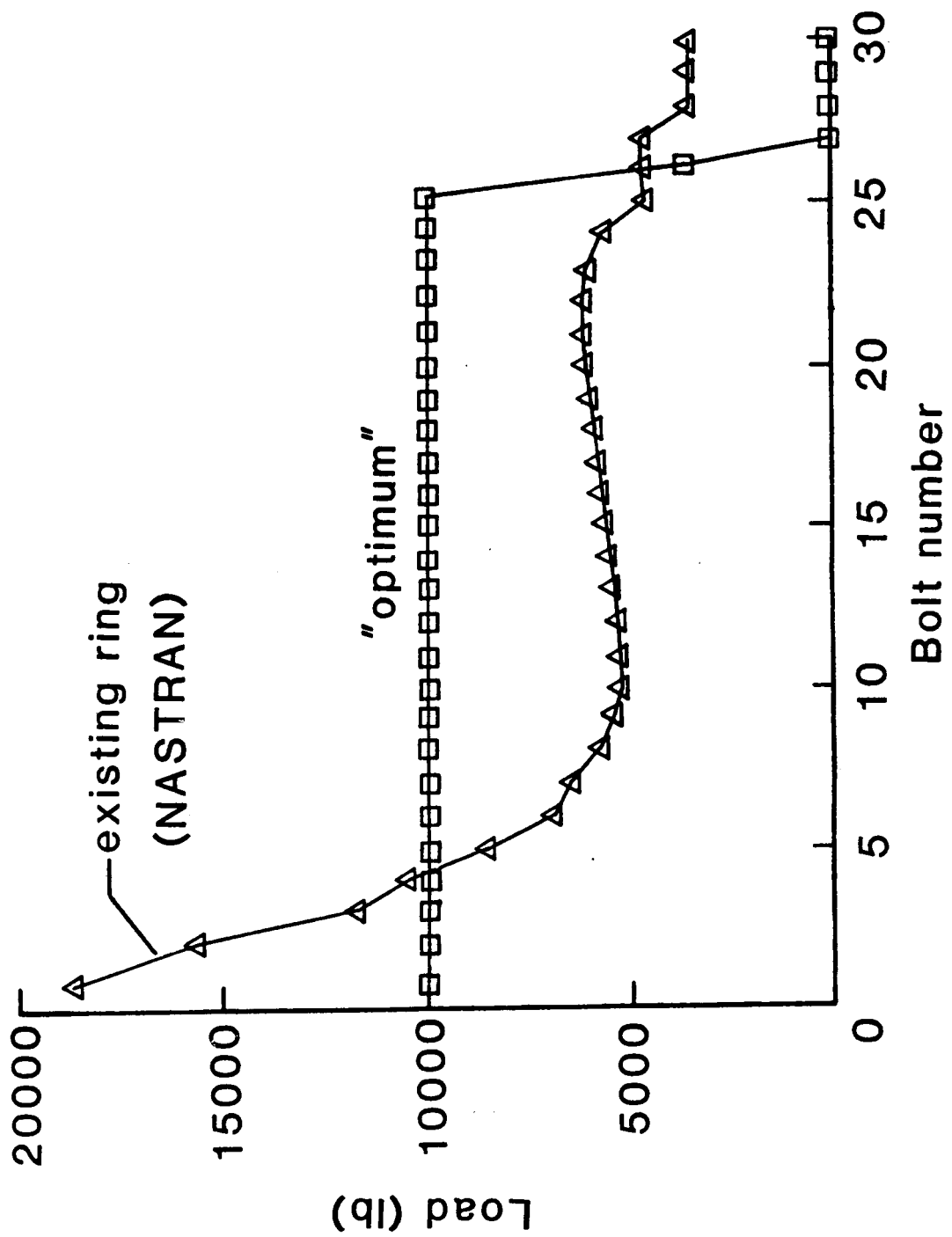


Figure 28.

MODIFIED AREA PROFILE

INCLUDES RING "SHEAR LAG" AND BOLT FLEXIBILITY

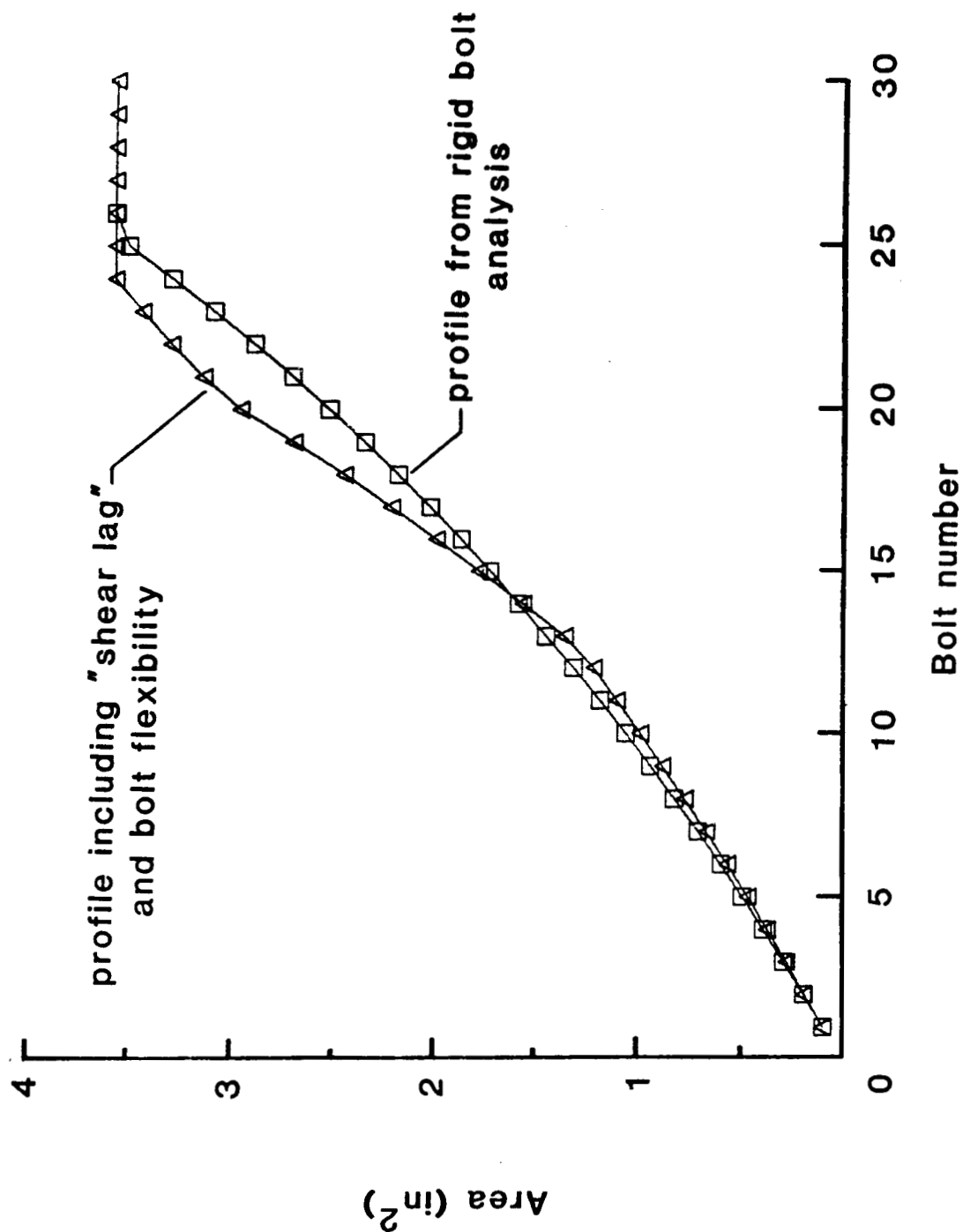


Figure 29.

PREDICTED TANG BOLT LOADS

INCLUDES RING "SHEAR LAG" AND BOLT FLEXIBILITY

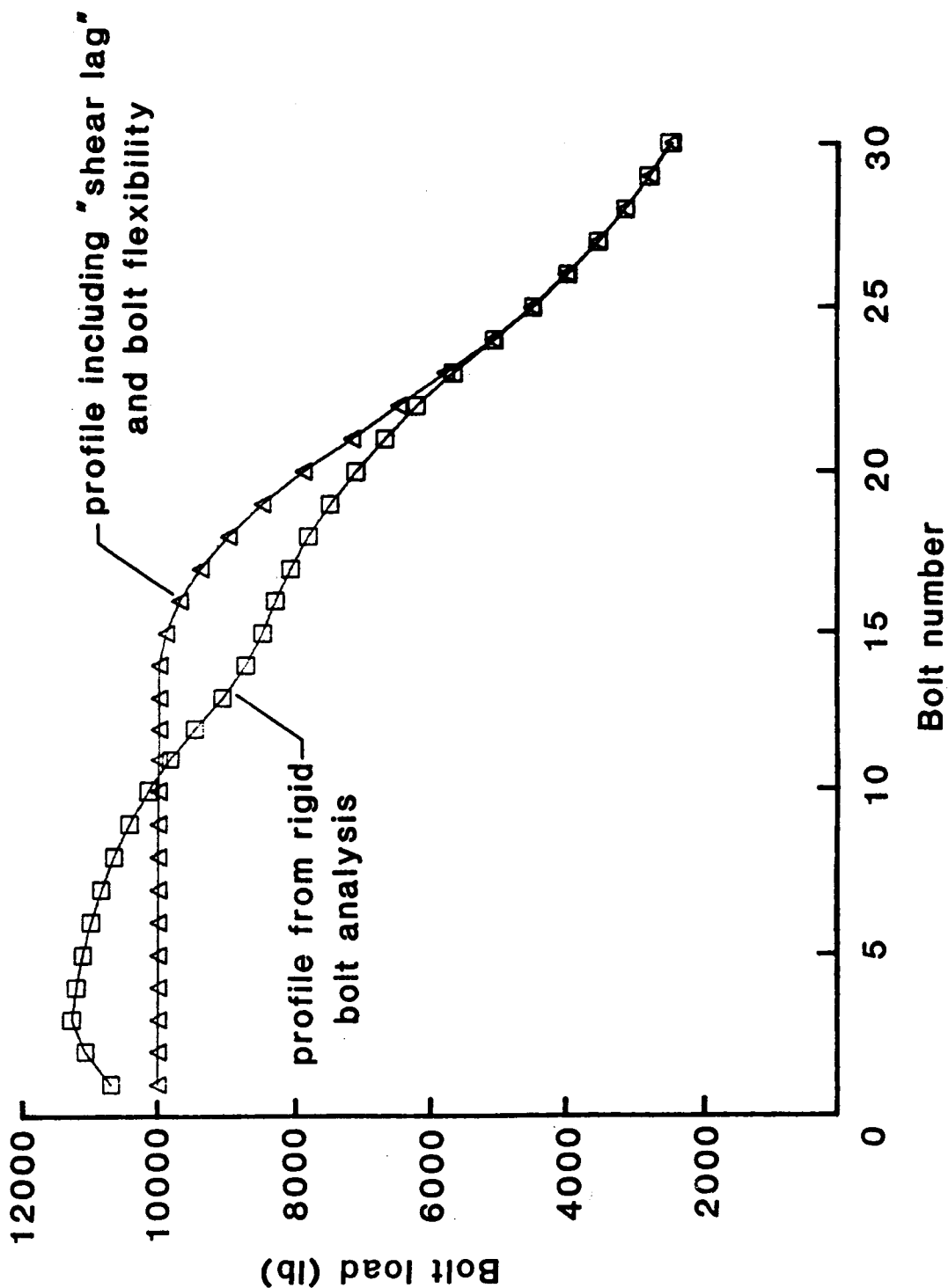


Figure 30.

2-D PLANAR MODEL

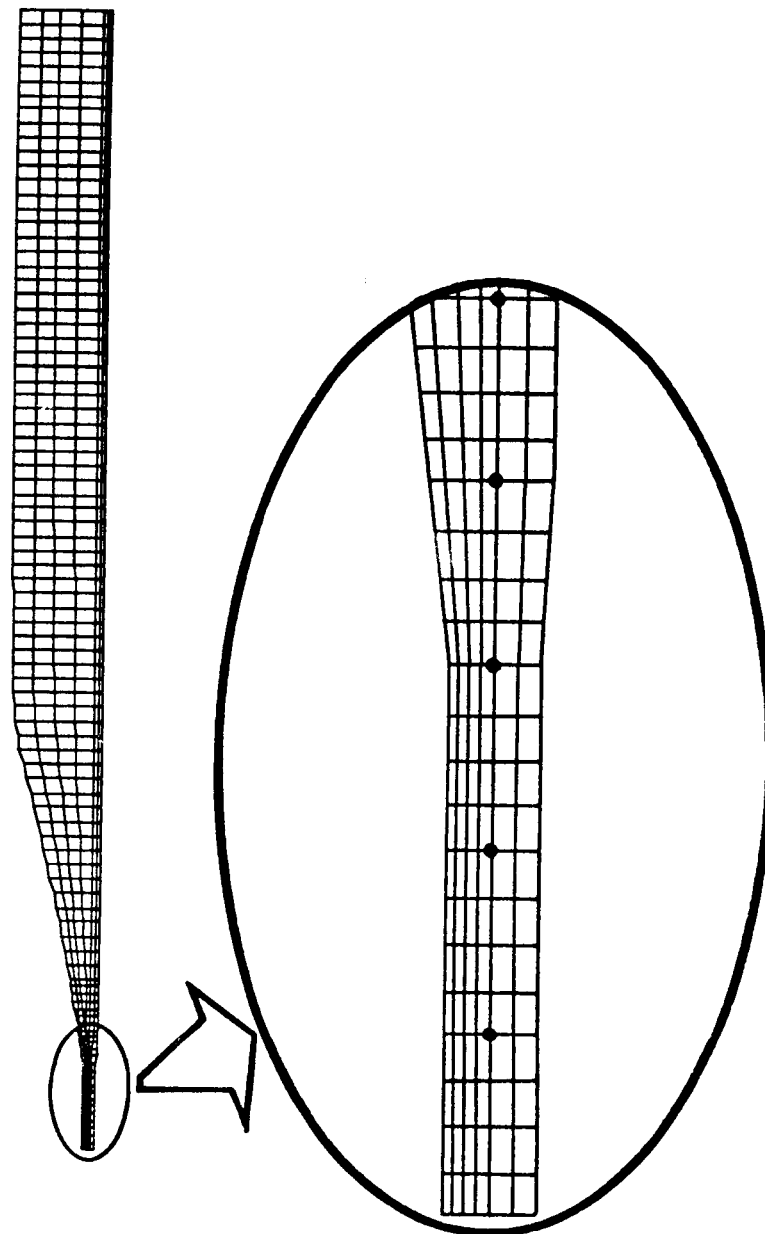


Figure 31.

3-D PLANAR MODEL

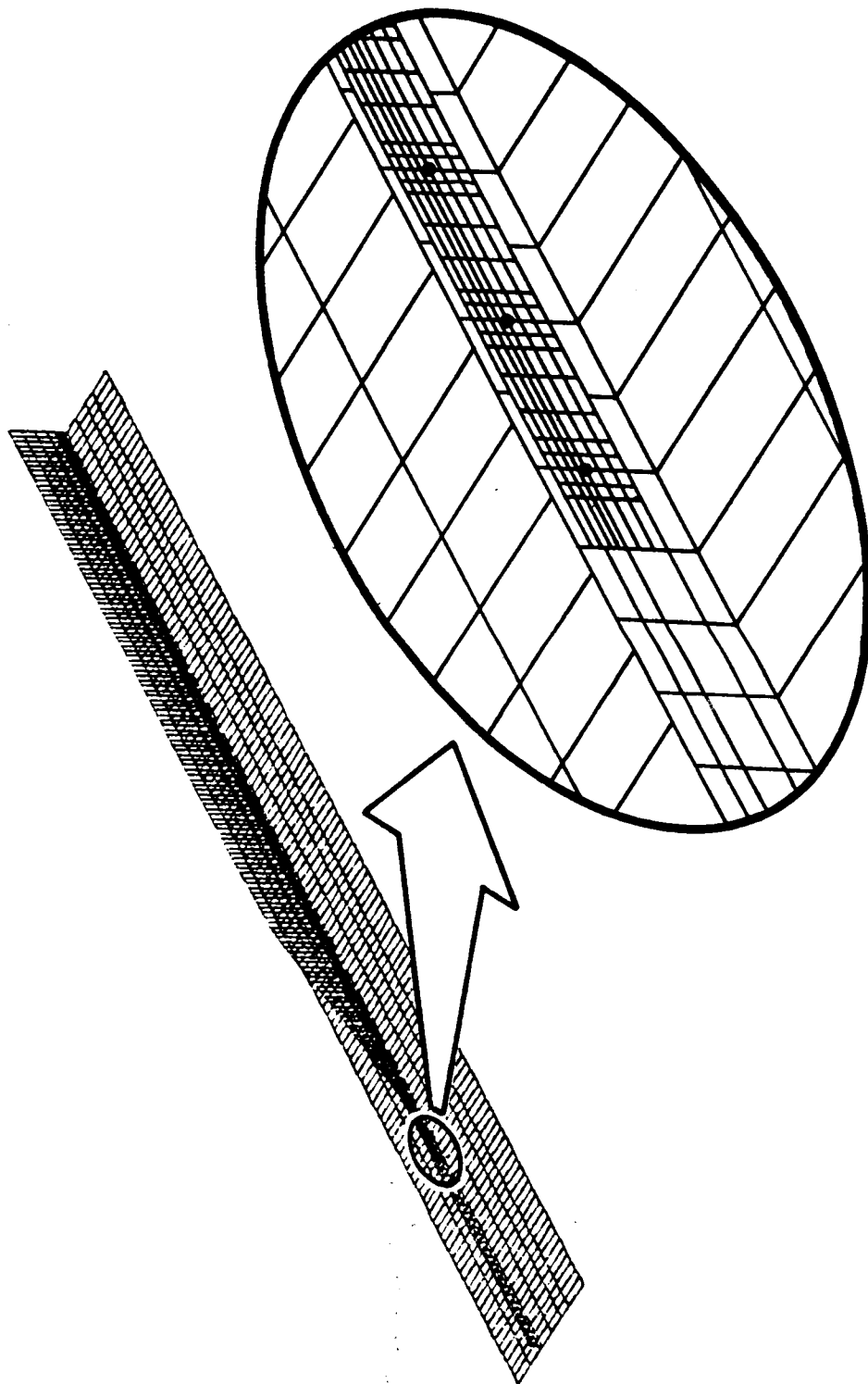


Figure 32.

COMPARISON OF 2-D AND 3-D PLANAR MODELS

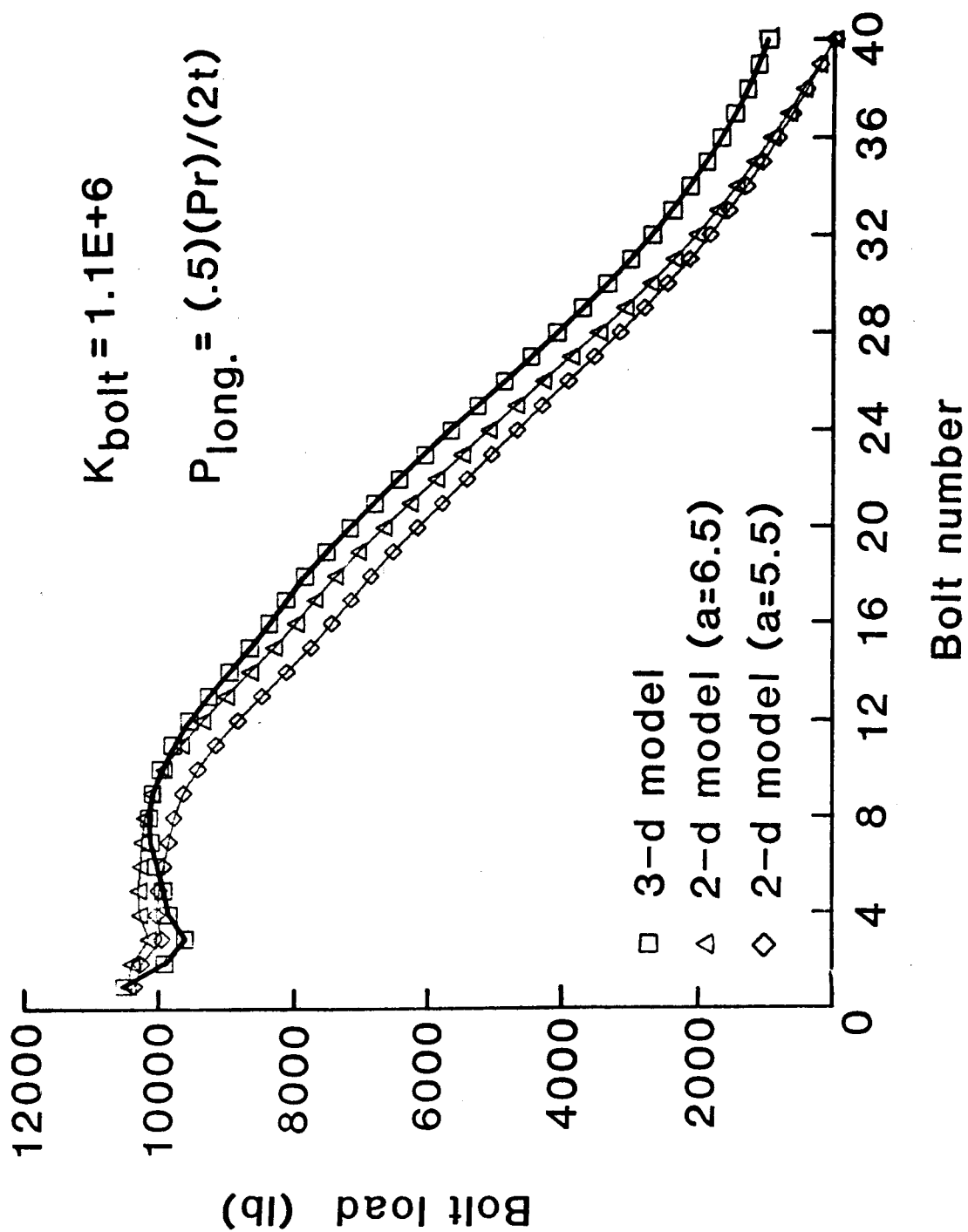


Figure 33.

BOUNDING OF MSFC RESULTS WITH 2-D PLANAR MODEL

$$k_{\text{bolt}} = 1.3 \times 10^6 \text{ lb/in} \quad a_{\text{shell}} = 6.5 \text{ in}^2$$

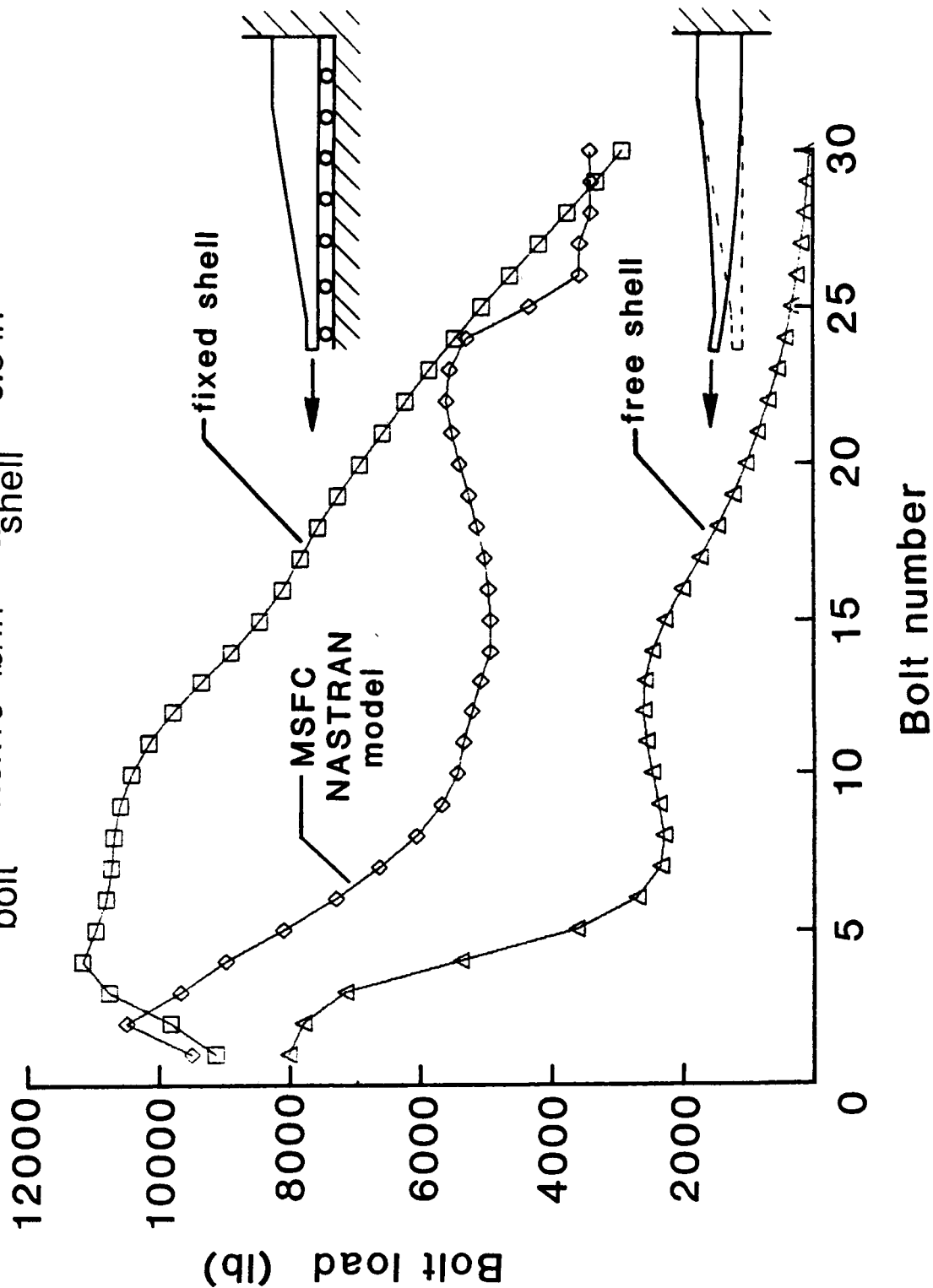
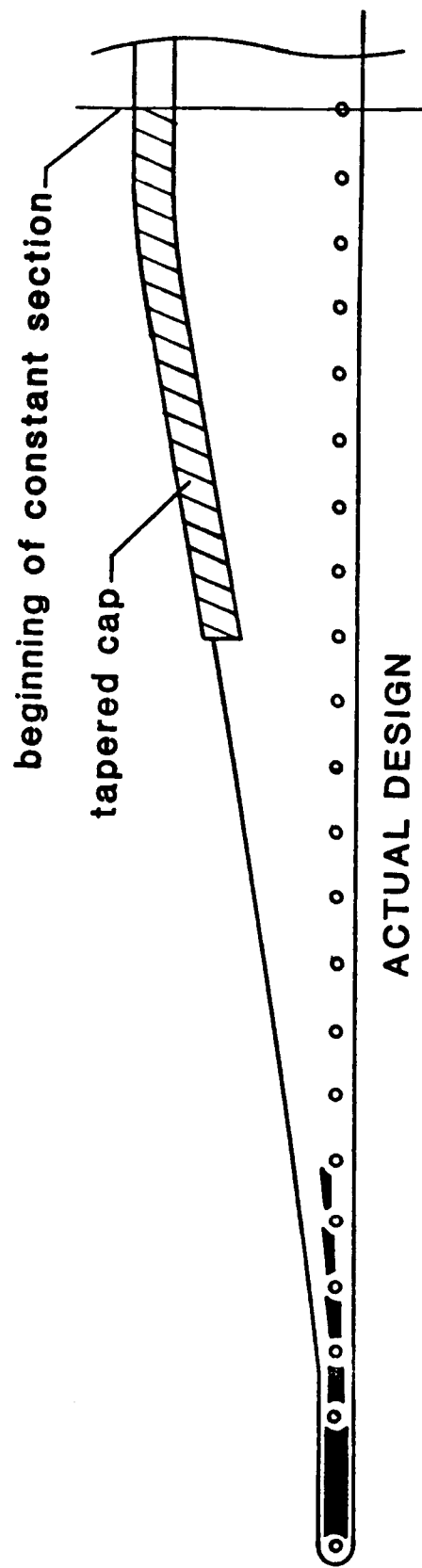


Figure 34.

F.E. MODEL OF REDESIGNED RING



63

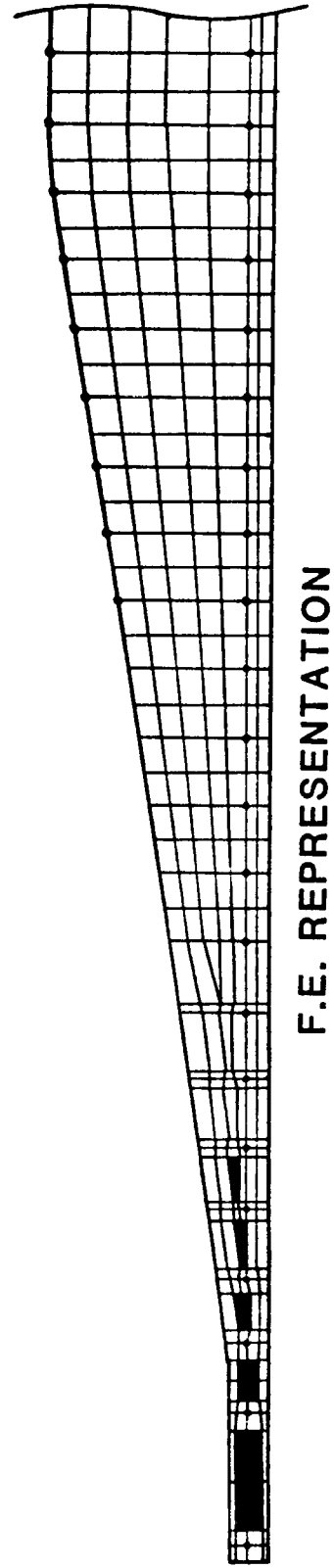


Figure 35.

REDESIGNED ETA RING BOLT LOADS

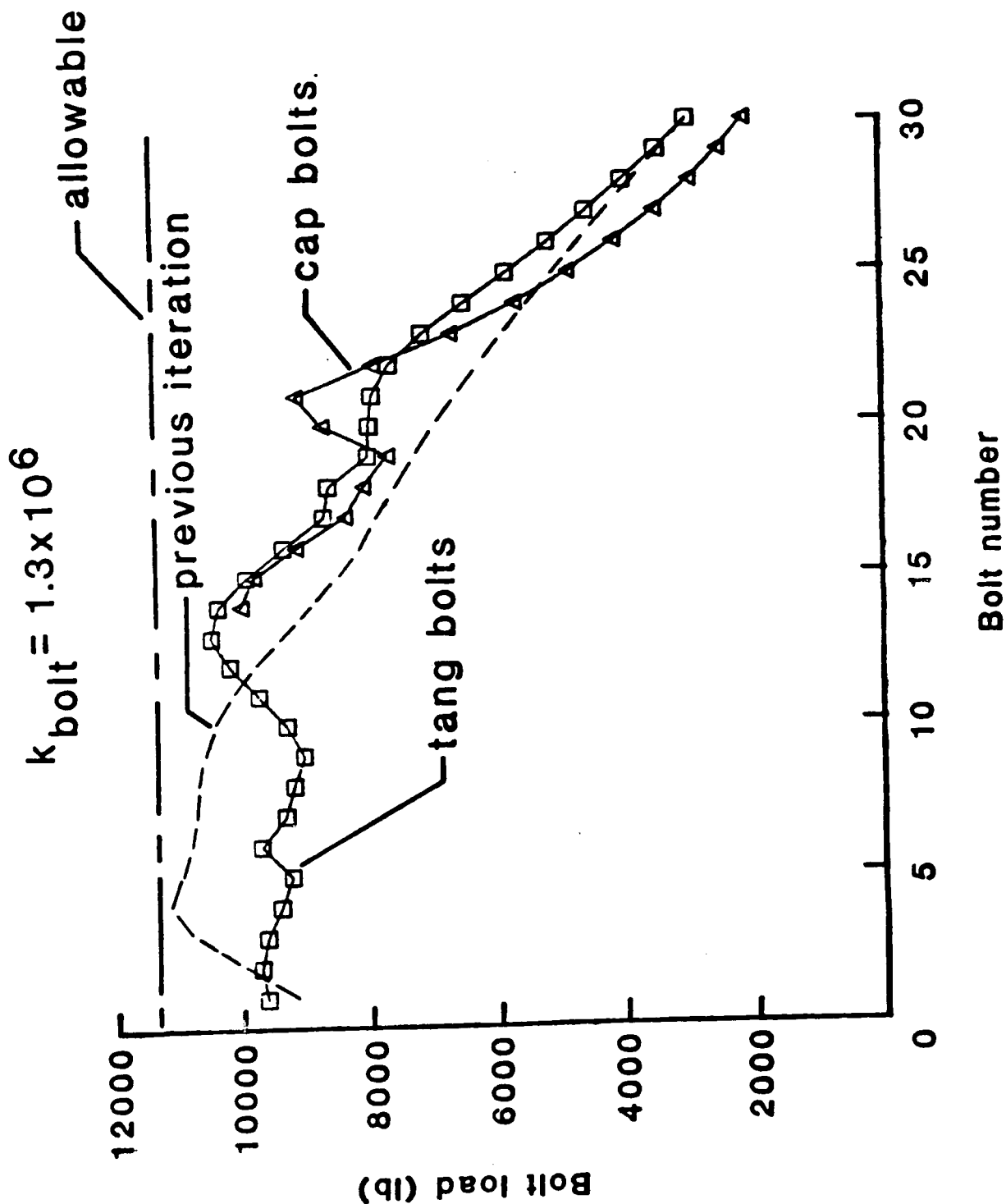


Figure 36.

SENSITIVITY OF BOLT LOADS TO BOLT STIFFNESS

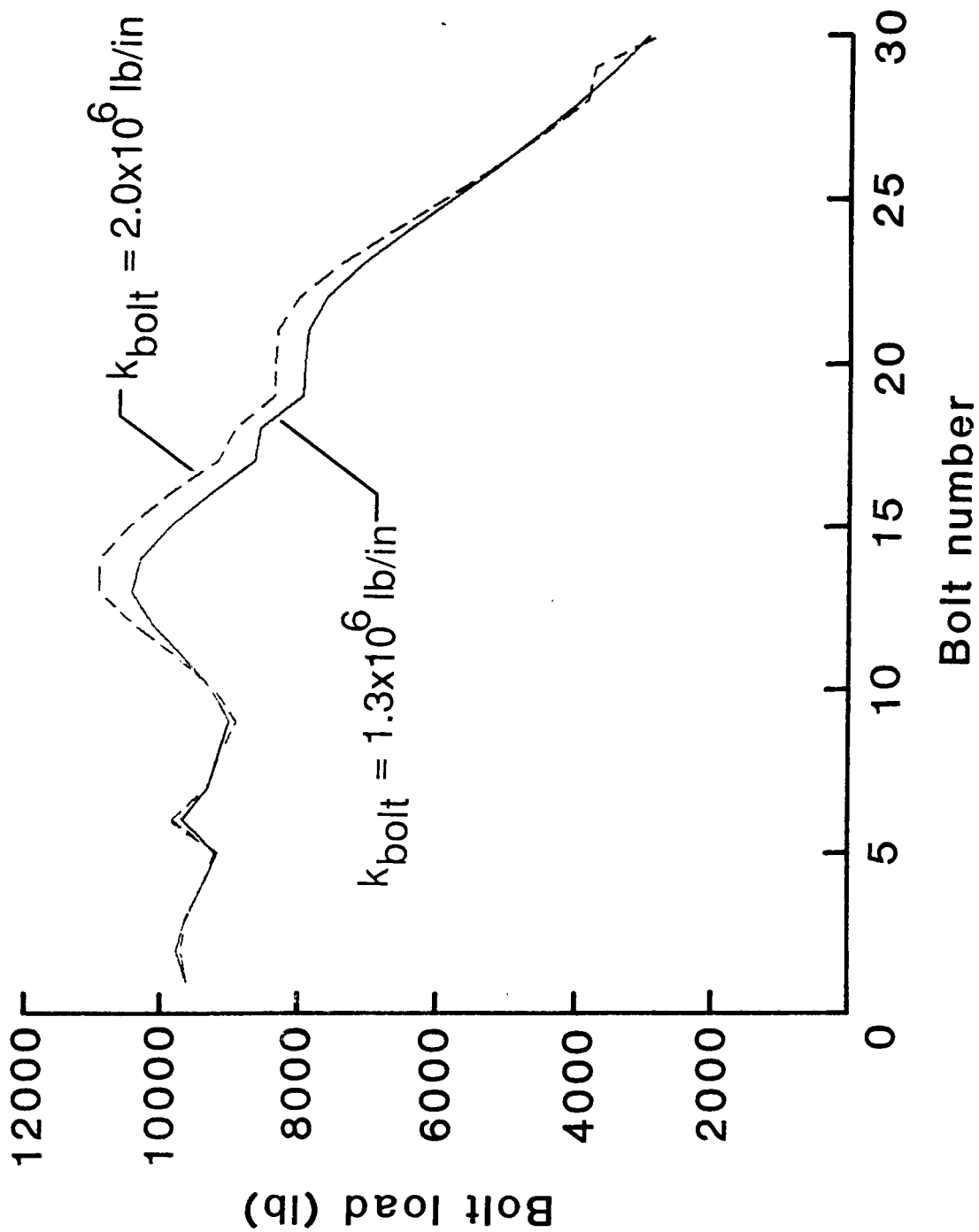


Figure 37.

EFFECT OF FAILED BOLTS

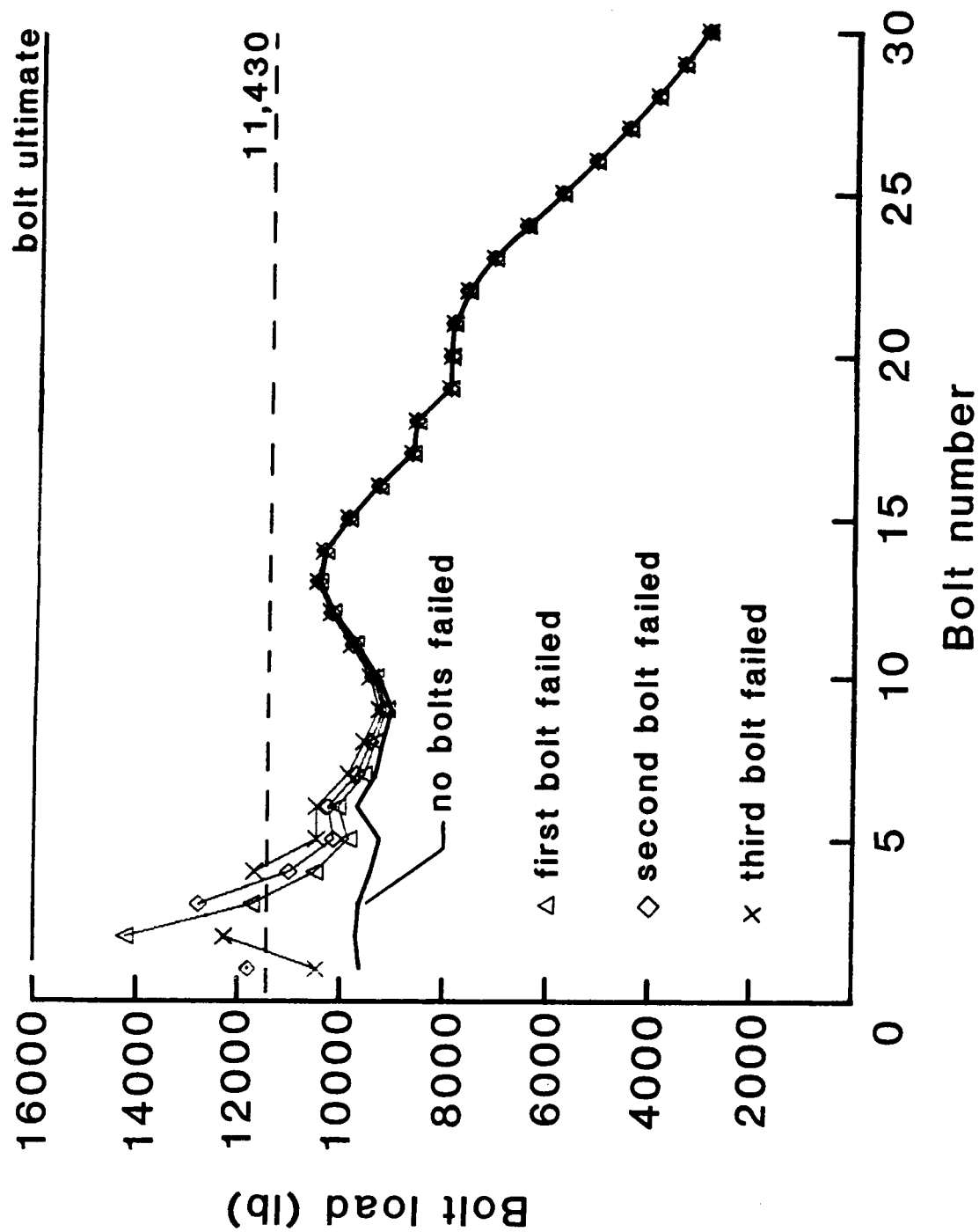
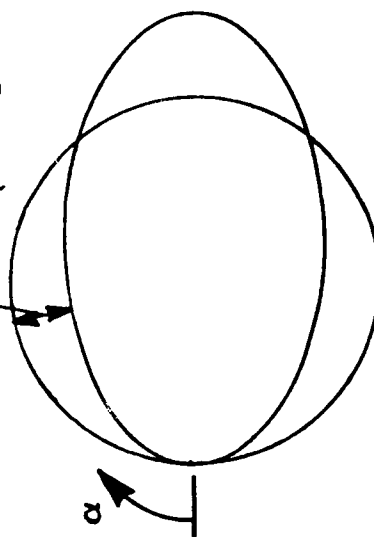


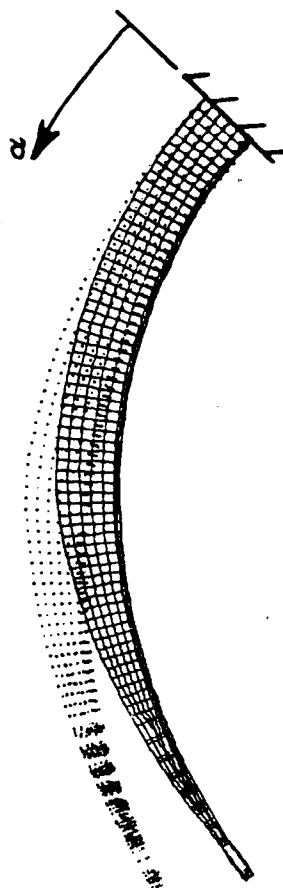
Figure 38.

RING ATTACHMENT TO OUT-OF-ROUND MOTOR CASE MODELED

$$r\Delta R = A\{\sin 2[\alpha + 45] - 1\}$$



OUT-OF-ROUND CASE REPRESENTATION



APPLIED DISPLACEMENT SHAPE FOR
CURVE RING MODEL

Figure 39.

BOLT LOADS DUE TO CASE OUT-OF-ROUND*

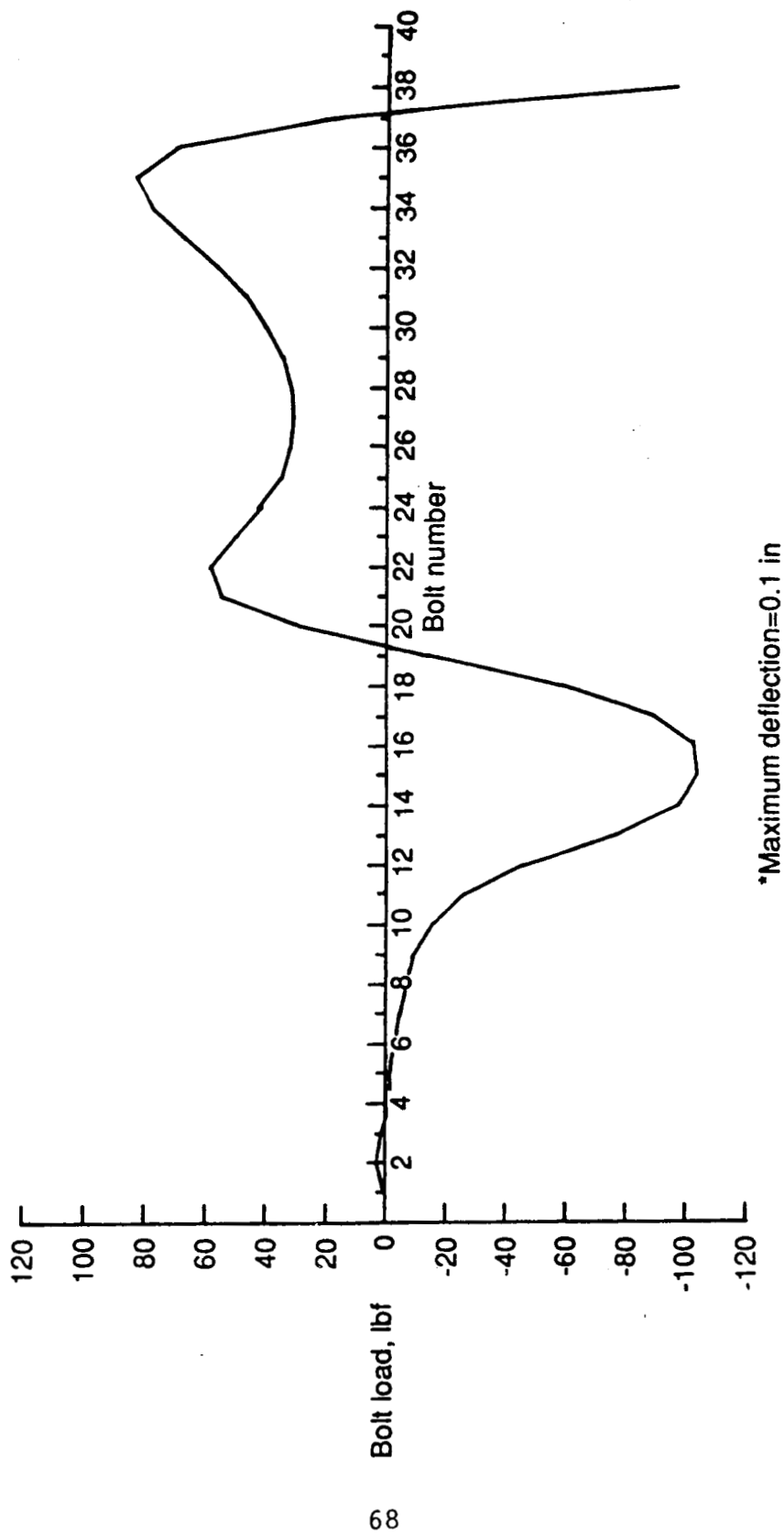


Figure 40.

ETA RING TANG BOLT LOADS

(PRESSURE PLUS STRUT LOADS)

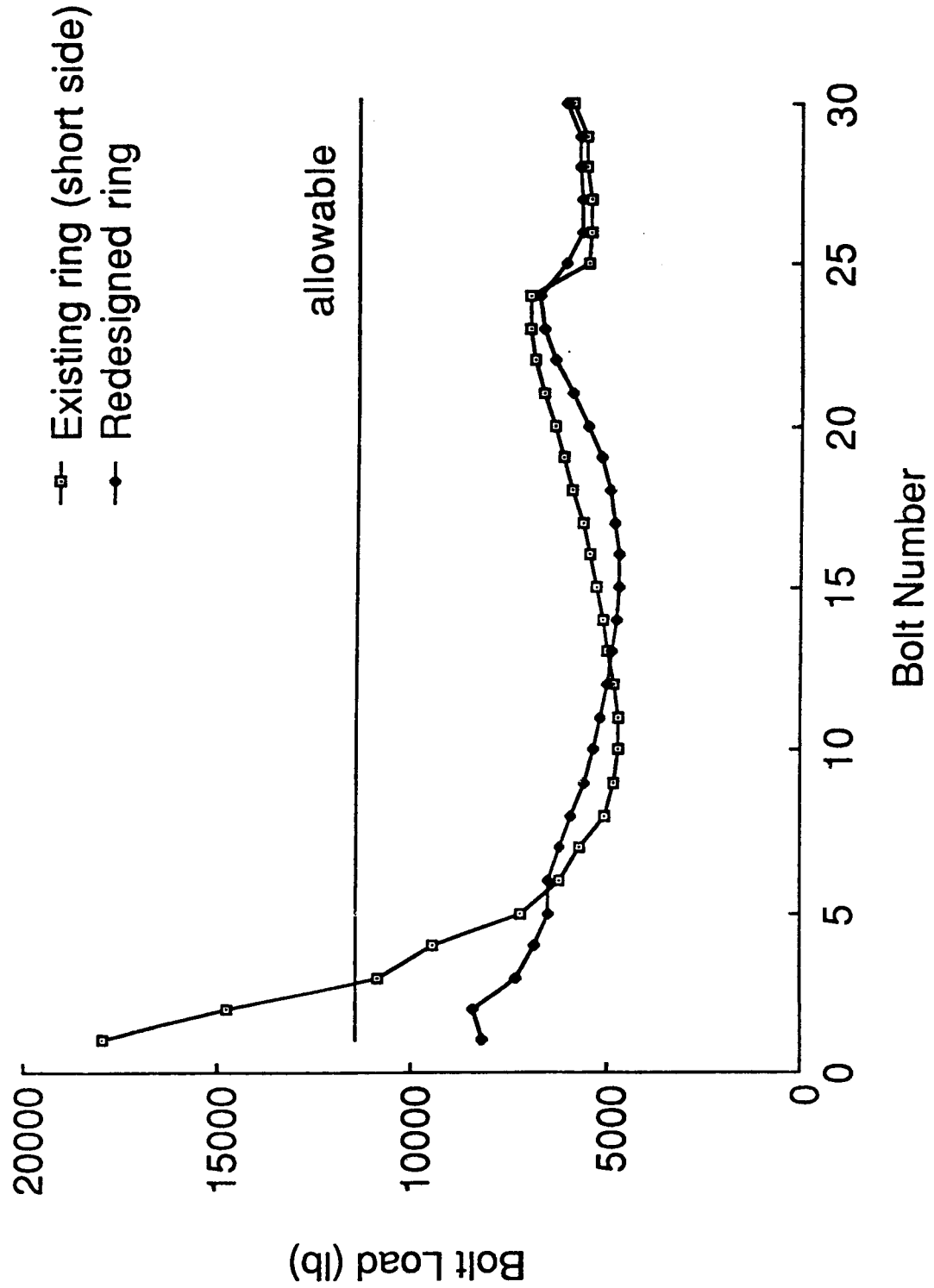


Figure 41.

REDESIGNED ETA RING TANG BOLT LOADS

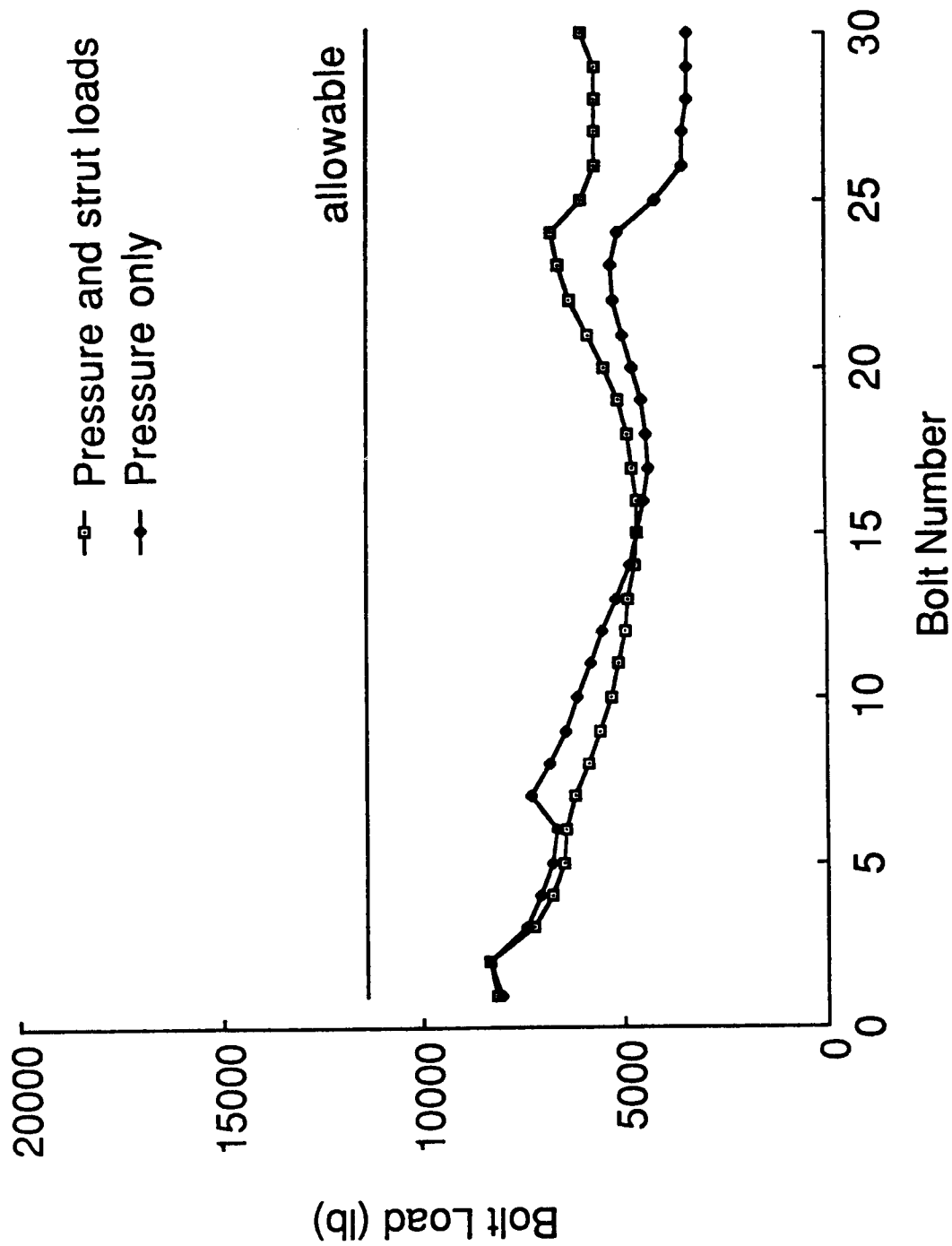


Figure 42.

EQUIVALENT BUSHING STIFFNESS

(PRESSURE ONLY)

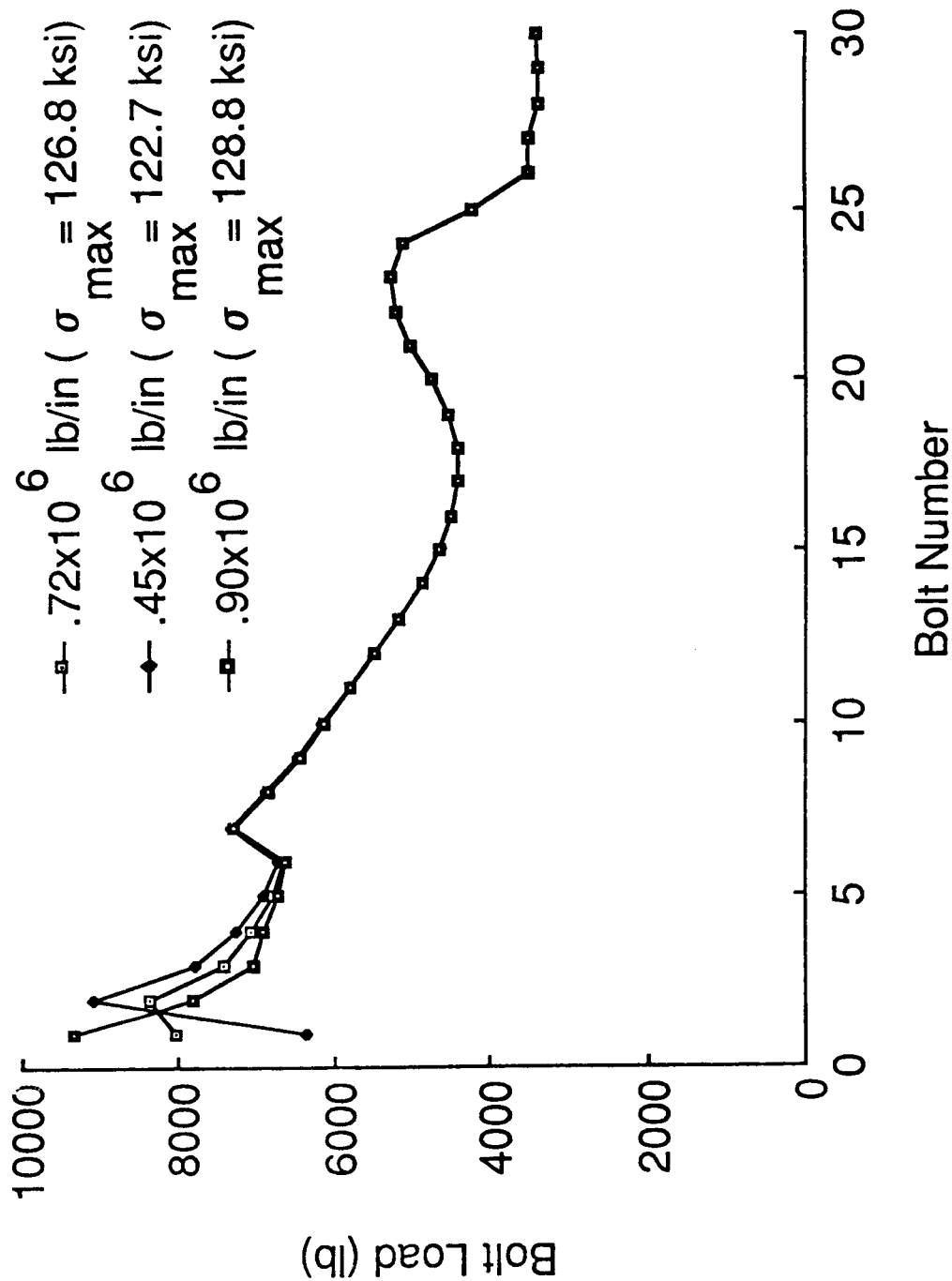


Figure 43.

TEST COMPONENT AND FIXTURE ASSEMBLY

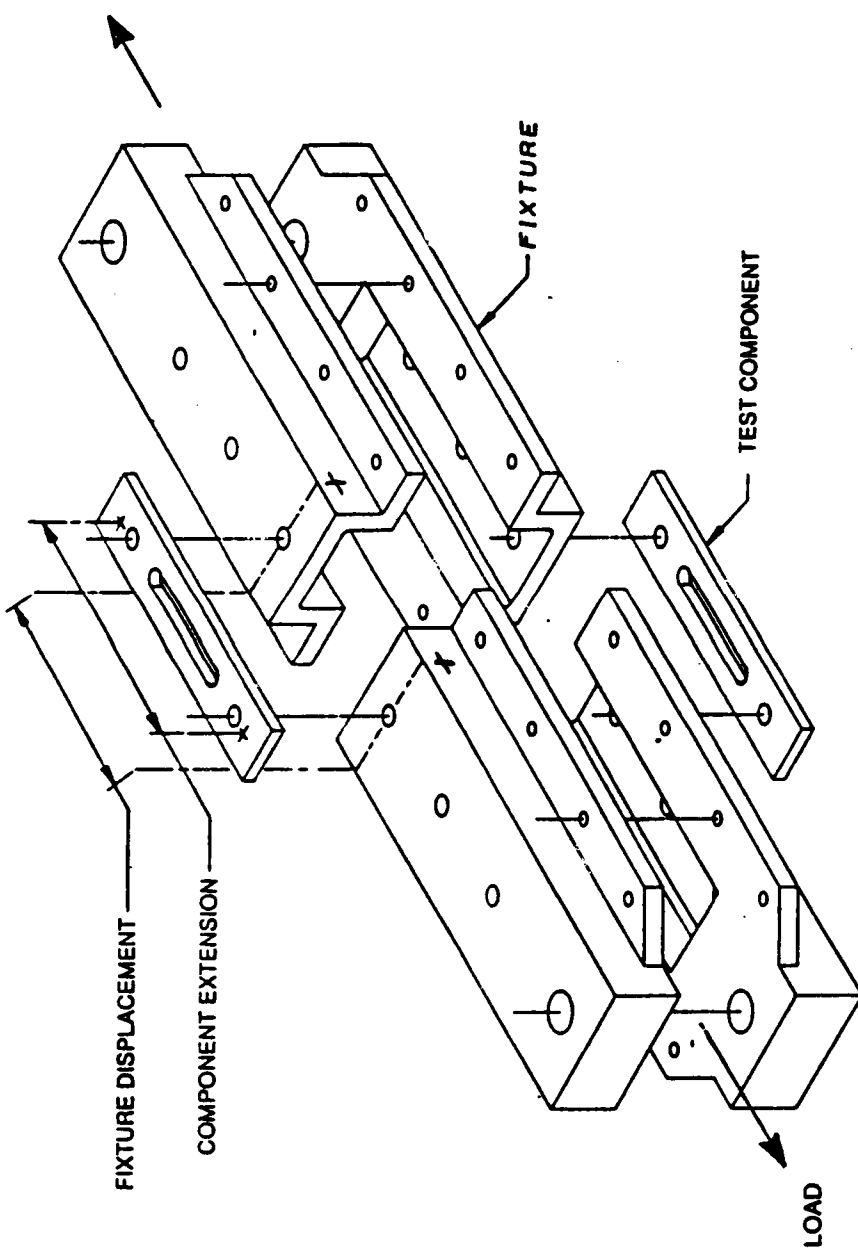


Figure 44.

LOAD-DISPLACEMENT RESPONSE
OF DOUBLE-BAR WEB END SECTION

C1C

DEFLECTIONS

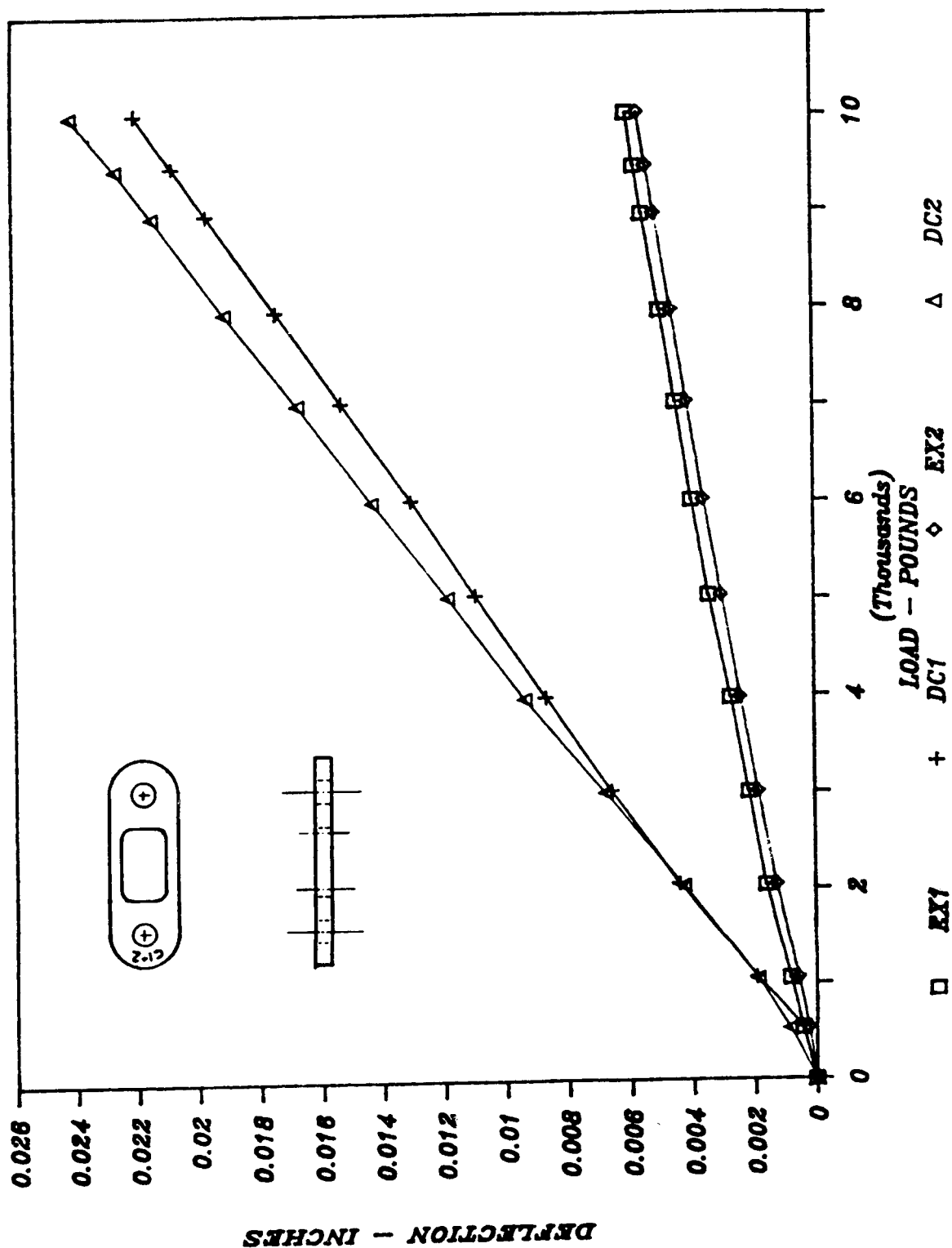


Figure 45.

WEB END SECTION TEST RESULTS SUMMARY

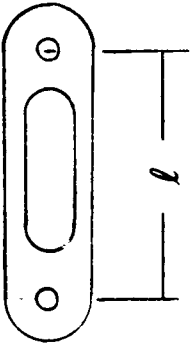
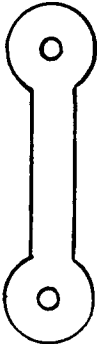

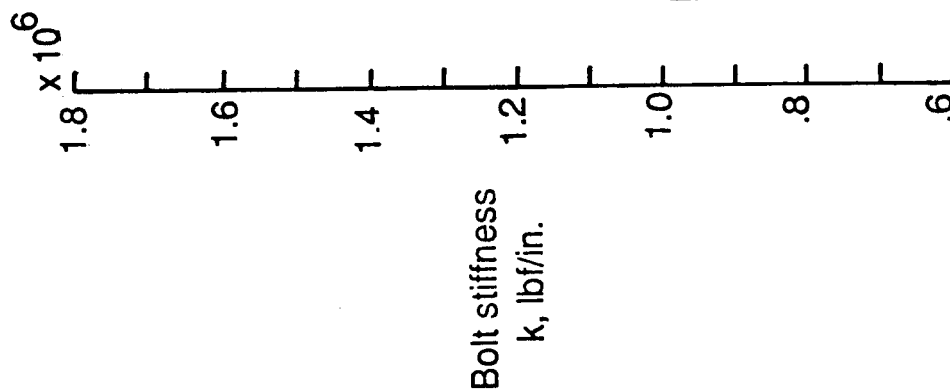



| Component | $l, \text{ in.}$ | Comp. Hole Dia Fixt. Hole Dia | EA, lbf 10^6 | K, lbf/in 10^6 | Remarks |
|---|------------------|----------------------------------|-------------------|---------------------|-----------------------------|
|  | 2.25 | .375"/.375" | 3.99 | 1.16 | Large Corner Fillets |
| | 2.25 | .391"/.375" | 6.66 | 1.18 | Section 2 |
| | 2.25 | .391"/.391" | 3.62 | 1.29 | Large Corner Fillets |
| | 2.25 | .391"/.391" | 3.08 | 1.13 | Corner Material Removed |
| | 4.50 | .391"/.391" | 3.21 | 1.50 | Large Corner Fillets |
| | 4.50 | .391"/.391" | 3.01 | 1.13 | Corner Material Removed |
| | 4.50 | .391"/.391" | 2.95 | 1.33 | Corner Material Removed |
| | 4.50 | .391"/.391" | 2.93 | 1.33 | Corner Material Removed |
| | 4.50 | .391"/.391" | 2.92 | 1.03 | Tolerances Reduced/Machined |
| | 2.25 | .391"/.375" | 3.61 | 1.08 | |
|  | 4.50 | .391"/.391" | 3.06 | 1.17 | |
| | 4.50 | .391"/.391" | | | |
| | 4.50 | .375"/.375" | 3.33 | 1.51* | *End Rotation Restrained |
|  | 4.50 | .375"/.375" | 5.44 | 1.65* | Section 2 |
| | 4.50 | .391"/.375" | 3.14 | 1.46* | |
| | 4.50 | .391"/.375" | 5.37 | 1.40* | Section 2 |
| | 4.50 | .391"/.391" | 2.93 | 1.28 | |

Figure 46.

BOLT STIFFNESS FOR VARIOUS COMPONENTS AND FIXTURE HOLE SIZES

3/8 IN. TANG BOLTS



 .375"/.375"
  .391"/.375"
  .391"/.391"

Component / Fixture hole combinations

Figure 47

EFFECTIVE BOLT STIFFNESS WITH VARIOUS THICKNESSES
OF 2024-T4 ALUMINUM BUSHINGS

3/8 IN. TANG BOLTS

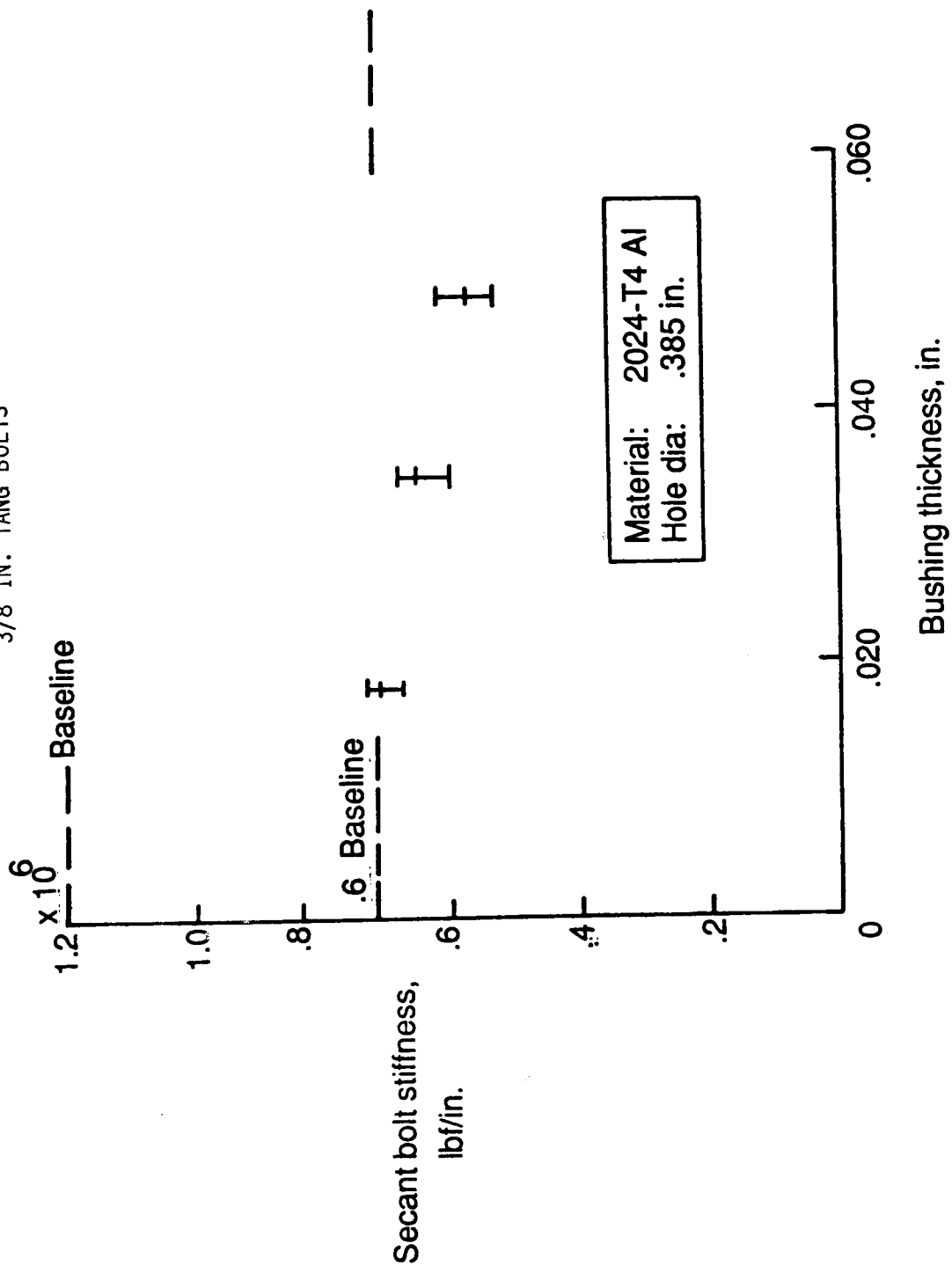
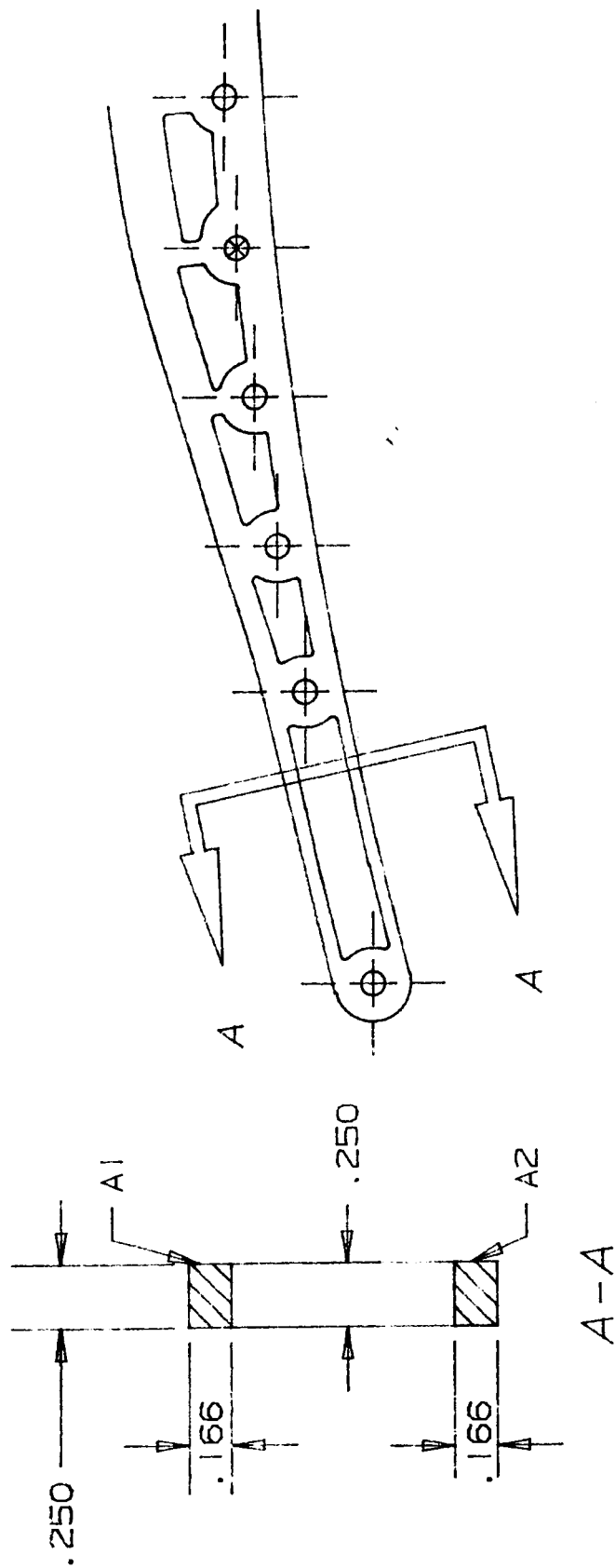
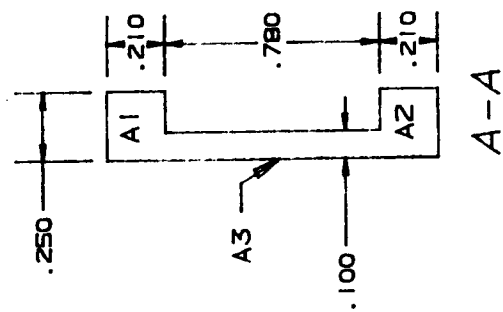
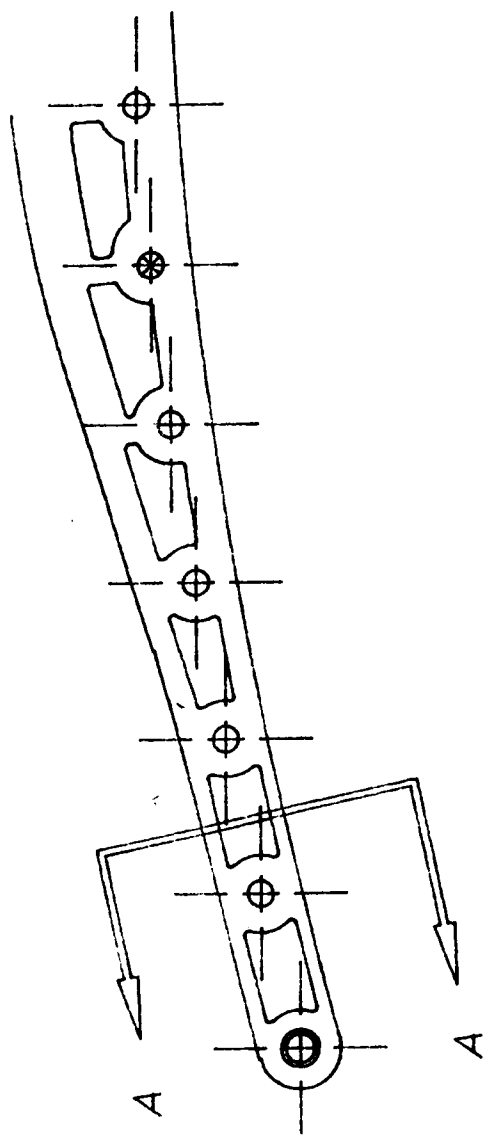


Figure 48.



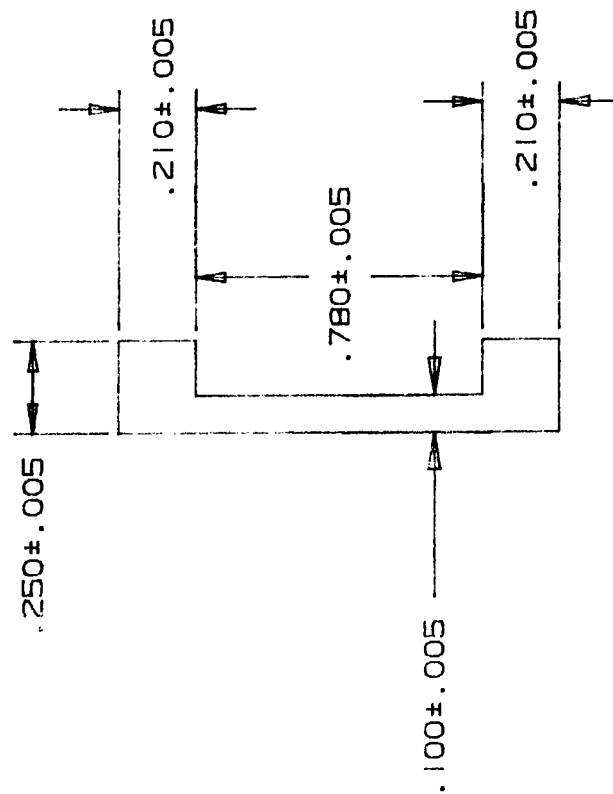
SUB AREA BREAKDOWN OF MINIMUM CROSS SECTION
DOUBLE BEAM CONCEPT

Figure 49.



SUBAREA BREAKDOWN OF CRITICAL CROSS SECTION
BUSHED CONCEPT
NOMINAL DIMENSIONS

Figure 50.



DIMENSIONING SCHEME OF CRITICAL CROSS SECTION AREA BETWEEN BOLTS 1 & 2

Figure 51.

NET SECTION STRESS VS BOLT NO.

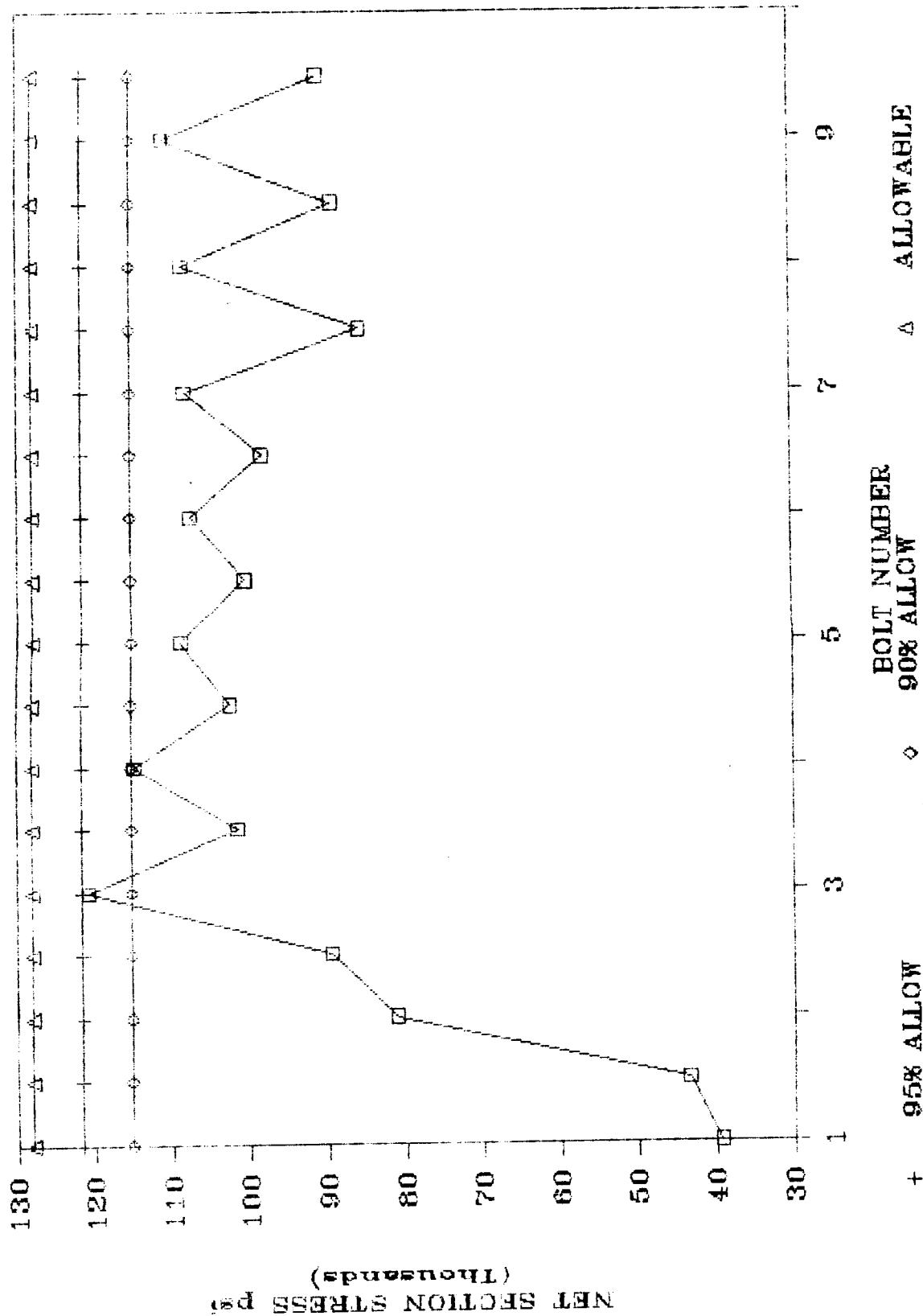


Figure 52.

APPENDIX A

LOADS

by Thomas C. Jones
Mail Stop 431
Langley Research Center
Hampton Va. 23665
Phone (804) 865-4508

June 3, 1987

for William F. Hunter
Thomas C. Jones, Author

William F. Hunter
Dr. W. F. Hunter, Reviewer

for Harold J. Bush
Dr. M. M. Mikulas Jr., Project Engineer

DH Butler 7/2/87
D. H. Butler, Project Manager

APPENDIX A

LOADS

- REF: (a) MSFC internal Letter from ED01/Dr. McDonough to SA41/Mr. Smith, "Interim IVBC-3 Design Loads for use in SRB and SRM Steel Case Redesign and Recertification," December 16, 1986.
- (b) MSFC Report SE-109-142-2H, "Solid Rocket Booster Venting Analysis," Revision A, July 1981.

Reference (a) defines loads which are to be used in the steel case redesign and recertification at MSFC. These same loads are also being used in the aft ET Attach Ring redesign activities at LaRC.

Reference (a) defines worst case internal forces and moments grouped in flight events as a function of SRB X-station. No time-related data is available; hence, an interpretation of the information is necessary and helpful for application to the effort currently ongoing at LaRC in support of the SRB ET Attach Ring redesign and SRB Aft Skirt evaluation. Emphasis is placed on an interpretation of data to assist the structural analyst and designer in obtaining the worst case set of loads. Since both the ET Attach Ring and Aft Skirt are large and complex structures, no one set of loads may be sufficient to completely design either structure. Therefore, the designer and structural analyst must work together with the loads analyst in designing and assessing these structures. This understanding of loads must also be used in the development and application of loads for certification test purposes.

The SRB motor case's radial growth due to pressure was initially examined based on the longitudinal internal force of:

$$F_x = p \pi R^2$$

$$\text{where } p = 912 \text{ psia}$$

$$R = 72.50 \text{ in}$$

$$\text{or } F_x = 15,600,000 \text{ lb}$$

This value of longitudinal internal force does not account for the thrust and inertia loadings which will tend to reduce the 15 million pounds. The

roll maneuver is the event where this peak pressure occurs; hence, it has been the event or period in flight for which the structure has been analyzed. Specifically, the largest "local" pressure creates the largest radial growth. This radial growth is reduced by the Poisson effect of the longitudinal internal force (an increase in longitudinal internal force reduces the radial growth). The formula for radial growth in a cylinder subjected to both circumferential and longitudinal stress is given by:

$$\delta R = (R/E) \times (S1 - \nu S2)$$

where R = radius of cylinder
 E = modulus of elasticity
 S1 = circumferential stress
 S2 = longitudinal stress
 ν = Poisson's ratio

Inspection of this relationship shows that the circumferential stress due to internal pressure tends to increase the radius (and the circumference) of the cylinder and the longitudinal stress (tension) tends to reduce the radius. Therefore, if we examine the case radial growth using the longitudinal internal force of 15 million pounds rather than a reduced value, the analysis of the ET attach ring is non-conservative. The design case should in fact use the proper longitudinal F_x .

Reference (a) presents design forces and moments for six flight events, beginning with SSME ignition and ending with SRB separation (no water impact loads are presented). For each of these events, in addition to pressure vs. SRB station, data is presented as "largest" and "smallest" beam-type internal forces and moments (F_x , F_y , F_z , M_x , M_y , M_z) as a function of SRB X-station. Thrust, internal pressure, change in mass due to motor burning, gust wind loads and aerodynamics are considered in determining these loads for each event. Families of transient response analysis representing each of these six events are performed which develop the "beam type" internal forces and moments. MSFC develops the finite-element models for the SRBs and external tank and JSC develops the FEM for the orbiter. Rockwell International, Inc., integrates these models and performs the transient response analysis at their Space Division.

Some of the structural analysis which is currently underway at LaRC is simplified and makes use of only the internal case pressure without considering the effects of a longitudinal force component. More complete analysis is also being performed at LaRC using FEM techniques applied to a portion of the SRB motor case which includes the "tang" ring. During the roll maneuver event, the local internal rocket case pressure is maximum. The following procedure is used to obtain a "complete" load set.

Reference (a) gives the largest internal SRB pressure as 911.8 psia [reference table A1, attached; table 3 in reference (a)] occurring at 18 seconds into flight, or during the roll maneuver. This is a three-sigma value and should be used (after an adjustment for the ambient pressure of 13 psia)

in the design and testing. Figure A1 [figure 4 of reference (a)] shows the coordinate system used to define the forces and moments. Positive forces and moments are shown positive on a "left-face" (the face of a segment of SRB case where the SRB X-axis is pointing inward) of a segment taken from the SRB. F_x is designated as SHEAR X on figure A2 [figure 3-1 of reference (a)]. The values of F_x (at SRB-station of about 1504) range from 13,000,000 pounds to 13,500,000 pounds in tension. F_x has an uncertainty factor of 0.05 [note that the uncertainty factor is given for each event; for the roll maneuver, see section 3 of reference (a)] which is accounted for by adjusting the extreme values by 0.05. The design values to use are:

$$F_x(\min) = 0.95 \times (-13,000,000 \text{ lb}) = -12,400,000 \text{ lb}$$

$$F_x(\max) = 1.05 \times (-13,500,000 \text{ lb}) = -14,200,000 \text{ lb}$$

Note that the lower value of -12,400,000 lb is significantly different from the -15,600,000 lb calculated using the formula:

$$F_x = p \pi R^2$$

The remaining beam-type internal forces and moments given for F_y , F_z , M_x , M_y , M_z are found on figures A3 through A7 [figures 3-2 through 3-6 of reference (a)] for the right SRB. These forces and moments are adjusted from those values read from the figures by 0.05 (uncertainty factor for the roll maneuver) and are summarized below for the SRB X-station of about 1504.

$$-14,200,000 < F_x < -12,400,000 \text{ lb}$$

$$-122,850 < F_y < 112,350 \text{ lb}$$

$$-92,400 < F_z < 18,900 \text{ lb}$$

$$-4,150,000 < M_x < 340,000 \text{ in-lb}$$

$$24,700,000 < M_y < 36,200,000 \text{ in-lb}$$

$$-44,100,000 < M_z < -34,200,000 \text{ in-lb}$$

To understand the relative importance of these forces and moments, consider their effects on stress and radial growth of a cylinder with the approximate dimensions similar to those of the SRB case, where:

$$R = 72.5 \text{ in}$$

$$p = 912 \text{ psi}$$

$$t = .45 \text{ in}$$

$$F_x = -12,400,000 \text{ lb}$$

$$I = \pi R^3 t = 538,737 \text{ in}^4$$

$$F_y = -122,850 \text{ lb}$$

$$J = 2 \times I = 1,077,473 \text{ in}^4$$

$$M_x = -4,150,000 \text{ in-lb}$$

$$E = 30,000,000 \text{ lb/in}^2$$

$$M_z = -44,100,000 \text{ in-lb}$$

$$G = 11,000,000 \text{ lb/in}^2$$

$$\nu = 0.3$$

For the example loadings, the stresses are found to be:

$$S1 = \text{Circumferential stress} = (p R)/t = 146,933 \text{ psi}$$

$$S2 = \text{Longitudinal stress} = -F_x/(2\pi R t) \\ = 60,491 \text{ psi (tension)}$$

$$S3 = \text{Average Shear Stress} = -F_y/(2\pi R t) \\ = 599 \text{ psi (max.)}$$

$$S4 = \text{Bending Stress} = -(M_z R)/I = 5,935 \text{ psi}$$

$$S5 = \text{Torsional Stress} = -(M_x R)/J = 279 \text{ psi}$$

$$\delta R = (R/E) \times (S1 - \nu S2) = 0.3097 \text{ in}$$

By inspection of the above numerical results, it is clear that the circumferential stress due to pressure and the longitudinal stress are much larger than the stresses due to "shear," "bending," or "torsion."

The above is a description of how the information in the reference should be interpreted to obtain maximum/minimum forces and moments at a section. Since that information is event-grouped or related as opposed to time-phased, and since the external forces and moments are not readily available, it is not possible to construct a "free-body" diagram which is in equilibrium from the referenced data. To do so will require us to obtain and examine the data as a function of time.

To evaluate the stresses in the ET attach ring/SRB case fasteners, a finite-element model of the ET attach ring and a portion of the SRB case are required. It must have sufficient modeling detail to accurately describe the structure. That level of detail should include provisions for inputting strut loads as well as the internal pressure. One end of the model is properly restrained with the other end having forces and moments imposed (\bar{F}_x , F_y , F_z , M_x , M_y , and M_z) which are obtained from the figures of reference (a) for the

case being examined. For example, the forces and moments applied to an end of a FEM which started at SRB X-station 1550 for the roll maneuver (uncertainty factor included) would be:

$$F_x = -12,400,000 \text{ lb}$$

$$F_y = -121,000 \text{ lb}$$

$$F_z = -99,000 \text{ lb}$$

$$M_x = 300,000 \text{ in-lb}$$

$$M_y = 32,000,000 \text{ in-lb}$$

$$M_z = -38,000,000 \text{ in-lb}$$

The other end of the FEM would be properly restrained. Strut loads in KIPS are given in reference (a) for the roll maneuver event [uncertainty factor included, struts identified on figure A1, figure 4 of reference (a)] as:

$$77 < p8 < 112$$

$$138 < p9 < 147$$

$$-117 < p10 < -79$$

These strut loads as well as the forces and moments listed above for X-station 1550 are not time-related. Therefore, all combinations of the strut loads must be evaluated with combinations of the end forces and moments. To these forces and moments, the internal pressure of 898.8 psid is added.

Bending stresses due to moments M_y and M_z vary as a cosine function from their respective peaks. Theta (θ) is in the SRB y-z plane and is measured from the y-axis using a right-handed rule. Moments are interpreted for use in FEM application by adding their contribution to F_x per unit of circumference. The total axial load per unit of circumference is N_x and is the sum of F_x per unit of circumference and the moment contribution. Stated mathematically, the distributed axial load as a function of theta is:

$$N_x(\theta) = (F_x)/(2\pi R) - (M_y/\pi R^2) \times \cos(90^\circ + \theta) - (M_z/\pi R^2) \times \cos(\theta)$$

Aero loads are added directly to the ET attach ring based on a dynamic pressure of 100 psf which produces an ET attach ring drag load of about 3,000 pounds for the roll maneuver. Aero loads are obviously larger during the high-q flight regime while other event-related loads are less.

The ET Attach Ring assembly itself is a pressure vessel and can be subjected to an internal pressure of 15.2 psid during ascent. Pressure, both "burst" and "crush", are defined for other conditions throughout the entire SRB flight in reference (b).

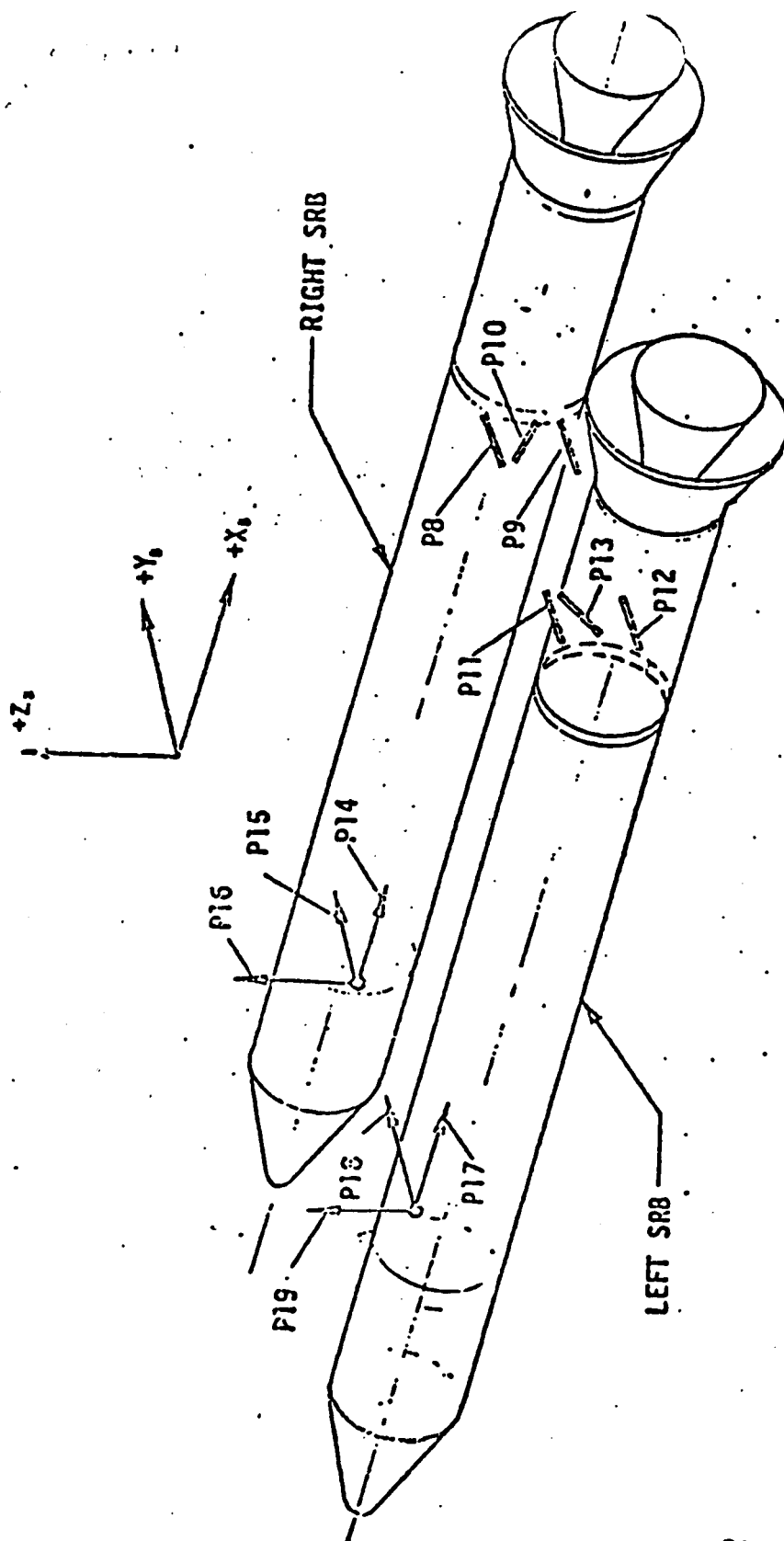
In summary, the beam-type loads and SRB case internal pressure loads are defined in reference (a) for use in the design and evaluation of modifications to the SRB ET attach ring. This letter gives an example of how to use reference (a) as well as stating a specific set of loads occurring during the roll maneuver flight event.

Thomas C. Jones
4508

TABLE A1

HPH LIGHT-WEIGHT MOTOR
AT MEOP OPERATING CONDITION
AT 90 DEG F AND AN INCREASE IN BURN RATE TO +3 SIGMA CONDITIONS

| TIME | ----- X LONGITUDINAL LOCATIONS ----- | | | | | | | NOZZLE STAGNATION PRESSURE |
|------|--------------------------------------|-------------------|-------------------|---------------------|--------------------|--------------------|--------------------|----------------------------------|
| | 486.4 HEADEND | 530.0 FWD DOME | 851.5 F/FC JNT | 1171.5 FC/AC JNT | 1491.5 AC/A JNT | 1577.5 AFT FACT | 1816.7 AFT DOME | |
| | CHAMBER PRESSURES (PSIA) | | | | | | | |
| 0.2 | 468.4 | 467.9 | 451.9 | 440.8 | 431.1 | 431.0 | 436.1 | 304.0 |
| 0.4 | 940.0 | 938.7 | 880.1 | 842.5 | 808.8 | 808.1 | 823.8 | 721.2 |
| 0.6 | 1012.2 | 987.2 | 921.1 | 871.2 | 824.4 | 823.5 | 847.4 | 698.6 |
| 0.8 | 1014.4 | 1002.2 | 938.5 | 889.7 | 844.4 | 843.6 | 866.6 | 903.4 |
| 1.0 | 1007.1 | 1006.0 | 945.4 | 898.6 | 855.1 | 854.3 | 876.2 | 897.6 |
| 2.0 | 995.8 | 995.9 | 941.7 | 897.6 | 856.4 | 855.2 | 875.6 | 898.1 |
| 4.0 | 984.1 | 983.3 | 937.8 | 898.0 | 860.4 | 858.9 | 876.5 | 902.0 |
| 6.0 | 988.1 | 987.6 | 947.9 | 911.4 | 878.3 | 874.8 | 890.3 | 919.3 |
| 8.0 | 986.1 | 985.7 | 952.0 | 918.9 | 889.2 | 884.8 | 897.9 | 924.7 |
| 10.0 | 985.3 | 984.9 | 956.1 | 926.1 | 899.0 | 894.1 | 905.4 | 930.0 |
| 12.0 | 982.0 | 981.7 | 956.7 | 929.6 | 904.6 | 899.9 | 909.4 | 932.1 |
| 14.0 | 975.4 | 975.2 | 953.5 | 929.0 | 906.0 | 901.3 | 909.5 | 930.2 |
| 16.0 | 971.5 | 971.3 | 952.2 | 930.0 | 908.8 | 904.3 | 911.2 | 930.3 |
| 18.0 | 968.7 | 968.5 | 951.7 | 931.5 | 911.8 | 907.5 | 913.4 | 931.0 |
| 20.0 | 960.2 | 960.1 | 945.9 | 927.6 | 909.1 | 905.1 | 909.9 | 925.9 |
| 22.0 | 921.5 | 921.4 | 910.1 | 894.1 | 877.1 | 873.2 | 876.9 | 891.0 |
| 24.0 | 885.9 | 885.8 | 876.8 | 862.7 | 847.1 | 843.5 | 846.3 | 858.7 |
| 26.0 | 856.9 | 856.8 | 849.6 | 837.1 | 822.8 | 819.4 | 821.4 | 832.4 |
| 28.0 | 831.7 | 831.7 | 825.8 | 814.8 | 801.5 | 798.3 | 799.7 | 809.6 |
| 30.0 | 808.3 | 808.3 | 803.6 | 793.7 | 781.5 | 778.4 | 779.3 | 788.3 |
| 32.0 | 786.3 | 786.3 | 782.5 | 773.8 | 762.4 | 759.5 | 760.1 | 768.1 |
| 34.0 | 764.9 | 764.9 | 762.0 | 754.2 | 743.7 | 741.0 | 741.2 | 748.4 |
| 36.0 | 745.8 | 745.8 | 743.5 | 736.6 | 726.8 | 724.2 | 724.2 | 730.7 |
| 38.0 | 727.6 | 727.6 | 725.9 | 719.7 | 710.6 | 708.2 | 708.0 | 713.9 |
| 40.0 | 712.9 | 712.8 | 711.5 | 706.0 | 697.5 | 695.2 | 694.8 | 700.3 |
| 42.0 | 701.0 | 701.0 | 699.9 | 694.9 | 687.0 | 684.8 | 684.3 | 689.4 |
| 44.0 | 690.1 | 690.1 | 689.2 | 684.8 | 677.3 | 675.2 | 674.5 | 679.2 |
| 46.0 | 676.0 | 676.0 | 675.2 | 671.0 | 664.0 | 662.0 | 661.3 | 665.8 |
| 48.0 | 664.6 | 664.6 | 663.9 | 660.0 | 653.4 | 651.6 | 650.8 | 655.1 |
| 50.0 | 666.9 | 666.9 | 666.3 | 662.6 | 656.3 | 654.6 | 653.8 | 657.9 |
| 52.0 | 672.7 | 672.7 | 672.1 | 668.6 | 662.6 | 660.9 | 660.1 | 664.0 |
| 54.0 | 677.8 | 677.8 | 677.3 | 673.9 | 668.2 | 666.6 | 665.8 | 669.6 |
| 56.0 | 683.4 | 683.4 | 682.9 | 679.7 | 674.2 | 672.7 | 671.9 | 675.5 |
| 58.0 | 687.9 | 687.9 | 687.4 | 684.4 | 679.1 | 677.7 | 676.9 | 680.3 |
| 60.0 | 692.3 | 692.3 | 691.8 | 689.0 | 684.0 | 682.6 | 681.8 | 685.1 |
| 62.0 | 695.8 | 695.8 | 695.4 | 692.7 | 687.9 | 686.6 | 685.8 | 689.0 |
| 64.0 | 699.2 | 699.2 | 698.8 | 696.2 | 691.7 | 690.4 | 689.6 | 692.7 |
| 66.0 | 701.1 | 701.1 | 700.7 | 698.3 | 693.9 | 692.7 | 691.9 | 694.8 |
| 68.0 | 702.2 | 702.2 | 701.8 | 699.5 | 695.3 | 694.2 | 693.4 | 696.2 |
| 70.0 | 702.5 | 702.5 | 702.2 | 700.0 | 695.9 | 694.9 | 694.1 | 696.8 |
| 72.0 | 696.1 | 696.1 | 695.7 | 693.6 | 689.7 | 688.6 | 687.8 | 690.6 |
| 74.0 | 678.3 | 678.3 | 677.9 | 675.9 | 672.1 | 671.0 | 670.3 | 673.1 |
| 76.0 | 661.8 | 661.8 | 661.5 | 659.5 | 655.8 | 654.8 | 654.1 | 656.9 |
| 78.0 | 642.3 | 642.3 | 642.0 | 640.0 | 636.5 | 635.5 | 634.8 | 637.7 |
| 80.0 | 619.1 | 619.1 | 618.8 | 617.0 | 613.7 | 612.7 | 611.9 | 614.9 |
| 82.0 | 600.3 | 600.3 | 600.0 | 598.2 | 595.0 | 594.1 | 593.4 | 596.3 |
| 84.0 | 591.2 | 591.2 | 590.9 | 589.2 | 586.1 | 585.2 | 584.6 | 587.4 |
| 86.0 | 574.9 | 574.8 | 574.6 | 573.0 | 570.0 | 569.1 | 568.6 | 571.3 |
| 88.0 | 553.9 | 553.9 | 553.7 | 552.1 | 549.2 | 548.4 | 548.0 | 550.6 |
| 90.0 | 539.0 | 539.0 | 538.8 | 537.3 | 534.4 | 533.6 | 533.3 | 535.9 |



Truss Members: P8 to P13
 Positive Tension
 Negative Compression

Orthogonal Loads: P14 to P19
 Positive Directions Shown
 Loads Applied to SRB's

FIG. A1 · SRB Attach Member Load Locations

ORIGINAL PAGE IS
 OF POOR QUALITY

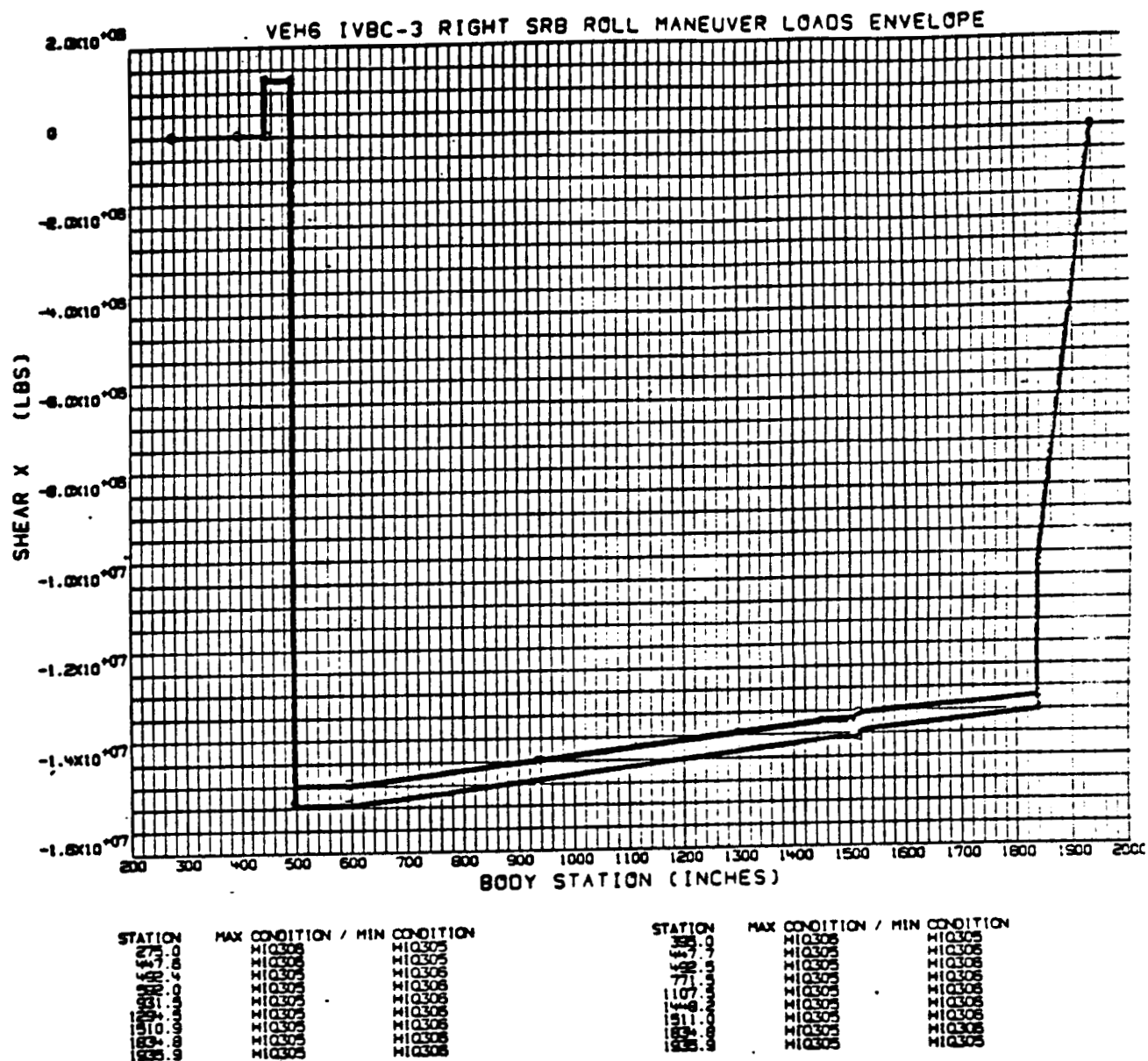


FIG. A2

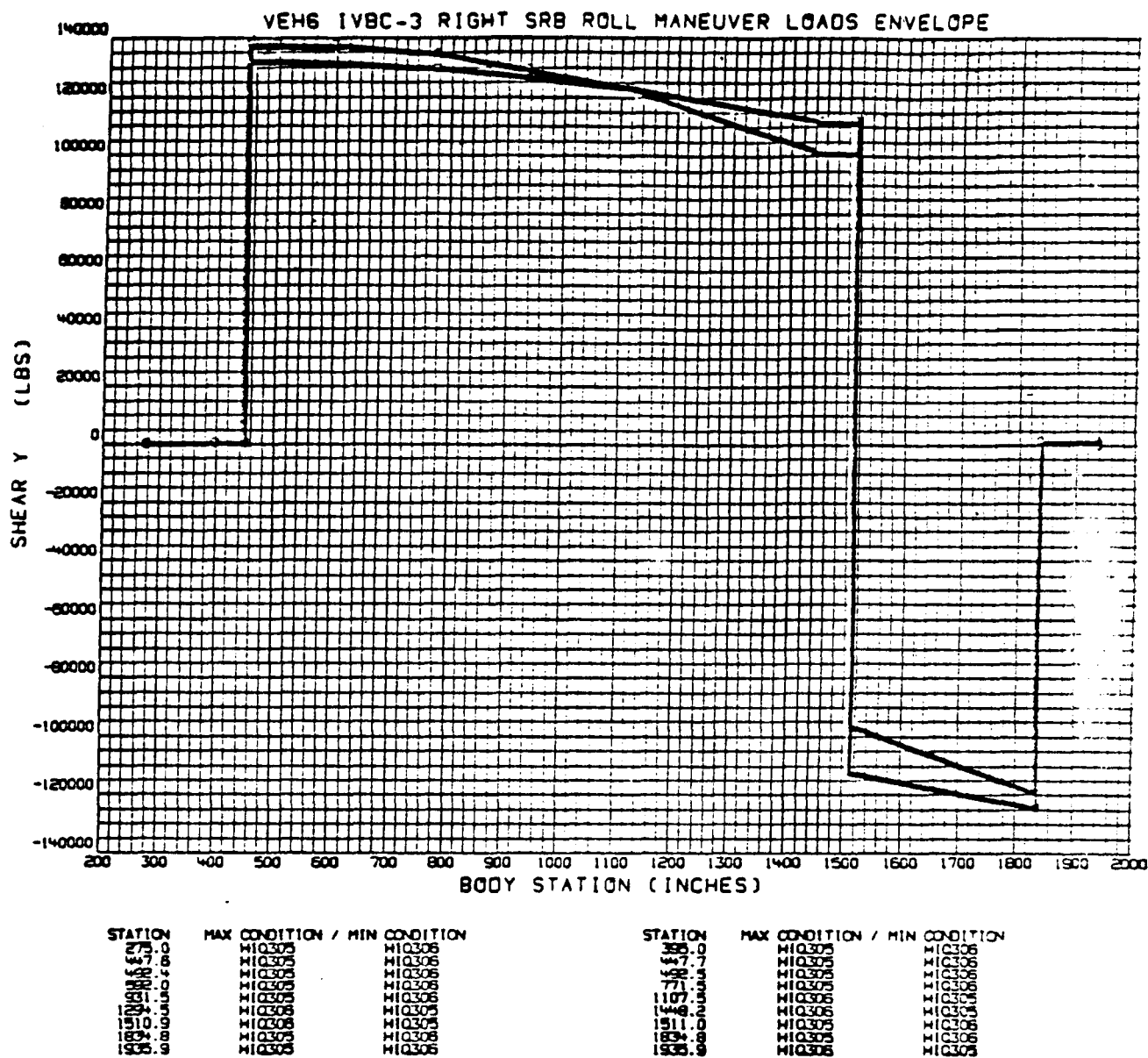


FIG. A3

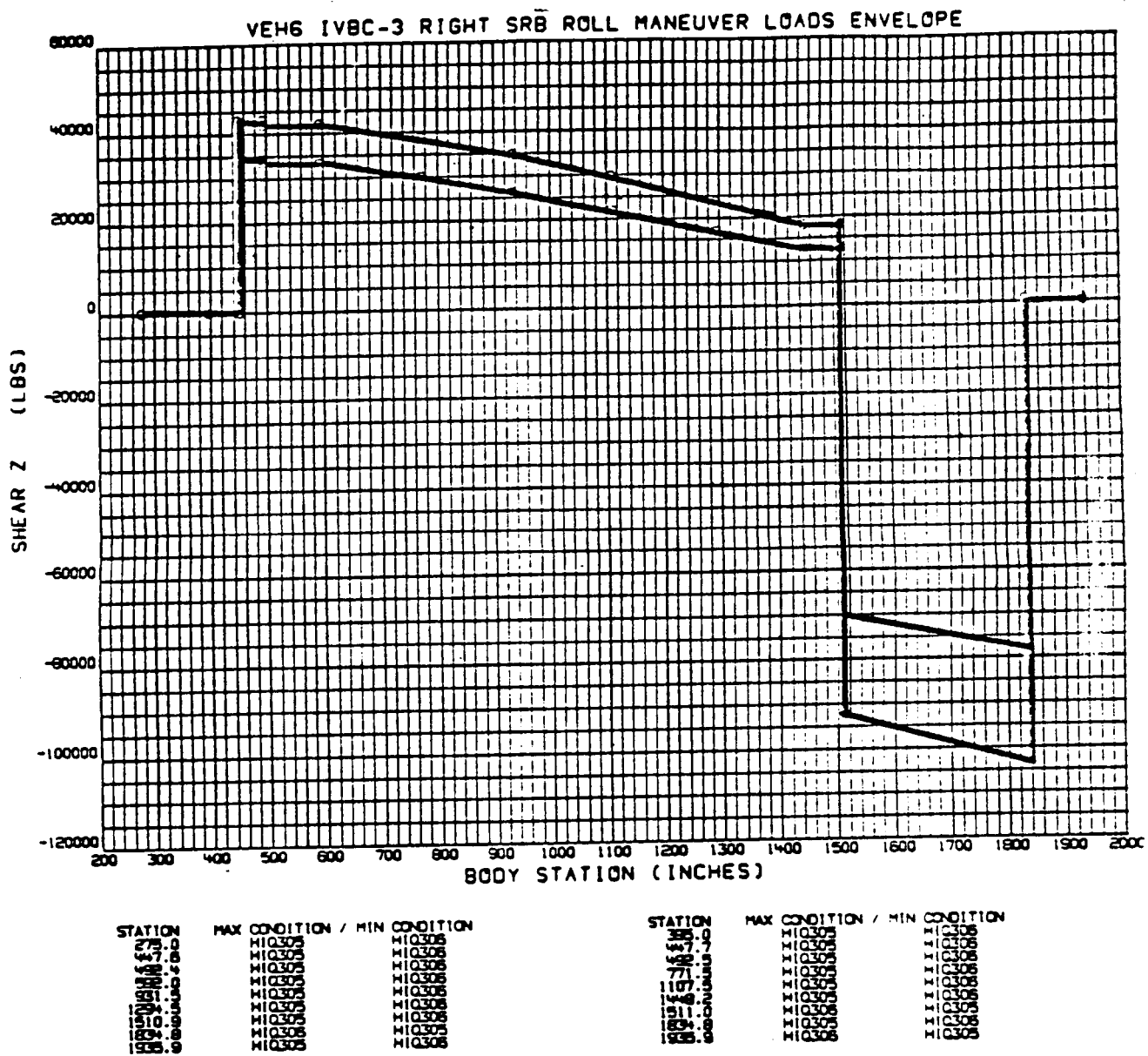


FIG. A4

TRACY JK
02/2/88

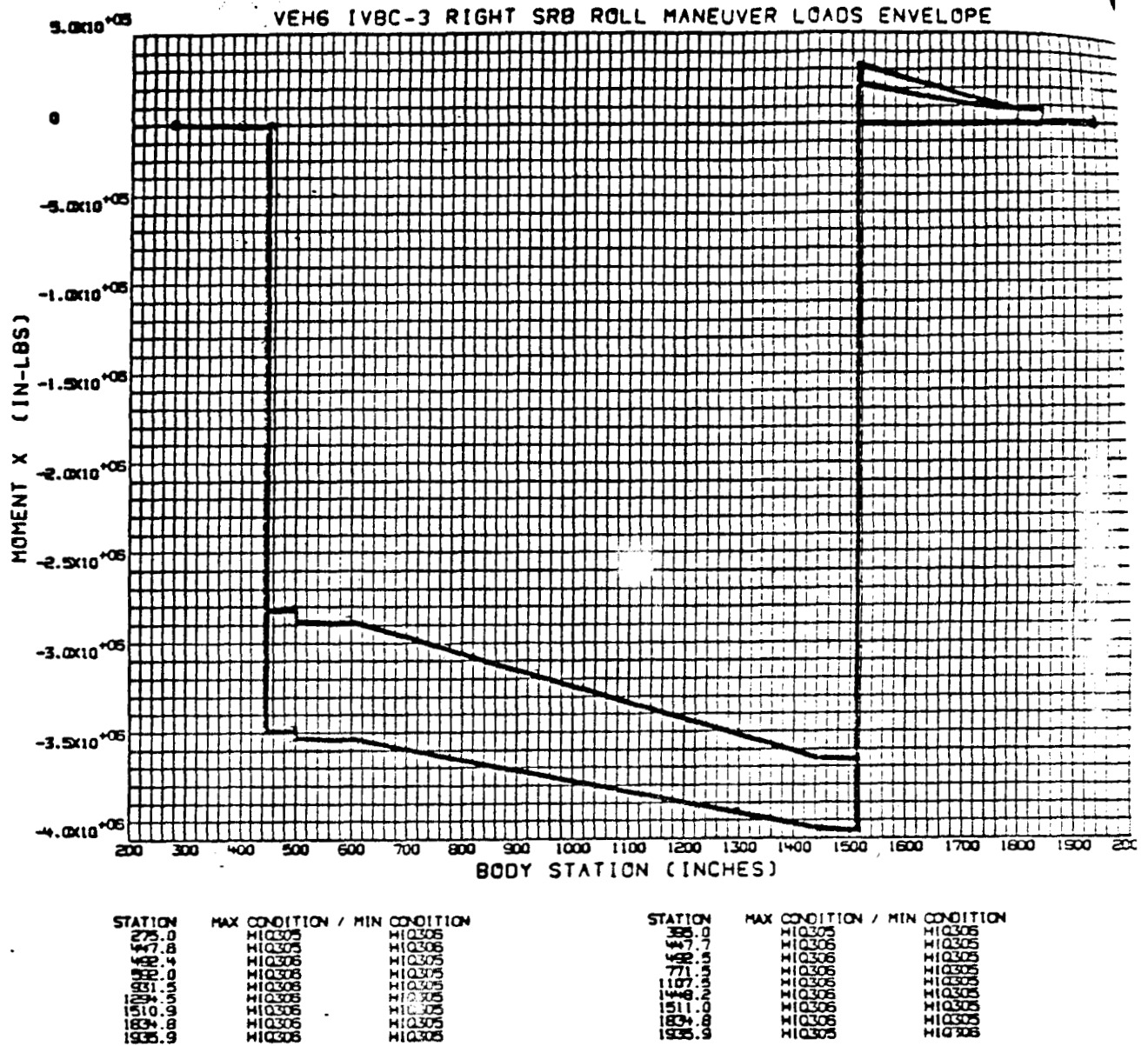
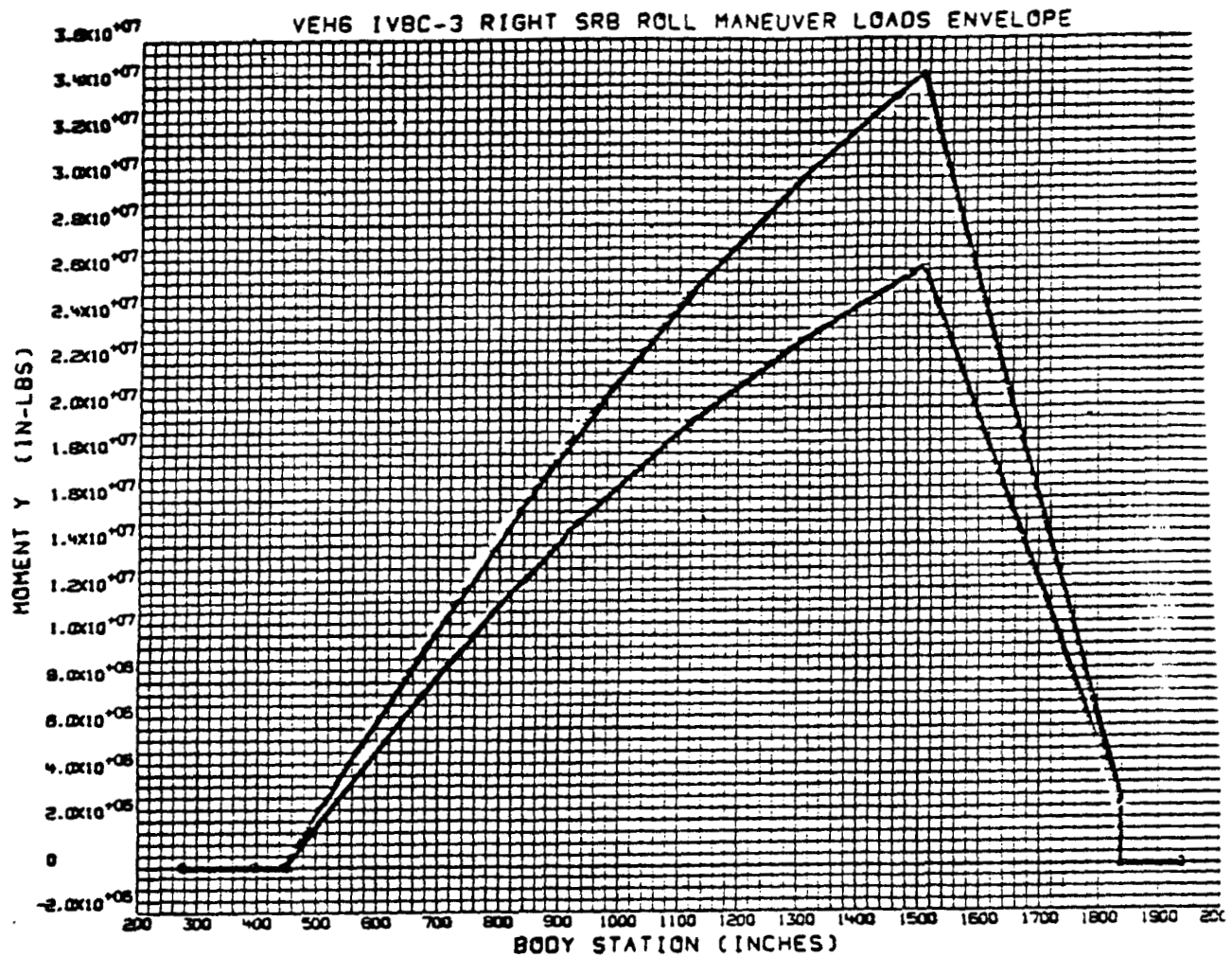


FIG. A5

ORIGINAL PAGE IS
OF POOR QUALITY

TRACY, JX
08/25/88



| STATION | MAX CONDITION / MIN CONDITION | STATION | MAX CONDITION / MIN CONDITION |
|---------|-------------------------------|---------|-------------------------------|
| 279.0 | H10305 / H10306 | 385.0 | H10305 / H10306 |
| 447.0 | H10305 / H10306 | 447.0 | H10305 / H10306 |
| 500.0 | H10305 / H10306 | 500.0 | H10305 / H10306 |
| 550.0 | H10305 / H10306 | 550.0 | H10305 / H10306 |
| 600.0 | H10305 / H10306 | 600.0 | H10305 / H10306 |
| 650.0 | H10305 / H10306 | 650.0 | H10305 / H10306 |
| 700.0 | H10305 / H10306 | 700.0 | H10305 / H10306 |
| 750.0 | H10305 / H10306 | 750.0 | H10305 / H10306 |
| 800.0 | H10305 / H10306 | 800.0 | H10305 / H10306 |
| 850.0 | H10305 / H10306 | 850.0 | H10305 / H10306 |
| 900.0 | H10305 / H10306 | 900.0 | H10305 / H10306 |
| 950.0 | H10305 / H10306 | 950.0 | H10305 / H10306 |
| 1000.0 | H10305 / H10306 | 1000.0 | H10305 / H10306 |
| 1050.0 | H10305 / H10306 | 1050.0 | H10305 / H10306 |
| 1100.0 | H10305 / H10306 | 1100.0 | H10305 / H10306 |
| 1150.0 | H10305 / H10306 | 1150.0 | H10305 / H10306 |
| 1200.0 | H10305 / H10306 | 1200.0 | H10305 / H10306 |
| 1250.0 | H10305 / H10306 | 1250.0 | H10305 / H10306 |
| 1300.0 | H10305 / H10306 | 1300.0 | H10305 / H10306 |
| 1350.0 | H10305 / H10306 | 1350.0 | H10305 / H10306 |
| 1400.0 | H10305 / H10306 | 1400.0 | H10305 / H10306 |
| 1450.0 | H10305 / H10306 | 1450.0 | H10305 / H10306 |
| 1500.0 | H10305 / H10306 | 1500.0 | H10305 / H10306 |
| 1550.0 | H10305 / H10306 | 1550.0 | H10305 / H10306 |
| 1600.0 | H10305 / H10306 | 1600.0 | H10305 / H10306 |
| 1650.0 | H10305 / H10306 | 1650.0 | H10305 / H10306 |
| 1700.0 | H10305 / H10306 | 1700.0 | H10305 / H10306 |
| 1750.0 | H10305 / H10306 | 1750.0 | H10305 / H10306 |
| 1800.0 | H10305 / H10306 | 1800.0 | H10305 / H10306 |
| 1850.0 | H10305 / H10306 | 1850.0 | H10305 / H10306 |
| 1900.0 | H10305 / H10306 | 1900.0 | H10305 / H10306 |
| 1950.0 | H10305 / H10306 | 1950.0 | H10305 / H10306 |
| 2000.0 | H10305 / H10306 | 2000.0 | H10305 / H10306 |

FIG. A6

C-2

TRACY, X
08/25/88



95

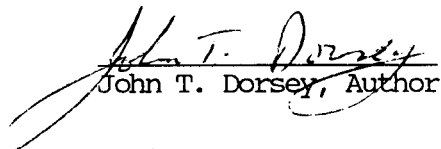
APPENDIX B

GLOBAL LINEAR AND NONLINEAR STRUCTURAL ANALYSIS

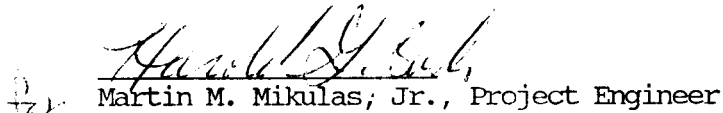
by John T. Dorsey
Mail Stop 190
NASA Langley Research Center
Hampton, VA 23665

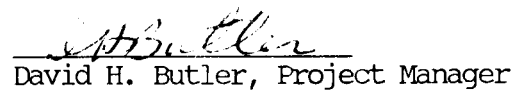
Phone: (804) 865-2892

June 11, 1987


John T. Dorsey, Author


Mark S. Lake, Reviewer


Martin M. Mikulas, Jr., Project Engineer


David H. Butler, Project Manager

APPENDIX B

GLOBAL LINEAR AND NONLINEAR STRUCTURAL ANALYSIS

INTRODUCTION

In this appendix the global finite element models and analysis results which contributed to the LaRC External Tank Attach (ETA) ring redesign effort are described. The analysis is considered global because the entire ETA ring as well as the portion of the Solid Rocket Motor (SRM) case where the ring is attached is modeled. Other finite element analyses which deal with local regions, such as the end of the web, were also performed and details appear in other appendices.

The finite element models described in this appendix are also considered to be simplified models because they do not contain structural details such as H-fittings, splice plates, intercostals, or tang-to-web and web-to-cap bolts. These simplifications have been made to reduce computer run times while retaining the basic physical and mechanical behavior of the ETA ring as well as its interaction with the SRM case so that only details which affect global behavior are studied. In particular, it is desired to understand how stresses are developed in the ETA ring when the SRM is pressurized. Finally, stress results obtained with the global model are used as input for some of the local analyses described in other appendices.

ANALYSIS

Loads

The design loads defined in Appendix A correspond to the Shuttle roll maneuver, at which time the pressure inside the SRM is 912 psia. The internal rocket pressure can be resolved into two components, a radial component and an axial component as shown in figure B1. The axial load component is a result of the internal pressure acting on the forward dome and tends to elongate the rocket.

One effect which needs to be understood and quantified is the loading induced in the ETA ring due to the axial load component. A stiffener attached to a plate, as shown in figure B2, is given as a simplified representation of the ETA ring attached to the SRM. When the plate is loaded in tension parallel to the stiffener (as on the left side of figure B2), the poisson effect causes the plate to contract in a direction perpendicular to the loading which does not add any load to the stiffener. However, when a tension load is applied perpendicular to the direction of the stiffener as shown on the right side of figure B2, the stiffener restrains the plate from contracting. Thus the poisson effect now causes a compressive load to develop in the stiffener. Similarly, the axial load component in the SRM will induce a compressive load in the ETA ring due to the poisson effect and the importance of this effect must be assessed.

Finite Element Model

The simplified finite element model developed for the global analyses is shown in figure B3. The partial ring shown is the existing design which was

flown on flight 51-L. For ease of modeling, a plane of symmetry is assumed to exist between the two webs of the ETA ring and thus, only one web and half of the cover plate is modeled as shown at the top of figure B3. The total length of SRM case modeled is 34.4 inches, which is long enough so that the stresses in the free shell away from the web agree with the theoretical solution for an infinite cylinder with internal pressure loading. The average radius for the SRM case, or shell, wall is 72.8 inches. The thickness of the case wall in the region of the attach ring is 0.58 inch and in the free shell away from the ring, 0.479 inch.

The finite element model is comprised of five components; the SRM case wall (shell), the tang, the web, the cap, and the cover plate. All five components are assumed to be made of steel and have a Young's modulus of 30.0 million psi. The finite element model has approximately 13,000 degrees of freedom and 2517 elements grouped as follows: the cap is represented by 137 beam elements; the tang is represented by 191 beam elements; the case wall is represented by 1528 plate elements; the web is represented by 520 plate elements; and the cover plate is represented by 141 plate elements. The cover plate has orthotropic properties giving it stiffness in the booster longitudinal direction (which prevents the two webs from deflecting laterally relative to each other), but no circumferential stiffness (so that it does not add to the hoop stiffness of the ETA ring). Since tang-to-web and web-to-cap bolts are not included, the model represents a one piece structure (that is, acts like it is welded together).

The boundary conditions at the top of the model (at the cut between the two webs) are chosen to make the R-theta plane a symmetry plane. At the bottom of the model (the free shell end), radial and axial displacements are allowed while circumferential displacements are constrained. An internal pressure of 912 psi is applied to the inside of the booster to give the radial load component. The total axial load on the booster corresponding to 912 psi is 15.1 million pounds. The total axial load is applied as a lineal load of 33,078 lbf/in in the -Z direction around the circumference at the free end of the shell.

A finite element model was also constructed for a full (360°) ETA ring concept. The details of this model are the same as those described for the partial ring concept, except that the tang, web, cap and cover plate completely encircle the SRM case. The full ring model has approximately 13,500 degrees of freedom, 360 beam elements and 2340 plate elements.

Linear Results

Figure B4 shows the circumferential stresses in the partial ring model due to an internal pressure of 912 psi. The stresses shown are taken at the section labeled A-A on figure B5, a point which is located in the portion of the ring midway between the two ring ends. Globally, the maximum circumferential stresses in the cap, web, and tang occur at this location. Stresses are shown in these components for two load cases: (1) the radial component of pressure only, and (2) both the radial and the axial pressure components. The compressive stress induced by the poisson effect discussed in figure B2 reduces the stress levels in all of the ETA ring components by approximately 18 percent.

Similarly, stress results are shown in figure B6 for the full ring model at the section A-A shown in figure B7. The maximum stresses in the cap, web, and tang are almost identical for the full ring and the partial ring models.

The full ring model also shows an approximately 18 percent reduction in stresses in the ETA ring due to the poisson effect induced by the axial load component.

Circumferential stresses in the partial ring model are shown along the length of the shell at section B-B (see figure B5) in figure B8. Location B-B corresponds to the section of case wall where no ring exists and is midway between the two ring ends. The boundaries and thicknesses of the plate elements making up the shell are indicated and the ETA ring is attached at the boundary between the second and third element from the top. Stresses for 912 psi internal pressure are given for the 2 load cases; the radial pressure component only, and both the radial and axial pressure components. These are compared to an analytical solution for the shell ($\text{stress} = \text{pressure} \times \text{radius} / \text{thickness}$). As expected, the axial load component has negligible effect on the circumferential stresses in the case wall. In the vicinity of the ring however, the case wall circumferential stresses are reduced from those predicted by the analytical solution by approximately 10 percent whereas away from the ring, the finite element and analytical solutions agree to within 1 percent.

In the actual SRM case, the center of a field joint is located 19.5 inches from the midpoint between the two webs of the ETA ring. A simplified representation of the field joint is added to the partial ring model to determine the effect of the field joint on ring stresses. The field joint, represented by an annulus with a width of 6 inches and a thickness of 1.1 inches, is centered 13.5 inches down from the tang. Because of the symmetry boundary condition imposed at the top of the model however, the actual situation being modeled is one where a field joint is on both sides of the ETA ring. Figure B9 shows the circumferential stresses at section A-A of the partial ring model with and without the field joint present. The presence of the field joint has little effect (<2 percent) on stresses in the ETA ring.

Nonlinear Results

A geometric nonlinear analysis using full Newton-Raphson integration was also run for the partial ring model for the 912 psi internal pressure loading case. The nonlinear analysis allows the bending stiffness due to membrane stresses in the case wall to be included in the problem. The purpose of running the nonlinear analysis is to assess the effect of this added shell bending stiffness as well as to ascertain if any unforeseen nonlinearities change the solution significantly from that obtained in the linear analysis.

The deflection shape of the partial ETA ring model (as viewed along the Z axis) is shown in figure B10. The linear and nonlinear radial displacements at various locations around the shell are also shown (the displacements shown are given at the location along the shell corresponding to where the web is attached). The nonlinear displacements at the two ends of the web are approximately 8 percent larger than the corresponding linear displacements. The largest difference between the linear and nonlinear displacement is approximately 23 percent and occurs at a location one fourth of the way between the two ends of the web. The partial ring deflection at A-A for the linear (.149 inch) and the nonlinear (.140 inch) solutions can be compared to the full ring linear displacement which is .141 inch.

Stresses in the various components of the partial ring model are compared for the nonlinear and linear cases of a 912 psi internal pressure load in figure B11. This figure summarizes the global stress results in that only the

circumferential stress at the center of an element is included for the plate elements, and only the axial stress for the beam elements is included. For each component, all of the stress results are scanned and only the maximum, and or minimum are given, with no reference to location in the model. The figure indicates that nonlinearities have a small (<8 percent) effect on global stresses.

Locally however, nonlinearities can have a slightly larger effect on element stresses as shown in figure B12. In this figure, the maximum stress in the tang at the end of the web (on the end where the cap does not go all the way to the end) is shown. The nonlinear solution gives a 7.8 percent reduction in the tang axial load (consistent with the results shown in the previous figure) and a 20.1 percent reduction in the tang bending moment. Thus the maximum stress in the tang outer fiber is reduced by 12.1 percent.

CONCLUSIONS

In summary, the following conclusions can be drawn from the analyses presented in this appendix:

1. The maximum stresses in the ETA ring are the same for the full ring and partial ring concepts.
2. The field joint which is located near the ETA ring has negligible effect on the ring stresses.
3. Nonlinearities have a small effect (<8 percent) on stresses globally, but can have a moderate effect (on the order of 12 percent) on local stresses.

APPLIED LOADS FOR EXTERNAL TANK ATTACH RING FINITE ELEMENT MODEL

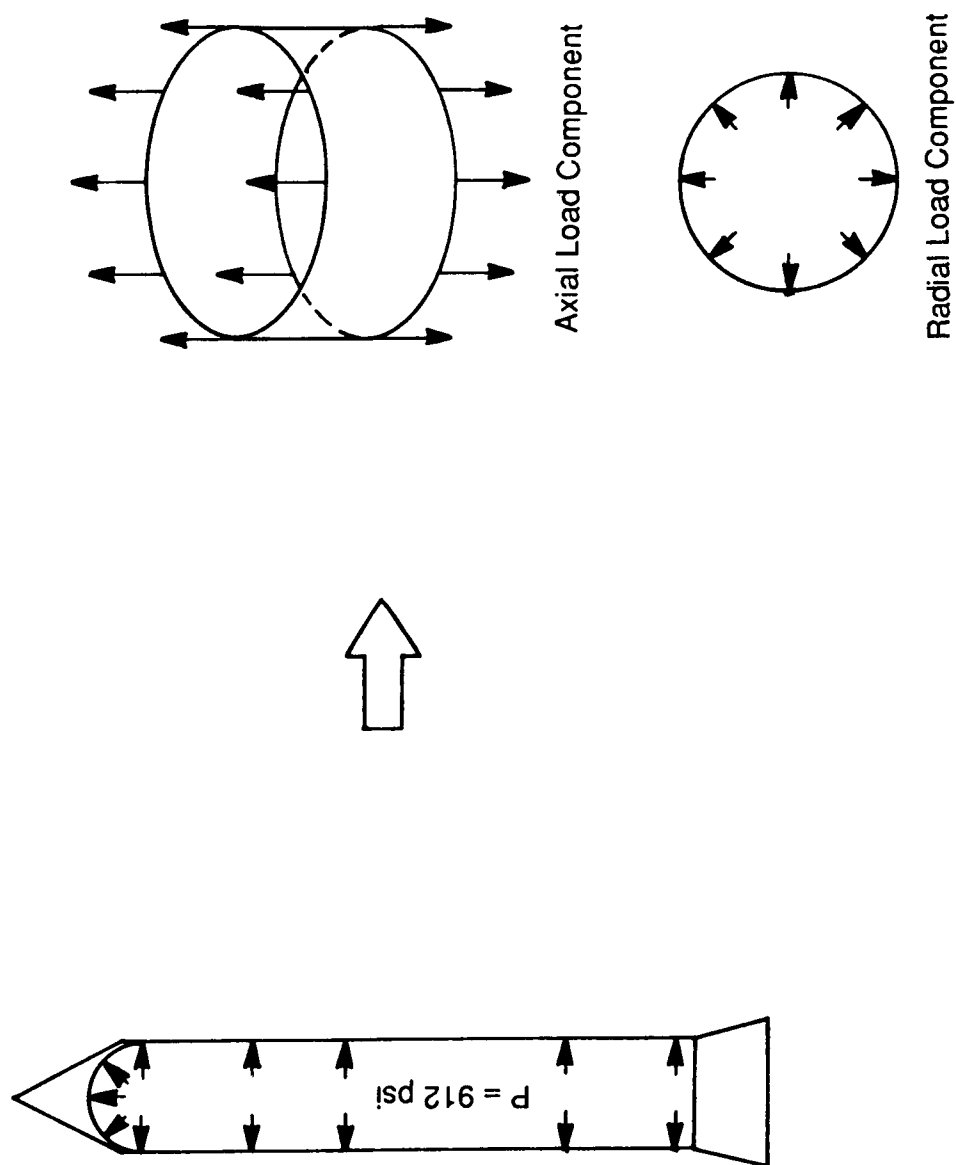
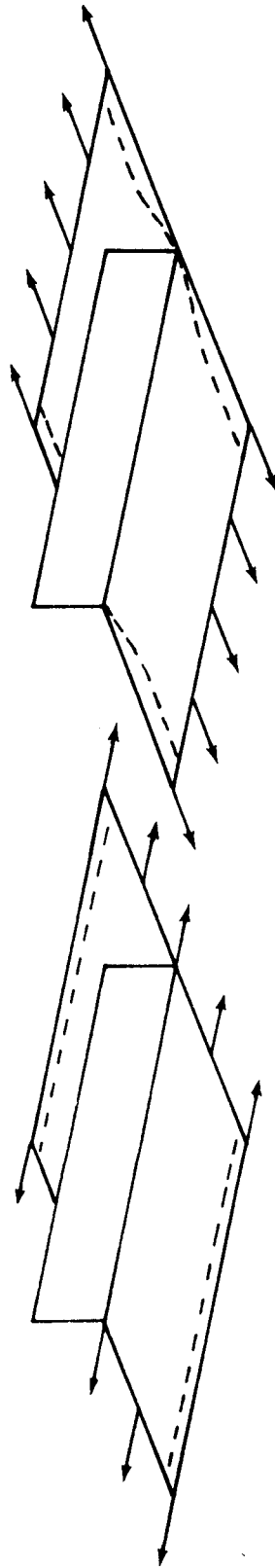


Figure B1.

POISSON EFFECT CAUSES LOADING IN WEB



Poisson effect causes no load
in stiffner

Poisson effect causes compression load
in stiffner

Figure B2.

PARTIAL RING FINITE ELEMENT MODEL

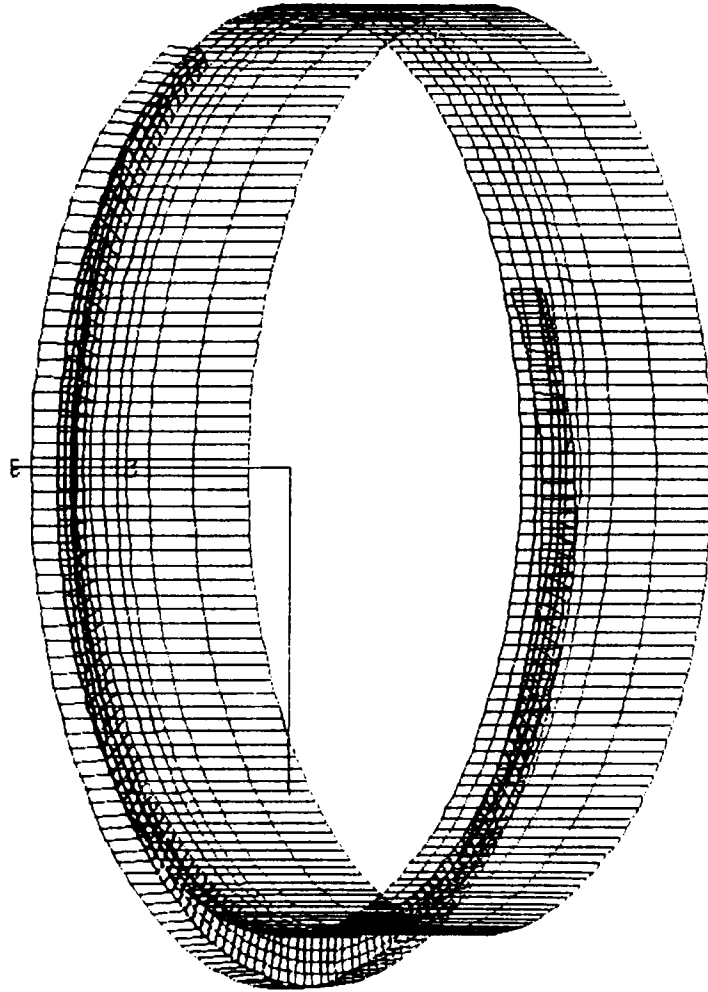


Figure B3.

CIRCUMFERENTIAL STRESSES IN RING OF PARTIAL RING MODEL (912 psi Internal Pressure)

| STRESS, ksi | | Radial load component only | A |
|--------------------------------------|------|-------------------------------|---|
| Radial plus axial load components | | | |
| 45.1 | 54.6 | CAP | A |
| 49.3 | 60.2 | | |
| 50.8 | 62.0 | WEB | A |
| 52.4 | 64.1 | | |
| 53.5 | 66.0 | | A |
| 57.2 | 69.8 | TANG | |
| 78.4 | 74.5 | CASE WALL | A |

Figure B4.

PARTIAL RING MODEL - WEB PLATFORM

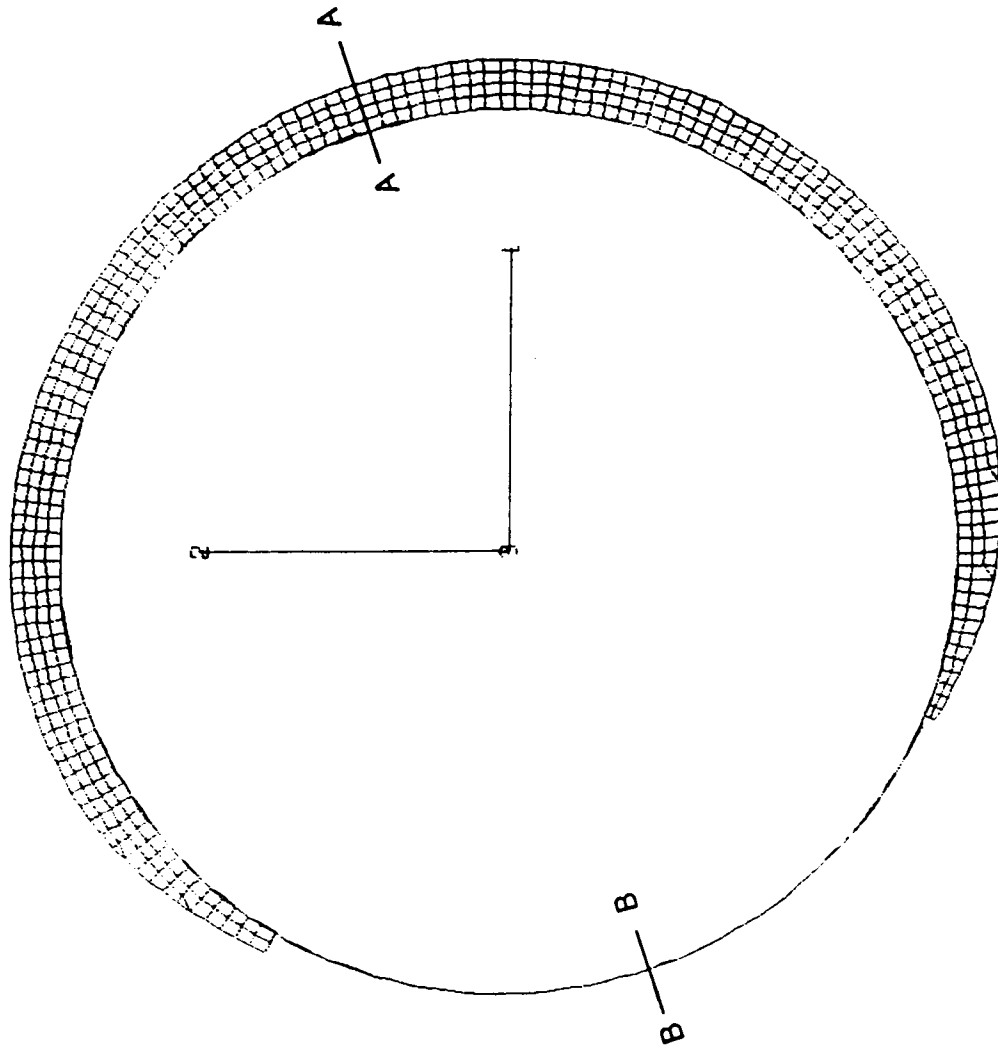


Figure B5.

CIRCUMFERENTIAL STRESSES IN RING OF FULL RING MODEL (912 psi Internal Pressure)

STRESS, ksi

| Radial plus axial load components | Radial load component only | A |
|--------------------------------------|-------------------------------|-----------|
| 45.5 | 55.1 | CAP |
| 49.7 | 60.7 | |
| 51.0 | 62.3 | WEB |
| 52.5 | 64.1 | |
| 53.9 | 65.8 | |
| 57.0 | 69.6 | TANG |
| 78.1 | 74.2 | CASE WALL |
| | | A |

Figure B6.

FULL RING MODEL - WEB PLATFORM

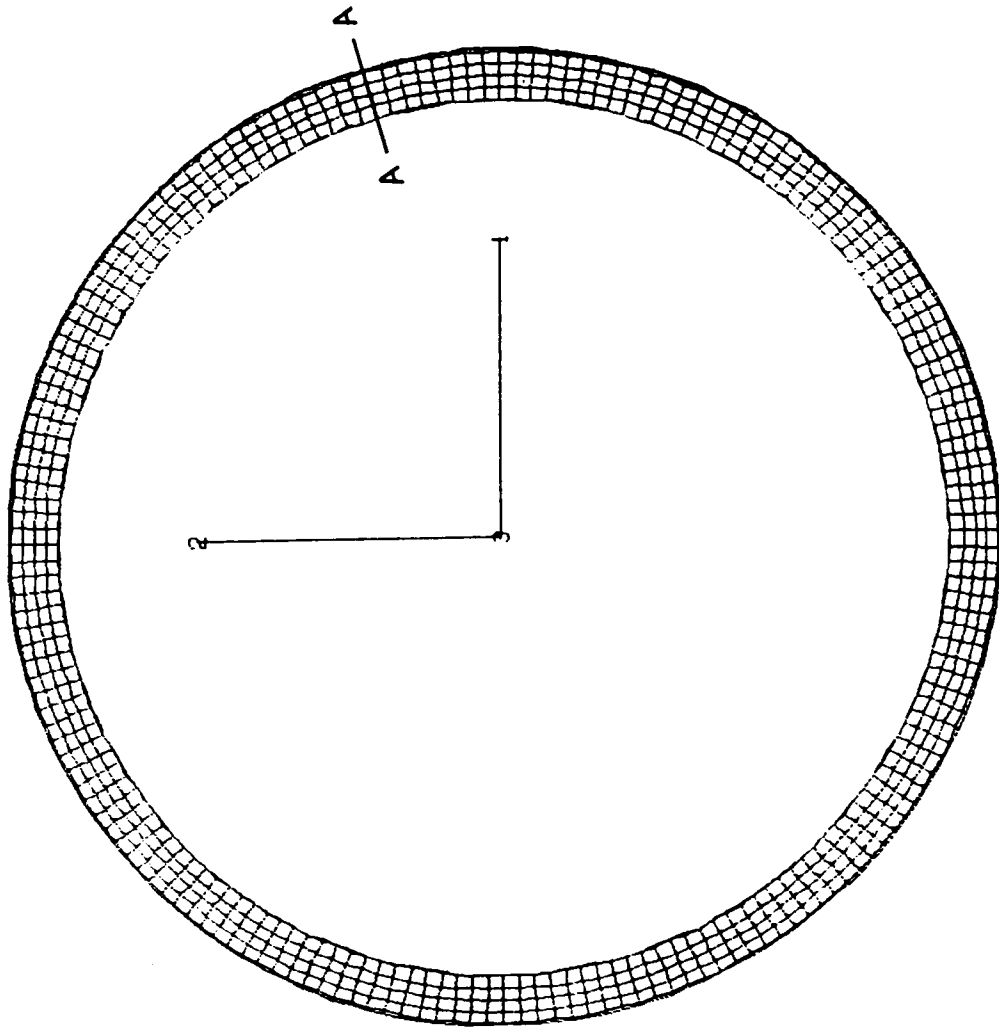


Figure B7.

CIRCUMFERENTIAL STRESSES IN SHELL OF PARTIAL RING MODEL (912 psi Internal Pressure)

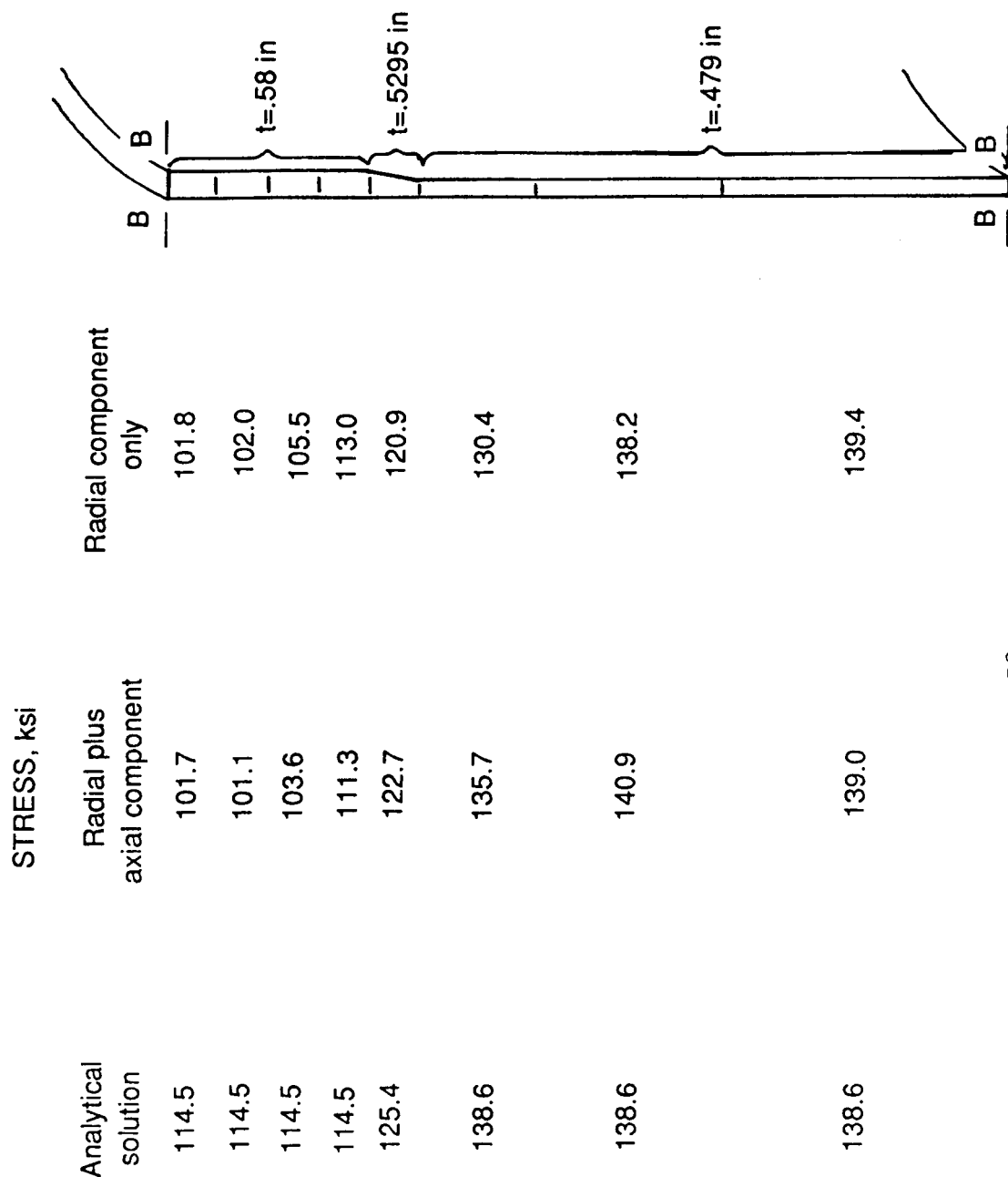


Figure B8.

EFFECT OF FIELD JOINT ON PARTIAL RING STRESSES (912 psi Internal Pressure)

STRESS, ksi

| No field joint | With field joint | Δ % | |
|----------------|------------------|------------|-----------|
| 45.1 | 45.8 | +1.6 | CAP |
| 49.3 | 49.7 | +0.8 | |
| 50.8 | 51.2 | +0.8 | |
| 52.4 | 52.8 | +0.8 | WEB |
| 53.5 | 54.4 | +1.7 | |
| 57.2 | 57.5 | +0.5 | TANG |
| 78.4 | 78.2 | -0.3 | CASE WALL |
| WEB MAX: 95.9 | 96.7 | +0.8 | |

Figure B9.

RADIAL DISPLACEMENTS ON PARTIAL RING MODEL DUE TO INTERNAL PRESSURE (912 psi)

Radial Deflection (in) = Linear/Nonlinear

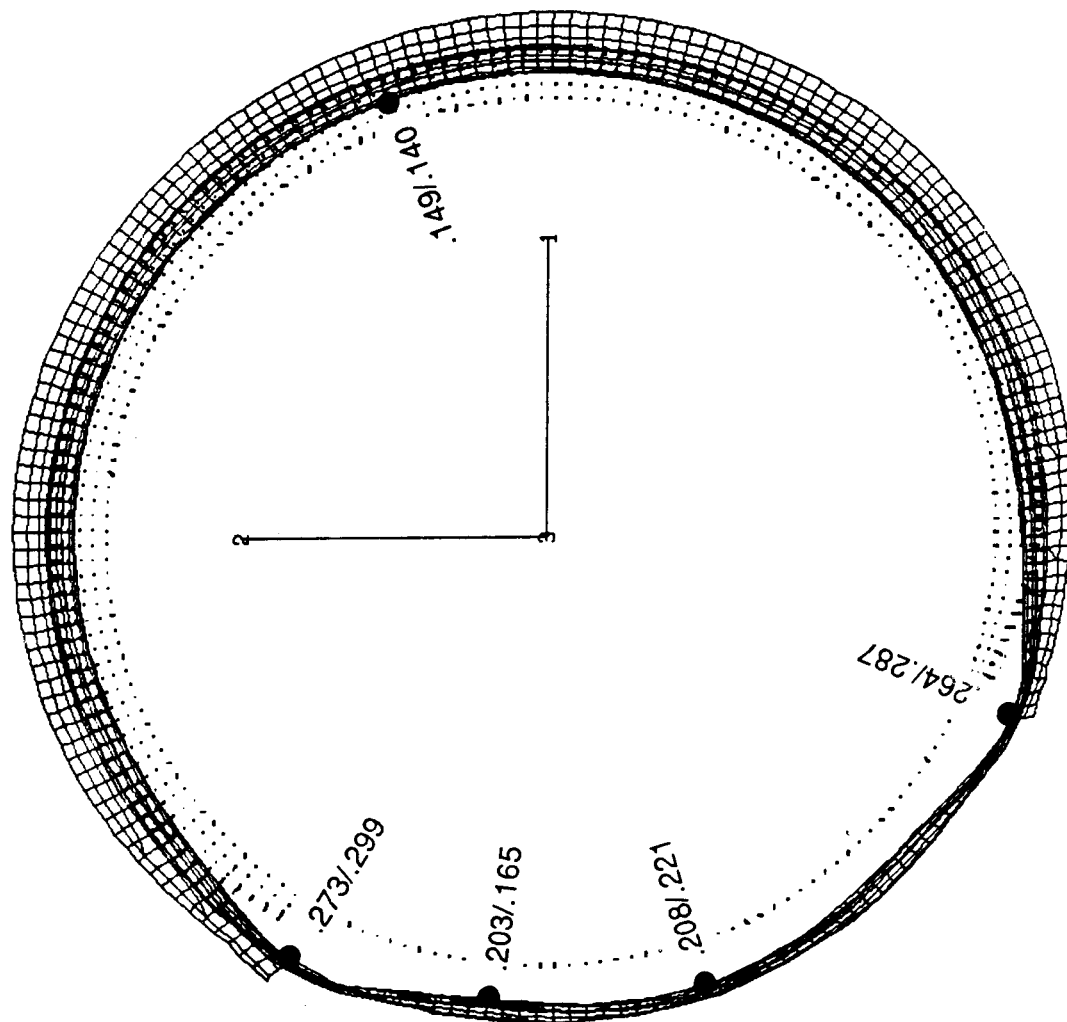


Figure B10.

PARTIAL RING - SUMMARY OF STRESS RESULTS*

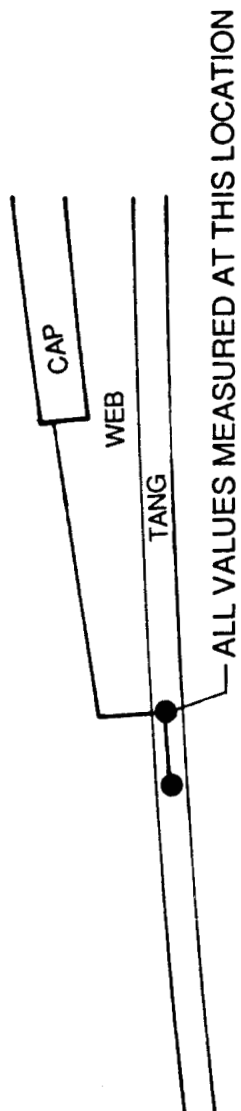
| Component† | STRESS, ksi | | Δ % |
|------------|-------------|-----------|------|
| | Linear | Nonlinear | |
| CAP | 45.1 | 48.0 | +6.4 |
| TANG | 57.2 | 60.9 | +6.5 |
| | 130.0 | 119.9 | -7.8 |
| CASE WALL | | | +4.4 |
| | | | -3.3 |
| WEB | 50.8 | 54.2 | +6.6 |

*912 psi internal pressure, radial and axial components

†Max/Min given for each component

Figure B11.

LOCAL TANG BENDING AT END OF WEB (912 PSI)



| | LINEAR | NONLINEAR | Δ % |
|------------------------|--------|-----------|------------|
| PZ, lbf | 86443. | 79734. | -7.76 |
| MY, in-lbf | 11818. | 9348. | -20.90 |
| σ_{MAX}^* , ksi | 195.5 | 171.8 | -12.12 |

$$*\sigma = \frac{PZ}{A} + \frac{MY \times Z}{I} : A = .6616 \text{ in}^2 \quad Z = .827 \text{ in} \quad I = .1508 \text{ in}^4$$

Figure B12.

APPENDIX C

RING AREA TAPERING ANALYSIS

by Mark S. Lake and W. B. Fichter
Mail Stop 190
Langley Research Center
Hampton, Virginia 23665
Phone (804) 865-2414, -3596

June 23, 1987

Mark S. Lake
Mark S. Lake, Co-Author

W. B. Fichter
W. B. Fichter, Co-Author

John T. Dorsey
John T. Dorsey, Reviewer

Harold M. Mikulas
for Martin M. Mikulas, Jr., Project Engineer

D. H. Butler
David H. Butler, Project Manager

INTRODUCTION

The existing Space Shuttle Solid Rocket Booster (SRB) external tank attachment (ETA) ring includes two different tapered end designs. Both ends exhibit high loads in the web-to-tang and web-to-cap bolts due to insufficient tapering of the web and cap cross-sections. The primary goal of this redesign effort is to develop a tapered design for the ETA ring which has bolts loaded well below their limit values while maintaining acceptable stress levels within the web and cap. The analyses that have been developed to optimize the cross-sectional area taper profile of the ETA ring are discussed in this appendix along with a summary of the appropriate design loads applied to the ring.

RING LOADS

In order to develop analyses to optimize the ring area taper profile it is important to understand the loads applied to the ring. Figure C-1 shows a segment of the existing ETA ring and SRB motor case wall extending from just beyond the end of the ring to a location where the ring cross-section and stresses are constant. The loads applied at these two boundaries represent average circumferential stress resultants within the motor case and ring for an internal motor case pressure of 912 psi. As shown in Appendix B the corresponding stresses are approximately 110 ksi. in the motor case beyond the end of the ring, 80 ksi. in the motor case, and 55 ksi. in the constant cross-section area of the ring.

If shear stresses in the motor case are neglected, balancing forces in the circumferential direction results in equation (C-1), which defines an effective motor case area, A_{eff} , that must be assumed to transfer load into the ring.² For the given stresses and the nominal ring cross-sectional area of 3.56 in², that effective motor case area is 6.5 in².

$$(110 \text{ ksi})(A_{eff}) = (55 \text{ ksi})(3.56 \text{ in}^2) + (80 \text{ ksi})(A_{eff}) \quad (C-1)$$

Stresses within the ring result from the loads in the bolts that attach the ring to the motor case tang. An important observation is that the circumferential stress resultant at any cross-section around the ring must be equal to the sum of the circumferential component of bolt loads up to that point. Therefore, in a redesigned tapered ring having constant bolt loads of 10,000 lb for example, 20 bolts are required to develop the existing stress resultant of 196,000 lb. In the following sections, the analyses needed to design a taper profile for the ETA ring with correctly prescribed bolt load distributions are presented.

RING AREA TAPERING WITH RIGID BOLT ASSUMPTIONS

A simplified 1-D analysis is developed to study the transfer of circumferential load from the pressurized shell (motor case) through the tang

bolts to the ring, and to also investigate tapering of the ring area. The assumptions for this analysis are as follows: (1) tang bolts are rigid, (2) strains in the ring and shell between any two adjacent tang bolts are constant, (3) the shell can be represented as a bar with constant cross-sectional area of 6.5 in² (as calculated in the previous section), (4) curvature in the shell and ring can be neglected and, (5) the cap area is lumped with the web area and cap bolts are not considered. Furthermore, from assumption (2) it follows that the ring can be treated as having constant area between any two adjacent tang bolts, and that any changes in ring area occur coincident with a tang bolt. Figure C-2 illustrates this simplified representation of the ring and shell.

Equilibrium of forces at the nth section of the ring between the tang bolts numbered n and n+1 requires that the sum of the ring stress resultant, P_{rn}, and the shell stress resultant, P_{sn} equal the applied far-field shell stress resultant P_{ff}, or

$$P_{ff} = P_{rn} + P_{sn} \quad (C-2)$$

The rigid bolt assumption forces equality of ring and shell strains in every section. Hence, equation (C-2) can be rewritten as

$$P_{ff} = E \epsilon_n (A_{rn} + A_s) \quad (C-3)$$

where A_{rn} is the ring cross-sectional area in the nth section, A_s is the shell cross-sectional area, which is assumed constant, and E is their common Young's modulus. Therefore, the strain in the nth section of both the ring and shell is

$$\epsilon_n = \frac{P_{ff}}{E(A_{rn} + A_s)} \quad (C-4)$$

Applying Hooke's law to equation (C-4) at the nth section of the ring gives an expression for the stress resultant at that section:

$$P_{rn} = EA_{rn} \epsilon_n = \frac{P_{ff} A_{rn}}{(A_{rn} + A_s)} \quad (C-5)$$

The load in a bolt (P_{bn}) that borders the two sections n and n-1 is given by the difference between the stress resultants in those two sections, or

$$P_{bn} = P_{rn} - P_{r(n-1)} = P_{ff} \left(\frac{A_{rn}}{A_{rn} + A_s} - \frac{A_{r(n-1)}}{A_{r(n-1)} + A_s} \right) \quad (C-6)$$

Given an area taper profile for the ring, A_{rn} , the recursion relation of equation (C-6) can be used to calculate a bolt load distribution, P_{bn} . Conversely, equation (C-6) can be rewritten to give a recursion relation for calculating the area taper profile if the bolt load distribution is specified:

$$A_{rn} = \frac{A_s [P_{bn}/P_{ff} + A_{r(n-1)}/(A_{r(n-1)} + A_s)]}{[1 - P_{bn}/P_{ff} - A_{r(n-1)}/(A_{r(n-1)} + A_s)]} \quad (C-7)$$

A first-iteration optimized area profile for the ETA ring is determined using equation (C-7) and assuming the constant 10,000 lb tang bolt load distribution mentioned in the previous section. The resulting "optimum" area taper is plotted in figure C-3 where it is compared to the area taper of the existing ETA ring "long side". The greatly decreased area at the end of the ring is a dramatic departure from the existing ring design. The effect of this is illustrated in figure C-4 where the bolt loads of the "optimum" design are compared to those predicted for the existing ring by finite element analysis. This simplified analysis shows that considerable tapering of the ring area is required to reduce the first bolt load to an acceptable level. Ring area tapering analysis which includes bolt and web shear flexibility is presented in the following section.

RING AREA TAPERING INCLUDING BOLT AND WEB SHEAR FLEXIBILITY

Bolt flexibility and web "shear lag" flexibility are included in a modified 1-D discrete planar model. Both the ring and the effective shell are again modeled by series of linear springs whose stiffnesses are proportional to cross-sectional area. Load is transferred between these parallel spring assemblages through an array of linear shear springs whose compliance represents the sum of the bolt and web shear compliances. Figure C-5 illustrates this representation of the ring and shell.

Stiffnesses of the n^{th} ring and shell segments and the n^{th} "effective" bolt are K_{rn} , K_s (assumed constant for all n), and K_{bn} , respectively which are defined by

$$\begin{aligned} K_{rn} &= \frac{EA_{rn}}{\ell} \\ K_s &= \frac{EA_s}{\ell} \\ K_{bn} &= \frac{K_b}{1 + (K_b/K_{wn})} \end{aligned} \quad (C-8)$$

where K_{wn} is the assumed web shear stiffness, K_b is the bolt stiffness, and ℓ is the spacing between tang bolts numbered n and $n+1$. By assuming strains to be constant in each segment (see figure C-5), the corresponding stress resultants, P_{rn} , P_{sn} , and P_{bn} , are related to the ring and shell displacements, u_{rn} and u_{sn} , at the n^{th} station by

$$\begin{aligned}
P_{rn} &= K_{rn}(u_{rn} - u_{r(n-1)}) \\
P_{sn} &= K_s(u_{sn} - u_{s(n-1)}) \\
P_{bn} &= K_{bn}(u_{r(n-1)} - u_{s(n-1)})
\end{aligned} \tag{C-9}$$

Eliminating the displacements from equations (C-9) yields the following equation in terms of forces alone:

$$\frac{P_{b(n+1)}}{K_{b(n+1)}} - \frac{P_{bn}}{K_{bn}} = \frac{P_{rn}}{K_{rn}} - \frac{P_{sn}}{K_s}, \quad n = 1, 2, 3, \dots, N-1 \tag{C-10}$$

where N is the total number of bolts being considered. Assuming that the total force on the n^{th} shell and ring segments is constant and equal to the far-field force, P_{ff} , equation (C-2) applies for all n from 1 to $N-1$

$$P_{rn} + P_{sn} = P_{ff}, \quad n = 1, 2, 3, \dots, N-1 \tag{C-11}$$

The force in the n^{th} ring segment is equal to the sum of the first n bolt forces, i.e.,

$$P_{rn} = \sum_{i=1}^n P_{bi} \tag{C-12}$$

Inserting equations (C-11) and (C-12) into equations (C-10) gives

$$\left(\frac{1}{K_{rn}} + \frac{1}{K_s}\right) \sum_{i=1}^n P_{bi} + \frac{P_{bn}}{K_{bn}} - \frac{P_{b(n+1)}}{K_{b(n+1)}} = \frac{P_{ff}}{K_s}, \quad n = 1, 2, \dots, N-1 \tag{C-13}$$

Requiring equality of far-field strains in the shell and ring yields

$$\sum_{i=1}^N P_{bi} = \frac{P_{ff} K_{rn}}{K_{rn} + K_s} \tag{C-14}$$

Equations (C-13) and (C-14) constitute a set of N linear algebraic equations in the N unknowns, P_{bn} , when all stiffnesses are assumed known (i.e. when the ring area profile is given). This is analogous to the recursion relation given in equation (C-6). On the other hand, if all stiffnesses except K_{rn} are assumed known, then specification of all bolt forces, P_{bn} , leads to a system of equations for the ring stiffnesses, K_{rn} , from which an area profile for the ring can be obtained through the relation given in equation (C-8). This second set of equations is analogous to the equations (C-7).

To determine the effect of bolt and web shear flexibility on bolt loads, the optimum area profile developed from the rigid bolt analysis and presented in figure C-3 is analysed using the system of equations (C-13) and (C-14). The web shear stiffness chosen is $K_{wn} = G/t_n / .6h_n$ (where t_n and h_n are the thickness and height of the n^{th} section of web and G is the shear modulus) and the bolt stiffness (K_b) is assumed to be 1.3×10^6 lb/in (see Appendix I). Figure C-6 shows the bolt load distribution predicted from this analysis (note curve titled "profile from rigid bolt analysis"). This distribution differs significantly from the design distribution of constant 10,000 lb loads shown in figure C-4.

Using the system of equations (C-13) a new area profile can be generated which gives constant bolt loads when bolt and web shear flexibility are included. The second curve on figure C-6 is a bolt load distribution which satisfies equation (C-14) and has constant 10,000 lb bolt loads for the first 15 bolts. It should be noted that specifying a bolt load distribution with large changes in load between adjacent bolts will lead to the prediction of an unreasonable area profile. Because of this, the bolt loads beyond the 15th bolt have been gradually tapered off. The area profile predicted using this bolt load distribution and equations (C-13) is shown in figure C-7 and is compared to the "optimum" area profile generated from the rigid bolt analysis. The lower slope for the first 12 bolts is responsible for lowering the high bolt loads in that region as seen in figure C-6. Similarly, the higher slope after the 12th bolt is commensurate with the higher bolt loads in that area. This comparison indicates that the effects of bolt and web shear flexibility can be significant and should be included in area profile prediction.

DEVELOPMENT OF THE REDESIGNED ETA RING AREA PROFILE

The area profiles presented in figure C-7 taper to very small sections at the end (A_{r1}), which gives rise to manufacturing and handling concerns. Evaluating equation (C-7) for $n=1$ shows that A_{r1} is nearly proportional to P_{b1} , the load in the first bolt. Therefore increasing the area tends to raise the first bolt load if all bolts are assumed rigid. However, if bolt flexibility is included, two mechanisms are available to increase the ring area without affecting the load in the first bolt. These mechanisms (shown in figure C-8) are (1) increase the bolt stiffness ratio, K_{b2}/K_{b1} and (2) decrease the bolt load ratio, P_{b1}/P_{b2} . Using either or both approaches in a design allows the first area to be increased as the first bolt load remains constant while causing the average stress in the first section to go down. Although this example is worked for the first section of the ring it is possible to employ these mechanisms wherever the ring area is too small or the stress is too high. These mechanisms are used to develop the final area profile design by modifying the area profile shown in figure C-7.

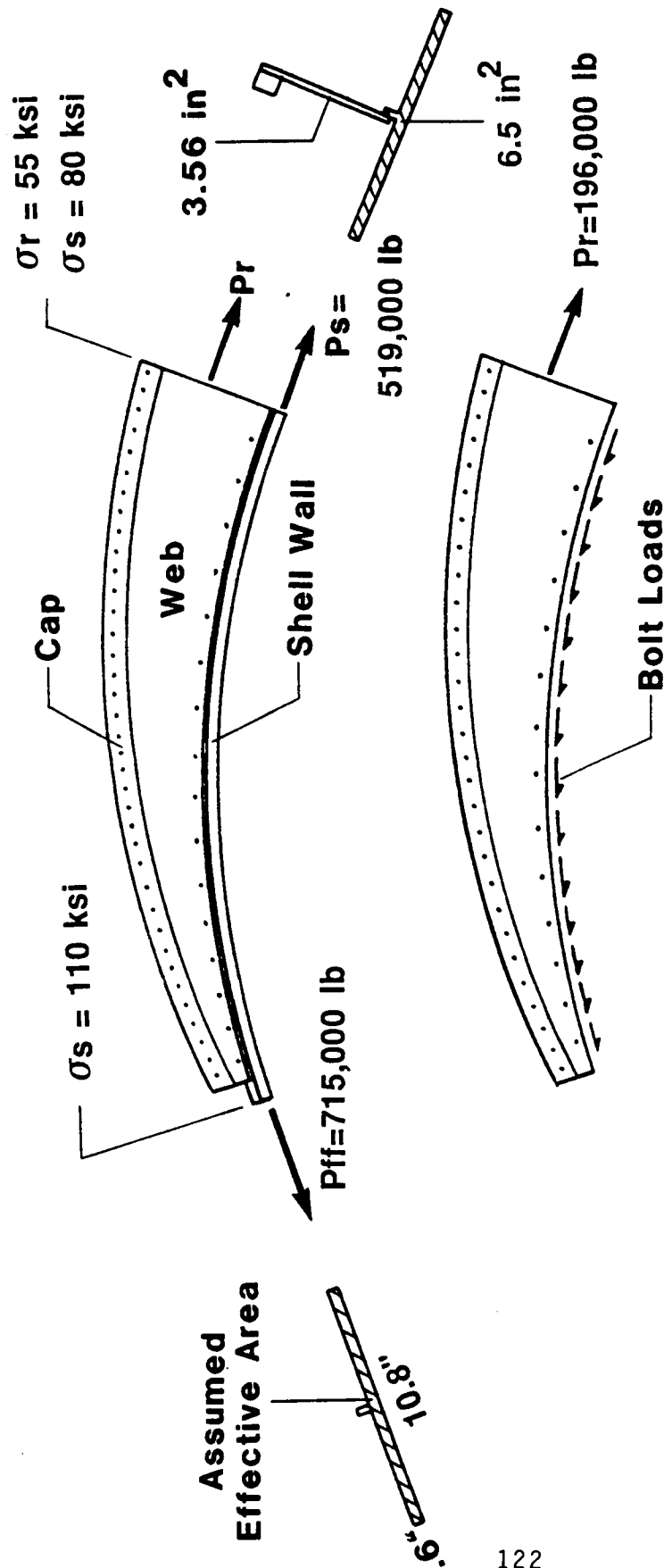
For the final design, the area at the end of the ring (A_{r1}) is increased by using a first bolt with reduced stiffness (see Appendix I) and specifying the bolt loads to decrease between the second and fourth bolts. Additionally, to increase the margin of safety, the bolt loads at the end of the ring are specified to lie between 7,000 and 8,000 lb. instead of at 10,000 lb. The profile that results from these modifications is shown in figure C-9 and

compared to the previous profile from figure C-7. It is seen that the area at the first bolt has been increased while, as a result of the decreased bolt loads, the slope of the curve near the first bolt has been decreased.

Bolt loads derived from the present analyses agree favorably with results from finite element analysis in the first few sections of the ring and tend to be conservative throughout the rest of the ring. Additionally, details of the web stresses are not predicted with these analyses because of the simplifying assumptions that have been made. Consequently, the area profile presented in figure C-9 represents a first-iteration version of that design which can be further developed using finite element analysis. Therefore, the final configuration of the redesigned ETA ring, presented in the accompanying report, differs slightly from this profile.

SIMPLIFIED RING TANG BOLT LOAD ANALYSIS

($p=912$ psi)



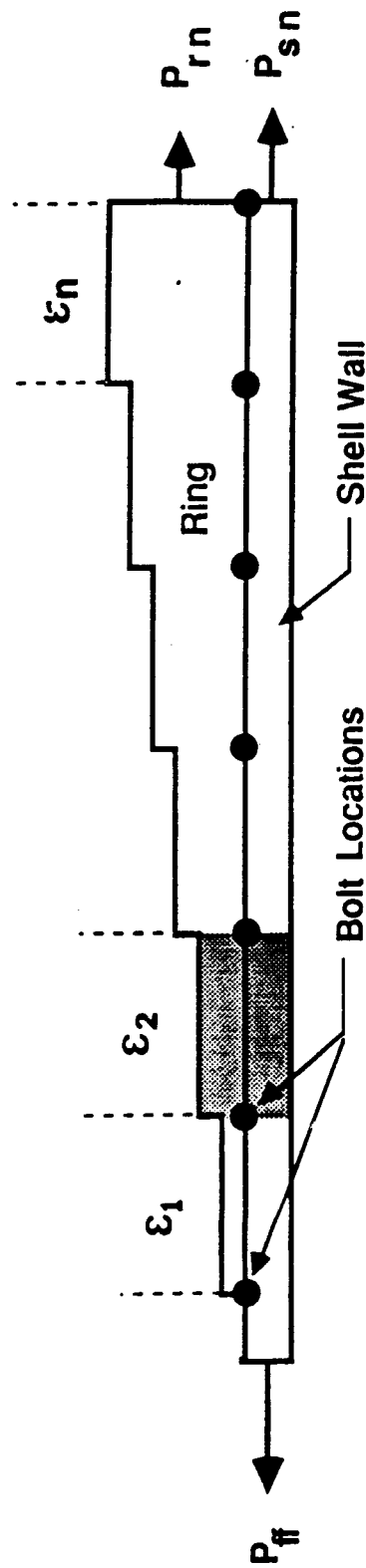
Sum of bolt loads = 196,000
 Assume each bolt carries 10,000
 $N(10,000) = 196,000$
 $N = 20$ bolts

Figure C-1

SIMPLIFIED RING ANALYSIS

ASSUMPTIONS:

- NO BOLT FLEXIBILITY
- NO RING "SHEAR LAG" FLEXIBILITY
- IDEALIZED RING SEGMENT (FLAT)



$$P_{ff} = P_{ring} + P_{shell}$$

$$P_{ff} = E \epsilon_n (A_{rn} + A_s)$$

$$\epsilon_n = \frac{P_{ff}}{E(A_{rn} + A_s)}$$

$$\therefore P_{rn} = E \epsilon_n A_n = \frac{P_{ff} A_{rn}}{A_{rn} + A_s}$$

$$(P_{bolt})_n = P_{rn} - P_{rn} - 1 = P_{ff} \left[\frac{A_{rn}}{A_{rn} + A_s} - \frac{A_{rn} - 1}{A_{rn} - 1 + A_s} \right]$$

$$A_{rn} = \frac{A_s \left[\frac{(P_{bolt})_n}{P_{ff}} + \frac{A_{rn} - 1}{A_{rn} - 1 + A_s} \right]}{\left[1 - \frac{(P_{bolt})_n}{P_{ff}} - \frac{A_{rn} - 1}{A_{rn} - 1 + A_s} \right]}$$

ETA RING AREA TAPER PROFILE

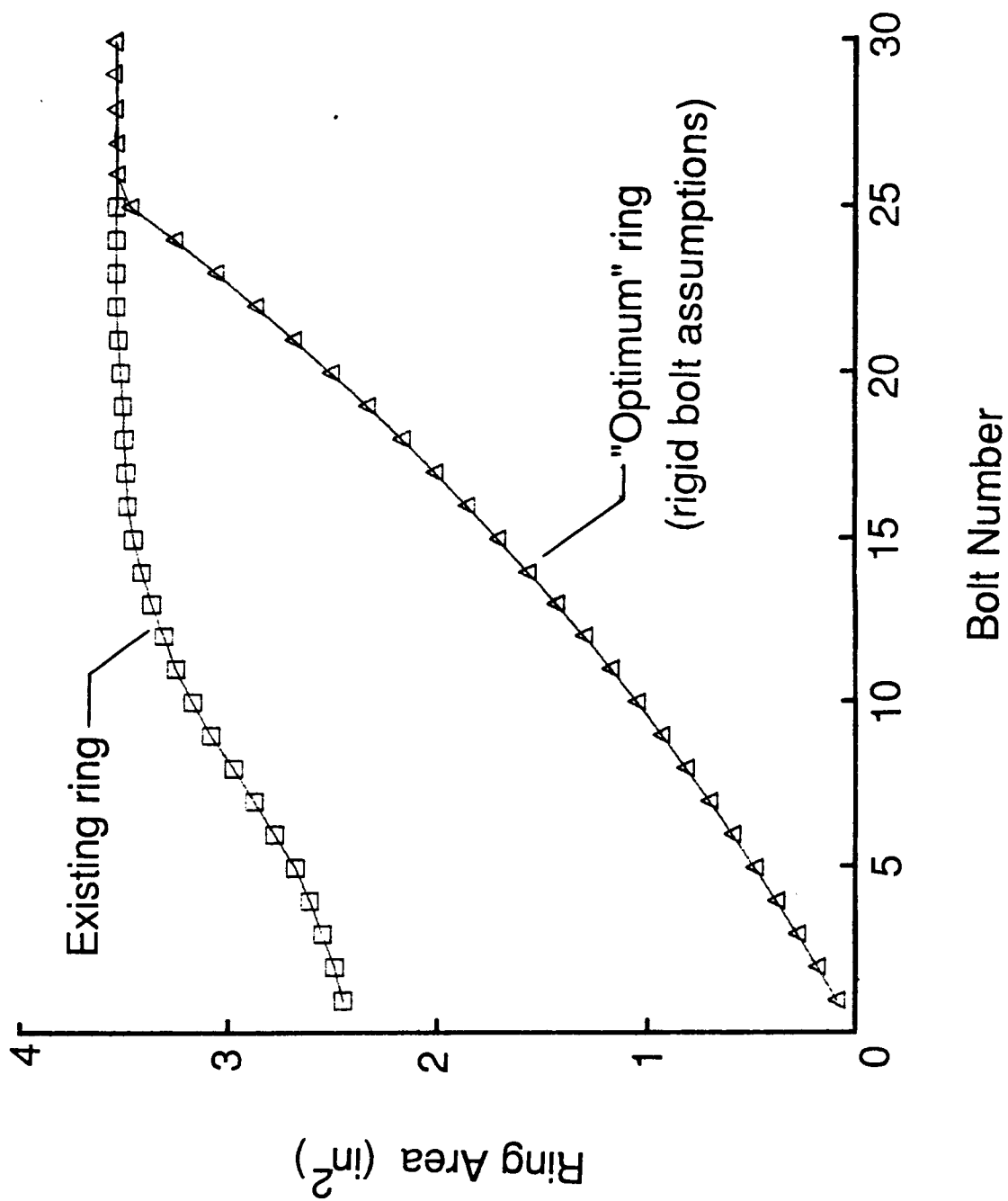


Figure C-3

TANG BOLT LOADS

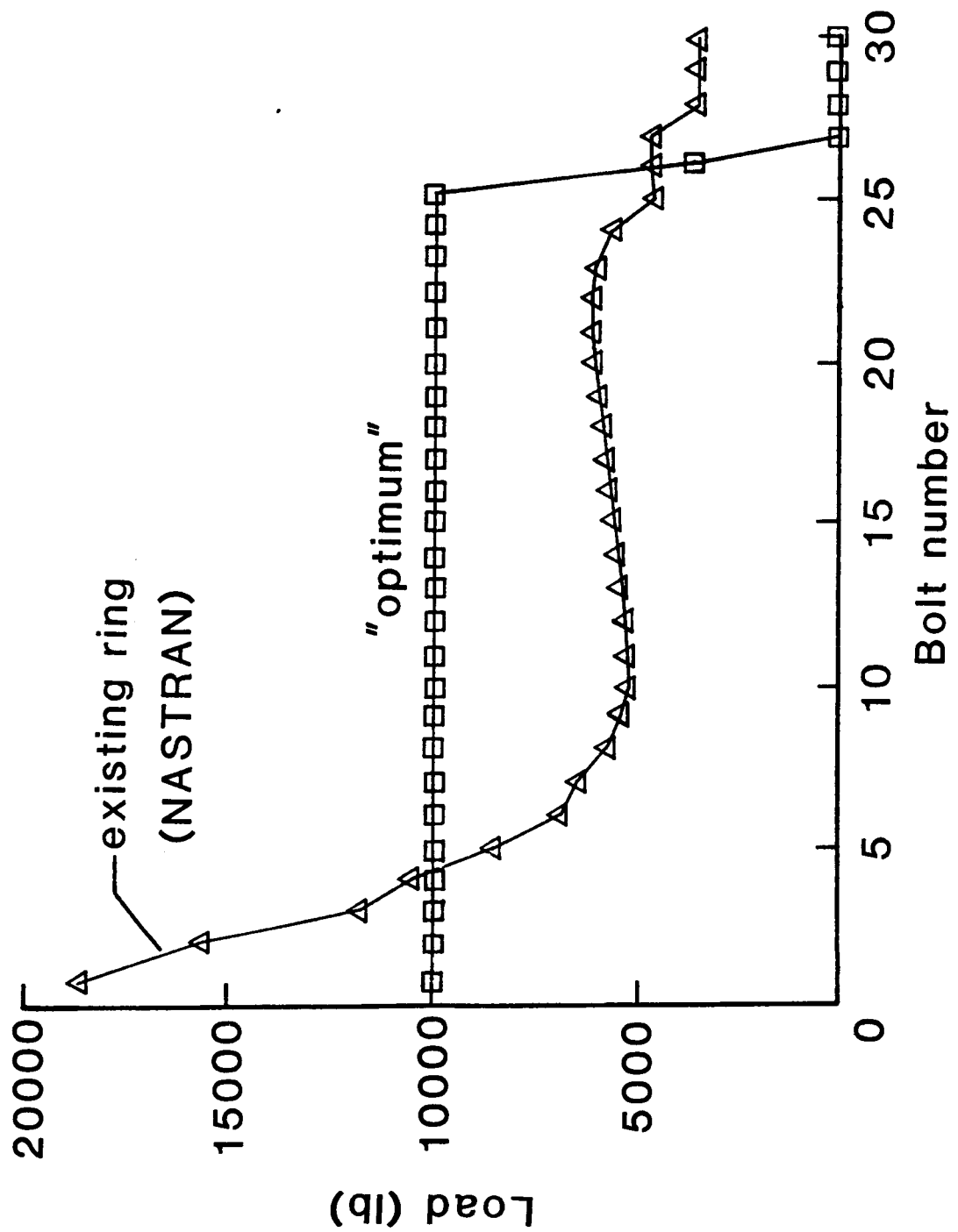
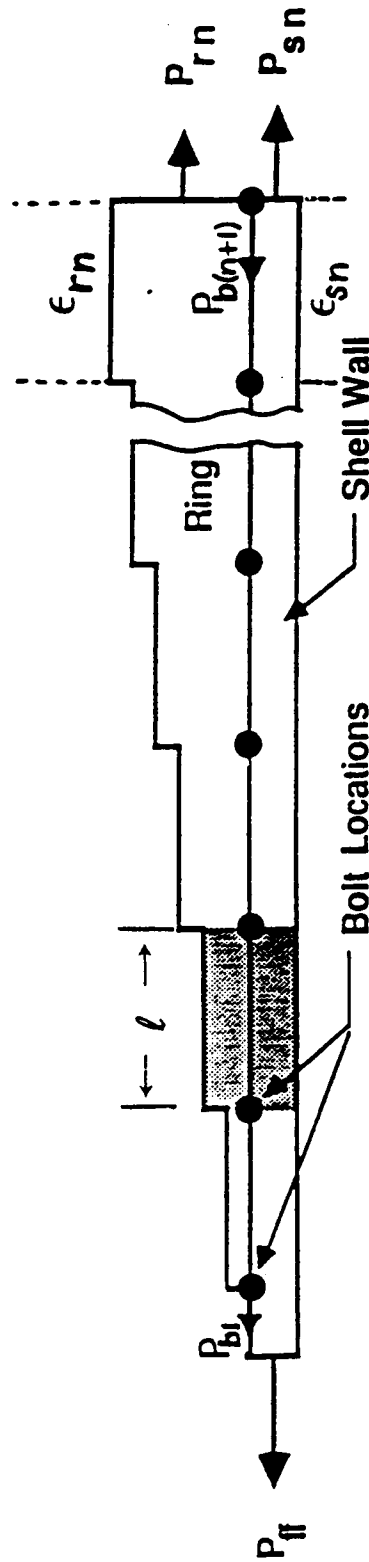


Figure C-4

SIMPLIFIED RING ANALYSIS

INCLUDES RING "SHEAR LAG" AND BOLT FLEXIBILITY



$$P_{ff} = P_{rn} + P_{sn}$$

$$K_{bn} = \frac{K_b K_{wn}}{K_b + K_{wn}}$$

$$K_{wn} = GJ \left(\frac{t_w}{h_w} \right)_n$$

$$\epsilon_{rn} = \frac{P_{rn}}{EA_{rn}}$$

$$\epsilon_{sn} = \frac{P_{sn}}{EA_{sn}}$$

$$A_{rn} \left\{ \frac{P_{ff} - \sum_{i=1}^n P_{bi}}{A_s} - \frac{E}{l K_{bn}} P_{bn} + \frac{E}{l K_{b(n+1)}} P_{b(n+1)} \right\} = \sum_{i=1}^n P_{bi}$$

and

$$\sum_{i=1}^N P_{bi} = \frac{A_{rn} P_{ff}}{A_{rn} + A_s}$$

Figure C-5

PREDICTED TANG BOLT LOADS

INCLUDES RING "SHEAR LAG" AND BOLT FLEXIBILITY

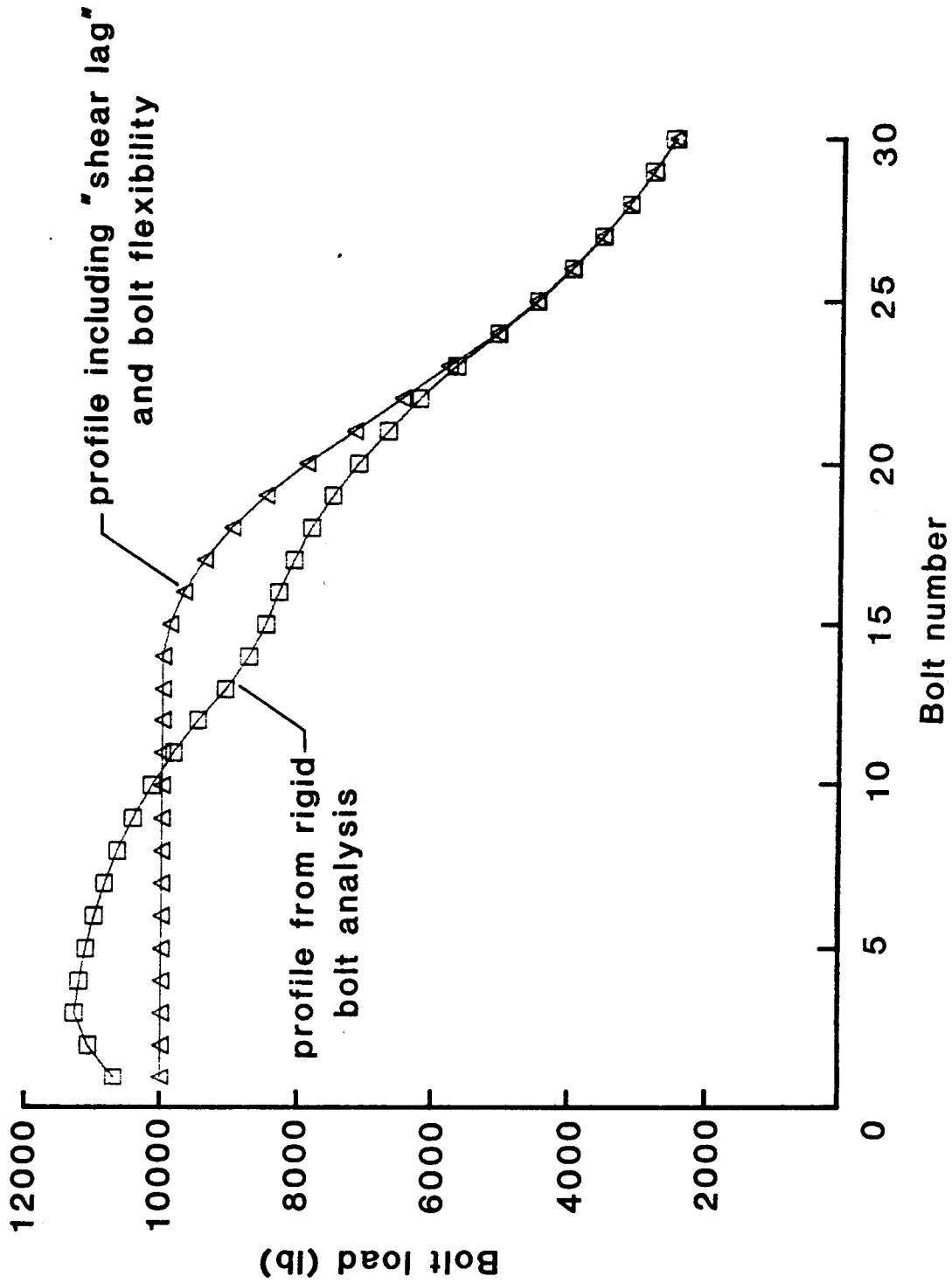


Figure C-6

MODIFIED AREA PROFILE

INCLUDES RING "SHEAR LAG" AND BOLT FLEXIBILITY

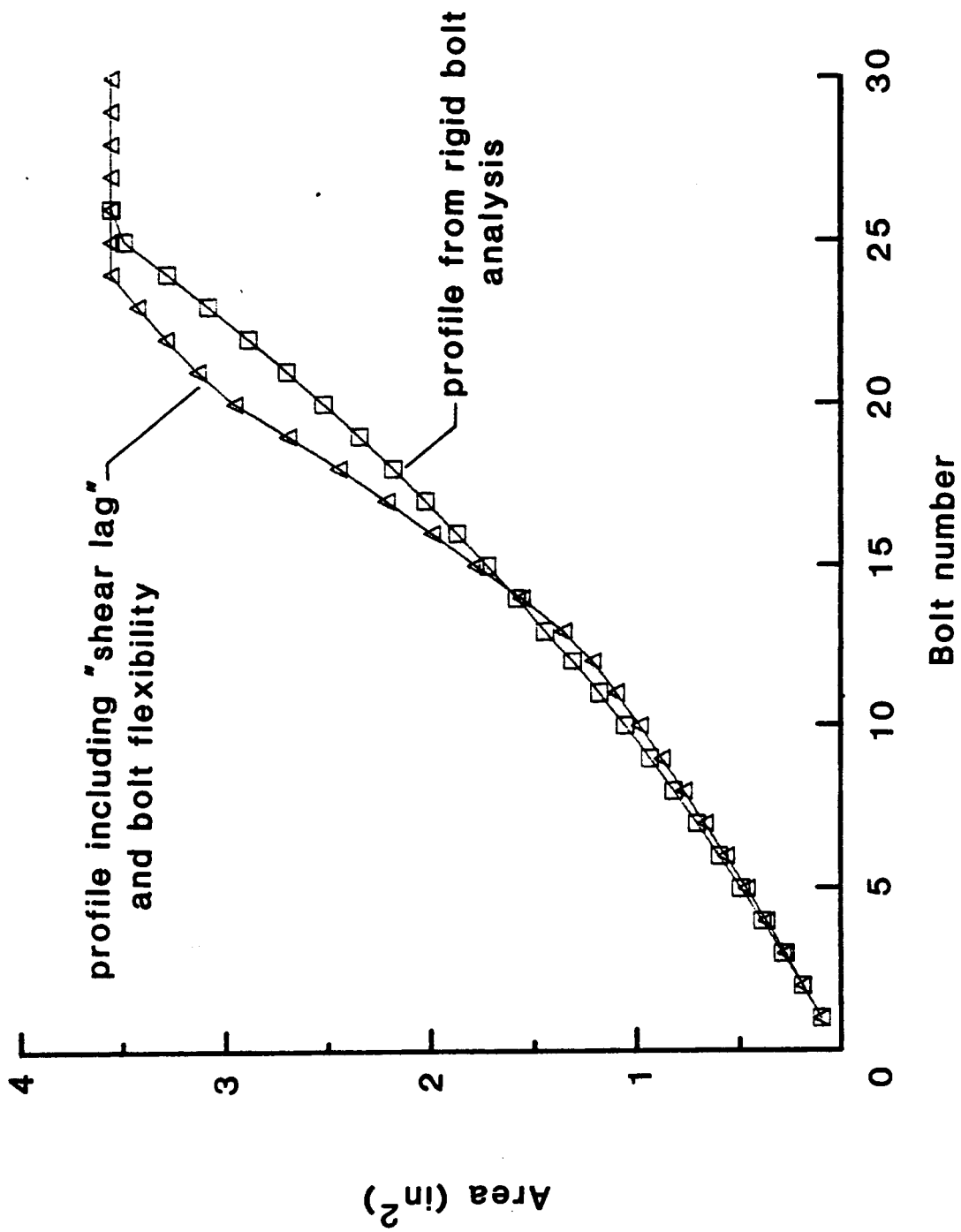


Figure C-7

MECHANISMS FOR INCREASING RING AREA AND REDUCING RING STRESS

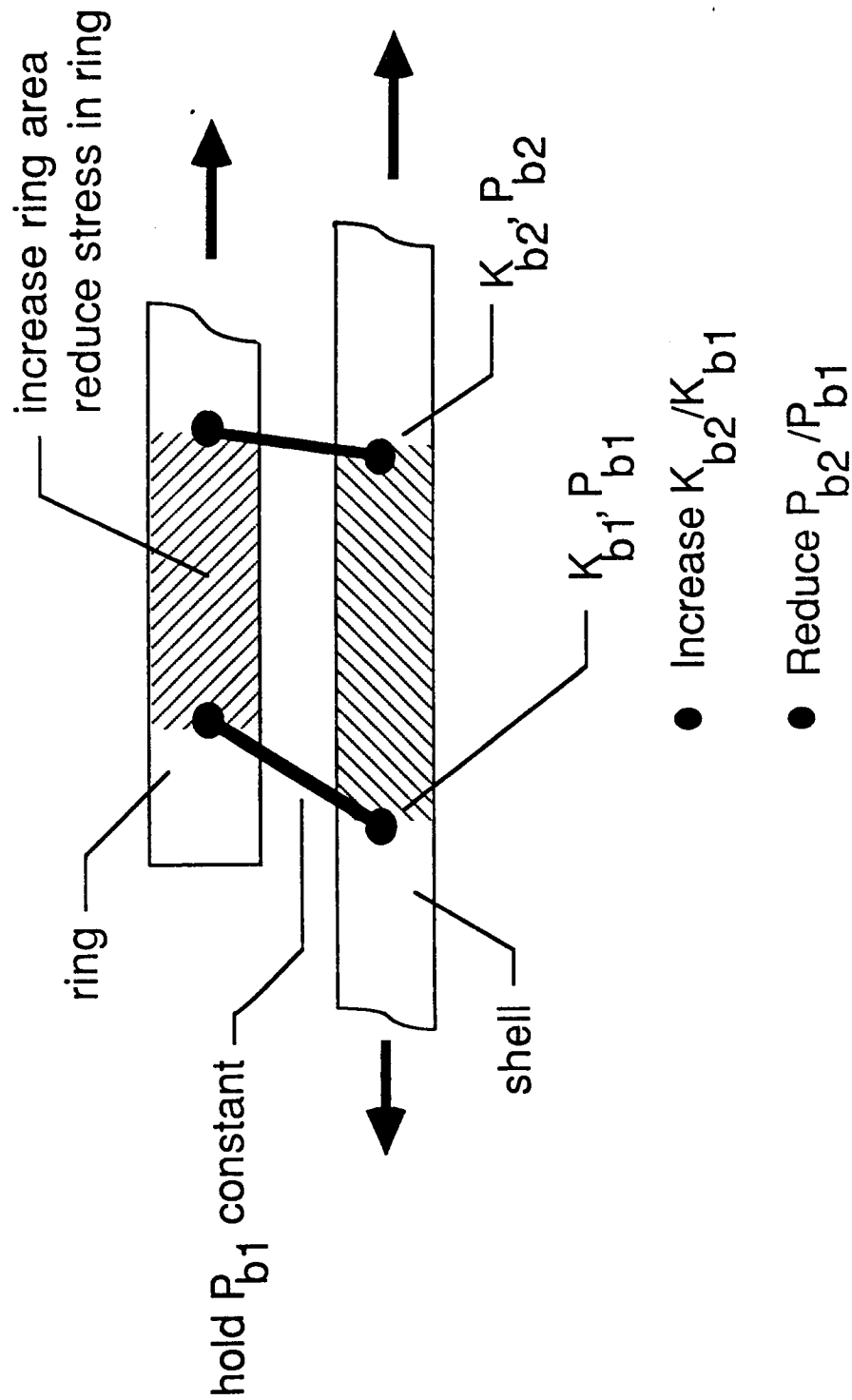


Figure C-8

REDESIGNED ETA RING AREA PROFILE

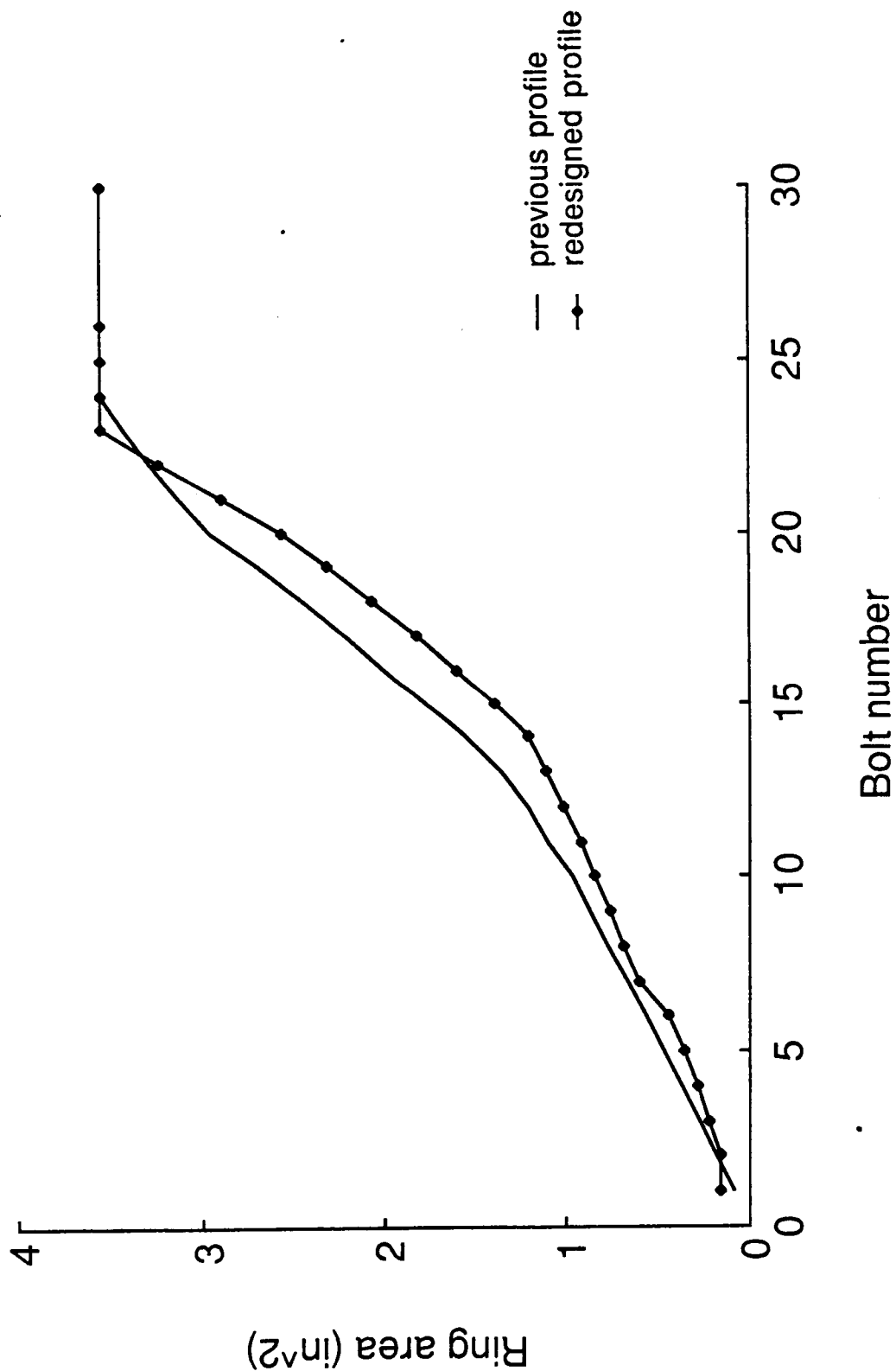


Figure C-9

APPENDIX D

SPLICE ANALYSIS

BY

Obie H. Bradley, Jr.
NASA-Langley Research Center
Mail Stop 434
Ph. (804)865-4571

and

Robert Davis
NASA-Langley Research Center
Mail Stop 431
Ph. (804)865-4571

June 9, 1987

Obie H. Bradley, Jr.
Obie H. Bradley, Jr.
Robert B. Davis
Robert Davis

Reviewed by *Carl E. Gray, Jr.*
Project Engineer *Arnold J. Bush*
for Martin M. Mikulas, Jr.
Project Manager *David H. Butler*
David H. Butler

APPENDIX D

Splice Analysis

Introduction

The original splice in the ET attachment ring, located between the strut attachment brackets, was found to have negative margins of safety when analyzed using a finite element code. This splice as well as splices for modified end segments for the partial ring were required to complete the design of the new partial ring. Fig. D1 shows the locations of the splices. Fig. D2 shows the splice configuration, hereafter referred to as the existing splice, which replaces the original splice. Fig. D3 shows the new end splice on the short side of the partial ring. The original splice used 3/8" bolts throughout the cap and web areas, while the splice designs which shall be considered in this analysis use 1/2" bolts in the cap and 3/8" bolts in the webs.

Analysis

To analyze the existing splice (between the struts), a finite element model of half of the splice was constructed. This model is shown in Fig. D4. The node numbering system is explained in Fig. D5. The finite element model is assumed to be fixed at the plane of symmetry. The structural computer program EAL was used. A listing of the input is included in Table D1.

The web and splice plates were simulated by plate elements. Solid elements were used to model the cap. The bolts were simulated by general beam elements which required that the elastic constants be input. Shear stiffness values of 1.2 million lb/in. and 2.2 million lb/in., which correspond to the shear stiffness of 3/8" and 1/2" bolts, were input in the program.

The loads which were imposed on the model were derived from another finite element model of a segment of the motor case developed by J. Dorsey. A separate appendix covers this work. Table D2 gives a summary of the stress results of this analysis which were used to develop the loads for the splice analysis. In the model 78,898 lb were applied to the cap, and 93,091 lb were applied to the web.

Analysis Results

The bolt shear forces which were calculated are shown in Figs. D6 and D7. The highest shear force in the existing splice was found to be 9,390 lb. The highest shear force in the new end splice was 13,050 lb. These are well within the allowable load of 20,000 lb for a 1/2" diameter fastener (145 ksi shear).

The maximum stresses calculated for the new end splice plates, web, and cap are shown in Figs. D8, D9, D10, and D11. The highest stresses occur on the inner splice near the joint. The stress level at this location is about 115 ksi. A summary of the highest stresses and loads is given on the following page. The ultimate strength of the material used for the margin calculations was 180 ksi.

The modeling did not consider the curvature of the splice and the motor case. Therefore, some error can be anticipated. The analysis does indicate positive margins, however. Incorporation of models of the splices in a full segment model of the motor case will be required for final approval.

Stress and Load Summary

| <u>Location</u> | <u>Stress or Load</u> | <u>Margin of Safety</u> (alt.) |
|------------------------------|-----------------------|-----------------------------------|
| Existing Splice | | |
| Bolt (Cap, $\frac{1}{2}$ ") | 9390 lb. | 1.16 |
| Bolt (Web, $\frac{3}{8}$ ") | 6280 lb. | .82 |
| New End Splices | | |
| Bolt (Cap, $\frac{1}{2}$ ") | 13050 lb. | .56 |
| Bolt (Web, $\frac{3}{8}$ ") | 7370 lb. | .55 |
| Cap | 52000 psi | 1.47 |
| Inner Splice Plate | 114,766 psi | .12 |
| Outer Splice Plate | 100,769 psi | .28 |
| Cap Splice Plate | 108,633 psi | .18 |

FINITE ELEMENT PROGRAM INPUT LISTING

```

79 0. 5.5 0. 12. 5.5 0. 13 1
* CHAR $*!M!:>
* XQT TAB
START 600
MATC
1 3.+7 .3 .263
JLDC
1 0. 1.38 0.
2 .698 1.38 0.
3 2.112 1.38 0.
4 3.525 1.38 0.
5 4.939 1.38 0.
6 6.353 1.38 0.
7 7.766 1.38 0.
8 9.180 1.38 0.
9 9.606 1.38 0.
10 0.0 1.94 0.
11 .698 1.94 0. 9.180 1.94 0. 7 1
18 9.606 1.94 0.
19 0.0 3.52 0.0
20 .698 3.52 0.0 9.180 3.52 0. 7 1
27 9.606 3.52 0.0
28 0.0 5.56 0.0
29 .698 5.56 0.0 9.180 5.56 0.0 7 1
36 9.606 5.56 0.0
37 0.0 6.35 0.0
38 .698 6.35 0.0 9.180 6.35 0.0 7 1
45 9.606 6.35 0.0
46 0.0 7.46 0.0
47 .698 7.46 0.0 9.180 7.46 0.0 7 1
54 9.606 7.46 0.0
101 0.0 1.38 0.01
102 .698 1.38 0.01 9.180 1.38 0.01 7 1
109 9.606 1.38 0.01
110 0.0 1.94 0.01
111 .698 1.94 0.01 9.180 1.94 0.01 7 1
118 9.606 1.94 0.01
119 0.0 3.52 0.01
123 .698 3.52 0.01 9.180 3.52 0.01 7 1
127 9.606 3.52 0.01
128 0.0 5.11 0.01
129 .698 5.11 0.01 9.180 5.11 0.01 7 1
136 9.606 5.11 0.01
137 0.0 6.35 0.01
138 .698 6.35 0.01 9.180 6.35 0.01 7 1
145 9.606 6.35 0.01
146 0.0 7.23 0.01
147 .698 7.23 0.01 9.180 7.23 0.01 7 1
154 9.606 7.23 0.01

```

TABLE D1 (Continued)

| | | | | | | | | |
|-----|-------|------|------|-------|------|------|---|---|
| 161 | 0.0 | 0.0 | 0.01 | | | | | |
| 162 | .698 | 0.0 | 0.01 | 9.180 | 0.0 | 0.01 | 7 | 1 |
| 169 | 9.606 | 0.0 | 0.01 | | | | | |
| 170 | 0.0 | 0.46 | 0.01 | | | | | |
| 180 | 9.606 | 0.46 | 0.01 | | | | | |
| 171 | .698 | .46 | 0.01 | 9.180 | 0.46 | 0.01 | | |
| 173 | 2.112 | .46 | 0.01 | 2.112 | 0.46 | 0.01 | | |
| 174 | 3.525 | .46 | 0.01 | 3.525 | 0.46 | 0.01 | | |
| 175 | 4.939 | .46 | 0.01 | 4.939 | 0.46 | 0.01 | | |
| 176 | 6.353 | .46 | 0.01 | 6.353 | 0.46 | 0.01 | | |
| 177 | 7.776 | .46 | 0.01 | 7.776 | 0.46 | 0.01 | | |
| 179 | 9.180 | .46 | 0.01 | 9.180 | 0.46 | 0.01 | | |
| 180 | 9.606 | .46 | 0.01 | 9.606 | 0.46 | 0.01 | | |
| 172 | 1.159 | .46 | 0.01 | | | | | |
| 178 | 8.553 | .46 | 0.01 | | | | | |
| 278 | 8.553 | .46 | 0.02 | | | | | |
| 272 | 1.159 | .46 | 0.02 | | | | | |
| 201 | 0.0 | 1.38 | 0.02 | | | | | |
| 202 | .698 | 1.38 | 0.02 | 9.180 | 1.38 | 0.02 | 7 | 1 |
| 209 | 9.606 | 1.38 | 0.02 | | | | | |
| 210 | 0.0 | 1.94 | 0.02 | | | | | |
| 211 | .698 | 1.94 | 0.02 | 9.180 | 1.94 | 0.02 | 7 | 1 |
| 218 | 9.606 | 1.94 | 0.02 | | | | | |
| 219 | 0.0 | 3.52 | 0.02 | | | | | |
| 220 | .698 | 3.52 | 0.02 | 9.180 | 3.52 | 0.02 | 7 | 1 |
| 227 | 9.606 | 3.52 | 0.02 | 9.606 | 3.52 | 0.02 | | |
| 228 | 0.0 | 5.11 | 0.02 | | | | | |
| 229 | .698 | 5.11 | 0.02 | 9.180 | 5.11 | 0.02 | 7 | 1 |
| 236 | 9.606 | 5.11 | 0.02 | | | | | |
| 261 | 0.0 | 0.0 | 0.02 | | | | | |
| 262 | .698 | 0.0 | 0.02 | 9.180 | 0.0 | 0.02 | 7 | 1 |
| 269 | 9.606 | 0.0 | 0.02 | | | | | |
| 270 | 0.0 | 0.46 | 0.02 | | | | | |
| 271 | 0.698 | 0.46 | 0.02 | | | | | |
| 273 | 2.112 | 0.46 | 0.02 | | | | | |
| 274 | 3.525 | 0.46 | 0.02 | | | | | |
| 275 | 4.939 | 0.46 | 0.02 | | | | | |
| 276 | 6.353 | 0.46 | 0.02 | | | | | |
| 277 | 7.776 | 0.46 | 0.02 | | | | | |
| 279 | 9.180 | 0.46 | 0.02 | | | | | |
| 280 | 9.606 | 0.46 | 0.02 | | | | | |
| 337 | 0.0 | 6.35 | 0.02 | | | | | |
| 338 | .698 | 6.35 | 0.02 | 9.18 | 6.35 | 0.02 | 7 | 1 |
| 345 | 9.606 | 6.35 | 0.02 | | | | | |
| 381 | 0.0 | 5.56 | 0.02 | | | | | |
| 382 | .698 | 5.56 | 0.02 | 9.18 | 5.56 | 0.02 | 7 | 1 |
| 389 | 9.606 | 5.56 | 0.02 | | | | | |
| 346 | 0.0 | 7.46 | 0.02 | | | | | |
| 347 | .698 | 7.46 | 0.02 | 9.18 | 7.46 | 0.02 | 7 | 1 |

TABLE D1 (Continued)

```

354 9.606 7.46 0.02
437 0.0 6.35 1.02
438 .698 6.35 1.02 9.18 6.35 1.02 7 1
445 9.606 6.35 1.02
481 0.0 5.56 1.02
482 .698 5.56 1.02 9.18 5.56 1.02 7 1
489 9.606 5.56 1.02
446 0.0 7.46 1.02
447 .698 7.46 1.02 9.18 7.46 1.02 7 1
454 9.606 7.46 1.02
537 0.0 6.35 1.03
538 .698 6.35 1.03 9.18 6.35 1.03 7 1
545 9.606 6.35 1.03
581 0.0 5.56 1.03
582 .698 5.56 1.03 9.18 5.56 1.03 7 1
589 9.606 5.56 1.03
546 0.0 7.46 1.03
547 .698 7.46 1.03 9.18 7.46 1.03 7 1
554 9.606 7.46 1.03

```

MREF

FORMAT=2

1 1 100. 10. 100.

CON=1

ZERO 1,2,3,4,5,6:1:10:19:28:37:46

ZERO 1,2,3,4,5,6:20:210:219:228:261:270

ZERO 1,2,3,4,5,6:581:537:546

BA

TUBE 1 0.0 .010

TUBE 2 0.0 .1875

TUBE 3 0.0 .1

TUBE 5 0.0 .175

BB

1 1.24+6

0. 1.24+6

0. 0. 1.24+6

0. 0. 0. 0.0

0. 0. 0. 0. 0.0

0. 0. 0. 0. 0. 0.0

2 2.20+6

0. 2.20+6

0. 0. 2.20+6

0. 0. 0. 0.0

0. 0. 0. 0. 0.0

0. 0. 0. 0. 0. 0.0

SA

1 .25

2 1.0

3 .375

4 .4166

TABLE D1 (Continued)

```

5 .5833
6 .750
3 .375
*XQT AUS
TABLE(NI=31,NJ=1):PROP BTAB 2 21
J=1
.1>
3.33-8>
-1.-8 3.33-8>
-1.-8 -1.-8 3.33-8>
0. 0. 0. 8.66-8>
0. 0. 0. 0. 8.66-8>
0. 0. 0. 0. 0. 8.66-8>
1.-6 1.-6 1.-6 1. 1. 1. 1. 1. 1.
*XQT ELD
S81
GROUP 1
381 382 338 337 481 482 438 437
382 383 339 338 482 483 439 438
384 385 341 340 484 485 441 440
383 384 340 339 483 484 440 439
385 386 342 341 485 486 442 441
386 387 343 342 486 487 443 442
387 388 344 343 487 488 444 443
GROUP 2
388 389 345 344 488 489 445 444
GROUP 3
337 338 347 346 437 438 447 446
338 339 348 347 438 439 448 447
339 340 349 348 439 440 449 448
340 341 350 349 440 441 450 449
341 342 351 350 441 442 451 450
342 343 352 351 442 443 452 451
343 344 353 352 443 444 453 452
344 345 354 353 444 445 454 453
E41
NSECT=1
1 2 11 10 1 8 3$INSIDE FLANGE
NSECT=1
28 29 38 37 1 2 2
NSECT=1
30 31 40 39 1 2 2
NSECT=1
32 33 42 41 1 2 2
NSECT=1
34 35 44 43 1 2 2
GROUP 2$WEB
NSECT=1
101 102 111 110 1 8 5

```

TABLE D1 (Continued)

| | | | |
|----------------------------|-----|---------|---------------------------------|
| 161 | 162 | 171 | 170 |
| 170 | 171 | 102 | 101 |
| 163 | 164 | 174 | 173 |
| 173 | 174 | 104 | 103 |
| 164 | 165 | 175 | 174 |
| 174 | 175 | 105 | 104 |
| 166 | 167 | 177 | 176 |
| 176 | 177 | 107 | 106 |
| 168 | 169 | 180 | 179 |
| 179 | 180 | 109 | 108 |
| GROUP 3\$OUTTER FLANGE | | | |
| 201 | 202 | 211 | 210 1 0 3 |
| 261 | 262 | 271 | 270 |
| 270 | 271 | 202 | 201 |
| 263 | 264 | 274 | 273 |
| 273 | 274 | 204 | 203 |
| 264 | 265 | 275 | 274 |
| 274 | 275 | 205 | 204 |
| 266 | 267 | 277 | 276 |
| 276 | 277 | 207 | 206 |
| 268 | 269 | 280 | 279 |
| 279 | 280 | 209 | 208 |
| GROUP 4\$OUTTERMOST SPLICE | | | |
| NSECT=3 | | | |
| 581 | 582 | 538 | 537 1 2 |
| 537 | 538 | 547 | 546 1 2 |
| NSECT=3 | | | |
| 583 | 584 | 540 | 539 1 2 |
| 539 | 540 | 549 | 548 1 2 |
| NSECT=3 | | | |
| 585 | 586 | 542 | 541 1 2 |
| 541 | 542 | 551 | 550 1 2 |
| NSECT=3 | | | |
| 587 | 588 | 544 | 543 1 2 |
| 543 | 544 | 553 | 552 1 2 |
| E31\$WEB | | | |
| NSECT=1 | | | |
| 162 | 172 | 171:162 | 163 172:163 173 172:172 173 103 |
| 172 | 103 | 102:172 | 102 171:165 166 176:165 176 175 |
| 175 | 176 | 105:176 | 106 105:167 168 176:167 178 177 |
| 178 | 106 | 107 | |
| 168 | 108 | 178 | |
| GROUP 2\$OUTER PLATE | | | |
| 262 | 272 | 271:262 | 263 272:263 273 272:272 273 203 |
| 272 | 203 | 202:272 | 202 271:265 266 276:265 276 275 |
| 275 | 276 | 205:276 | 206 205:267 268 278:267 278 277 |
| 278 | 208 | 207:268 | 208 278:277 278 207 |
| E22\$INNER PLATE-----WEB | | | |
| GROUP 1 | | | |

TABLE D1 (Continued)

```

11 111:113 113:115 115:117 117
20 120:122 122:124 124:126 126
29 129:131 131:133 133:135 135
$WEB-----OUTER PLATE
172 272:174 274:176 276:178 278
120 220:122 222:124 224:126 226
111 211:113 213:115 215:117 217
129 229:131 231:133 233:135 235
$OUTER PLATE--SOLID BAR
$$SOLID BAR-----SPLICE
$25
$SECT=2
$6 515
$SIMULATES SPLICE
$WEB
$N1 161:502 170:503 101:504 110:505 119:506 128
$07 137:508 146
$SIMULATES DISCONUITY OF SOLID BAR
GROUP 2
NSECT=2
38 138: 40 140:42 142:44 144
138 338:140 340:142 342:144 344
438 538:440 540:442 542:444 544
E21
NSECT=3
337 338 1 8
437 438 1 8
*XQT PLTA
SPEC 1
KDTATE 15 1 35 2 55 3
S81 1:S81 2:S81 3
SPEC 2
E41 2:E31 1
*XQT PLTB
DISPLAY=UNDE
UPTION=10,26
PLOT 2
*XQT EXIT
*XQT SEQ
*XQT E
RESET G=380.
T=1.-20 -1.-3 1.-2 1.-2 4. 1.-4 1.-4 1.-4
*XQT EKS
*XQT TAN
*XQT K
*XQT RSI
*XQT AUS
SYSEEC
APPLIED FORCE 1

```

TABLE D1 (Concluded)

CASE 1

I=1:J=169:2925.

I=1:J=180:8775.

I=1:J=109:9410.

I=1:J=118:13607.

I=1:J=127:20158.

I=1:J=136:18567.

I=1:J=145:14054.

I=1:J=154:5595.

I=1:J=389:9862.0

I=1:J=354:9862.0

I=1:J=345:19725.

I=1:J=454:9862.0

I=1:J=445:19725.

I=1:J=489:9862.0

*XQT SSOL

*XQT VPRT

PRINT STATIC DISP

PRINT STATIC REACTIONS

*XQT GSF

*XQT PSF

*XQT PLTA

SPEC 1

ALL

*XQT PLTB

DISPLAY=UNDE

OPTION=26

PLOT 1

*XQT EXIT

TABLE D2

CIRCUMFERENTIAL STRESSES IN PARTIAL RING MODEL
(912 psi Internal Pressure)

| STRESS, ksi | | A |
|-----------------------------------|----------------------------|-----------|
| Radial Plus Axial Load Components | Radial Load Component Only | |
| 45.1 | 54.6 | CAP |
| 49.3 | 60.2 | --- |
| 50.8 | 62.0 | WEB --- |
| 52.4 | 64.1 | --- |
| 53.5 | 66.0 | --- |
| 57.2 | 69.8 | TANG |
| 78.4 | 74.5 | CASE WALL |
| | | A |

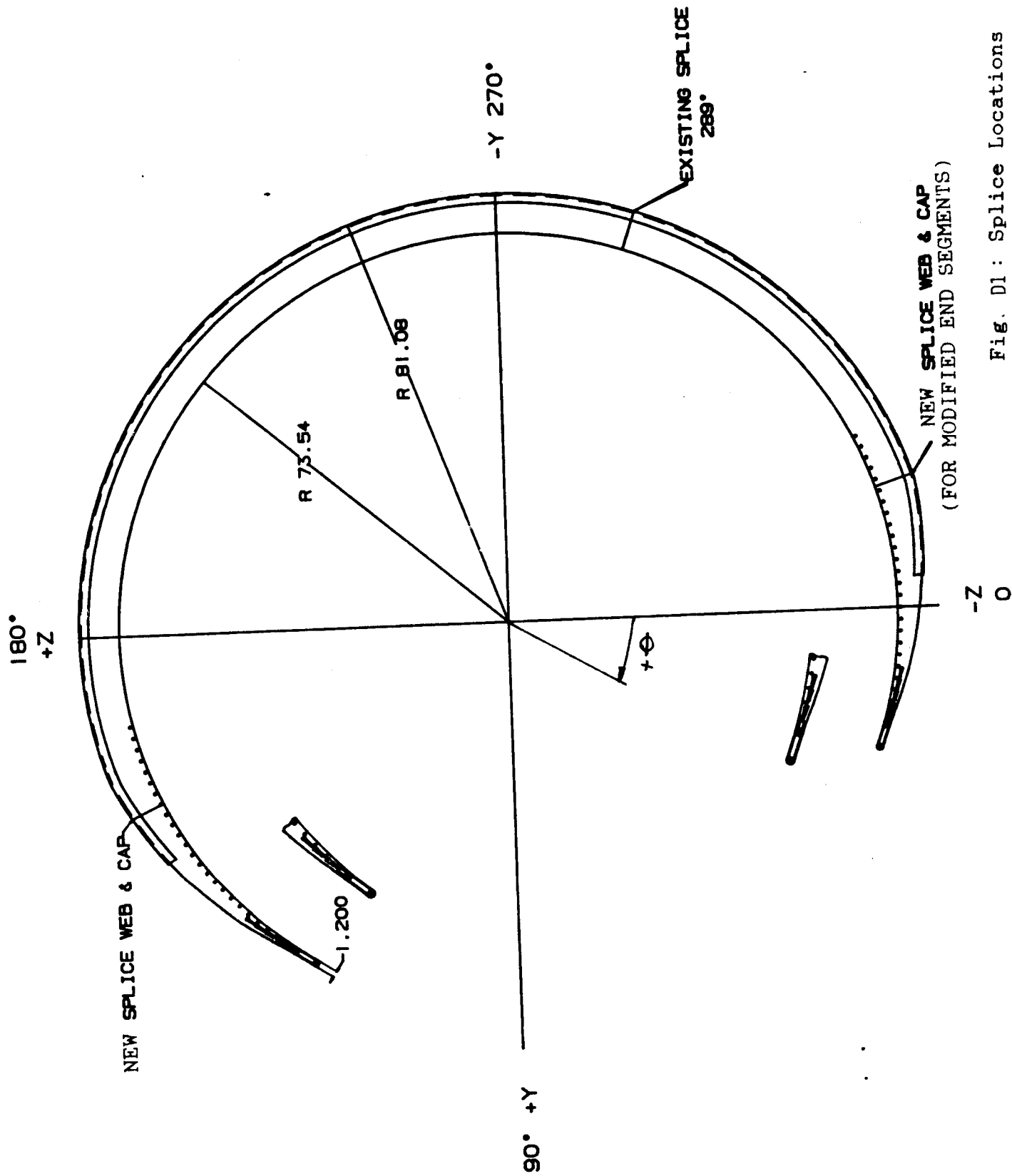


Fig. D1: Splice Locations

SPLICE JOINT

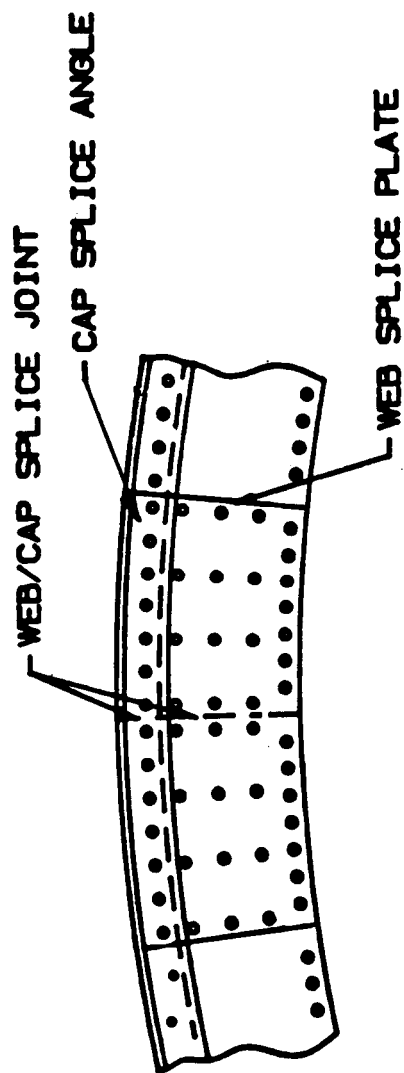


Fig. D2: Existing Splice Configuration

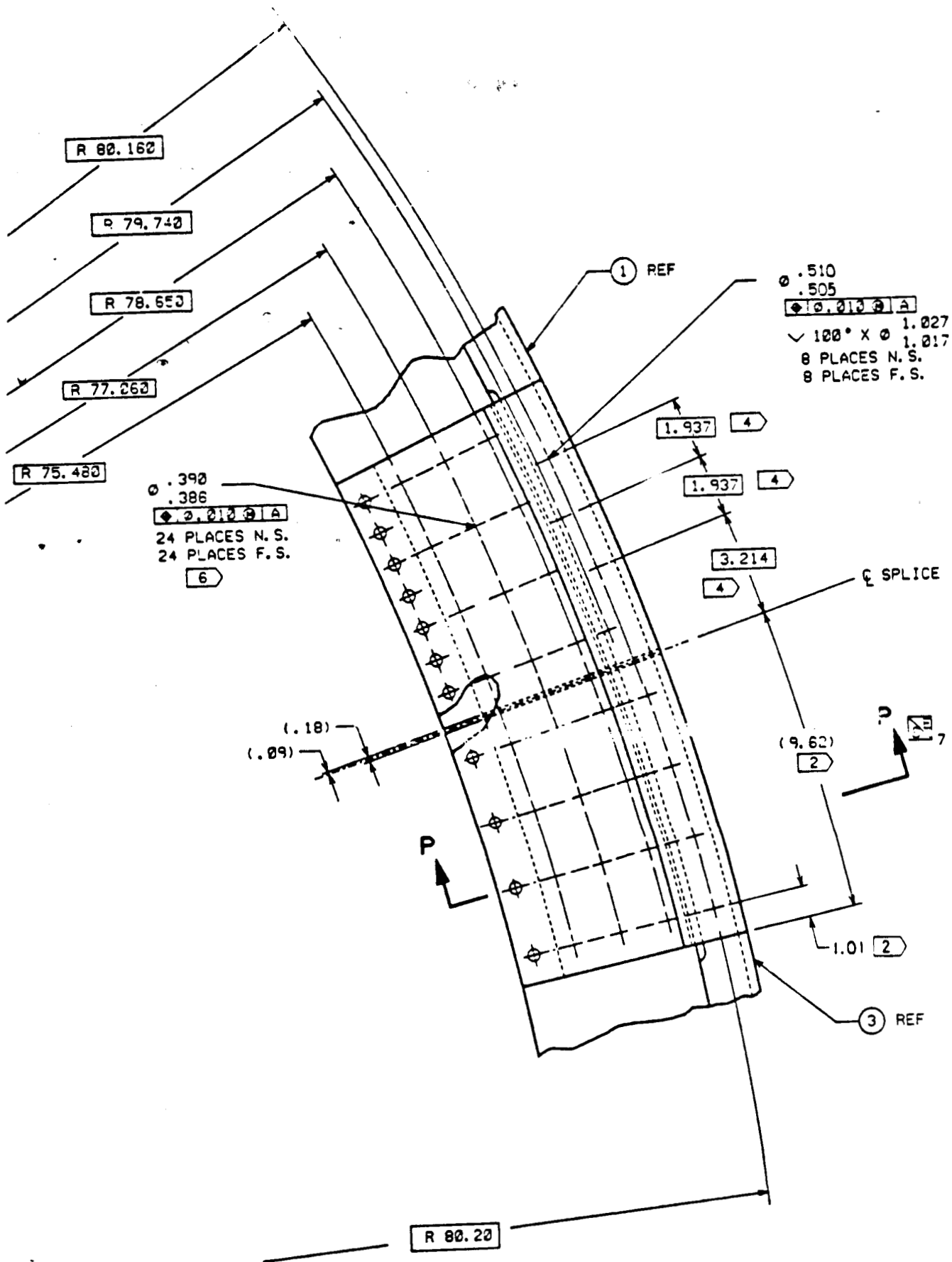


Fig. D3 : New End Splice (Short Side)

ORIGINAL PAGE IS
POOR QUALITY

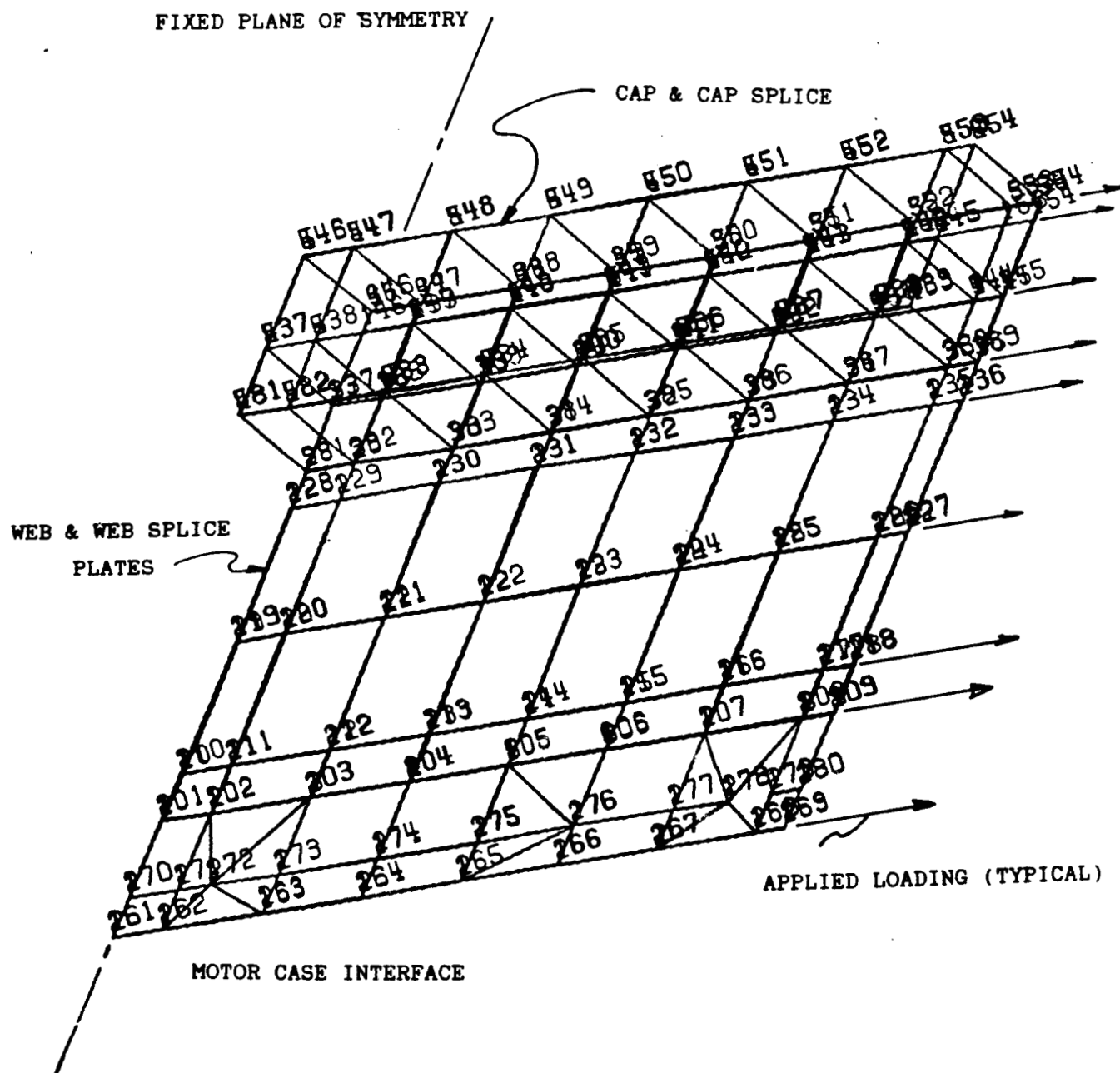


Fig. D4 : Finite Element Model--Existing Splice

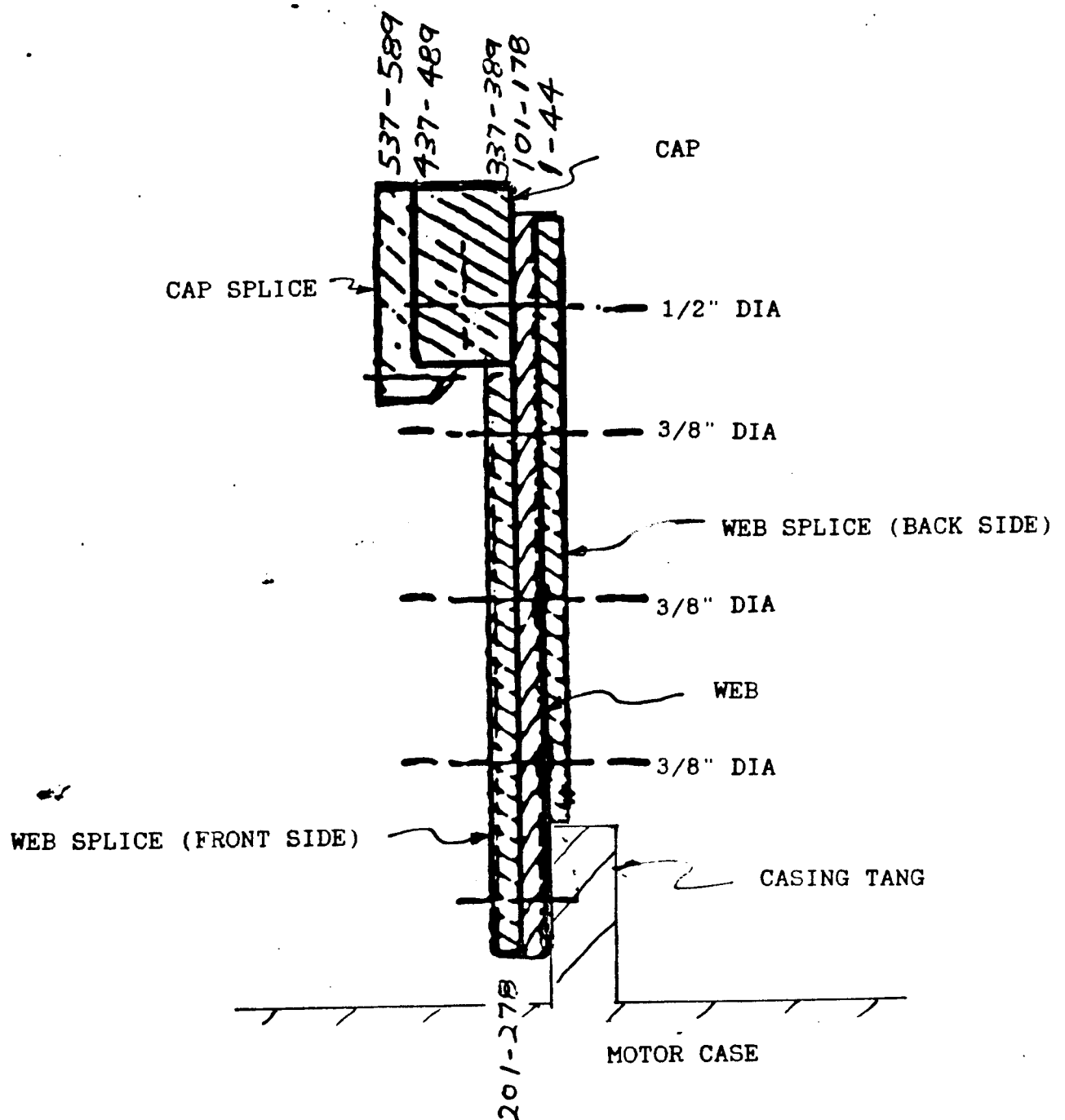


Fig. D5 : Node Numbering

KEY: XX-XXX X.XXX

NODE #'S FORCE, KIPS

| LOCATION | 38-138 | 39-139 | 6.87 | 40-140 | 5.56 | 41-141 | 4.98 | 42-142 | 5.12 | 43-143 | 5.94 | 44-144 | 7.29 |
|------------|---------|---------|---------|---------|---------|---------|---------|---------|---------|---------|---------|---------|------|
| WEB SPLICE | 9.39 | 6.00 | 139-339 | 5.71 | 140-340 | 5.35 | 141-341 | 5.10 | 142-342 | 4.91 | 143-343 | 4.86 | 4.66 |
| PL TO WEB | | | | | | | | | | | | | |
| WEB TO CAP | | | | | | | | | | | | | |
| CAP TO CAP | 8.73 | 439-539 | 6.72 | 440-540 | 5.41 | 441-541 | 4.78 | 442-542 | 4.74 | 443-543 | 5.40 | 444-544 | 6.41 |
| SPLICE | | | | | | | | | | | | | |
| | 29-129 | 0.71 | 31-131 | 0.36 | 33-133 | 0.43 | 35-135 | 0.53 | 37-137 | 0.53 | 39-139 | 0.53 | 0.53 |
| | 129-229 | 6.28 | 131-231 | 3.34 | 133-233 | 3.00 | 135-235 | 4.57 | 137-237 | 4.57 | 139-239 | 4.57 | 4.57 |
| | 20-120 | 4.65 | 22-122 | 3.42 | 24-124 | 3.73 | 26-126 | 5.59 | 28-128 | 5.59 | 30-130 | 5.59 | 5.59 |
| | 120-220 | 4.51 | 122-222 | 2.41 | 124-224 | 2.36 | 126-226 | 4.18 | 128-228 | 4.18 | 130-230 | 4.18 | 4.18 |
| | 11-111 | 3.17 | 13-113 | 2.73 | 15-115 | 3.35 | 17-117 | 5.16 | 19-119 | 5.16 | 21-121 | 5.16 | 5.16 |
| | 111-211 | 2.93 | 113-213 | 1.74 | 115-215 | 2.00 | 117-217 | 3.95 | 119-219 | 3.95 | 121-221 | 3.95 | 3.95 |
| | 172-272 | 2.08 | 174-274 | 1.58 | 176-276 | 2.20 | 178-278 | 4.58 | 180-280 | 4.58 | 182-282 | 4.58 | 4.58 |

Fig. D6 : Bolt Shear Forces
(EXISTING DESIGN)

KEY: XX-XXX X.XXX

LOCATION NODE #'S FORCE, KIPS

| | | | | | | | | |
|-------------------------|-------------------|---------------|-------------------|--------------|-------------------|--------------|-------------------|--------------|
| WEB SPLICE PL TO WEB | 38-138 138-338 | 11.72 9.79 | 40-140 140-340 | 8.04 9.32 | 42-142 142-342 | 7.67 8.90 | 44-144 144-344 | 9.78 8.33 |
| WEB TO CAP | 38-538 | 13.05 | 440-540 | 9.96 | 442-542 | 9.13 | 444-544 | 10.34 |
| CAP TO CAP SPLICE | 29-129 129-229 | 0.64 7.37 | 31-131 131-331 | 0.28 3.95 | 33-133 133-333 | 0.36 3.41 | 35-135 135-335 | 0.58 4.89 |
| | 20-120 120-220 | 5.21 4.98 | 22-122 122-222 | 4.18 2.64 | 24-124 124-224 | 4.58 2.47 | 26-126 126-226 | 6.35 4.20 |
| | 11-111 111-211 | 3.38 3.04 | 13-113 113-213 | 3.11 1.78 | 15-115 115-215 | 3.77 2.01 | 17-117 117-217 | 5.47 3.93 |
| | 172-272 | 2.00 | 174-274 | 1.56 | 176-276 | 2.21 | 178-278 | 4.56 |

Fig. D7 : Bolt Shear Forces

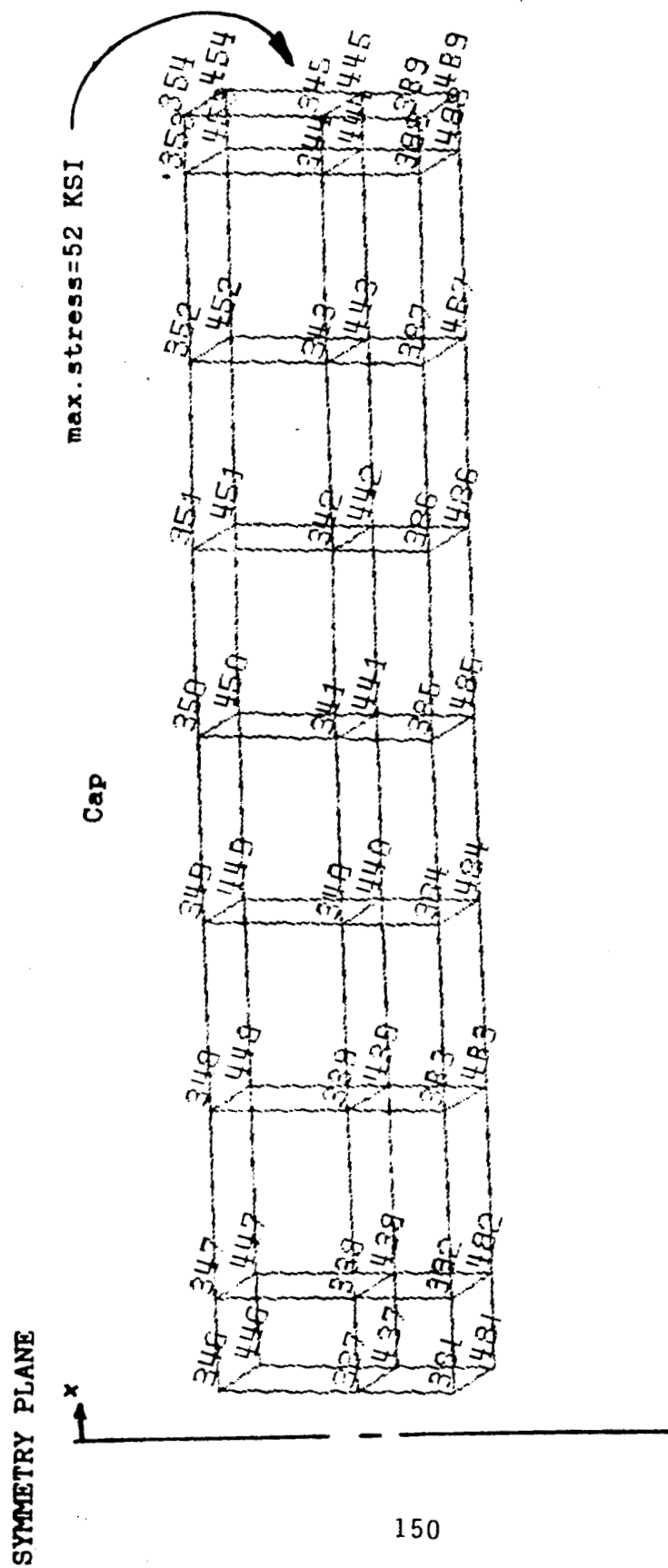


Fig. D8 : Maximum Stresses

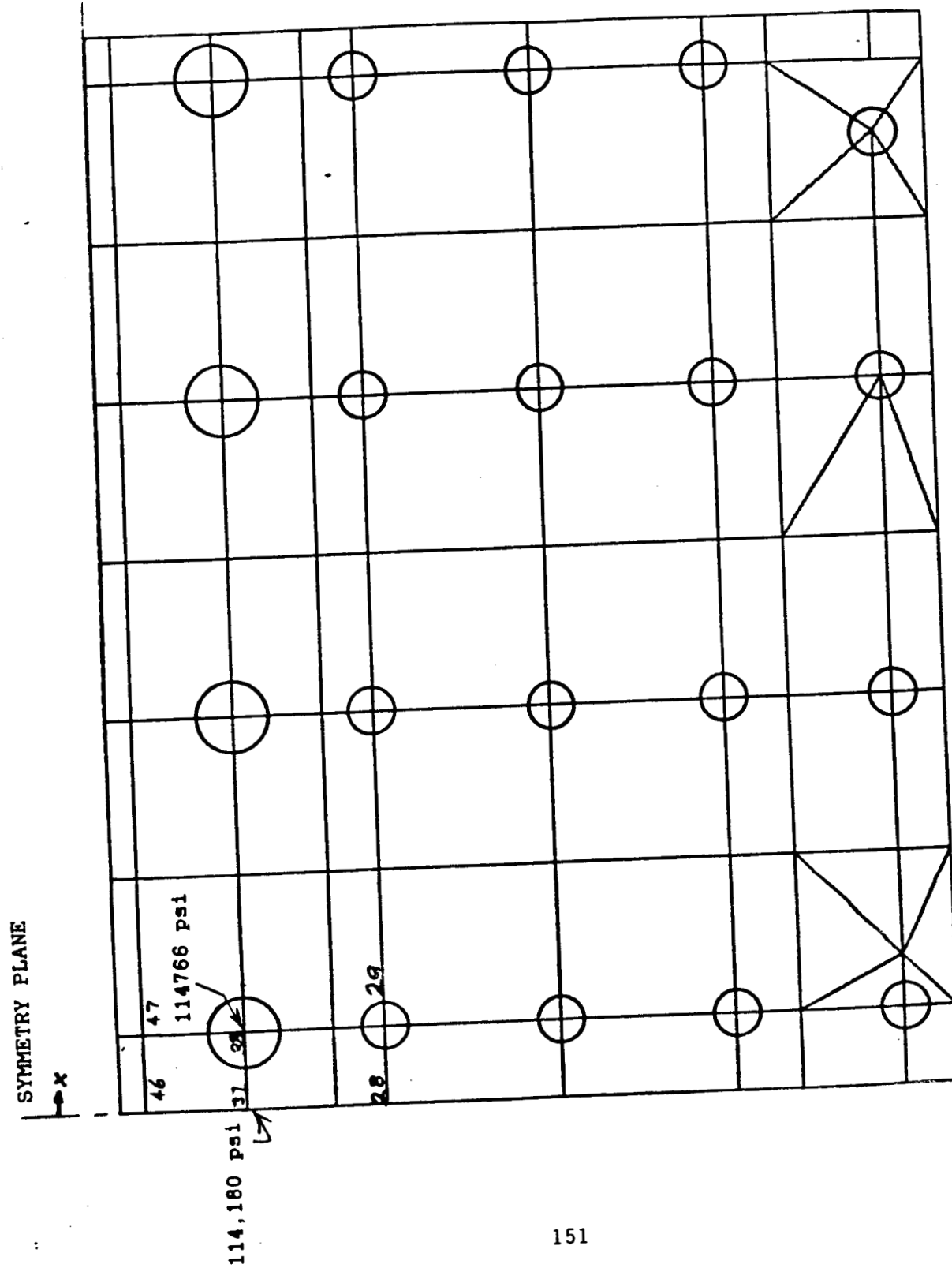


Fig. D9 : Maximum Stresses--Inner Splice Plate

SYMMETRY PLANE

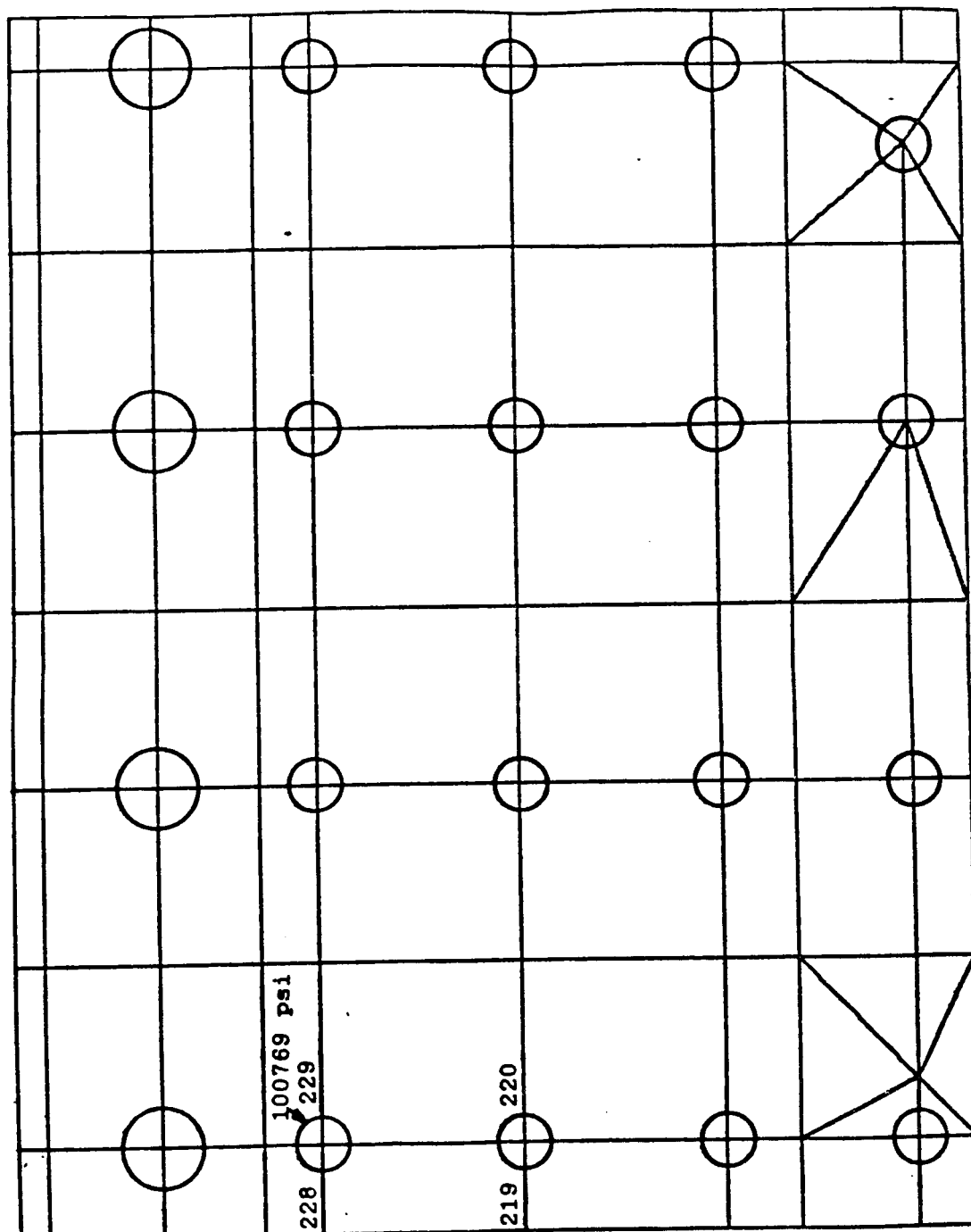


Fig. D10 : Maximum Stresses--Outer Splice Plate

SYMMETRY PLANE

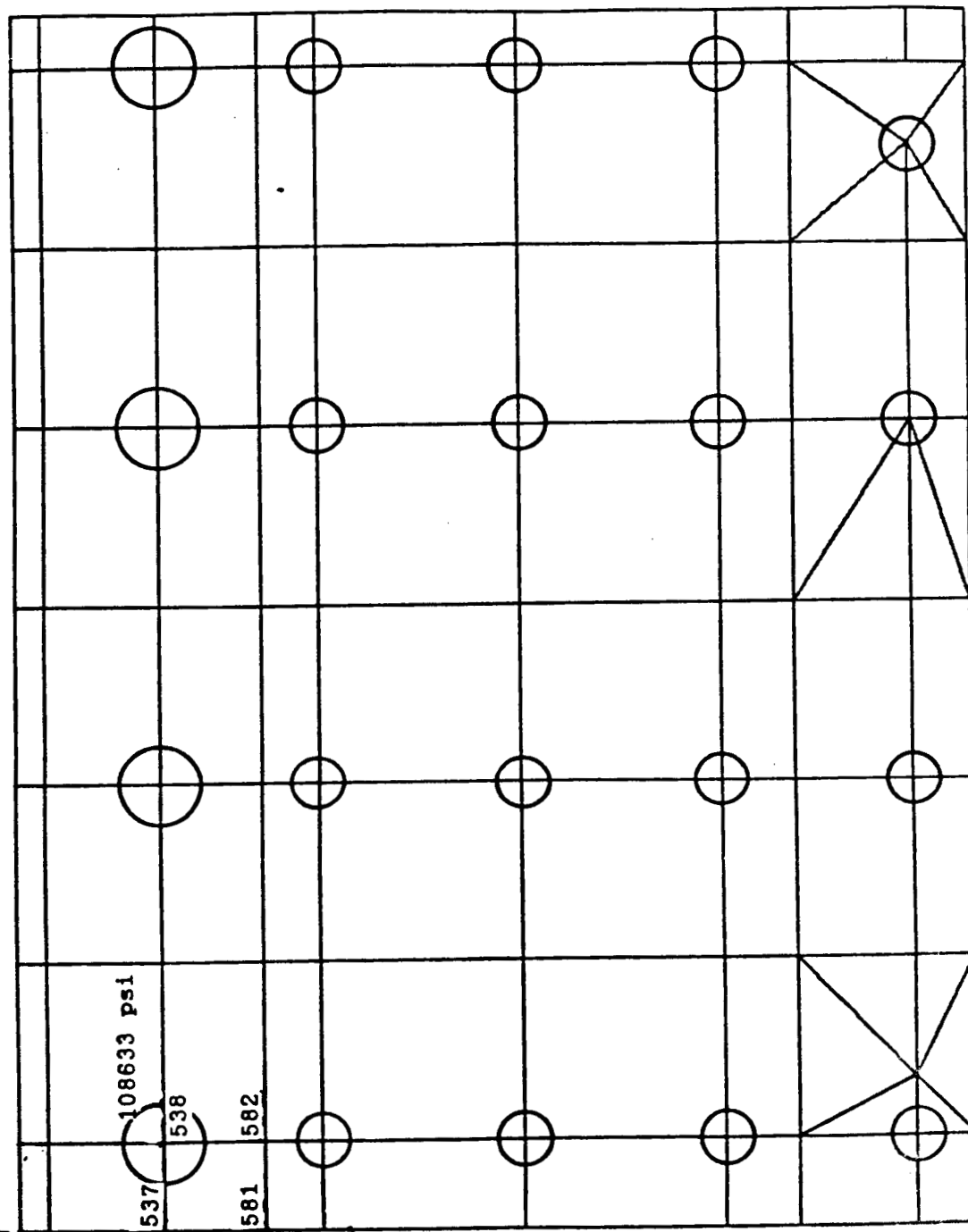


Fig. D11 : Maximum Stresses--Cap Splice Plate

APPENDIX E

ET/SRB ATTACH RING SYSTEMS COVER ANALYSIS

BY
Obie H. Bradley, Jr.
Mail Stop 434
Ph. (804)865-4571

June 9, 1987

Obie H. Bradley, Jr.
Obie H. Bradley, Jr.

Checked by *DH Butler*
Project Engineer *Martin M. Mikulas, Jr.*
Per *Martin M. Mikulas, Jr.*
Project Manager *DH Butler 7/6/87*
David H. Butler

Appendix E

ET/SRB Attach Ring Systems Cover Analysis

Introduction

The systems cover provides protection and attachment locations for wiring and electrical systems components from the ET attach ring to the systems tunnel. The cover is subjected to and must withstand a variety of loads including aerodynamic forces, acceleration, and internal and external pressure. Also, the cover is designed to prevent the transfer of forces and moments to the ET attach ring. At the splice of the ET attach ring ends and the existing ring body, the systems cover will transition to the existing cover assembly.

Hardware Description

Details of the hardware are shown in fig. E1 and fig. E2. The side rings are 3/32 inch thick curved angle segments of 4340 steel which attach to the motor case ring. The segments are attached to the motor case rigidly at only one bolt per segment side. The other bolt holes are slotted to allow expansion of the motor case without loading the side rings of the cover. The cover plate is made up of 3/16 inch thick segments of 4340 steel which attach to the side ring segments. Brackets are provided on 9 inch centers to provide additional stiffness for the rings.

The ring segments are connected to each other by a flexible joint. this joint allows for expansion between the rings while maintaining a weather-proof seal. The cover rings and plate meet the existing cover system at the point where the ET ring begins to taper. At this point a seal is formed to maintain pressure and weather-proof the systems tunnel. The systems cover and ET attach ring are covered with cork insulation before flight to minimize heat transfer.

Analysis

The following analysis considers the combined loading due to aerodynamic forces, acceleration forces, and internal or external pressure. Factors of safety based on MSFC-HDBK-505, Rev. A have been applied to determine the margins of safety. A summary of the worst case stresses and margins is included at the end of this section.

ANALYSIS

LOADS:

The loads which shall be considered are summarized below:

Acceleration : 3.2 g (max.) per JSC 07700 Volume XIV
Attachment 1

Differential Pressure: 26 psid per SE-019-142-2H
"Solid Rocket Booster
Venting Analysis"

Aerodynamic : 819 psf per SE-019-142-2H

Factors of Safety:

ORIGINAL PAGE IS
OF POOR QUALITY

F.S. on yield = 1.25

F.S. on ultimate = 2.00

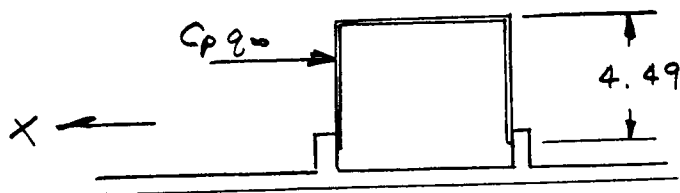
Material Allowables:

Rings and cover 4340 stl.

yield = 160 KSI

Ult = 180 KSI

Aerodynamic Force



$$C_p = 1.25$$

$$q = 819 \text{ psf}$$

$$F_{AERO} = C_p q_\infty A$$

$$= 1.25(819) A$$

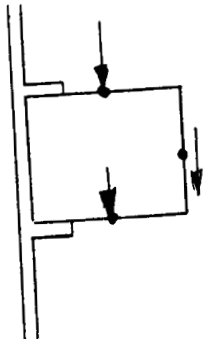
$$F_{AERO} = 1024 \text{ psf}$$

$$AREA_X = \frac{4.49}{12} \times 1 = .374 \text{ ft}^2/\text{ft. of ring}$$

values per SE-019-142-2H
"Solid Rocket Booster Venting Analysis"

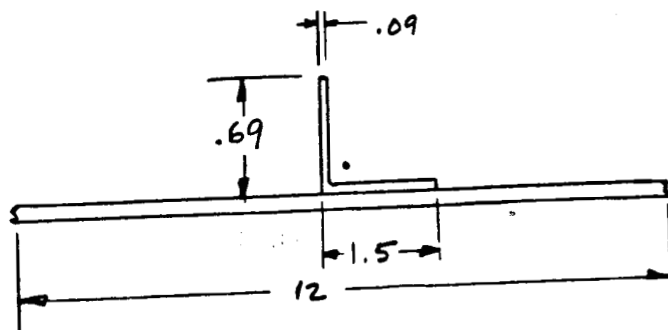
42 381 50 SHEETS 5 SQUARE
42 382 100 SHEETS 5 SQUARE
42 389 200 SHEETS 5 SQUARE

ORIGINAL PAGE IS
OF POOR QUALITY



$$\begin{aligned} F_{\text{Accel}} &= mg \\ &= 15.83 (3.2) \\ &= \underline{50.66} \text{ lb/ft} \end{aligned}$$

Moment of Inertia, I for side rings



$$I_{\text{vert. leg}} = \frac{bh^3}{12} = \frac{.09(.69^3)}{12} = .00246 \text{ in}^4 \quad \text{Area} = .09(.69) = .0621 \text{ in}^2$$

$$I_{\text{Horiz leg}} = \frac{bh^3}{12} = \frac{1.41(.09^3)}{12} = .0000857 \text{ in}^4 \quad \text{Area} = 1.41 \times .09 = .127 \text{ in}^2$$

$$I_{\text{plate}} = \frac{bh^3}{12} = \frac{12(.09^3)}{12} = .000729 \text{ in}^4 \quad \text{Area} = 12 \times .09 = 1.08 \text{ in}^2$$

Centroid of composite plate

$$\bar{X} = \frac{\sum Ax}{\sum A}$$

$$= \frac{.0621(.435) + .127(.135) + 1.08(.045)}{.0621 + .127 + 1.08}$$

$$\bar{X} = .073 \text{ in.}$$

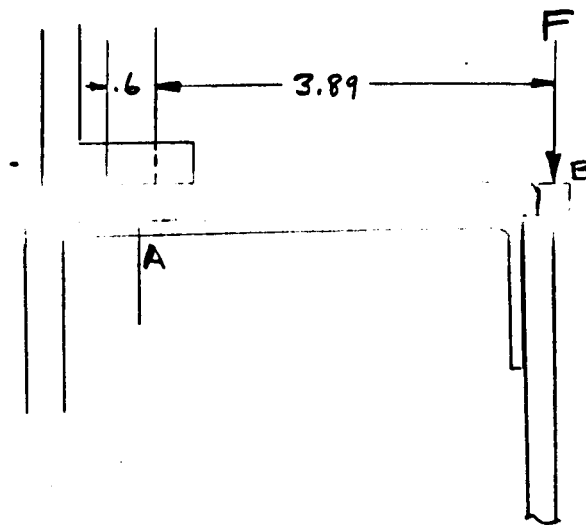
$$I = I_o + Ad^2$$

$$I = .00246 + .0000857 + .000729 + .0621(.435 - .073)^2$$

$$+ .0000857(.135 - .073)^2 + .000729(.073 - .045)^2$$

$$I = 0.113 \text{ in}^4$$

Stresses Due To Aerodynamic and Acceleration Forces



$$\text{Force} = F_{\text{Aero}} + F_{\text{Accel}}$$

$$= 383 + 50.66$$

$$F = 433.7 \text{ lb.}$$

Bending stress at A

$$\sigma = \frac{Mc}{I}$$

$$= \frac{433.7}{2} \frac{(3.89)(.707)}{.0113}$$

$$\sigma = \underline{52,178 \text{ psi}}$$

Deflection

$$\delta = \frac{Fl^3}{3EI} = \frac{433.7}{2} \frac{(3.89)^3}{3(30 \times 10^6)(.0113)} = .013 \text{ in.}$$

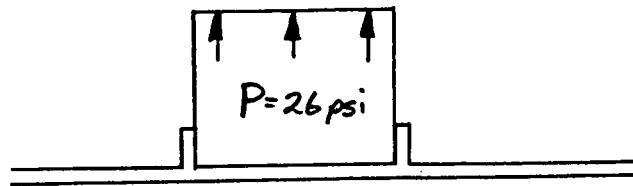
Bolt load

$$\sum M = 0$$

$$.6(F_{\text{bolt}}) = 4.49 \left(\frac{433.7}{2} \right) \times \frac{2.25}{12} \quad \text{bolt spacing}$$

$$F_{\text{bolt}} = \underline{304} \text{ lb.} \quad \text{tension}$$

Stresses Due To Pressure on Cover



$$\text{Stress in side ring} = \frac{P \times A_{\text{cover}}}{A_{\text{ring}}}$$

$$= \frac{26 (12)(12)}{12(.09)(2)}$$

$$= \underline{1733} \text{ psi} \quad \text{tension}$$

Shear in fasteners due to pressure

$$\text{Load} = \frac{P \times A}{\text{No. of fasteners}}$$

$$= \frac{26 \times 12 \times 12}{2 \times 12 / 2.25} = \underline{351} \text{ lb./fastener shear}$$

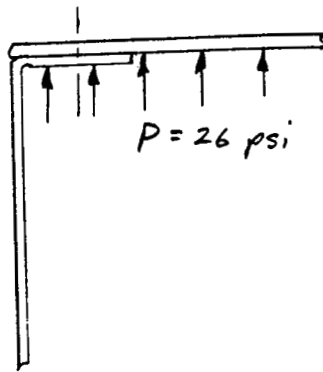
Cover (see following page for MSC-CASE output)

$$\sigma = \frac{6M}{t^2}$$

$$= \frac{6(323)}{.1875^2}$$

$$\sigma = \underline{55125} \text{ psi} \quad \text{due to bending in cover}$$

Cover bolt loads (tension)



ORIGINAL PAGE IS
OF POOR QUALITY

$$\text{bolt spacing} = 2.25''$$

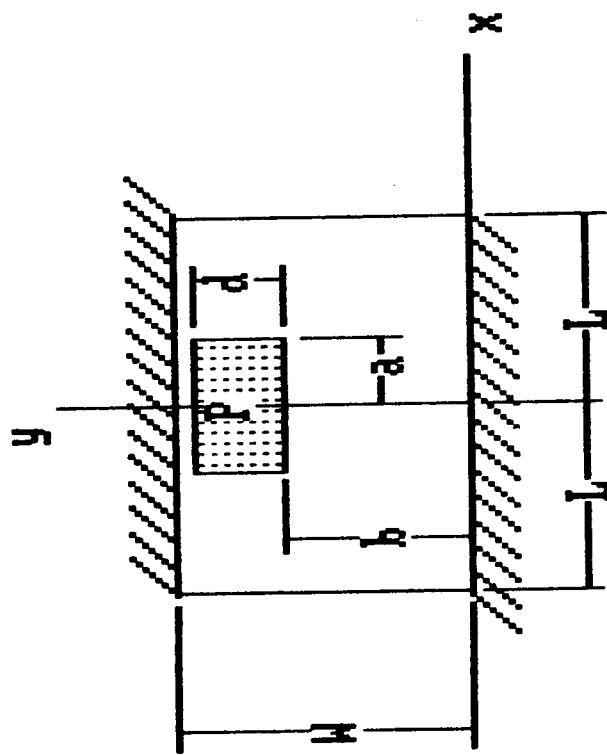
$$\text{Load per bolt} = P \times A_{\text{cover}} / \text{bolt}$$

$$= 26 \times 2.25 \times 12 / 2$$

$$F_{\text{bolt}} = 351 \text{ lb. Tension}$$

Module D-2: Plates - Rectangular

COVER PLATE



$M_x(\max) = 1.07E+02$
 $M_y(\max) = 3.23E+02$
 $M_{xy}(\max) = 2.89E+01$

LENGTH, $L = 7.875$
 WIDTH, $W = 12$
 THICKNESS, $t = .1875$

ELAST MOD, $E = 30e6$
 POISSON, $\nu = .33$
 LOAD, $P = 4914$

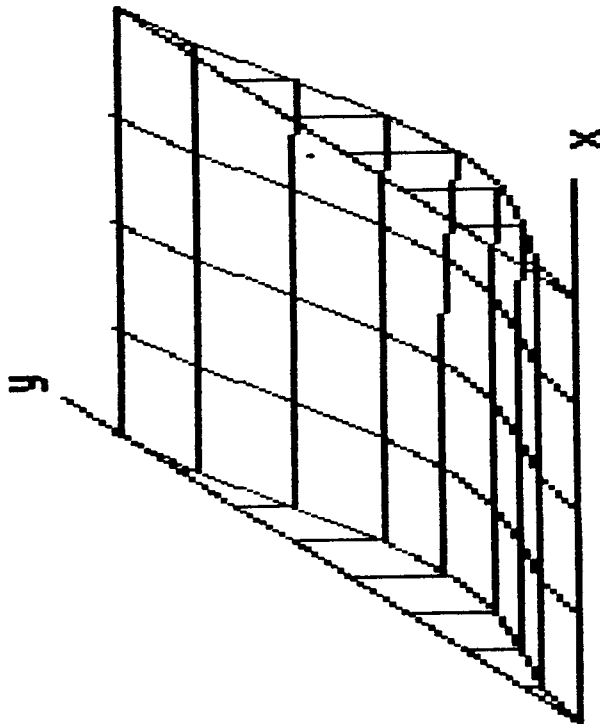
ENTER F6 FOR BOUNDARY REACTIONS OR
 F7 FOR BOUNDARY MENU

F2PRINT F3DISP

F6NEXT F7MENU

F8REDO F9SAVE F10TOP

Deflection



$w(\max) = 8.56E-02$

$a [1-4 \text{ only}] = 4(L/4)$
 $b [0-7 \text{ only}] = 0(W/8)$
 $d [1-8 \text{ only}] = 8(W/8)$

- side Ring Plates (see following page for MSC-CASE output)

$$\sigma = \frac{6M}{t^2}$$

$$= \frac{6(33.9)}{.092}$$

ORIGINAL PAGE IS
OF POOR QUALITY

$$\sigma = \underline{25111} \text{ psi} \quad T$$

- side to cover bolt loads (shear)

$$\text{bolt spacing} = 2.25''$$

$$\text{Load per bolt} = P \times A_{\text{side}} / \text{bolt}$$

$$= 26 \times 2.25 \times 3.89 / 2$$

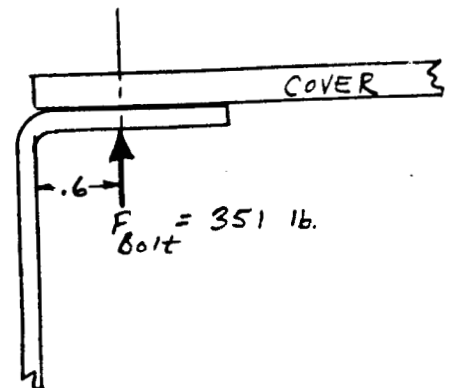
$$F_{\text{bolt}} = 114 \text{ lb.} \quad \text{shear}$$

- Bending stress in side angles

$$\sigma = \frac{Mc}{I}$$

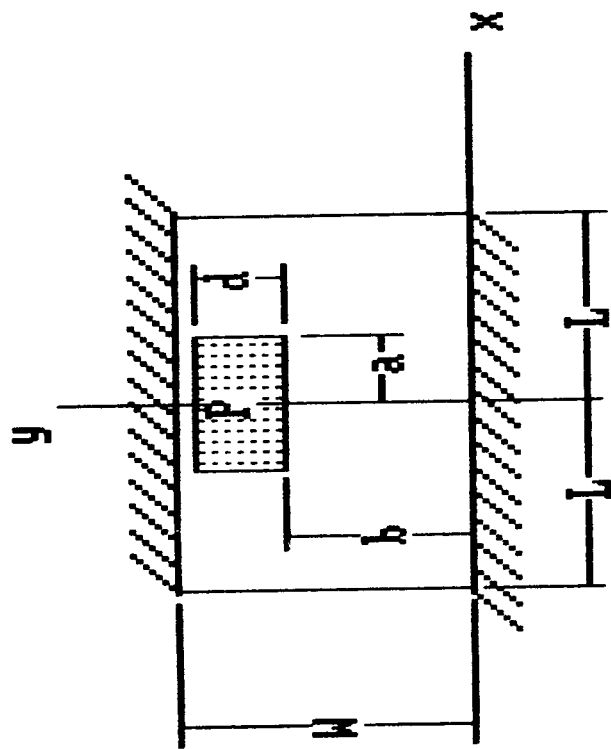
$$= \frac{351(.6)(.095)}{2.25 \frac{(.093)^3}{12}}$$

$$\sigma = \underline{69333} \text{ psi}$$



Module D-2: Plates - Rectangular

SIDE RING PLATE



$M_x(\text{max}) = 1.12\text{E}+01$
 $M_y(\text{max}) = 3.39\text{E}+01$
 $M_{xy}(\text{max}) = 2.49\text{E}+00$

LENGTH, L = 7.875
 WIDTH, W = 3.89
 THICKNESS, t = .09

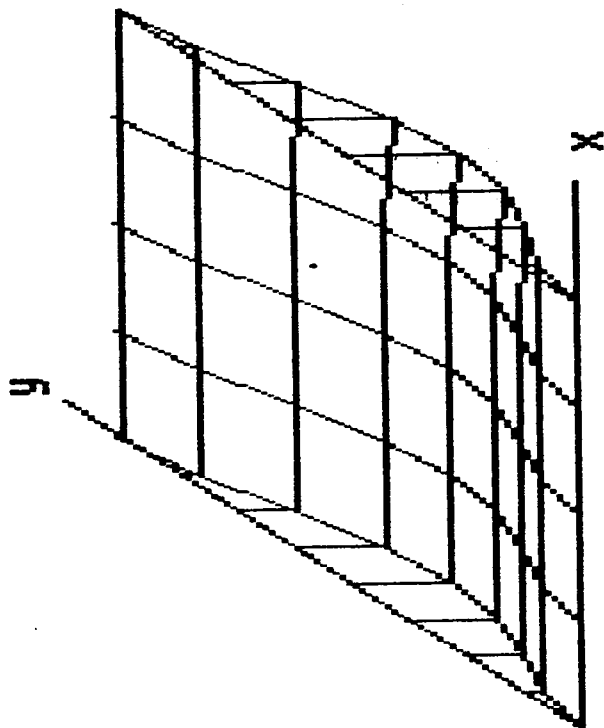
ELAST MOD, E = 30e6
 POISSON, ν = .33
 LOAD, P = 1593

ENTER F6 FOR BOUNDARY REACTIONS OR
 F7 FOR BOUNDARY MENU

F2PRINT F3DISP

F6NEXT F7MENU F8REDO F9SAVE F10TOP

Deflection



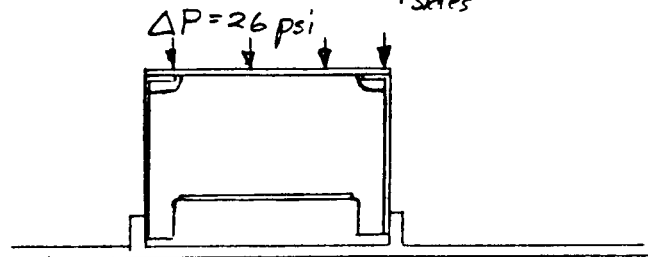
$w(\text{max}) = 8.26\text{E}-03$

a [1-4 only] = 4(L/4)
 b [0-7 only] = 0(W/8)
 d [1-8 only] = 8(W/8)

Buckling

Side rings - The buckling will be calculated for a flat plate. Brackets are provided on 9" centers which provide end fixity for the rings. The buckling stress, $\sigma_{cr} = 20880 \text{ psi}$ as shown on the following page which is output from the program MSC-CASE. For a maximum crushing pressure of 26 psi,

$$\text{Stress in side rings} = \frac{P \times A_{\text{corner}}}{A_{\text{sides}}}$$



$$\sigma_{\text{sides}} = \frac{26 (12 \times 9)}{9 (.09) 2}$$

$$\sigma_{\text{sides}} = \underline{1733} \text{ psi} \quad \text{Compression}$$

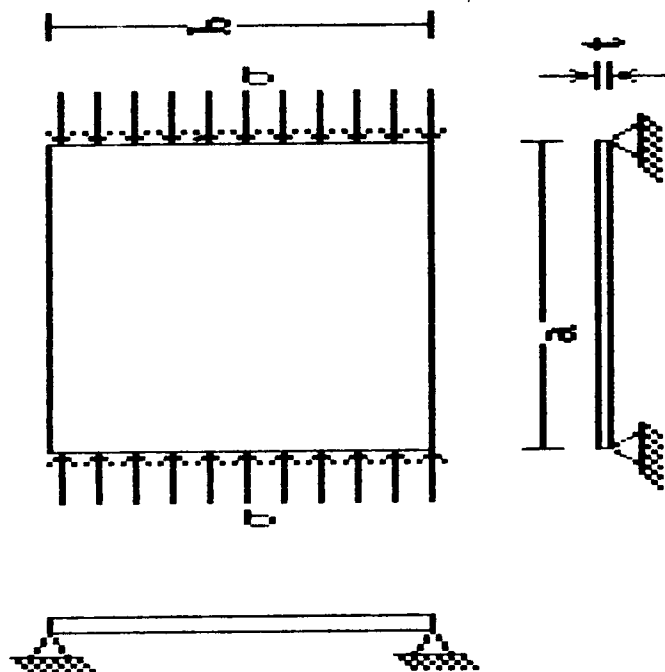
The pressure on the sides of the rings, however, will cause a deflection which could reduce σ_{cr} . The cross members control this and actually form a short column with the side rings. The buckling of the short column will be checked.

Module D-6: Buckling of Plates and Shells

Side Rings

DIMENSION a =3.89
 DIMENSION b =9
 THICKNESS t =.09
 ELAS MOD, E =30E6
 POISSON'S, ν =.33

$\omega_r = 2.088E+04$



ENTER F7 FOR LOADING CONDITION MENU

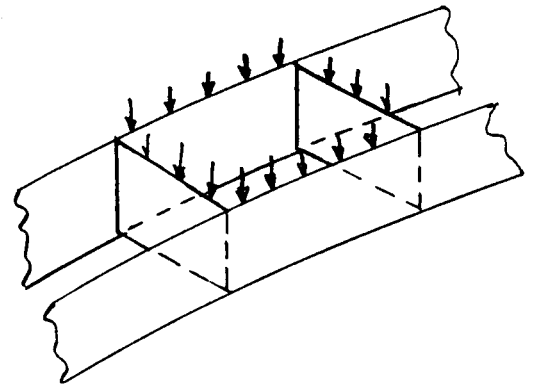
F2PRINT F3DISP

F7MENU F8REDO F9SAVE

Assume that the side rings and brackets form a short column. The moment of inertia of this column is (conservatively),

$$I \approx Ad^2$$
$$= 1.08 (6^2)$$

$$I = 38.9 \text{ in.}^4$$



The critical buckling stress is

$$\sigma_{cr} = 1.5 \times 10^9 \text{ psi} \quad \text{from MSC - Case program}$$

Therefore the section will yield before it buckles.

ORIGINAL PAGE IS
OF POOR QUALITY

Buckling of cover

From MSC-CASE the critical buckling-stress is , $\sigma_{cr} = 16680 \text{ psi}$ (see following page).

$$\sigma_{cover} = \frac{P \times A_{sides}/2}{A_{cover}}$$

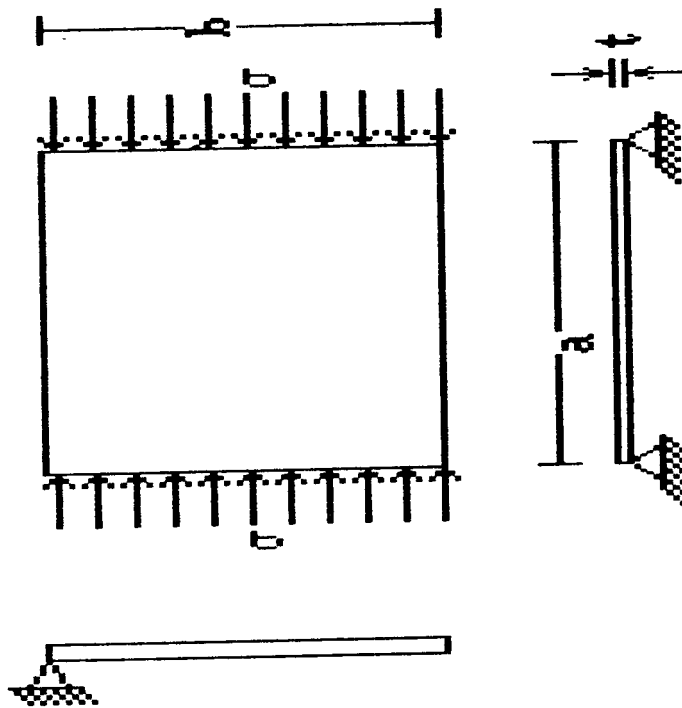
$$= \frac{26 \times 3.89 (15.75/2)}{.1875 \times 15.75}$$

$$\sigma_{cover} = \underline{270 \text{ psi}} \quad \text{Compression}$$

COVER Module D-6: Buckling of Plates and Shells

DIMENSION a =12
 DIMENSION b =15.75
 THICKNESS t =.1875
 ELAS MOD E =30E6
 POISSON'S ν =.33

$\sigma_{cr} = 1.668E+03$

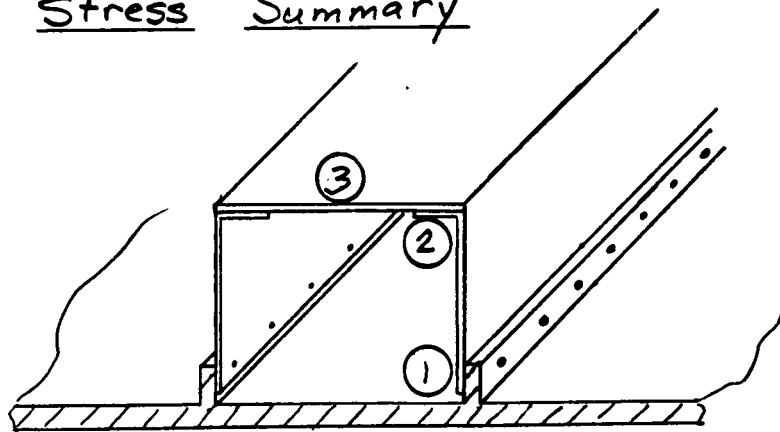


ENTER F7 FOR LOADING CONDITION MENU

F2PRINT F3DISP

F7MENU F8REDO F9SAVE

Stress Summary



| <u>Location</u> | <u>Max. Stress or Load</u> | <u>M.S. (ULT.)</u> |
|----------------------------|----------------------------|--------------------|
| ① Side rings near bolts | 79622 psi | .13 |
| ② Side angle | 69333 | .30 |
| ③ Cover | 55125 | .63 |

Fasteners

| | | |
|-------|-----------------|------|
| Tang | 304 lb. Tension | >2.0 |
| | 351 lb. Shear | >2.0 |
| Cover | 351 lb. Tension | >2.0 |
| | 114 lb. Shear | >2.0 |

Buckling Summary

| <u>Location</u> | <u>Stress</u> | <u>Buckling Stress</u> |
|-----------------|---------------|------------------------|
| Side rings | 1733 | 20880 |
| Cover | 270 | 16680 |

42 381 30 SHEETS 3 SQUARE
42 382 30 SHEETS 3 SQUARE
42 383 30 SHEETS 3 SQUARE
42 384 30 SHEETS 3 SQUARE



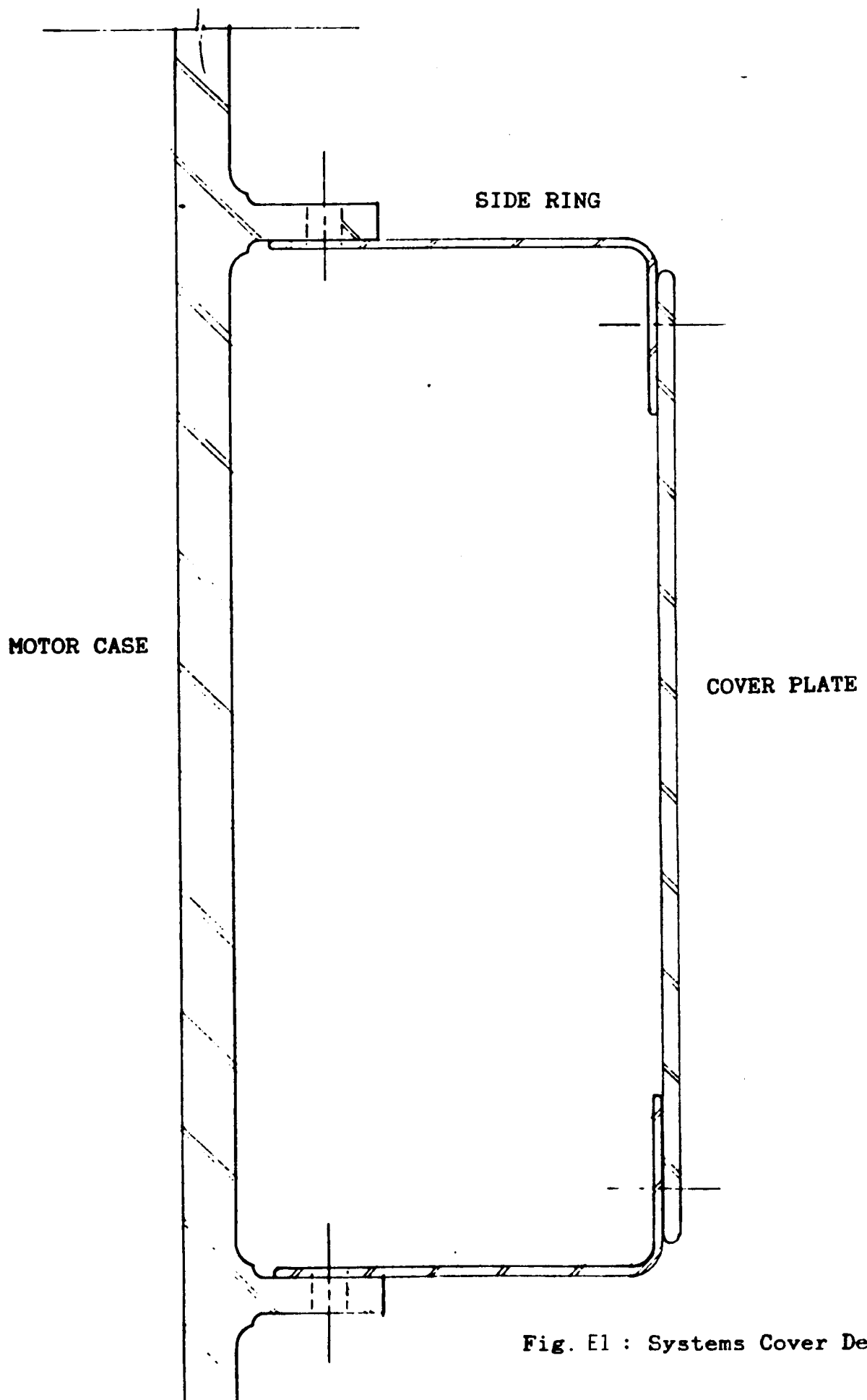


Fig. E1 : Systems Cover Detail

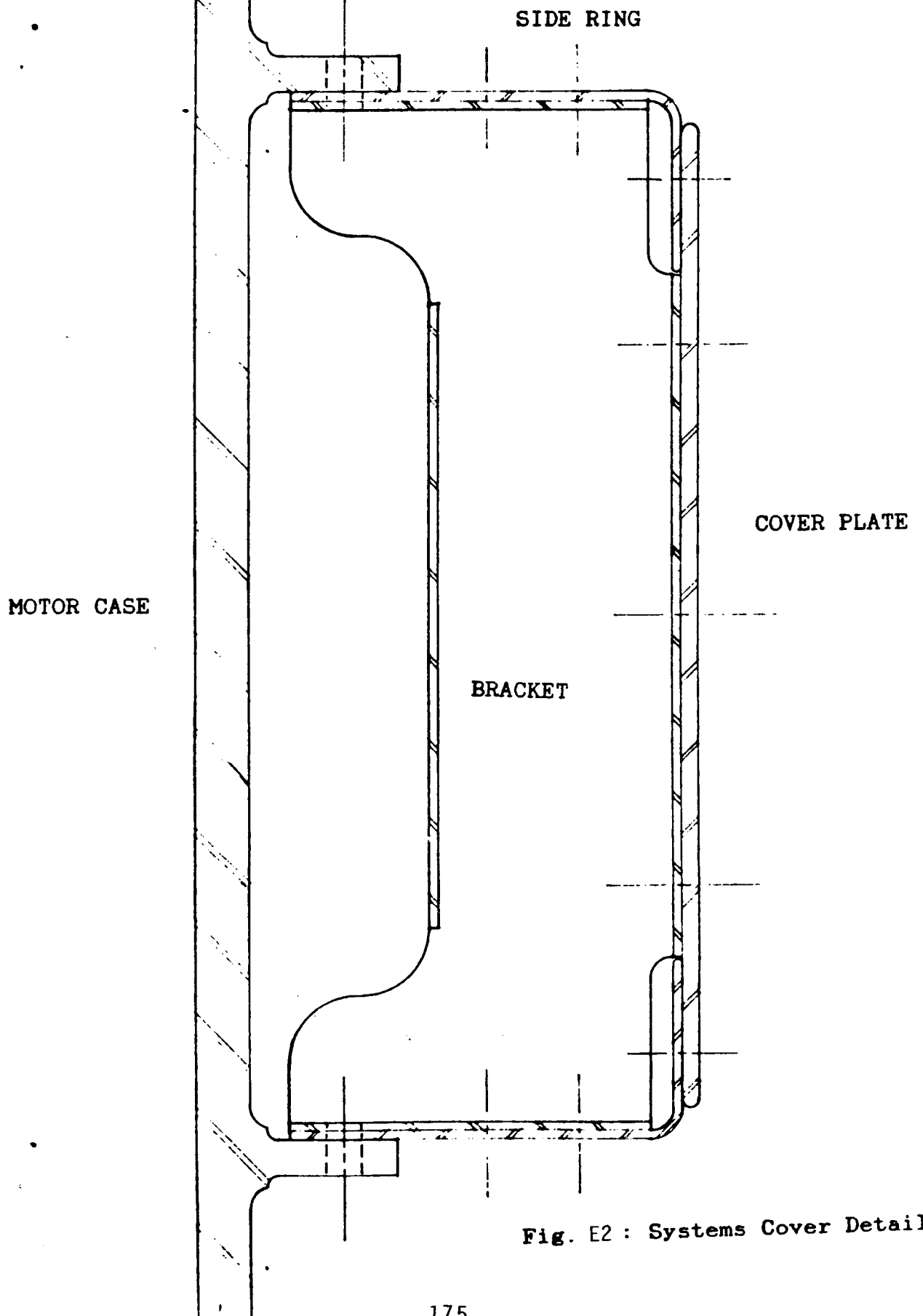


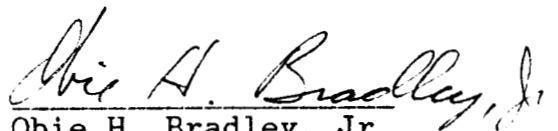
Fig. E2 : Systems Cover Detail

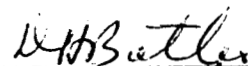
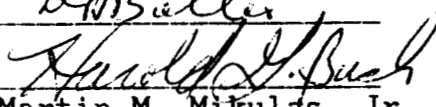
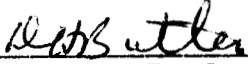
APPENDIX F

MARGINS OF SAFETY
AND
OTHER SUPPORTING ANALYSES

BY
Obie H. Bradley, Jr.
Mail Stop 434
Ph. (804)865-4571

June 9, 1987


Obie H. Bradley, Jr.

Checked by 
Project Engineer 
for Martin M. Mikulas, Jr.
Project Manager 
David H. Butler

APPENDIX F

MARGINS OF SAFETY

Margins of safety are provided in Table F1 for the worst case predicted stresses for the part or system location indicated. These margins, therefore, are the lowest values calculated for the locations. The following equation has been used to determine each value:

$$M.S. = \frac{\text{allowable stress}}{\text{predicted stress} \times \text{factor of safety}} - 1$$

For acceptance,

$$M.S. \geq 0.0$$

The factors of safety have been obtained from MSFC-HDBK-505, Rev. A. For the materials which have been specified, the margins are based on the ultimate allowable strength values since these are the most critical.

The stresses used are based on a number of analyses which combine the effects of SRB pressure, strut loads, aerodynamic drag, and acceleration. The approach taken in these analyses was to assume that structure responded in a linear-elastic manner.

TABLE F 1: MARGINS OF SAFETY

| LOCATION | STRESS OR LOAD | MARGIN OF SAFETY |
|--|---|-------------------------------------|
| RING (SEE FIG. F1) WEB--SECTION BETWEEN BOLTS 1-2 WEB--SECTION BETWEEN BOLTS 2-3 WEB--SECTION BETWEEN BOLTS 3-4 | 71600 PSI 126800 PSI 123200 PSI | .80 .01 .04 |
| RING NET SECTIONS AT BOLTS AT SHORT END OF RING BOLT 1 BOLT 2 BOLT 3 BOLT 4 | 39550 PSI 81500 PSI 121300 PSI 115300 PSI | 2.25 .58 .06 .12 |
| TANG BOLTS (SEE FIG. F2) BOLT 1 BOLT 2 BOLT 3 | 7950 LBS 8430 LBS 8000 LBS | .44 .36 .43 |
| SPLICE INNER SPLICE PLATE OUTER SPLICE PLATE CAP SPLICE PLATE BOLTS CAP, 1/2" WEB, 3/8" | 114800 PSI 100800 PSI 108600 PSI 13050 LBS 7370 LBS | .12 .28 .18 .55 .55 |

TABLE F1:MARGINS OF SAFETY (CONT'D)

| LOCATION | STRESS OR LOAD | MARGIN OF SAFETY |
|----------------------------|----------------|------------------|
| SYSTEMS COVER (SEE FIG.F3) | | |
| SIDE RINGS NEAR BOLTS | 79622 PSI | .13 |
| CRIPPLE ANGLE | 69333 PSI | .30 |
| COVER | 55125 PSI | .63 |
| BOLTS | | |
| TANG, 3/8" | 351 LBS | > 2.0 |
| COVER, 1/4" | 351 LBS | > 2.0 |

PRINCIPAL STRESSES

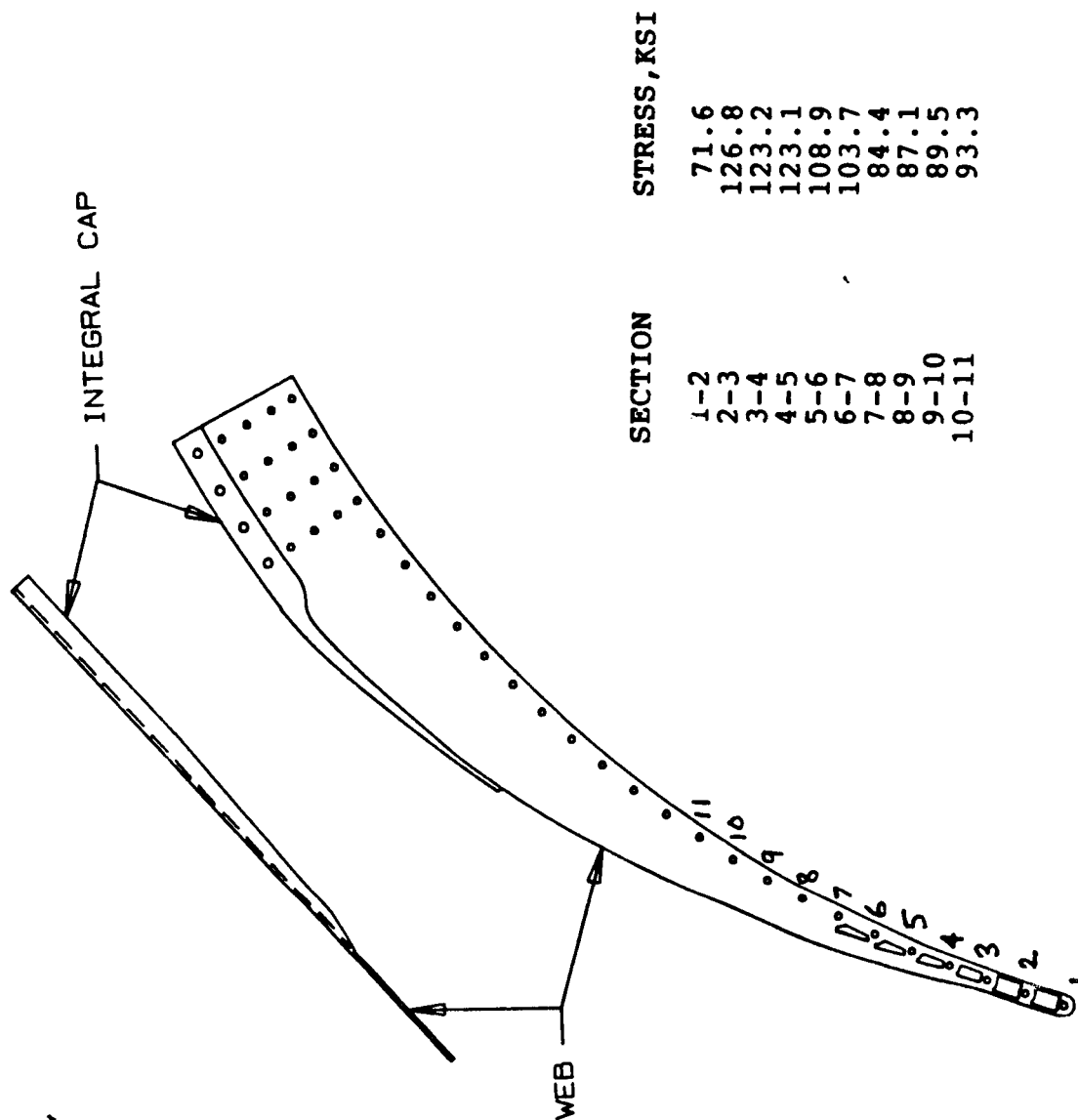


Fig. F1 : Ring Web Stresses

BOLT LOADS---SHORT END

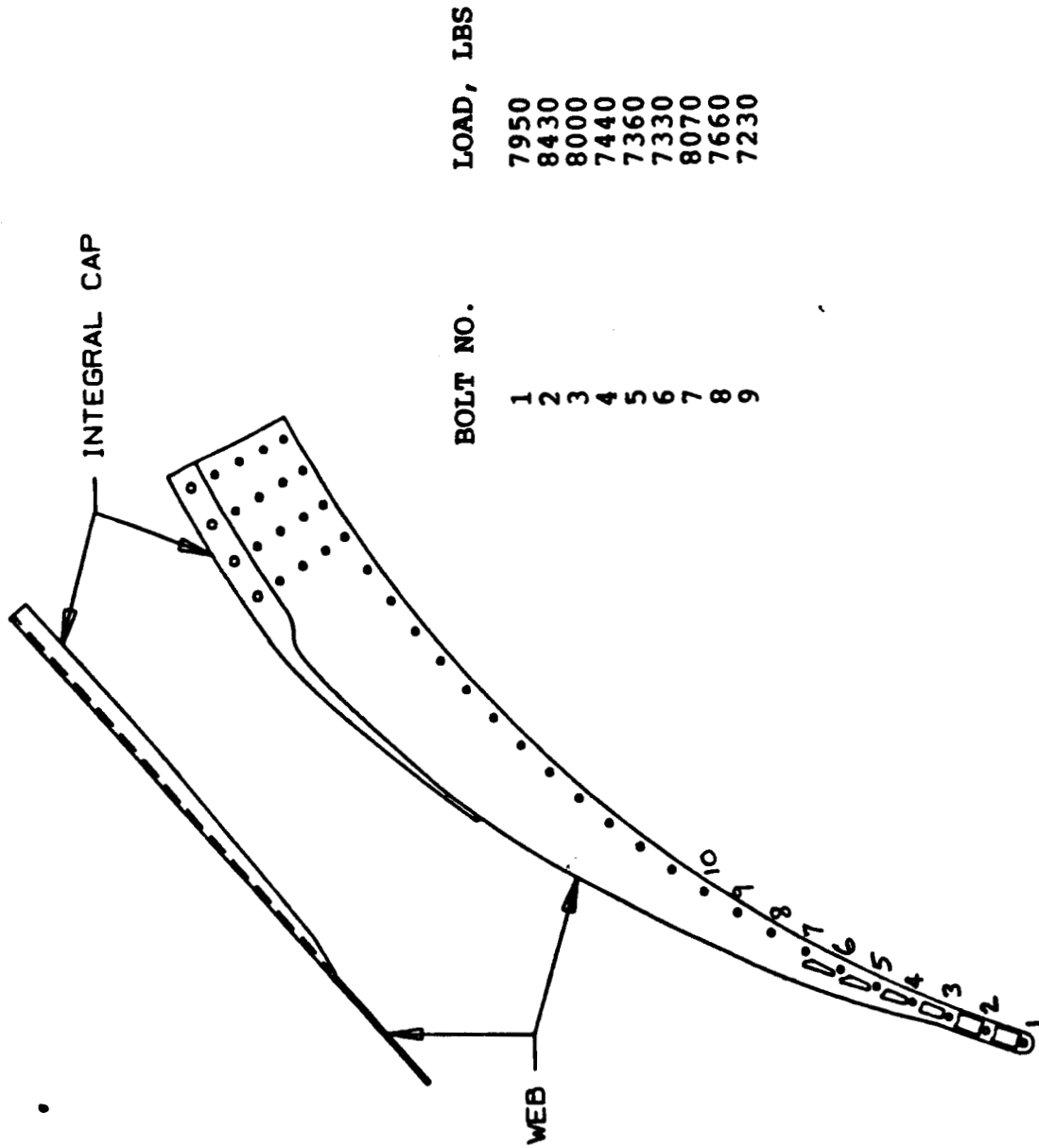
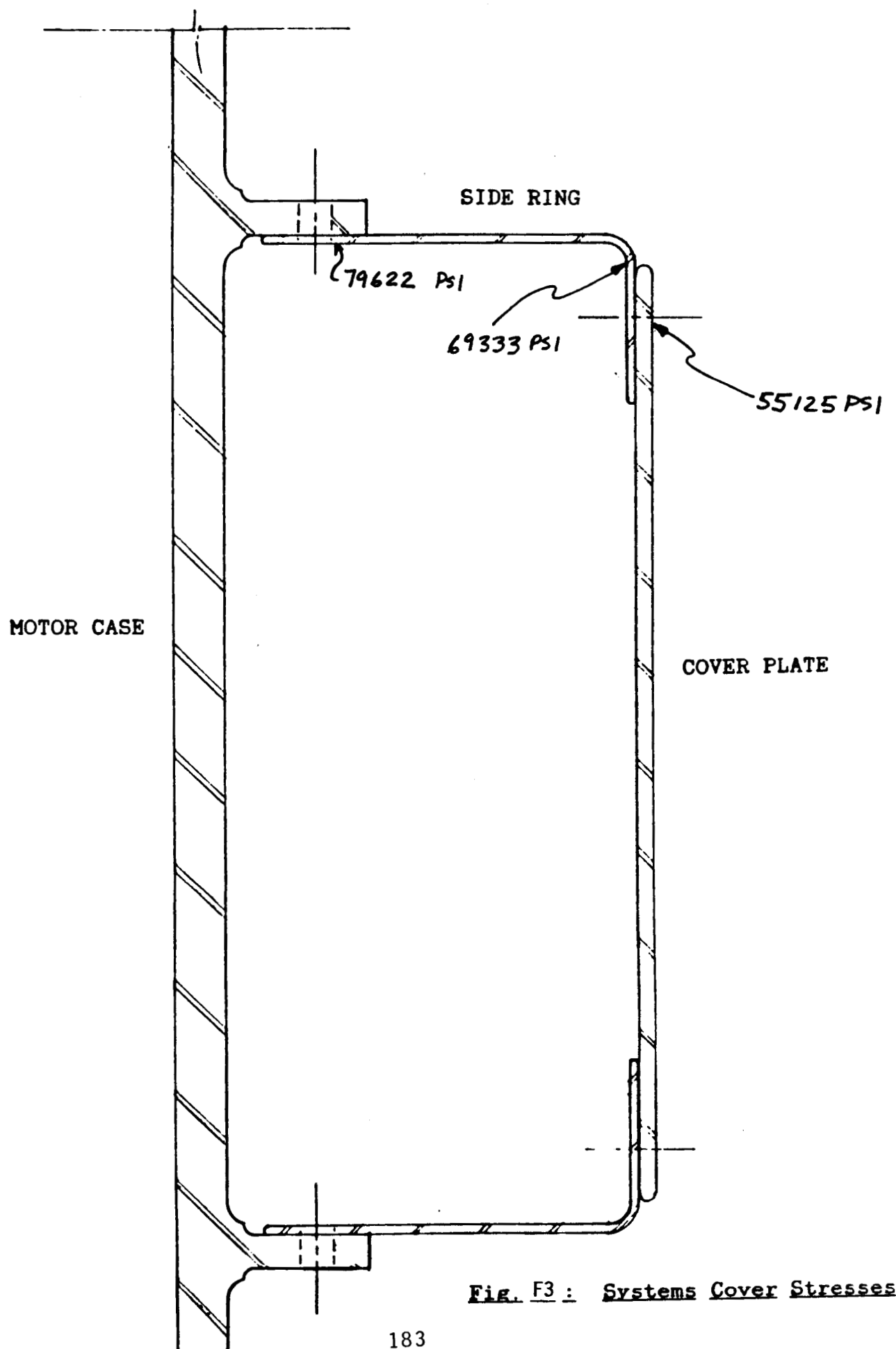


Fig. F2 : Tang Bolt Loads



ET RING STRESSES DUE TO AERODYNAMIC, ACCELERATION, AND PRESSURE LOADS

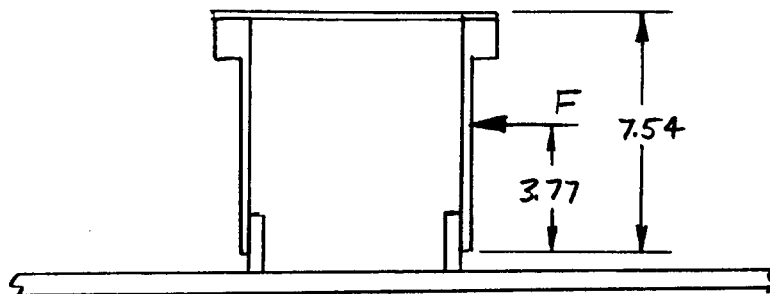
Introduction

The following analysis considers the contribution of aerodynamic, acceleration, and internal ring pressure loads on the ET ring. As a conservative case, the ring is considered to be full height when applying all of the loads. The stresses resulting from these loads are not directly additive to the stress contributions from internal SRB pressure and from strut loads. The stresses must be combined as a biaxial resultant. Also, the stresses calculated occur at time of approximately 60 seconds into the flight. The stresses due to SRB pressure are somewhat reduced at this time.

Results

The combined tensile stress from aerodynamic, acceleration and pressure loads is 18,291 psi. When this stress is combined with the stress due to SRB pressure and strut loads at this time (maximum 90,000 psi.) to give a principal stress, the result is 116,241 psi.

AERODYNAMIC LOADS



$$F = F_{AERO} + F_{ACCEL.}$$

$$F_{AERO} = C_p q A$$

$$C_p = \text{Press. coefficient} = 1.25$$

$$q = \text{Dynamic pressure} = 819 \text{ psf}$$

$$A = \text{Area}$$

Ref. SE-019-142-ZH
Rev A, "Solid Rocket
Booster Venting Analysis"

$$F_{AERO} = 1.25 (819) (1)$$

$$= 1024 \text{ psf}$$

$$F_{ACCEL.} = mg$$

$$m = 7.23 (.25) (12) (.283) + 1.75 (1) (12) (.283)$$

$$= 12.08 \text{ lbm / ft of ring}$$

$$g = 3.2$$

$$F = 1024 \left(\frac{12 \times 7.54}{144} \right) + 12.08 (3.2)$$

$$= \overset{\text{Aero.}}{643.4} + \overset{\text{Accel.}}{38.66}$$

$$F = 682 \text{ lb. / ft of ring}$$

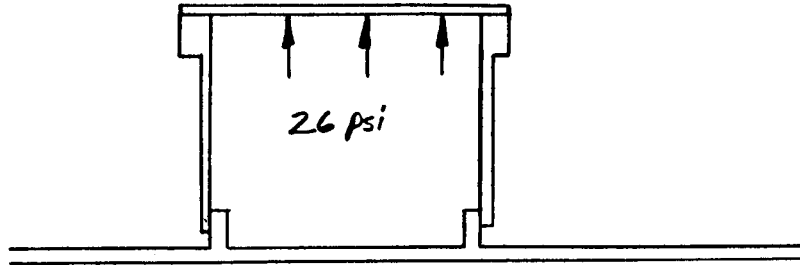
Stress

$$\sigma = \frac{Mc}{I}$$

$$= \frac{682 (3.77 - 1.2) (.125)}{(2) 12 \left(\frac{.25^3}{12} \right)}$$

$$\sigma = \underline{7011 \text{ psi}} = \text{stress due to bending from aerodynamic and acceleration loads}$$

PRESSURE LOADS



$$\text{Force on cover} = 26 \times (12 \times 12) = 3744 \text{ lb/ft.}$$

Stress at bolt line due to cover load

$$\begin{aligned} \sigma &= \frac{P_{\text{COVER}}}{A_{\text{SIDE}}} \\ &= \frac{3744}{2(12 \times .25)} \end{aligned}$$

$$\sigma = \underline{624 \text{ psi}} \quad T \uparrow$$

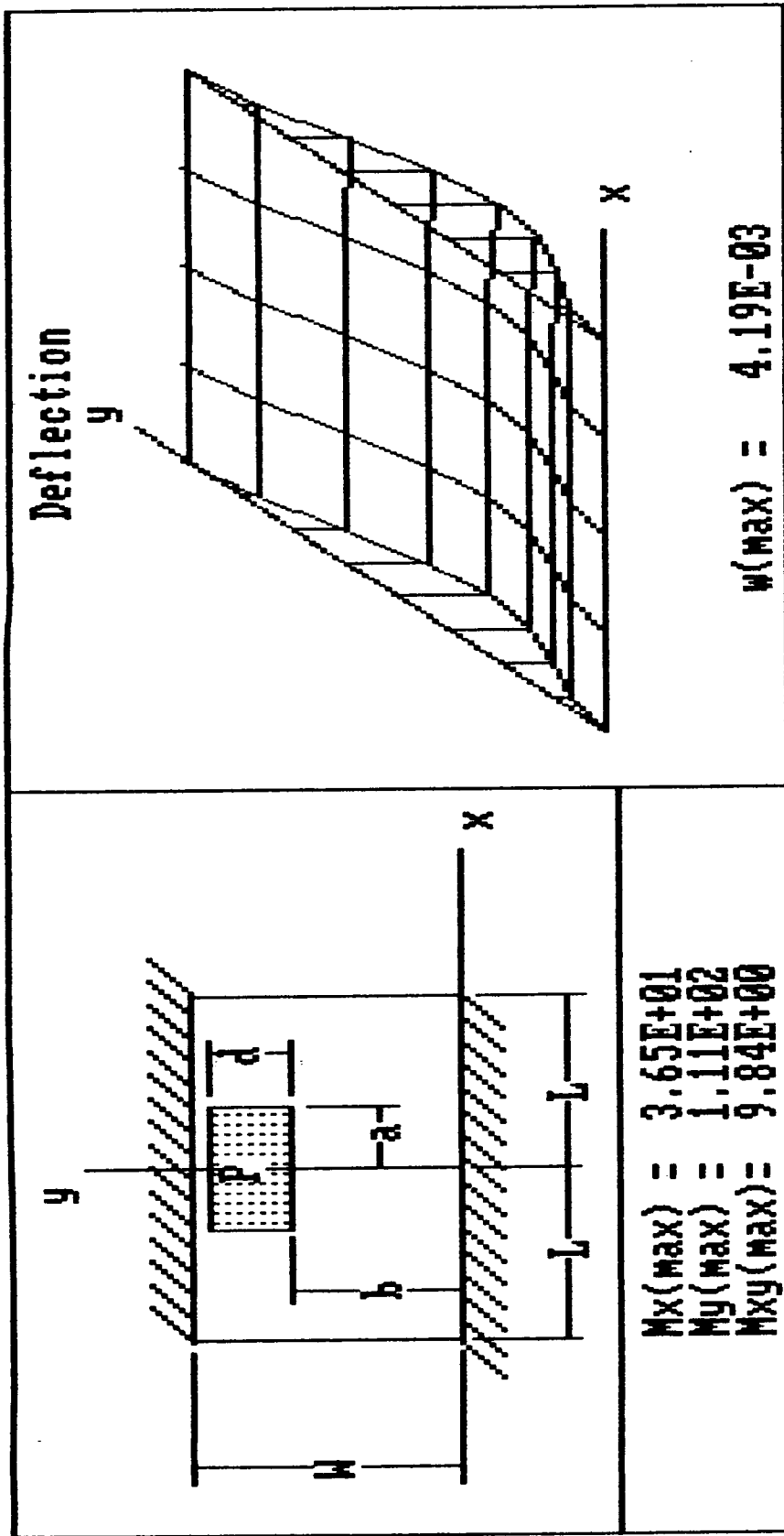
$$\text{Force on sides} = 26 \times (12 \times 7.23) = 2256 \text{ lb/ft.}$$

From MSC-CASE output (see following page) the max. moment is 111 in-lb. The max. stress is

$$\begin{aligned} \sigma &= \frac{6M}{t^2} \\ &= \frac{6(111)}{.25^2} \end{aligned}$$

$$\sigma = \underline{10656 \text{ psi}} \quad T \text{ or } C \uparrow$$

Module D-2: Plates - Rectangular



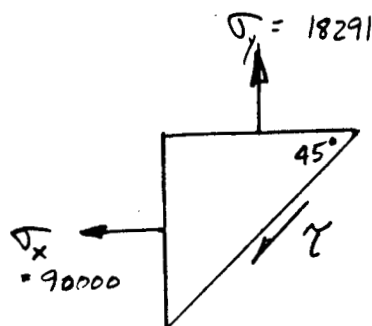
$Mx(\max) = 3.65E+01$
 $My(\max) = 1.11E+02$
 $Mxy(\max) = 9.84E+00$

LENGTH, $L = 6$
 WIDTH, $W = 6.94$
 THICKNESS, $t = .25$
 ELAST MOD, $E = 30e6$
 POISSON, $\nu = .33$
 LOAD, $P = 2256$
 $a [1-4 \text{ only}] = 4(L/4)$
 $b [0-7 \text{ only}] = 0(W/8)$
 $d [1-8 \text{ only}] = 8(W/8)$

ENTER F6 FOR BOUNDARY REACTIONS OR
 F7 FOR BOUNDARY MENU

F2PRINT F3DISP
 F6NEXT F7MENU F8REDO F9SAVE F10TOP

Stress at a point on the ring



Sum of tensile stresses
 $= 7011 + 624 + 10656$
 $= 18291$

$$\sigma_x \sin 45^\circ - \sigma_y \sin 45^\circ + \tau = 0$$

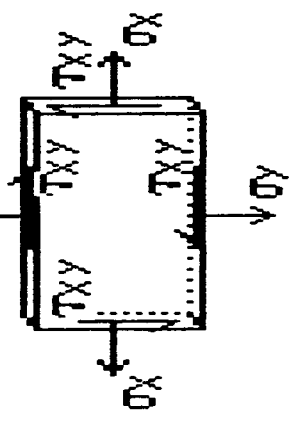
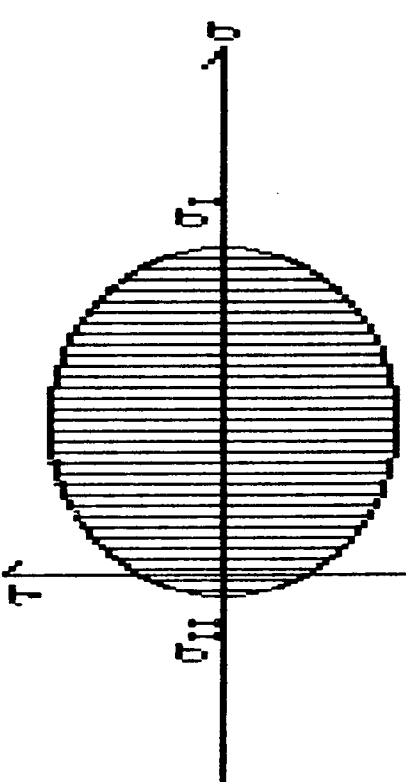
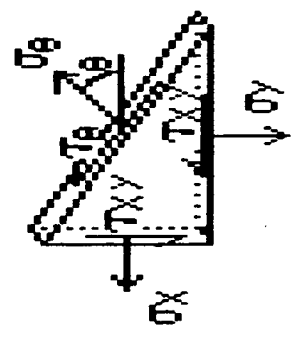
$$90000 (0.707) - 18291 (0.707) + \tau = 0$$

$$\tau = -50698 \text{ psi shear}$$

Principal stress

At the time of the roll maneuver (max. SRB pressure) the contributions from the aerodynamic, acceleration, and pressure loads are insignificant. At approximately 60 seconds into flight, the contributions add to the principal stress to a greater degree. The ring stress at this time is approximately 90000 psi (max.) due to SRB and strut loads. The principal stress is calculated on the following page to be 116241 psi.

Module F-1: Combined Stress

| | |
|--|---|
| <div> σ_θ τ_θ σ_I σ_{II} τ_{MAX} </div> <div> = 104843.5 = -35854.51 = 116240.8 = -7949.848 = 62095.35 </div> <div> (θ = 45.00) (θ = 45.00) (θ = 27.37) (θ = 117.37) (θ = -17.63) </div> | <div>2. Biaxial Stress</div> <div>  </div> |
| <div>  </div> <div> σ_x = 90000 σ_y = 18291 τ_{xy} = 50698 </div> <div> θ = 45 </div> | <div>  </div> |

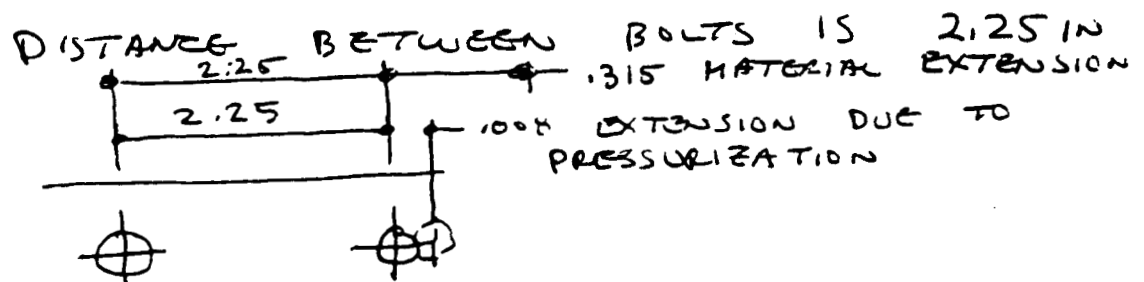
ENTER F7 FOR STATE OF STRESS MENU

F2PRINT F3DISP F7MENU F8REDO F9SAVE

PROBLEM: DETERMINE THE FS OF ELONGATION
TO FAILURE OF WEB MATERIAL RELATIVE
TO THE 1008 MIL CASE EXTENSION BETWEEN
BOLTS

SOLUTION:

MATERIAL IS AISI 4340 STEEL HEAT TREATED
TO 180-200 ksi. ELONGATION IS
14% (REF MODERN STEEL PP 124, 6th Ed)



|||||

$$FS = \frac{\text{ALLOWABLE EXTENSION}}{\text{ACTUAL EXTENSION}}$$

$$FS = 39$$

D. Bradley

NET FIELD STRESS
AT BOLTS

6-25-87

| Bolt # | Load | Σ Loads | Area at Bolt | σ , psi |
|--------|------|----------------|--------------|----------------|
| 1 | 7950 | 7950 | .201 | 39552 |
| 2 | 8430 | 16380 | .201 | 81493 |
| 3 | 8000 | 24380 | .201 | 121294 |
| 4 | 7440 | 31820 | .276 | 115290 |
| 5 | 7360 | 39180 | .359 | 109136 |
| 6 | 7330 | 46510 | .432 | 107662 |
| 7 | 8070 | 54580 | .504 | 108294 |
| 8 | 7660 | 62240 | .573 | 108621 |
| 9 | 7230 | 69470 | .625 | 111152 |

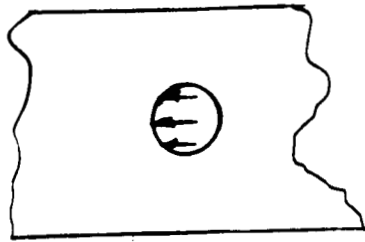


BoH loads include strut contributions

from P2 (155 KIPS), P9 (241 KIPS), P10 (267 KIPS)

22-141 50 SHEETS
22-142 100 SHEETS
22-144 200 SHEETS





ORIGINAL PAGE IS
OF POOR QUALITY

$$\text{Max. Bolt Load} = 8430 \text{ LB.}$$

$$\begin{aligned} \text{Area} &= .375 \times .25 \text{ in.} \\ &= .094 \text{ in.}^2 \end{aligned}$$

Stress

$$\sigma = \frac{P}{A}$$

$$= \frac{8430}{.094}$$

$$\sigma = \underline{89700} \text{ psi} \quad \text{bearing}$$

Margin of Safety

$$\text{ultimate bearing strength} = 347 \text{ KSI} \quad \begin{matrix} \text{Ref.} \\ \text{MIL-HDBK-5D} \end{matrix}$$

$$M.S. = \frac{347000}{89700(1.4)} - 1$$

$$M.S. = \underline{\underline{1.76}}$$

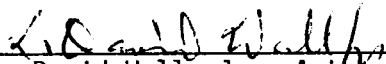
APPENDIX G


INELASTIC ANALYSIS


by L. David Wall, Jr.
Mail Stop 190
NASA Langley Research Center
Hampton, VA 23665

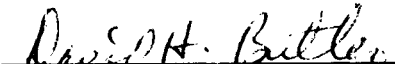
Phone: (804) 865-4585

June 12, 1987


L. David Wall, Jr., Author


James H. Starnes, Jr., Reviewer


Der Martin M. Mikulas, Jr., Project Engineer


David H. Butler, Project Manager

APPENDIX G

INELASTIC ANALYSIS

INTRODUCTION

Accurate stress analyses of large structures with local detailed features, such as the Solid Rocket Booster (SRB) External Tank Attach (ETA) ring bolted joints, can be conducted with a finite element code if enough elements are used to represent the structural details properly and if enough time and computer resources are available to obtain the desired solution. A large number of finite elements are usually needed to model accurately the stresses and stress gradients in such a bolted joint, and large amounts of computer time and storage capacity are needed to obtain solutions if material nonlinearities or inelastic effects are included in the analysis. To study the effects of varying bolted-joint parameters on the stresses and failure loads of the ETA ring bolted joint with a finite element code would require a large number of computationally-intensive computer analyses and a large amount of an analyst's time. An alternative to such a finite element analysis approach is to use an accurate and computationally-efficient continuum-mechanics-based analysis developed specifically for bolted joints. The continuum-mechanics-based A4EJ computer code (ref. G-1) was developed for detailed stress analyses of bolted joints and was selected to study the effects of varying bolt stiffnesses and bolt-hole clearances and tolerances on the stresses and failure loads of the ETA ring bolted joint. The results of this study are presented in this Appendix. Results of a study of the effects of bolt failure and bolt-failure sequence on joint strength are also included in this Appendix.

ANALYTICAL MODEL

An A4EJ model of the Langley tapered ETA ring joint design was developed for the joint segment containing the first 40 bolts from the ring end and the details of the model are shown in Figure G-1. The joint geometry of the end of the Langley tapered joint as modeled in a separate EAL finite element analysis (Ref. G-2) is shown in Figure G-1a and joint details for the first 10 bolts from the end of the joint are shown in Figure G-1b. The corresponding A4EJ models are shown in Figure G-1c and G-1d, respectively. The A4EJ code requires a model that is symmetric about the line of bolts and the A4EJ model shown in Figure G-1 was developed to match the bolt-load distribution predicted by the EAL model of Reference G-2 for limit load conditions. The effects of joint web, joint cap, and cap-bolt flexibilities were included in the A4EJ 40-bolt model by adjusting the individual bolt-station stiffnesses to correspond to the appropriate bolt loads. The model included 6.5 in.² of motor casing, the joint web and the case tang.

The A4EJ code uses a Ramberg-Osgood inelastic stress-strain formulation (Ref. G-3) in the analysis that includes a bilinear load-deflection curve for the bolts. The bolt stiffnesses used in the analysis are 1.3×10^6 lb/in. for the primary or elastic part of the bolt load deflection curve and approximately 20 percent of this value for the secondary or inelastic part of the load-deflection curve. The elastic moduli of the joint web and tang are 29×10^6 psi and 30×10^6 psi, respectively. The bolt strengths used are 12,812 lb at yield and 16,015 lb at ultimate. The Ramberg-Osgood parameters used are

$F_{0.7} = 171$ ksi and $n = 22.5$ for the tang and $F_{0.7} = 179$ ksi and $n = 50.0$ for the web. The strength properties used are $F_{TU} = 195$ ksi, $F_{BU} = 297$ ksi and $e_{TU} = 0.05$ for the tang and $F_{TU} = 180$ ksi, $F_{BU} = 250$ ksi and $e_{TU} = 0.15$ for the web. The limit load condition used for the case is 110 ksi stress at 715 kips load and the ultimate load condition used is 140 percent of limit load or 154 ksi stress at 1001 kips load.

RESULTS

A comparison of the results from the A4EJ continuum-mechanics-based joint analysis and the EAL finite element analysis at limit load is shown in Figure G-2. The bolt station stiffnesses of the A4EJ model were deliberately adjusted until the bolt loads from the A4EJ analysis matched the bolt loads from the EAL analysis as shown in Figure G-2a. This stiffness adjustment process resulted in the excellent correlation in the shell tang bypass stresses, ring bypass stresses and bolt bearing stresses as shown in Figures G-2b and G-2c and G-2d respectively. The excellent correlation of the results from the A4EJ and EAL models suggest that the A4EJ model gives results that are consistent with the EAL results and the A4EJ model was used to study effects of varying a number of joint parameters on joint strength and to study inelastic effects. The results of these A4EJ studies are described in the following paragraphs

Bolt Stiffness Effects

The bolt load distributions at joint failure for three different bolt stiffness distributions are shown in Figure G-3. Although the individual bolt loads differ significantly, the predicted joint failure loads differ by less than one percent. The curve with the absolute maximum bolt load represents the results for a model with a uniform bolt stiffness distribution of 1.3×10^6 lb/in. The other two curves represent the results for models with the individual bolt stiffnesses adjusted to include the effects of web, cap and cap bolt flexibilities. The individual bolt stiffnesses for these models range from 0.5×10^6 to 1.0×10^6 lb/in. These results indicate that bolt stiffness variations affect the individual bolt loads more than they affect joint strength. For determining joint strength, the precise bolt stiffness definition is necessary only when the bolts are loaded near their ultimate strength.

Effects of Clearances and Tolerances

Relative longitudinal motion between the two joint elements that are bolted together can occur at a given bolt station before the bolt begins to transmit any applied load. This relative motion is a result of the clearances and tolerances at a bolt as indicated in the left sketch on Figure G-4 and is referred to as the Potential Bolt Slip or PBS in this Appendix. The effects of this potential bolt slip due to bolt clearances and tolerances on the joint failure load is shown in Figure G-4. The curves on the figure represent joint failure loads as a function of potential bolt slip at a number of holes in the ETA ring joint and the hole numbers where potential bolt slip is assumed to occur are indicated to the right of each curve. Preliminary results indicate that, for an arbitrary value of potential bolt slip, the fourth bolt hole from the joint tapered end causes the largest reduction in joint strength when all

other bolt holes have zero potential bolt slip or are tightly fitted. The results also indicate that the most sensitive distribution of potential bolt slip when more than one bolt hole has the same potential bolt slip occurs when holes with the same arbitrary potential bolt slip alternate with holes with zero potential bolt slip. Examples of results for cases having alternating holes with arbitrary and zero potential bolt slip are shown in Figure G-4 and compared with the results (upper curve) for the case having holes with arbitrary, uniform potential bolt slip. In these examples, the first hole with potential bolt slip is the fourth hole from the tapered end of the joint, and holes not identified in the sequence to the right of the curves have zero potential bolt slip. The results indicate that the joint failure loads decrease as the magnitude of the potential bolt slip increases but become constant at a critical value of potential bolt slip for each case (indicated on Fig. G-4 by the critical PBS curve). Bolt holes with potential bolt slip do not carry any of the applied load for potential bolt slip values greater than the critical value indicated on the curves and any further increase in potential bolt slip at these holes does not affect joint failure and the particular bolt hole sequence becomes ineffective for longitudinal load transfer. The critical value of potential bolt slip is different for each bolt hole sequence on the figure and the critical value increases with the number of bolt holes in the sequence. For some bolt hole sequences, the joint strength is reduced to a value below the ultimate bolt failure load (1.4 times limit load) before the critical value of potential bolt slip is reached. None of the sequences shows a joint strength below limit load, but for moderately high values of potential bolt slip, joint failure load is reduced significantly. If all 40 holes have the same potential bolt slip (top curve), the joint failure load increases very slightly as potential bolt slip increases. In summary, alternating bolt holes with potential bolt slip affect joint strength more markedly than non-alternating holes with potential bolt slip. An alternating distribution of holes with potential bolt slip approximates the case where tolerances vary from bolt to bolt while clearances are uniform.

The results in Figure G-5 indicate that when the first, second, and third bolt holes from the end of the joint have potential bolt slip, the joint failure load first increases to a maximum value and then decreases to a constant value as potential bolt slip increases. Results for the cases when bolt holes number 1, 2 and 3 individually have potential bolt slip while all other holes are bearing against bolts are shown in Figure G-5a. Results for bolt hole number 4 from Figure G-4 are also included for comparison. Results are shown in Figure G-5b for bolt hole sequences 1-2 and 1-2-3 along with the bolt hole 1 results for comparison. The triangles (maximum joint failure load) mark the values of potential bolt slip for which the joint failure mechanism changes from a material failure in the web to failure of a tightly fitted bolt adjacent to one with potential bolt slip. The results in Figure G-5a indicate that if any one of the first four bolts is unloaded because of a high value of potential bolt slip, joint strength does not decrease significantly. The results shown in Figure G-5b indicate a significant reduction in joint strength for critical values of potential bolt slip, but these high potential bolt slip values would occur only for an extreme out-of-tolerance situation resulting from poor handling, fabrication or assembly practices or from material yielding in a prior flight. The concern here is not for critical potential bolt slip values, but that the results show that a moderately high value of potential bolt slip (triangles) can cause adjacent bolts to fail and weaken the joint.

Sequential Bolt Failure

The sensitivity of the failure mode to potential bolt slip suggests a way to examine sequential bolt failures and the results for the study of bolt-failure sequence is shown in Figure G-6. The variation of joint failure load is shown in Figure G-6a for cases when the critical (or higher) value of potential bolt slip causes one of the first 10 bolts to carry zero load thus simulating bolt failure. Each point on the curve represents one failed bolt and the notation by the point (e.g., W-3, B-2) indicates the next failure mode predicted after the initial bolt failure. The A4EJ code predicts tensile failure of the web at bolt number 3 (denoted as W-3 on the figure) when all bolts carry load. When bolts number 1, 2, or 3 are failed, an adjacent bolt (B-2, B-3, or B-4, respectively) fails as the next mode of joint failure. For bolts number 4 through 10, the next mode of failure is a web tensile failure at the indicated bolts. These results show that the loss of any one of the first ten bolts alone does not significantly lower the joint strength, but the loss of any one of the first three bolts tends to change the failure mode from the web to another bolt.

The effects on joint strength of a sequential bolt failure that initiates and continues to precipitate other failures in the joint are shown in Figures G-6b and G-6c. Each point on the figures represents the total number of bolts failed (modeled as unloaded bolts) as indicated by the bolt numbers in parentheses and the resulting joint strength. The next predicted failure mode for each point on the figures is also indicated (e.g., B-4, W-3). For the results in Figure G-6b, the sequential failure process starts by selectively unloading bolt number 3 because of the web failure at bolt number 3 as predicted by A4EJ when all bolts carry load. Unloading bolt number 3 causes a slight reduction in joint strength and the next failure event is predicted to be failure of bolt number 4 (B-4). The next failure event to occur is failure of bolt number 5 (B-5) which is determined by unloading bolts number 3 and 4 (assumed failed) for the A4EJ analysis. In this manner, the rest of the curve is generated by selectively unloading the bolts that are predicted to be the next "weak link" and this process is continued until the first 10 bolts are simulated as failed. (The notation W-1,2 at bolt number 7 indicates that the next failure mode is a web failure between the remaining bolt number 1 and the already failed bolt number 2.)

For the results shown in Figure G-6c, the failure sequence is initiated arbitrarily at bolt number 1. Each succeeding bolt failure is determined by unloading the next predicted failed bolt after applying the A4EJ analysis. In every subsequent step in the failure process after bolt number 1 has failed, A4EJ predicts a bolt failure as the next mode until all 10 bolts have failed. As a result, each point (at bolt number X) on the curve represents the joint strength after bolts number 1 through X have failed.

The results in Figures G-6b and G-6c represent upper and lower bounds of the sequential failure process if the first 10 bolts are progressively unloaded until all 10 bolts are simulated as failed. That is, selection of any one of the other 10 bolts as the first failed bolt and then sequentially unloading the next predicted "weak bolt" generates a curve which is similar to those in figures G-6b and G-6c and eventually merges with the curves on Figures G-6b or G-6c. All three curves from Figures G-6a, G-6b and G-6c are plotted in Figure G-6d for comparison. It is evident that the loss of 2 or 3 of the first 10 bolts can significantly weaken the joint depending on which bolts have failed and that the sequential loss of any 4 of these bolts reduces the joint strength to approximately that of limit load.

CONCLUDING REMARKS

When bolt station stiffnesses are selectively adjusted for web, cap and cap bolt flexibilities, the A4EJ computer code provides stress results for the ETA tapered end ring that are consistent with the elastic behavior results from the EAL computer code and provides significant insight into inelastic effects on ring strength. Precise bolt stiffness definition affects individual bolt loads more than it affects joint strength. Potential bolt slip caused by clearances and tolerances at bolt holes affects joint strength and failure mode significantly for certain sequences of bolt hole failures and certain values of potential bolt slip. Unloading or failure of one of the first three bolts from the end of the ring changes the failure mode from a web failure to a bolt failure, but a loss of any one of the first 10 bolts from the end of the ring does not affect joint strength significantly unless a sequential failure process is precipitated. If a sequential failure process is precipitated, the end of the ETA ring joint is significantly weakened by the loss of three bolts. The loss of four bolts reduces the strength of the ETA ring joint to about that of limit load.

REFERENCES

- G-1. Hart-Smith, L. J.: Design Methodology for Bonded-Bolted Composite Joints, Vols. I & II. Air Force Technical Report, AFWAL-TR-81-3154, Flight Dynamics Laboratory. Wright-Patterson Air Force Base, Ohio, February 1982.
- G-2. Lake, M.; and Fichter, W. B.: Ring Sizing and Analysis. Appendix C, Redesign of Solid Rocket Booster/External Tank Attachment Ring for the Space Transportation System, Compiled by Harvey G. McComb, Jr., Hampton, Virginia, June 1987.
- G-3. Bruhn, E. F.: Analysis and Design of Flight Vehicle Structures. Tri-State Offset Co., 1973.

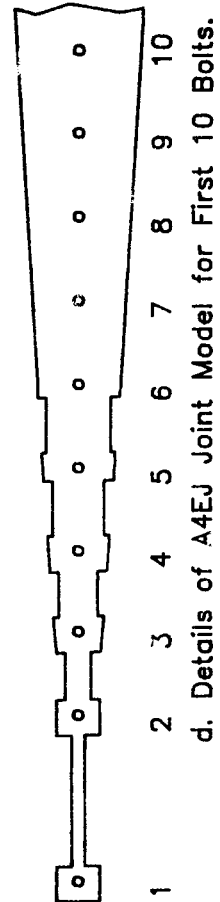
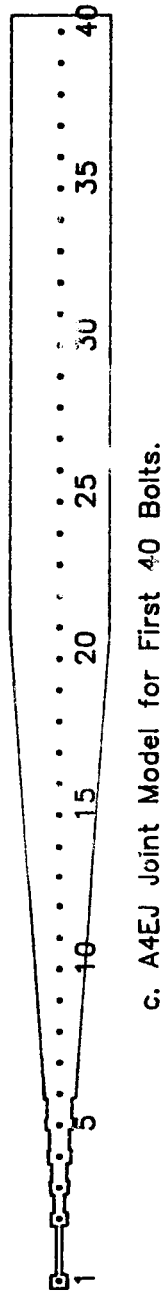
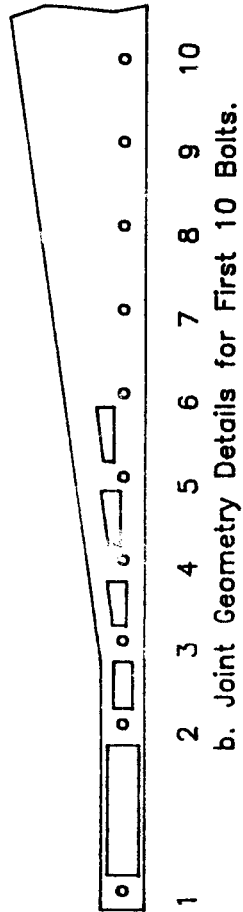
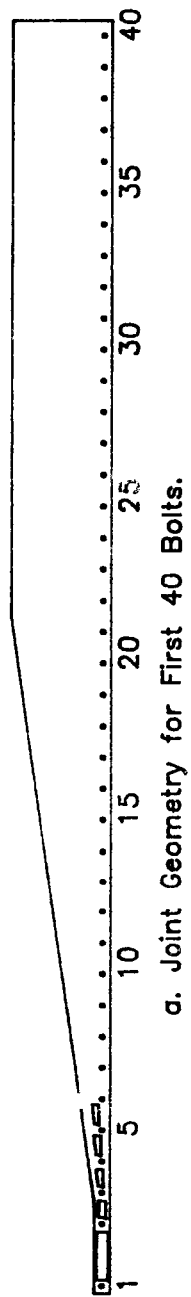


Figure G-1. Imperfect ETA Ring Model. The numbers on the figure are bolt station numbers.

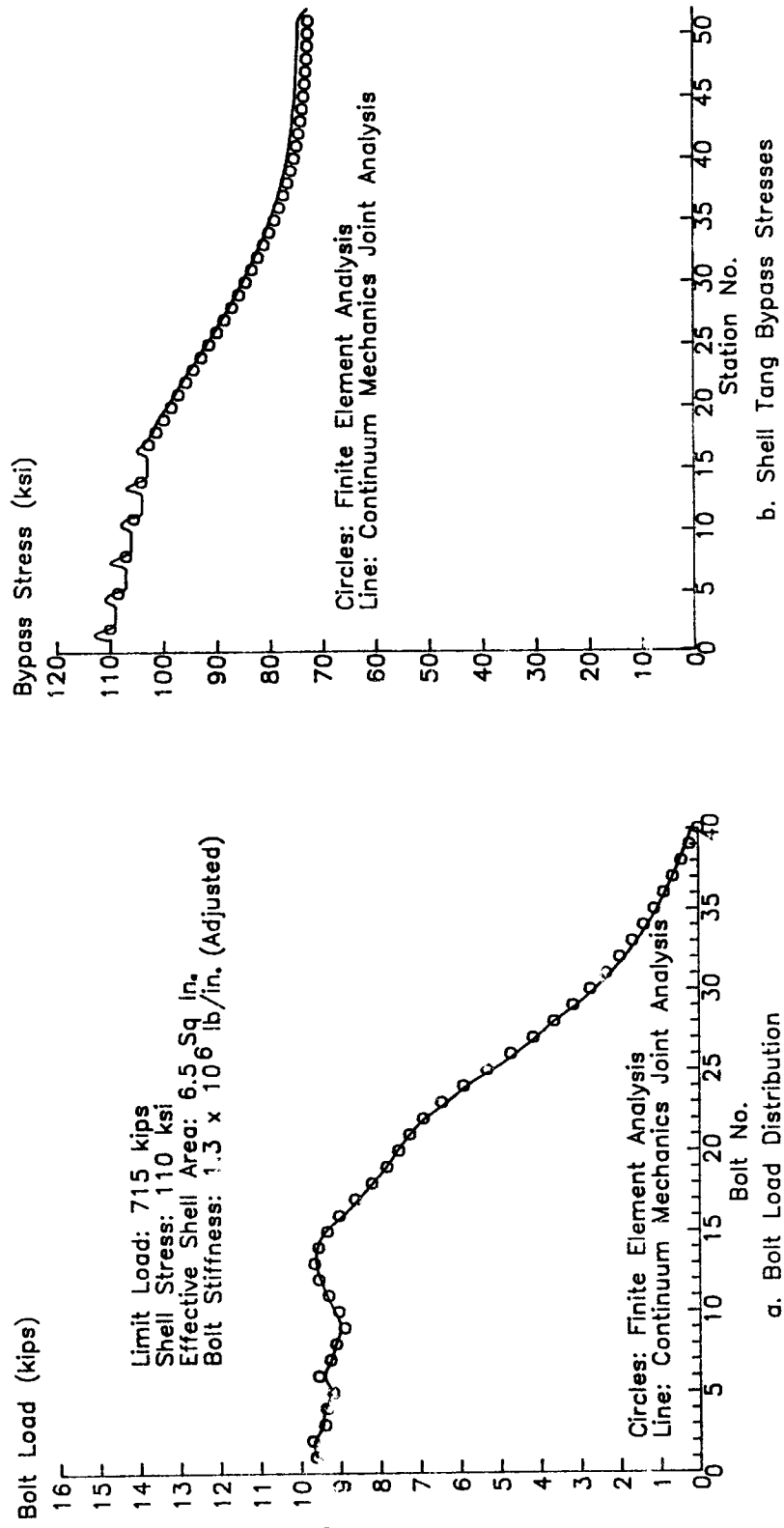
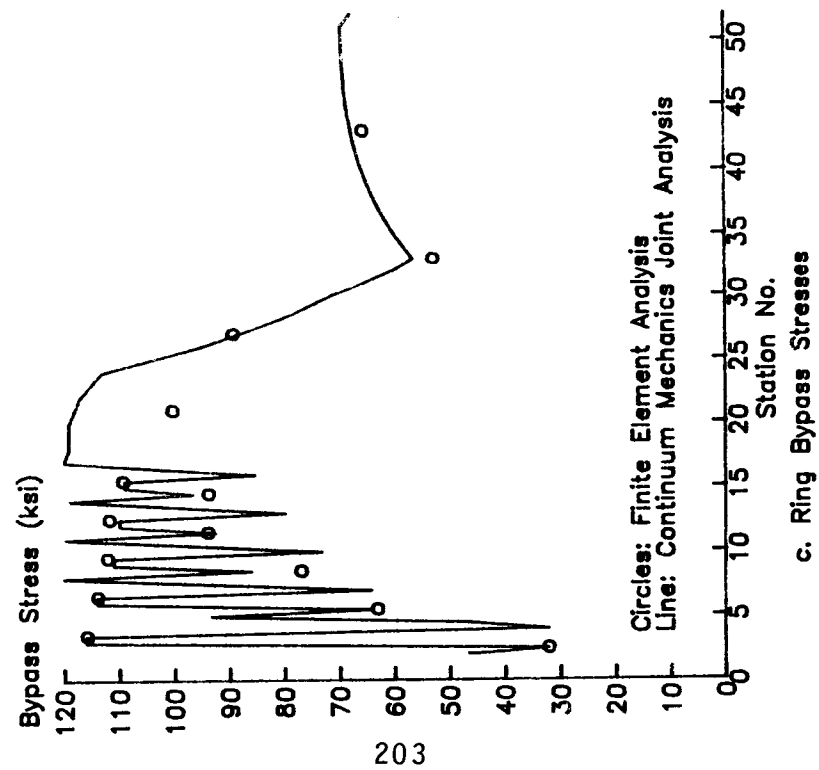
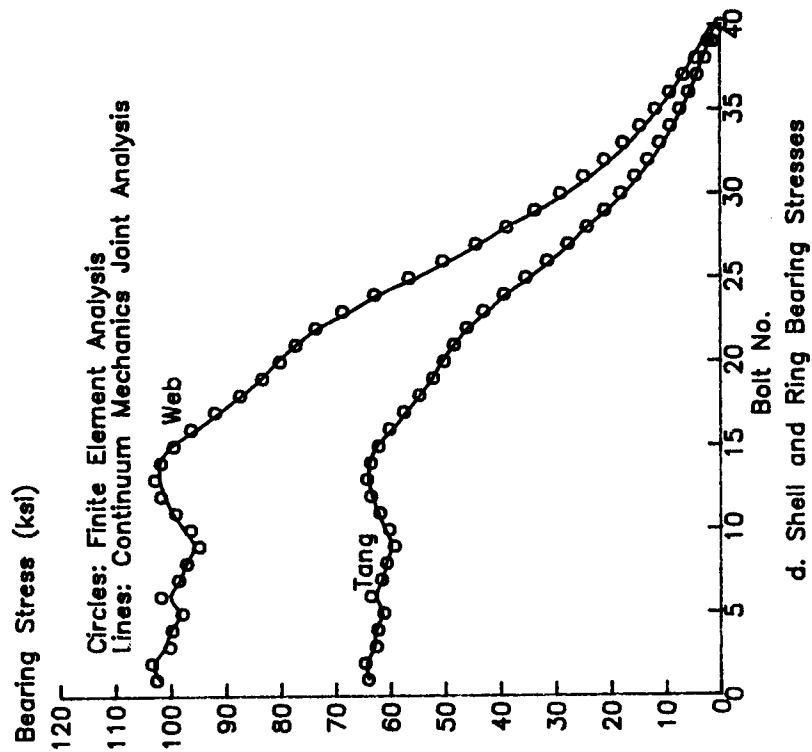


Figure G-2. Comparison of Continuum Mechanics Joint Analysis Results and Finite Element Analysis Results at Limit Load.



c. Ring Bypass Stresses



d. Shell and Ring Bearing Stresses

Figure G-2. (Concluded).

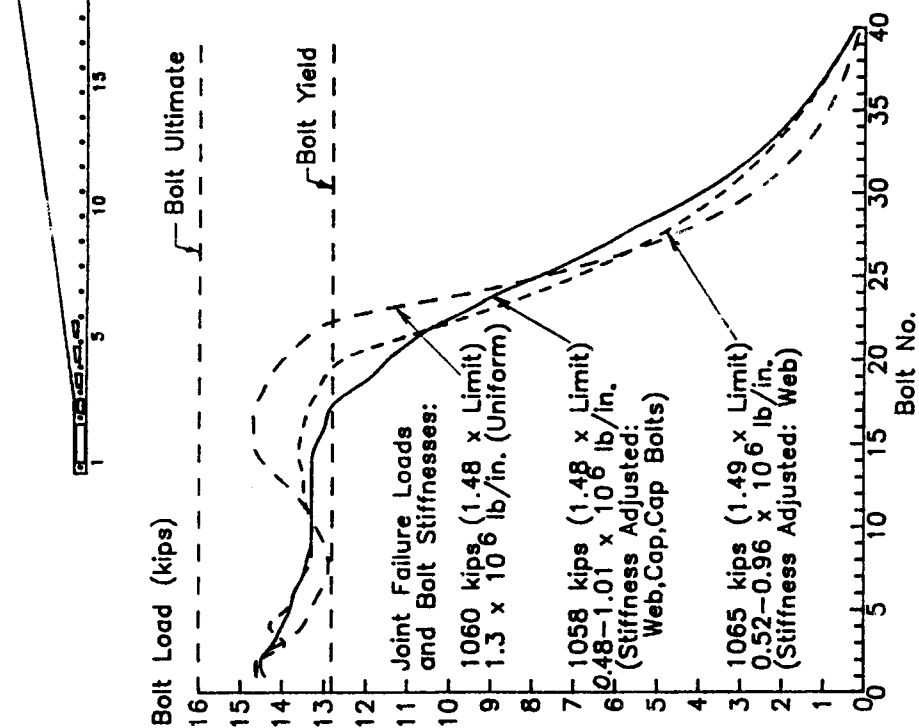


Figure G-3. Bolt Load Distribution at Joint Failure.

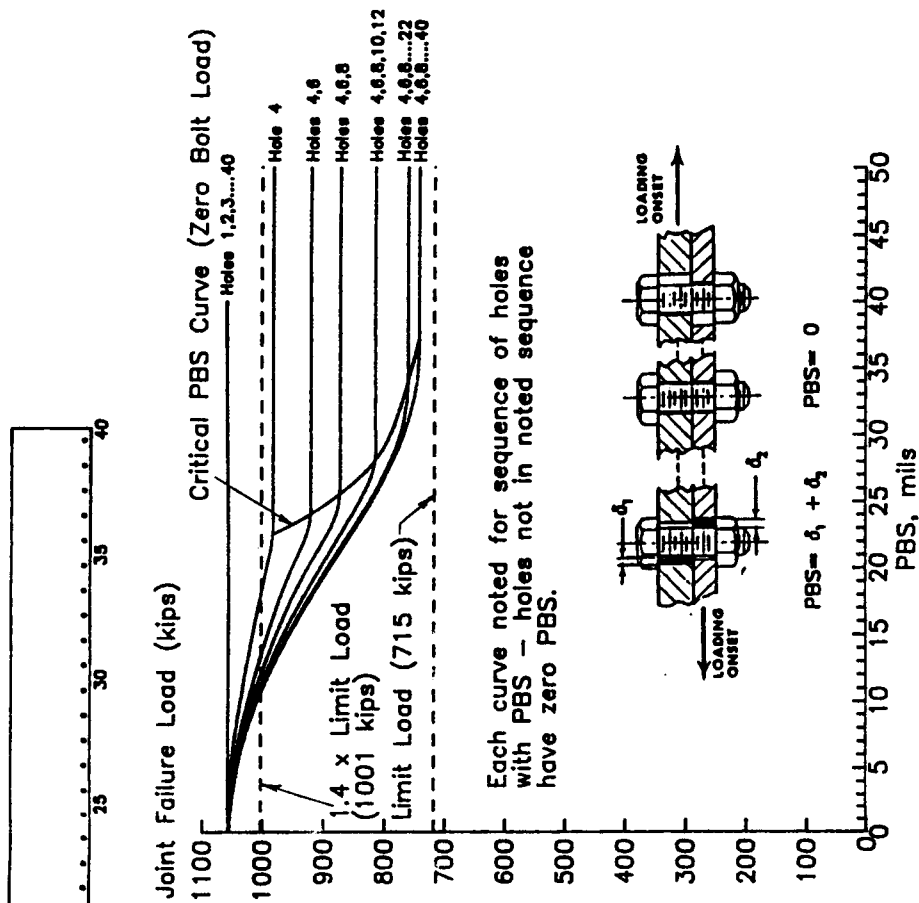


Figure G-4. Effect of Potential Bolt Slip on Joint Failure Loads.

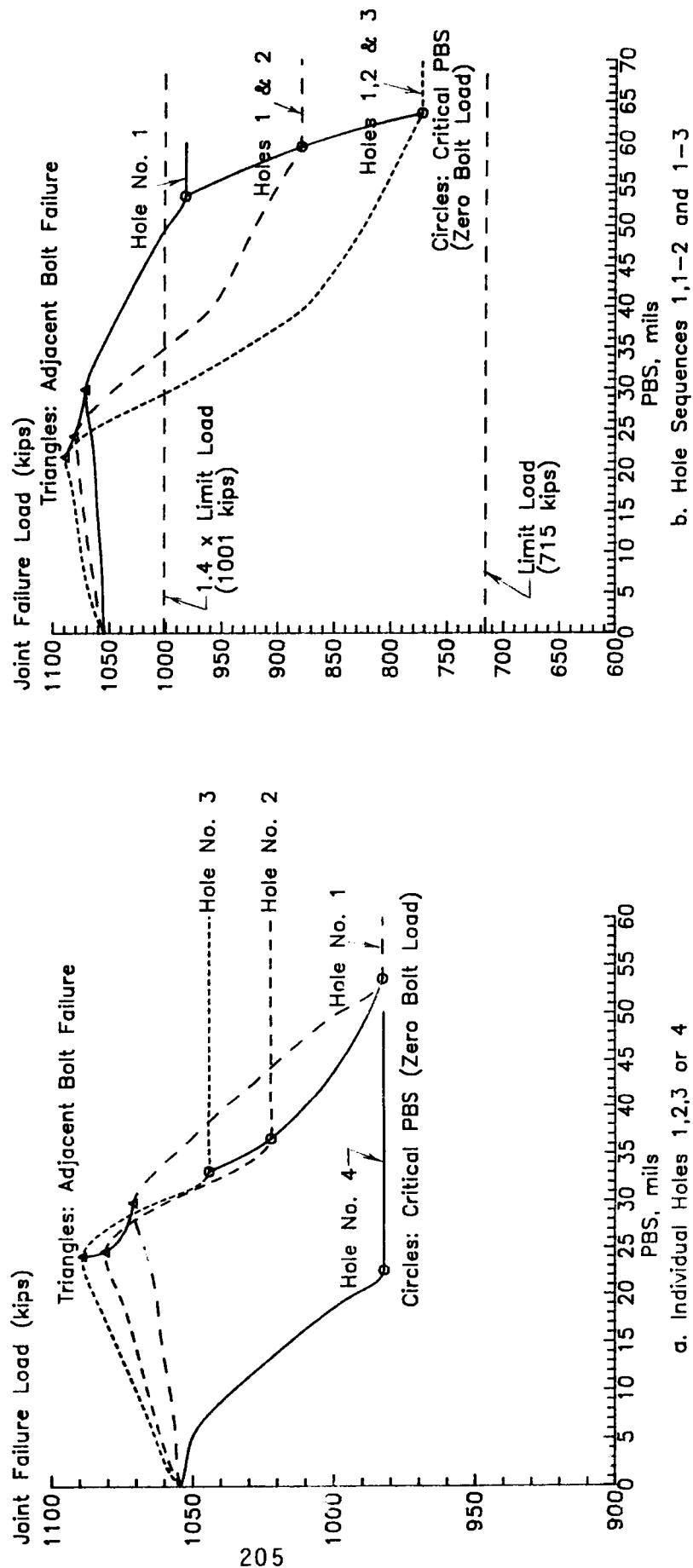


Figure G-5. Joint Failure Loads when Holes 1,2,3 and 4 Have Potential Bolt Slip (PBS).

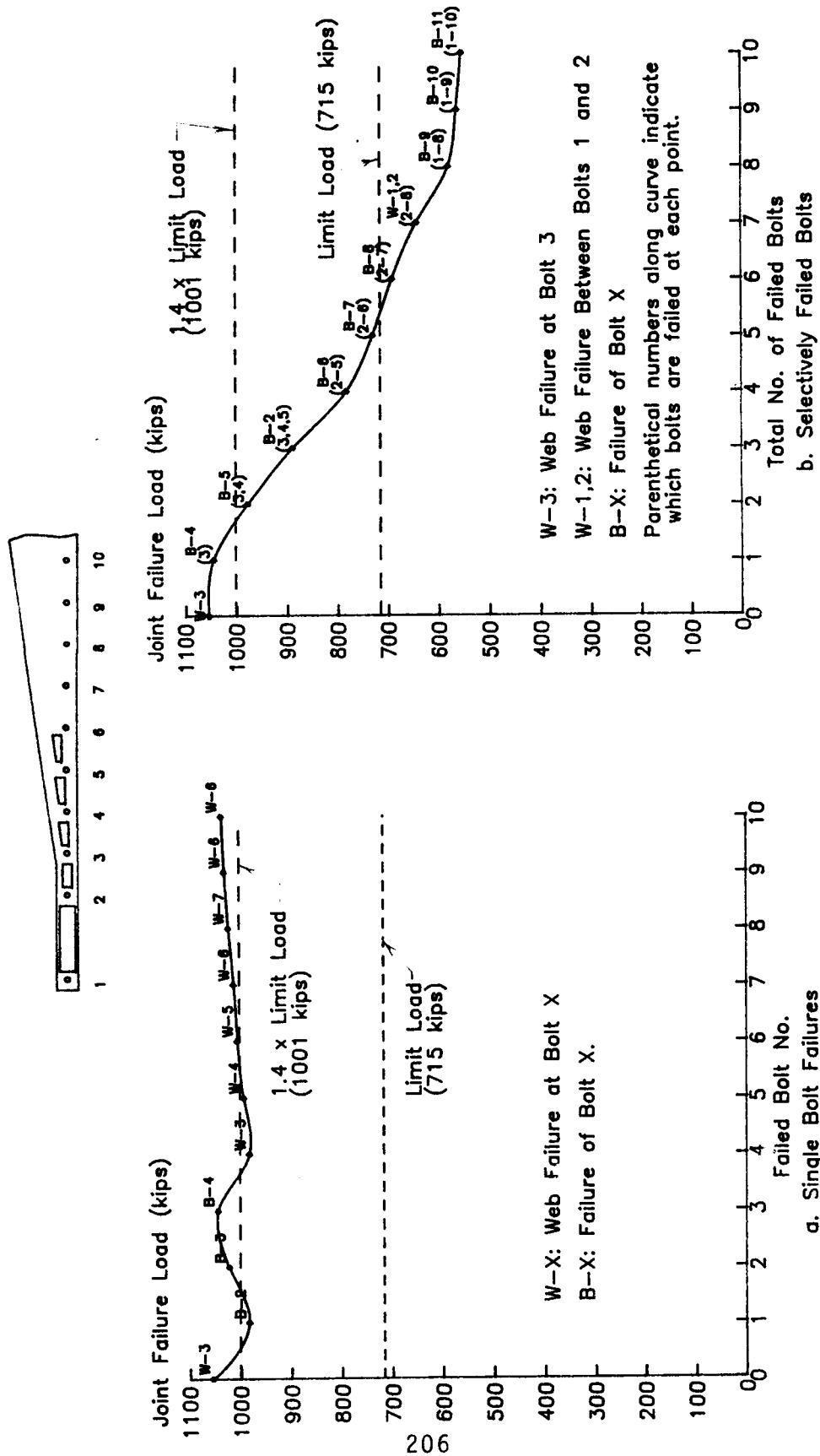


Figure G-6. Effects of Bolt Failure Sequence on Joint Failure Load.

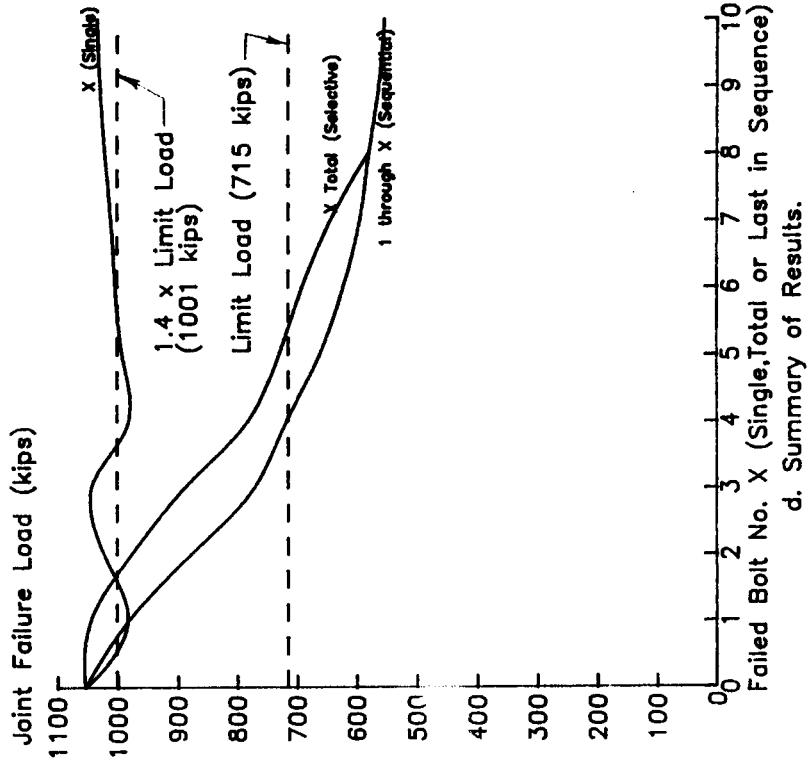
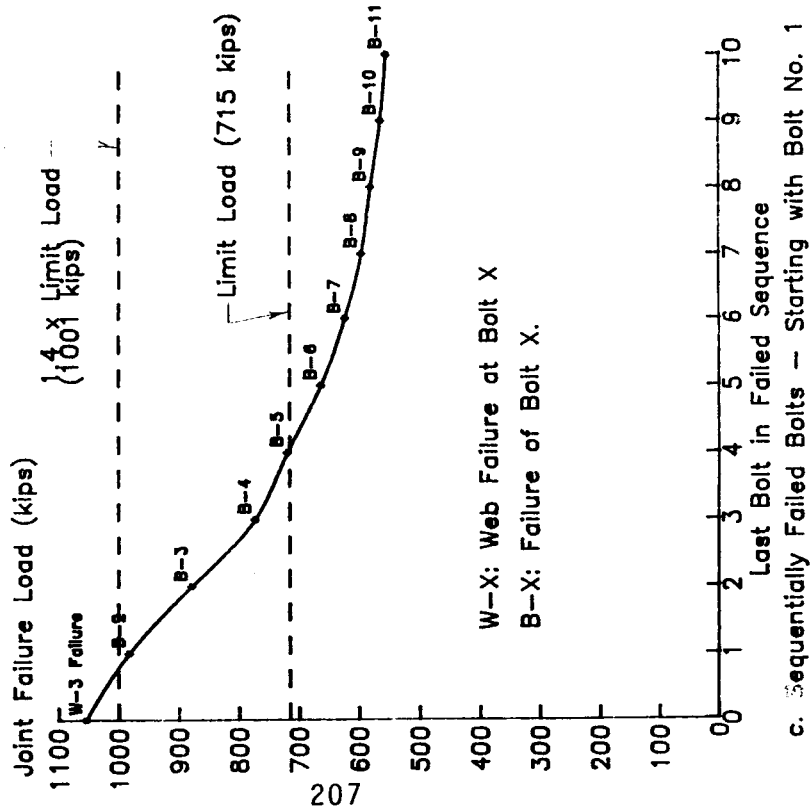
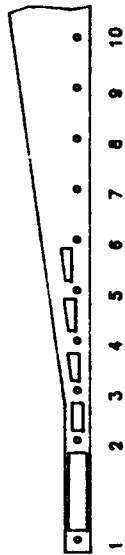


Figure G-6. (Concluded)

APPENDIX H

FRACTURE MECHANICS ANALYSIS

BY

Phillip L. Brown
Mail Stop 434
NASA Langley Research Center
Hampton, VA 23665
Phone: (804) 865-4571

AND

J. C. Newman, Jr.
Mail Stop 188E
NASA Langley Research Center
Hampton, VA 23665
Phone: (804) 865-3192

June 23, 1987

Phillip L. Brown
Phillip L. Brown

J. C. Newman, Jr.
J. C. Newman, Jr.

Reviewed by

Robert B. Davis
Robert Davis

Project Engineer

Martin M. Mikulas, Jr.
Martin M. Mikulas, Jr.

Project Manager

David H. Butler
David H. Butler

APPENDIX H

FRACTURE MECHANICS ANALYSIS

Introduction

A fracture mechanics analysis of the current Langley redesign of the SRB/ET attachment ring has been performed with the intent of establishing a useful service life for the ring. A goal of forty mission lives is sought with the exclusion of water impact loading and with verification of material surface condition (i.e. maximum initial crack size) by inspection. This analysis considers the propagation of cracks at locations in the ring where bolt loading and subsequent stresses are of high concern.

A computer code has been developed to address particular types of surface flaws which may cause fracture of the ring, and discussion of this analytical tool as well as the results of this analysis will be presented in this appendix.

ANALYSIS

Loads

First, it should be noted that the end portion of the short side of the ring up to and including the section through bolt number 4 encompasses the area of concern for this analysis. In order to bound the problem, the present configuration of the ring end was used to determine a maximum average bolt load which would not violate the allowable design stress level of 128 ksi. A simple load over area calculation was made for this purpose and did not include stress concentration effects of a local nature at the bolt holes. This resulted in a 8.57 kip maximum average load allowed at the first three bolt locations. Figure H-1 shows the present configuration and cross-sectional areas considered for determining the allowable bolt load. The area through bolt location three is the limiting area in this design for establishing the maximum average bolt load. For some crack cases however, the maximum allowable design stress of 128 ksi was used instead of the calculated section stress based on bolt loading in order to bound the problem.

Computer Program

A computer code utilizing the standard Paris crack growth rate equation was formulated for this analysis. Two types of failure were considered. One type of failure was a fracture failure. This occurred when the stress intensity,

K, exceeded the fracture toughness, K_{IC} , of the material. The other type of failure occurred when the net-section stress (plastic hinge failure) exceeded the ultimate strength of the material. Crack case solutions pertinent to the ring geometry were obtained from the NASA Flagro crack growth program and other recognized published sources (see references H1-H3). In particular, models were coded for through crack and corner crack cases for cracks growing from a pin loaded lug and for a single-edge crack in a plate. Linear-cumulative damage calculations were made (crack-growth retardation or acceleration was not considered) for constant-amplitude and spectrum loading cases. Under constant-amplitude loading, one cycle was considered one flight. Under spectrum loading, 506 cycles was considered one flight. The basic approach in establishing a spectrum load profile was to use a steady state nominal bolt load based on the maximum internal motor case pressure (to remain constant throughout a flight at 912 psi for this analysis), and add to this the oscillatory contributions of the struts at the ring end basing those values on the relative changes of the P9 strut during liftoff and flight. In considering the crack cases that were subject to spectrum loading, a maximum average bolt load value of 8.57 kips was used. This value included the maximum input at the ring end which would be induced by strut loading. A maximum of 0.30 kips was used as an average maximum input for the first three bolt locations due to strut loading at "max Q." Therefore, a nominal steady state load of 8.27 kips was used when spectrum loading cases were run. The loading profile was established by using the "Preliminary Fatigue Loads for SRB" (ref H4) for the P9 strut and was used in conjunction with the SE-019-057-2H loads document (ref H5), pages 4.19-1 and 4.19-26. The strut loads reacted into the ring are reduced to small levels near the ends, and the value of 0.30 kips for the maximum appears to be in good agreement with the load values predicted by an optimum design and as revealed by the latest finite element analyses. When stress levels were used in the spectrum loading cases instead of bolt loads, the levels for the loading profile were ratioed in the same manner as above. A plot of the spectrum loading used for this analysis is shown in Figure H-6.

Paris Crack Growth Rate: $DA/DN = C(DK)^N$

where: DK = stress-intensity factor range

C = growth rate coefficient

N = growth rate exponent

values of C and N were obtained

from NASA/FLAGRO for each stress ratio

Material Properties:
(4340 Steel)

Ultimate strength = 190 ksi

Yield strength = 160 ksi

Fracture toughness = 90 ksi(in)^{0.5}

C = 2.34 E-09 in/cyc

N = 2.314

Model Application

The present configuration of the ring design dictates that the maximum web section stress will be experienced in the web located between bolts 2 and 3 on the short end of the ring. For this web section, two crack cases were considered.

One case considered a through crack starting at the edge of the web section. A sketch of this model is shown in Figure H-2. In this particular case, a constant web thickness of 0.10 inch was assumed across the total 1.20 inch width of the component. This case neglected those portions of the beam segments in excess of 0.10 inch, and therefore, was conservative. The worse case analysis for this model used an average cross-sectional area stress of 128 ksi.

The second case considered was a corner crack originating in the beam section of the web. A sketch of this model is shown in Figure H-3. For this case, once the crack became critical in this cross-section, a 0.21 inch wide by a 0.25 inch thick section, it was considered a failure. This also was judged to be somewhat conservative because the influence of the 0.10 inch thick shear web adjacent to the beam section was neglected in the analysis. Again, for this crack model, a average cross-section stress of 128 ksi was used.

Likewise, using the present design, another critical area for considering a crack was at bolt location number 3. For this area, a corner crack growing from the bolt hole was considered. A sketch of this model is shown in Figure H-4. For this crack case, the average load for input into the model was 8.57 kips. This was the maximum value which would not violate the design stress allowable. The effects of stress concentration at the bolt hole are included in the fracture mechanics analysis of this crack case. These effects are accounted for in calculating the stress-intensity factor, K , for use in this model.

Results

The results of this analysis are limited to 4340 steel. This is due to the fact that 4340 is being recommended as the material of choice. Similar results can be expected with 4130 steel, although actual crack cases should be run for this material if it is selected.

Analysis results for all crack cases considered show that forty mission lives of the attachment ring can be achieved. A service life factor (scatter factor) of 4 must be met in order to satisfy the fracture control requirements (ref H6) of the attachment ring. Using this factor, lifetimes of 160 flights (40 times 4) or greater are required to meet

Langley's design goal. The expected cyclic lifetimes of the particular models that were run are given in Tables H-1T through H-3T. For all cases, an initial crack size of 0.075 inch was used. This appears to be a very reasonable value for inspection purposes since it is larger than the standard damage tolerant flaw size of 0.050 inch commonly used by the U.S. Air Force. Spectrum loading results are given only for the two crack cases with the shortest lifetimes. A decrease in lifetime of less than two percent was experienced in both cases under spectrum loading. All analyses thus far show that based on the present design no flaws smaller than 0.075 inch will grow to critical size in less than forty mission lives of the ring using either a maximum of 8.57 kips applied at the bolt holes or 128 ksi section stress. For the case of a through crack at the edge of the web section between bolts 2 and 3, a lifetime of 602 flights can be expected. For the corner crack in the pin-loaded lug (bolt location 3) case, a lifetime of 571 flights can be expected. This latter case shows that a factor of 3.5 (571/160) or better exists beyond that required and leads to an added degree of confidence given any shortcomings in the analytical approach. The finite element analysis of the present ring design predicts lower bolt loads and web stresses than those considered in this analysis. Thus, the actual service life of the ring would be larger than predicted.

Limitations

It is important to note that the fatigue-crack growth and fracture analyses performed were linear elastic. Based on present finite element analyses, some local yielding can be expected at holes 2, 3, and 4 when stress concentration effects are considered. A plot of the stress concentration factor based on the lug configuration is shown in Figure H-5. As previously mentioned in the section on model application, the effects of local stress concentration at the bolt holes were included in the fracture mechanics analysis. The effect of local yielding was not accounted for in the analysis. However, considering the additional amount of calculated mission lifetime beyond that required, local yielding effects would not offset this margin.

A final area of concern, an area which was not accounted for in the present analysis, is the contribution of water impact loading. It is felt that this load does not contribute to crack propagation in the ring. This type of loading would tend to cause some out of plane bending stresses in the ring but in a direction that would not promote any crack growth due to flight loading. Also, the ends of the attachment ring are for the most part supported by the motor case tangs in reaction to this load. This would further downplay water impact load effects in the areas of concern from a fracture mechanics standpoint.

Conclusion

In summary, the end of the present SRB/ET attachment ring design has undergone a fracture mechanics analysis. This was a linear elastic analysis designed to establish a lifetime of the ring based on calculated maximum allowable flight bolt loads of 8.57 kips applied at the first three bolt locations or based on the maximum allowable design stress of 128 ksi applied at the web sections. The highly stressed areas near the short end of the ring were evaluated and service lives greater than forty missions were obtained. A very reasonable initial flaw size of 0.075 inch can be inspected for in assuring that the ring meets its calculated goal. Using this initial flaw size, service lives greater than 14 (571/40) times the required goal of forty mission lives were calculated. Any uncertainties due to local yielding at pin holes, water impact loading, or even handling or rework, may have to be further evaluated, although it is felt that adequate margin exists beyond the required scatter factor of 4 to allow for this. In any event, flight safety can be met through periodic inspections.

References

- H1. Fatigue Crack Growth Computer Program, NASA/FLAGRO, JSC-22267, NASA Lyndon B. Johnson Space Center, August 1986.
- H2. Newman, J. C., Jr., "Fracture Analysis of Ductile Materials," ICM-3, Vol.3, Cambridge, England, August 1979.
- H3. Tada, H., Paris. P. C. and Irwin, G., "The Stress Analysis of Cracks Handbook, Del Research Corporation, 1973.
- H4. "Fatigue Loads Data for SRB," Panafax Transmission, MSFC to LaRC, J. Dozier to D. Butler, subject: SRB ETA Ring Fatigue Loads, April 30, 1987.
- H5. Solid Rocket Booster Design Loads, SE-019-057-2H, Book 1, SCN 049, 8 January 8, 1982.
- H6. Solid Rocket Booster Fracture Control Plan, United Technologies United Space Boosters, Document No. 10PLN-0023, Huntsville, Alabama, March 1987.

TABLE H-1T. FRACTURE MECHANICS RESULT FOR SRB/ET ATTACHMENT RING

MODEL: SINGLE EDGE THROUGH CRACK IN A PLATE (WEB BETWEEN BOLTS 2 & 3)

MAT'L: 4340 STEEL

MECHANICAL PROPS: $F_T = 180 \text{ ksi}$, $F_{TY} = 160 \text{ ksi}$

$K_{IC} = 90 \text{ ksi} \sqrt{\text{IN}}$

$C = 2.34 \times 10^{-9} \text{ IN/cycle}$ — (Ref: NASA/FLAGRO)

$n = 2.314$

ALLOWABLES: MAX DESIGN STRESS = 128 ksi

DIMENSIONS: WIDTH = 1.20 IN. THICKNESS = 0.10 IN.

| | APPLIED STRESS (ksi) | INITIAL CRACK SIZE, A_0 (IN.) | CYCLIC LIFE (FLIGHTS) | FAILURE MODE | FINAL CRACK SIZE (IN.) |
|------------------|----------------------|---------------------------------|-----------------------|----------------------------------|------------------------|
| CONSTANT AMPL. | 128 | .075 .060 .050 | 609 980 1299 | FRACTURE FRACTURE FRACTURE | .112 .112 .112 |
| SPECTROM LOADING | 128 | .075 | 602 | FRACTURE | .112 |

P.L. Brown 6-25-87
NASA - LARC

TABLE H-2T. FRACTURE MECHANICS RESULTS FOR SRB/ET ATTACHMENT RAIL

MODEL: CORNER CRACK IN A BAR (WEB SECTION BETWEEN BOLTS 2 & 3)

MAT'L: 4340 STEEL

MECH PROPERTIES: $F_{T0} = 180 \text{ ksi}$ $F_{TY} = 160 \text{ ksi}$

$$K_{1C} = 90 \text{ ksi} \sqrt{\text{in}}$$

$$C = 2.34 \times 10^{-9} \text{ in/cycle}$$

$$n = 2.314$$

(REF: NASA / FLAGRO)

ALLOWABLES: MAX DESIGN STRESS = 128 ksi

DIMENSIONS: WIDTH = .21 IN THICKNESS = .25 IN.

217

| APPLIED STRESS (ksi) | INITIAL CRACK SIZE, A_0 (in.) | CYCLE LIFE (FLIGHTS) | FAILURE MODE | FINAL CRACK SIZE (in.) |
|----------------------|---------------------------------|----------------------|---------------------|------------------------|
| 128 | .075 | 1361 | NET SECTION FAILURE | .113 |
| | .060 | 2298 | NET SECTION FAILURE | .113 |
| | .050 | 3135 | NET SECTION FAILURE | .113 |

P.L. BLOWN 6-25-87
NASA - LARC

TABLE H-3T. FRACTURE MECHANICS RESULTS FOR SRB/ET ATTACHMENT RING

MODEL: CORNER CRACK FROM A HOLE IN A LUG (BOLT LOCATION 3)

MAT'L: 4340 STEEL

MECH PROPERTIES: $F_{T0} = 180 \text{ ksi}$ $F_{TY} = 160 \text{ ksi}$

$K_{IC} = 90 \text{ ksi} \sqrt{\text{in}}$

$C = 2.34 \times 10^{-9} \text{ in/cycle}$ (Ref: NASA/FLAGRO)

$n = 2.314$

ALLOWABLES : MAX APPLIED LOAD = 8.57 KIPS, MAX APPLIED STRESS =

DIMENSIONS : WIDTH = 1.20 IN THICKNESS = .25 IN HOLE DIA. = .396 IN.

| | APPLIED LOAD/STRESS (KIPS / KSI) | INITIAL CRACK SIZE, A_0 (IN.) | CYCLIC LIFE (FLIGHTS) | FAILURE MODE | FINAL CRACK SIZE (IN.) |
|---------------------|-------------------------------------|------------------------------------|--------------------------|----------------------------------|---------------------------|
| CONSTANT AMPL. | 8.57 / 57.13 | .075 .060 .050 | 579 862 1077 | FRACTURE FRACTURE FRACTURE | .114 .114 .114 |
| SPECTRUM LOADING | 8.57 / 57.13 | .075 | 571 | FRACTURE | .114 |

P.L. BROWN (6-25-87)
NASA-LARC

AREAS

$A-A = .183 \text{ IN.}$

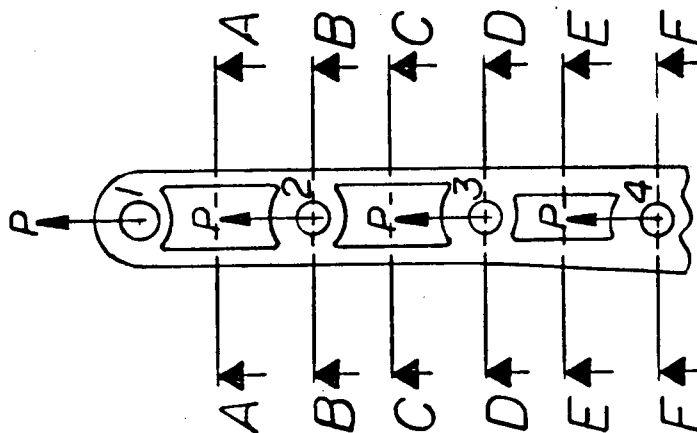
$B-B = .201 \text{ IN.}$

$C-C = .183 \text{ IN.}$

$D-D = .201 \text{ IN.}$

$E-E = .240 \text{ IN.}$

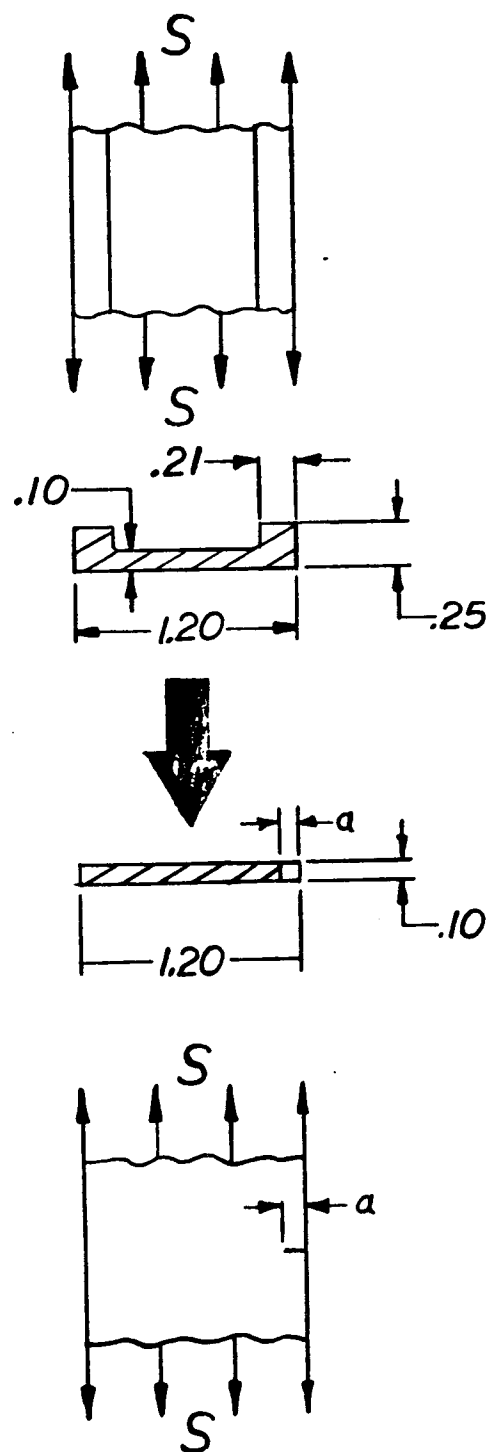
$F-F = .276 \text{ IN.}$



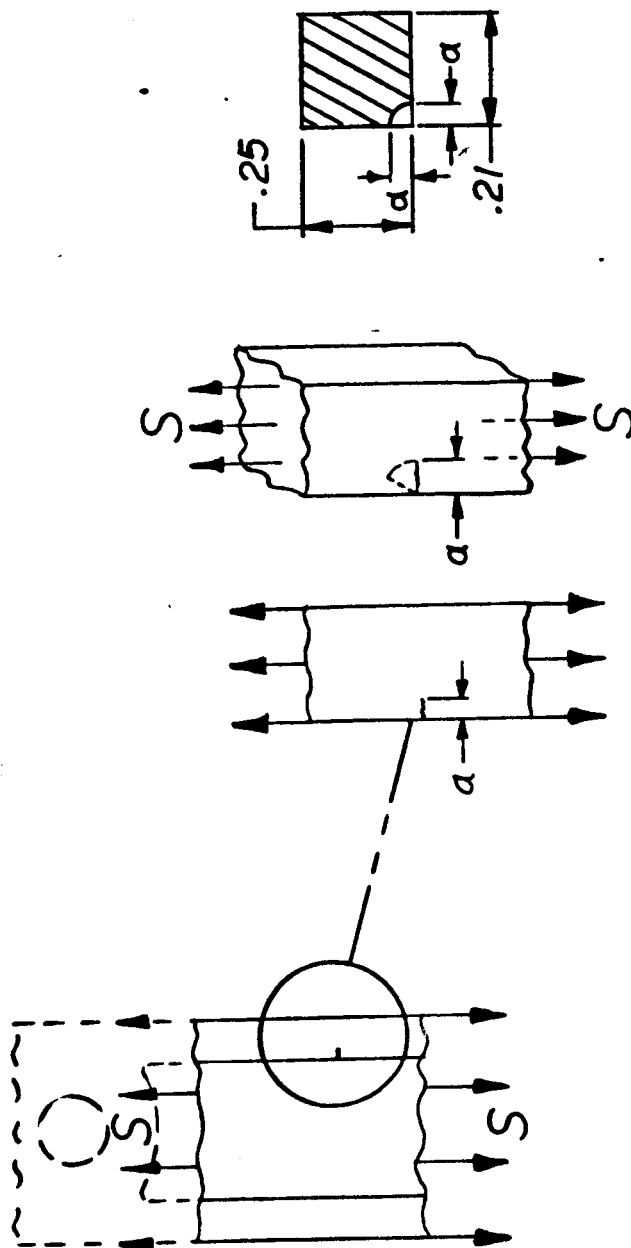
SRB/ET ATTACHMENT RING

(FIGURE H-1)

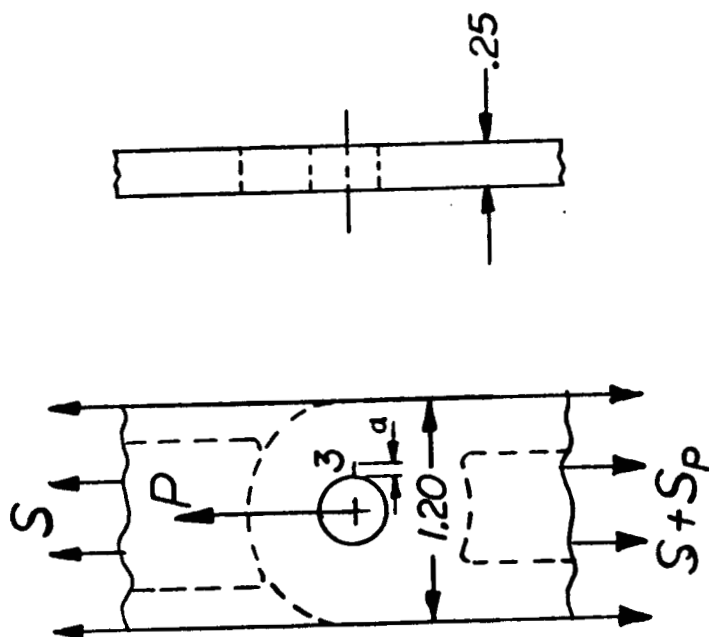
SINGLE EDGE THROUGH CRACK



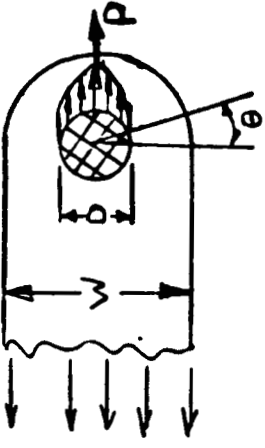
(FIGURE H-2)



CORNER CRACK IN A BAR
(FIGURE H-3)

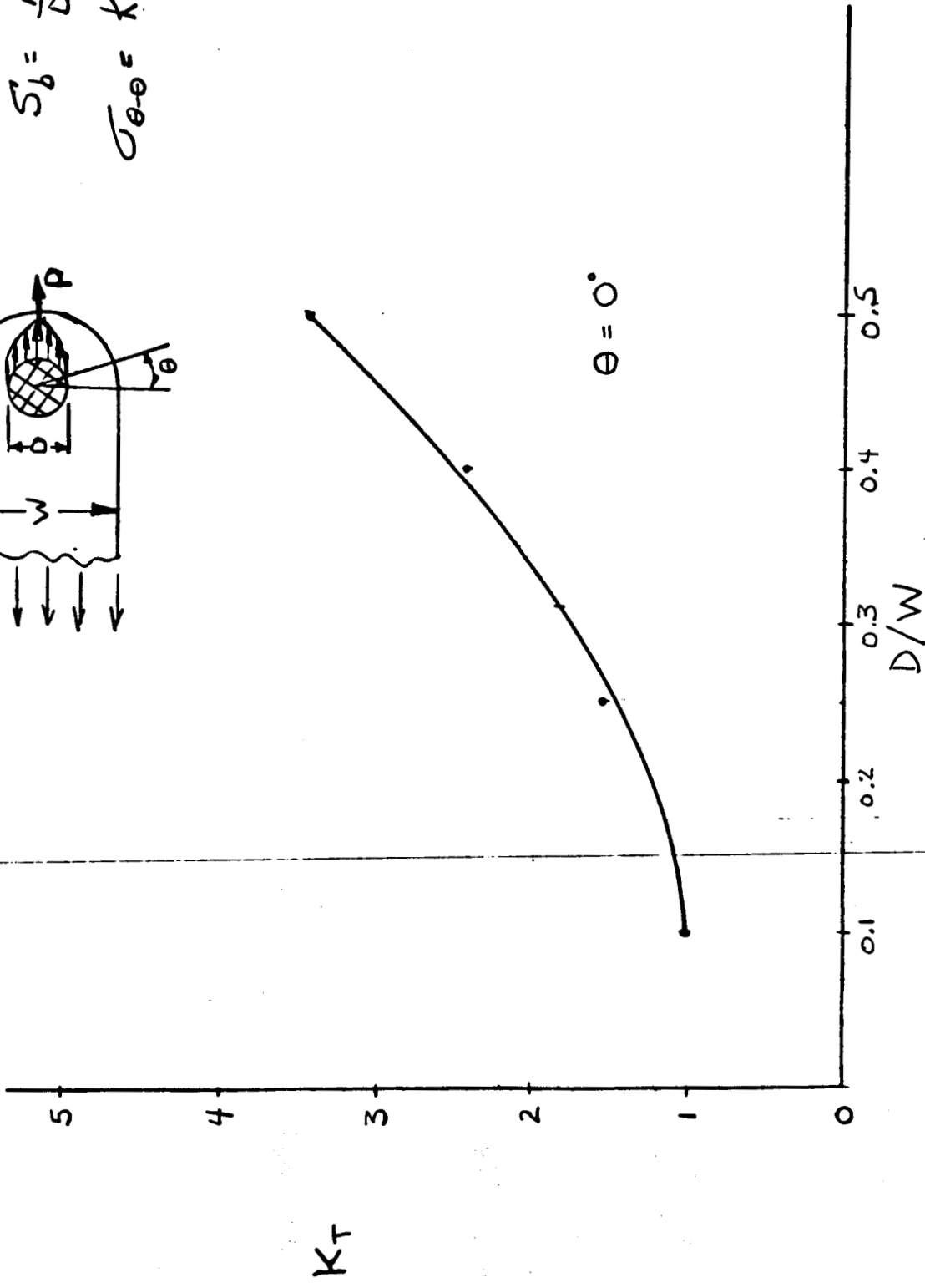


CORNER CRACK FROM PIN LOADED LUG
(FIGURE H-4)

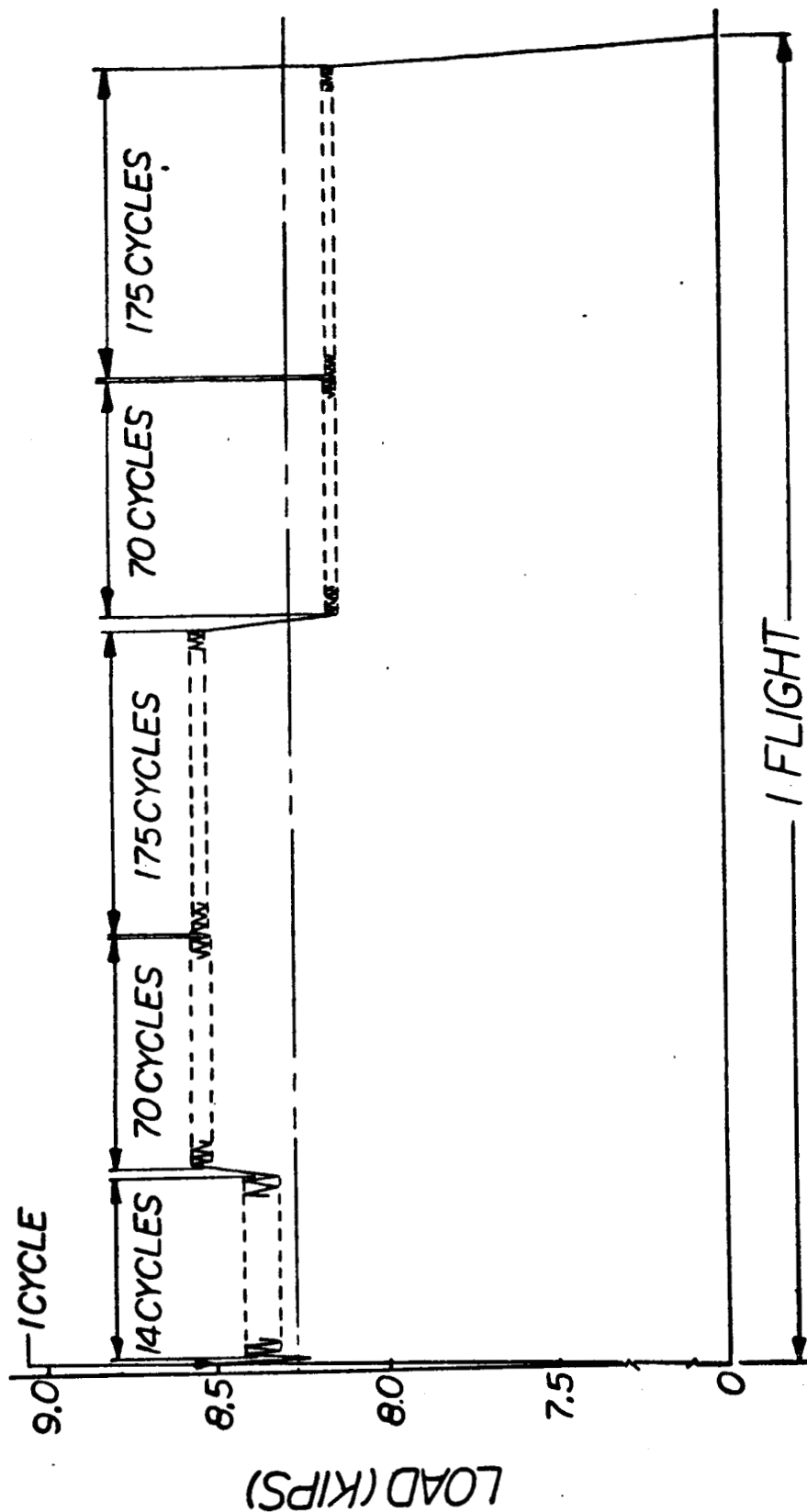


$$S_b = \frac{P}{Dt}$$

$$\sigma_{\theta=0} = K_T S_b$$



STRESS CONCENTRATION FACTORS FOR PIN LOADED LUG
(FIGURE H-5)



SPECTRUM LOADING
(FIGURE H-6)

P.L. BROWN 7-1-87
NASA - LARC


APPENDIX I


EXPERIMENTS

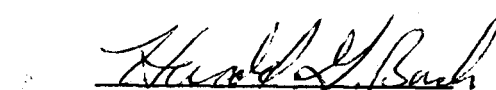
by Harold G. Bush
Mail Stop 190
Langley Research Center
Hampton, Virginia 23665

Phone: (804) 865-2498

June 3, 1987


Harold G. Bush, Author


Reviewer


Martin M. Mikulas, Jr., Project Engineer


David H. Butler, Project Manager

APPENDIX I - EXPERIMENTS

Introduction

Experiments were conducted to determine the elastic properties of a proposed partial SRB external tank attachment ring web. It was determined by analysis that the shear loading of the first (or end) bolt (see fig. 28) was extremely sensitive to the extensional stiffness (i.e., Young's Modulus \times cross-sectional area, EA) of the web section between the first and second tang bolts connecting the web to the SRB motor case. The required area of the redesigned first web section was analytically found to be small (see fig. 27) relative to the original web design. The first area was sufficiently small that the bolt boss area, required to transmit bolt forces into the web, substantially increased the section effective extensional stiffness. Therefore, various designs for the end web section were developed and fabricated for test to obtain a measure of the "actual" extensional stiffness.

Experiments to determine bolt stiffness and strength, material Young's modulus, and the effectiveness of various bushings in reducing bolt stiffness were also conducted.

Test Setup

The test fixture and component configuration used to load two web sections per test in single-shear are shown in Figure I-1. Two clam-shell fixture halves are used back-to-back to eliminate out-of-plane bending deformations of the fixture which would occur if web section components were tested singly in single shear. Details of the test fixture clam-shell halves are shown in Figure I-2. The test fixture was fabricated from 17-4 Ph steel heat-treated to a hardness of approximately Rockwell C 42 to approximate the SRB casing hardness and strength.

The component extension measurements (x) were taken adjacent to the bolt head (as shown in Figure I-1 and I-3) using electronic, knife edge extensometers. Attempts to obtain measurements from the bolt head were unsuccessful. Fixture displacements (y) were obtained by attaching rigid offsets to the fixture to support DCDT displacement measuring devices. To keep these measurements along the component centerline (to eliminate bending influence in that plane) the rigid offsets supported the DCDT instruments approximately 5 inches from the fixture clam-shell separation plane as shown in Figure I-3. This permitted the component extensometer and fixture displacement measurements to be obtained in a plane through the components' centerlines. Differential extension of the components (x_1 , x_2) will cause the fixtures to rotate (essentially as rigid bodies) as shown in an exaggerated view in Figure I-3, which has the effect of amplifying the resultant fixture displacements (y_1 , y_2). Since the rigid offsets constitute two straight lines, the centerline displacement (y) is equal to the average of y_1 and y_2 as shown in Figure I-3. The extension (x) is equal to the average of the two components (x_1 and x_2) tested.

Elastic Property Determination

The elastic properties (component extensional stiffness, EA and bolt stiffness, K) were determined as defined in Figure I-4. Since it is essentially impossible to measure those displacements needed to calculate the

elastic properties exactly, the most appropriate measurements were taken as shown in Figures I-3 and I-4. Bolt and component calculations were made from the analysis model and equations given in Figure I-4, and provided a basis for comparing various component designs for the end section.

Component Tests

Three designs for the end web section(s) were considered. These component configurations are shown in Figures I-5 thru I-7 which also show typical load-deflection response for the three web component designs tested using 4130 steel heat-treated to Rockwell C 42 hardness. The individual component extensions are labeled EX-1 and EX-2. The fixture displacement measurements are labeled DC-1 and DC-2. Bolt stiffness (K) and section extensional stiffness (EA) were determined using the methods outlined on Figure I-4 and are summarized in Figure I-8.

Bolt stiffness values are shown in Figure I-9 for the three component and fixture hole size combinations tested. While there is considerable scatter in the calculated values, there is an apparent trend to lower values of bolt stiffness for "sloppy" holes. For the tests shown in Figure I-8 and I-9, all components were "seated" (free-play removed) by applying load before data were recorded, therefore free-play or slippage did not contribute to the bolt stiffness scatter. Each component tested was loaded to 10,000 lbf (20,000 lbf total applied load).

Extensional stiffness calculation results are shown in Figure I-10 for the three component and fixture hole size combinations tested. Since none of the designs showed any distinct advantage (i.e., lower extensional stiffness) over the others, the double bar design was selected for refinement due to handling and fabrication considerations. Extra material was machined from the bolt boss area to reduce the effective extensional stiffness of the double bar components. It is shown in Figure I-10 that successive machining operations on the 4.5-inch component reduced the stiffness from 3.21×10^6 lbf to 2.92×10^6 lbf. The final configuration shown was still 5.8 percent above the target value of 2.76×10^6 which is based on the cross-sectional area of the bars only.

Web Bending

Single shear loading of bolts (i.e., current ET attach ring design) has the consequence of bending the web locally and distorting measurements taken from the component surface. This problem is depicted in Figure I-11 which shows the physical situation in the test setup used for the web end component tests. The bolt rotation essentially causes the bolt to bear non-uniformly on the bolt hole inside diameter resulting in a moment being applied to the component cross section as well as an axial force. It is shown in the Figure that displacement measurements taken on the "outside" surface of the test component would be less than the desired web midplane displacement required to accurately measure the component extensional performance. Since the component is bolted to a fixture, the points required for measurement (i.e., web midplane on loaded side of the bolt hole) are inaccessible. An attempt to quantify the bending effect under the bolt head is shown in Figure I-12. The displacement between two points on the "outside edge" and subsequently two points on the "inside edge" of a test component during loading were obtained using two optical micrometers. The measurement locations are shown in Figure I-12 and I-13. Each displacement measurement shown in Figure I-13 is the

average of five tests, since it was physically impossible to obtain the "inside" and "outside" measurements simultaneously. Figure I-13 shows the average test results for two series of tests. One series used only two bolts while the second series used a third bolt, finger tightened to preclude movement at that location away from the fixture. It is shown that the difference between midplane and surface displacement values is 0.0016 inch and 0.0018 inch for the "restrained" and "free" cases, respectively. It may be reasoned that such a "correction factor" should be applied to the extensometer measurements used to calculate the stiffness parameters listed in Figure I-8. As an example, "correcting" the double bar (4.5 inches) test results in Figure I-8 reduces the EA value range from $(3.21 - 2.92) \times 10^6$ lbf to $(2.86 - 2.62) \times 10^6$ lbf. Bolt stiffness, K_b , values also are increased from $(1.03 - 1.5) \times 10^6$ lbf/in to $(1.13 - 1.74) \times 10^6$ lbf/in.

Figure I-14 shows a comparison of a double-bar test result and a finite element analysis of that test. The finite element model did not include eccentric loading at the bolt hole, therefore, the analytical result does not include any out-of-plane bending deformations. The test results shown include the bending effects. The finite element analysis indicates a displacement of 0.0151 inches at the location where the "correction factor" was determined. Test results indicate a displacement of 0.0136 inches. Adding the 0.0018 inch "correction" displacement to the test value results in an experimental measurement of 0.0154 inches, which compares more favorable with the analytical result.

The extreme difficulty in obtaining the appropriate measurements for calculating the actual effective elastic properties of structural components loaded in single shear, as discussed herein, indicates that judicious use be made of "design" values deduced from experimental results. Simultaneous "numerical" experiments (analysis) of any experiment is highly recommended to identify and quantify anomalies (such as bending) which may be present.

Material Property Tests

In order to insure that the 4130 steel possessed the nominal modulus of 30×10^6 lbf/in², tests were performed to determine the actual Young's modulus of the specimens being manufactured at LaRC. Results of these tests are presented in Figure I-15 along with ultimate load test results for the 3/8-inch tang bolts being used. Test results shown in Figure I-15 confirmed the modulus of 4130 steel and exceeded the reported ultimate bolt shear strength (16,000 lbf).

Bushing Tests

To investigate design alternatives, a series of clearance fit bolt hole bushings were tested to determine their effectiveness in reducing bolt stiffness. Figures I-16 thru I-18 show the bolt load-deflection response of an end section design (dog-bone/4130 steel) without a bushing and the response of the same component machined and fitted with 1020 steel bushings of various thicknesses. It is shown in the Figures that thicker bushings are characterized by greater scatter in their load-deflection characteristics. Secant values of bolt stiffness were calculated from the results shown in Figures I-16 thru I-18 and are presented in Figure I-19. The calculated secant values of bolt stiffness at 10,000 lbf bolt load are shown for the three bushing thicknesses tested. The vertical bar indicates the scatter band width at each thickness and each tic-mark is a test result. The circled tests

were performed initially with bushings machined from different 1020 steel than were the other tests. A different fixture (of the same design) was also used for the initial tests. All fixtures initially had 0.391-inch bolt holes and all bushings had 0.385-inch bolt holes.

An effective secant bolt stiffness of 0.5 to 0.7 times the baseline stiffness (1.2×10^6 lbf/in) was found analytically to be desirable in reducing the load in the end tang bolt. Therefore, the 0.018-inch steel bushings were found suitable since all data fell within this band. A bolt stiffness value of 60 percent of the baseline was selected as the nominal value for analysis purposes.

Figure I-20 through I-22 show the bolt load-deflection response of 2024-T4 aluminum bushings tested similarly to the steel bushings. The performance of the aluminum bushings is approximately the same as the steel bushings but is characterized by more consistent (i.e., less scatter) behavior at all three thicknesses tested. Figure I-23 shows the calculated secant values of bolt stiffness for the three bushing thicknesses considered. It is shown that calculated bolt stiffness for both the 0.018-inch and 0.035-inch thick bushings fall within the desired range at 0.5 to 0.7 times the baseline bolt stiffness.

Bolt Hole-Minimum Section Test

End-section web designs being considered have an end web section height of 1.2 inches. The minimum cross-sectional area available to transmit bolt load occurs when a maximum thickness bushing is used. The maximum bushing diameter being considered is 0.4934 inches. A tensile test was performed using a 4130 steel dog-bone type component with a maximum width through bolt hole center equal to 1.2 inches. A hardened steel bushing was used (OD = .4934 inches and ID = .385 inches) in conjunction with 3/8-inch tang bolts to determine the load carrying capability of a minimum height web section with a maximum diameter bushing installed, including hole stress concentration effects. Two components were loaded simultaneously in the test fixture as described previously. A maximum load of 32,500 lbf was attained before yielding occurred away from the bolt hole, in the minimum cross-sectional area of the test component. No bolt yielding or web yielding was visible around the bolt hole and bushing.

TEST COMPONENT AND FIXTURE ASSEMBLY

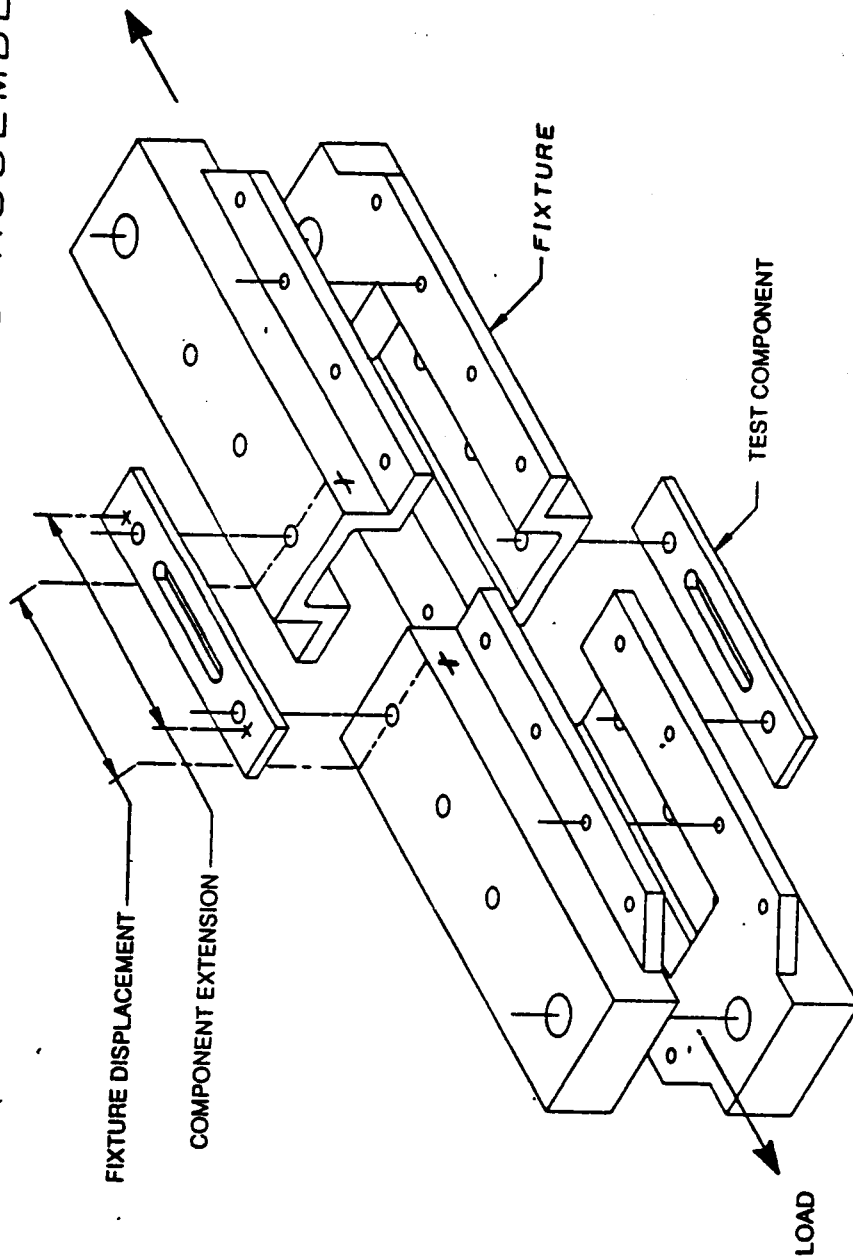


Figure I-1. Exploded view of test component and fixture configuration.

COMPONENT TEST FIXTURE

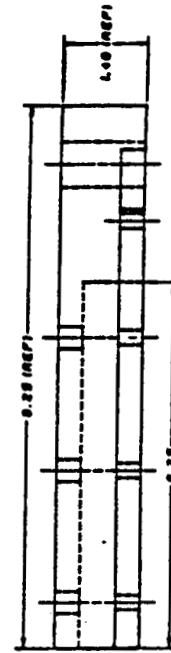
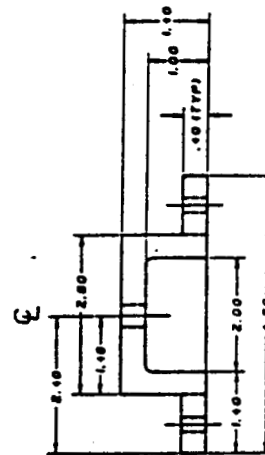
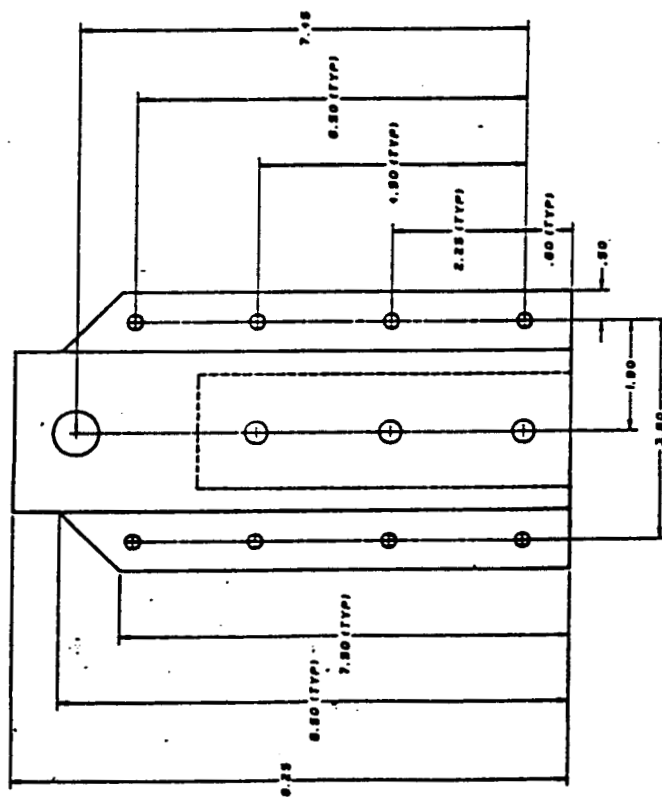


Figure I-2. Details of component test fixture.

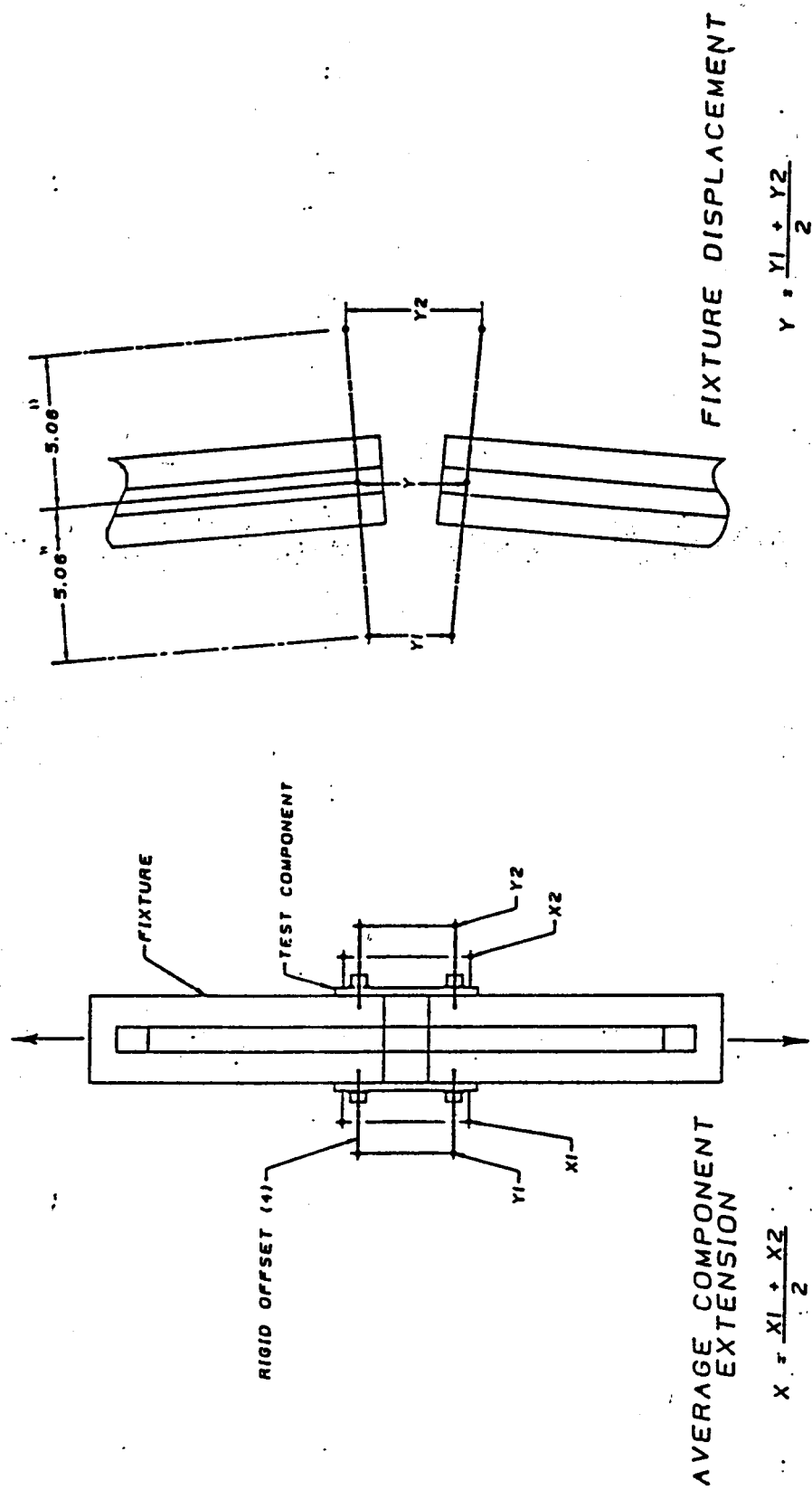
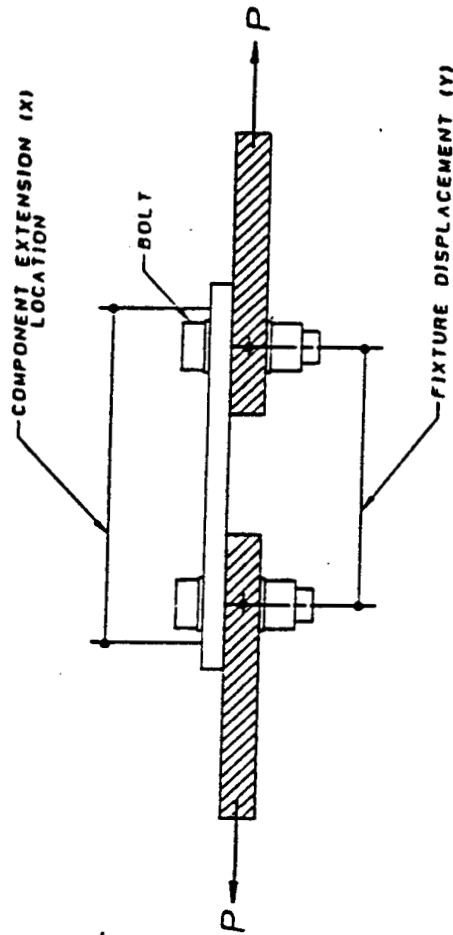


Figure I-3. Component and fixture displacement measurement locations.

EXPERIMENTAL BOLT STIFFNESS DETERMINATION

A - GEOMETRY



B - ANALYSIS MODEL

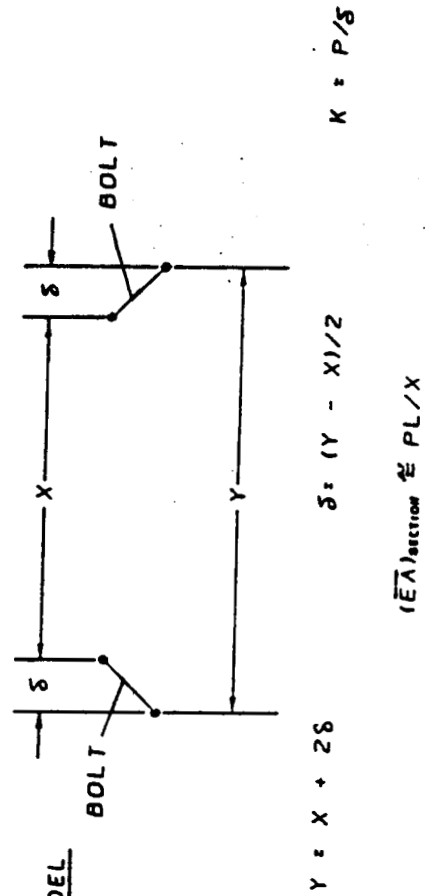


Figure I-4. Measurement locations for bolt stiffness determination.

B1A

DEFLECTIONS

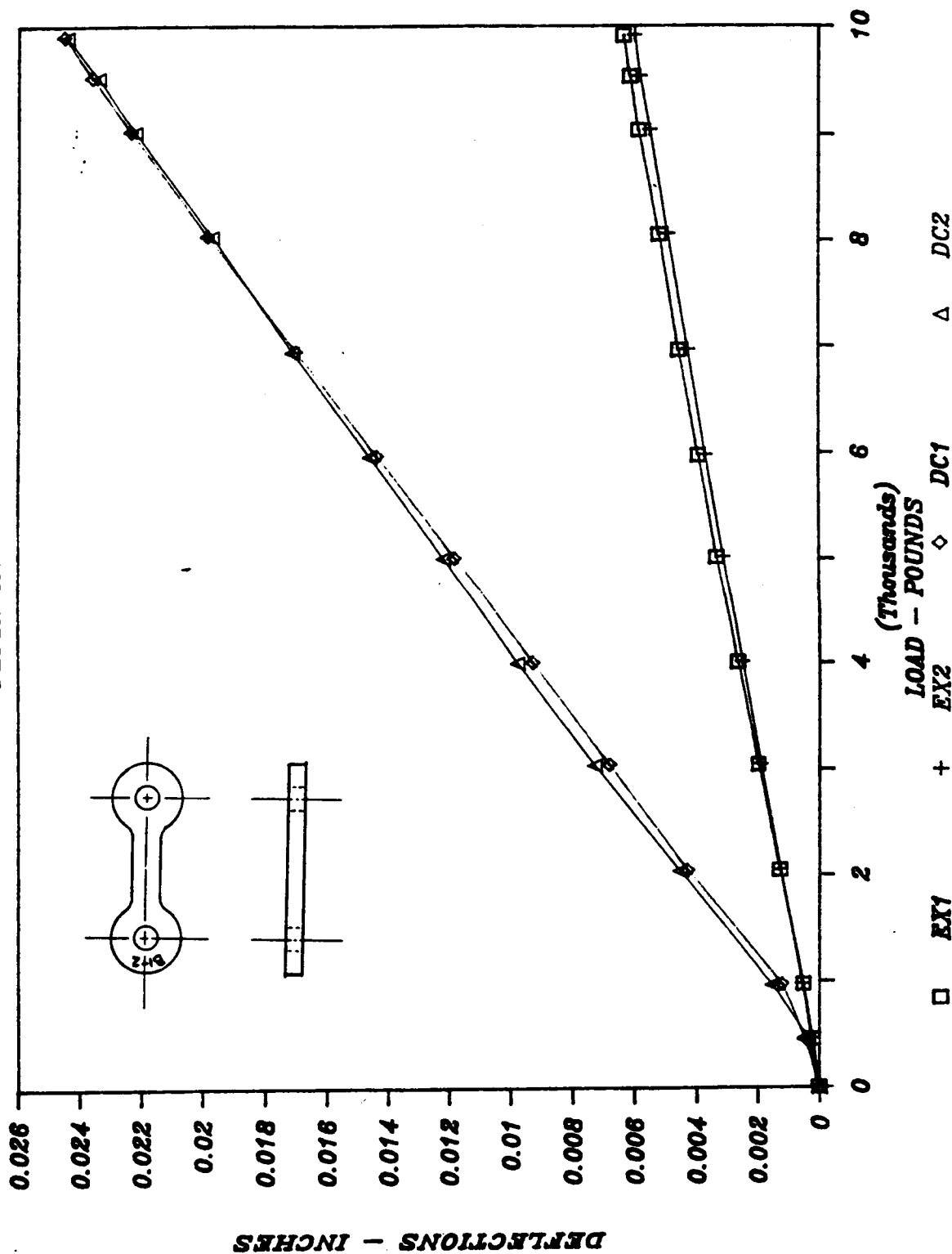


Figure I-5. Typical load-displacement response of dog-bone design end section.

C1C

DEFLECTIONS

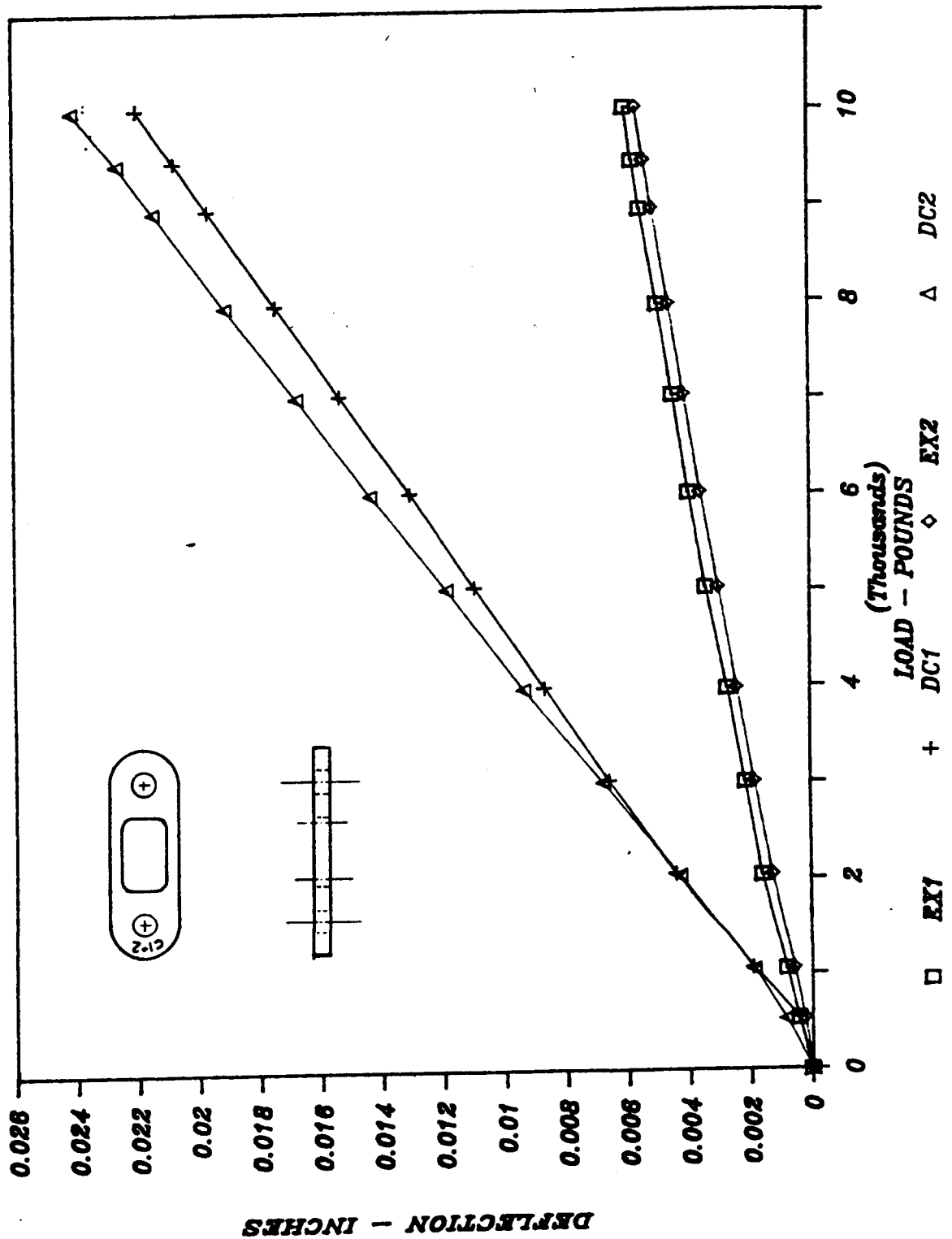


Figure I-6. Typical load-displacement response of double-bar design end section.

DR1B SEC. 1-2

DEFLECTIONS

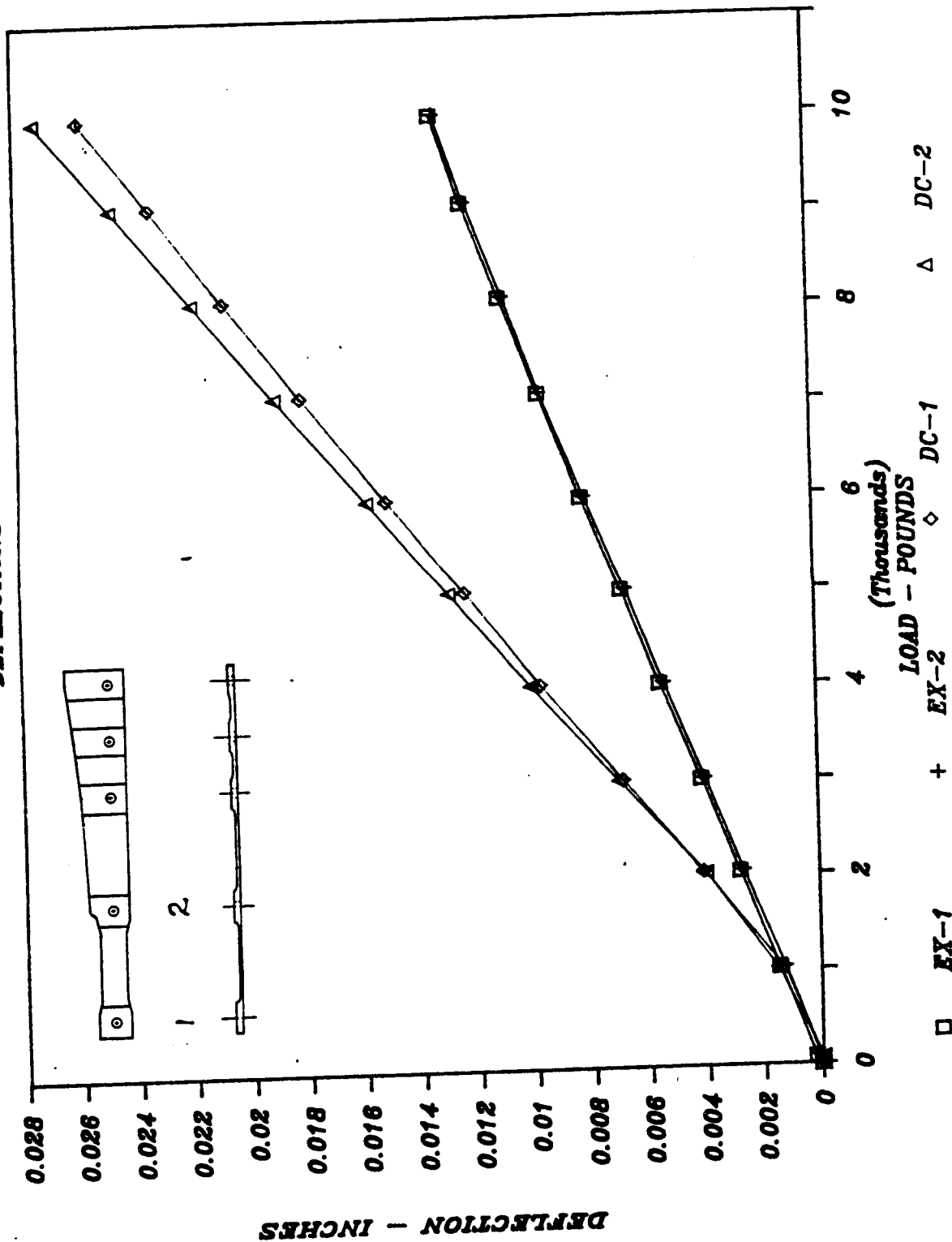


Figure I-7. Typical load-displacement response of scalloped design end section.

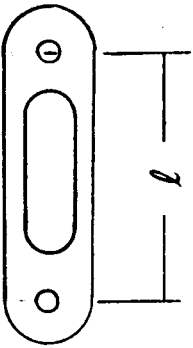
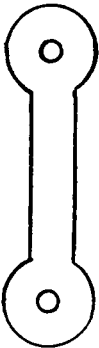

| Component | l , in | Comp. Hole Dia Fixt. Hole Dia | EA , lbf 10^6 | K , lbf/in 10^6 | Remarks |
|---|----------|----------------------------------|----------------------|------------------------|-----------------------------|
|  | 2.25 | .375"/.375" | 3.99 | 1.16 | Large Corner Fillets |
| | 2.25 | .391"/.375" | 6.66 | 1.18 | Section 2 |
| | 2.25 | .391"/.391" | 3.62 | 1.29 | Large Corner Fillets |
| | 2.25 | .391"/.391" | 3.08 | 1.13 | Corner Material Removed |
| | 4.50 | .391"/.391" | 3.21 | 1.50 | Large Corner Fillets |
| | 4.50 | .391"/.391" | 3.01 | 1.13 | Corner Material Removed |
| | 4.50 | .391"/.391" | 2.95 | 1.33 | Corner Material Removed |
| | 4.50 | .391"/.391" | 2.93 | 1.33 | Corner Material Removed |
| | 4.50 | .391"/.391" | 2.92 | 1.03 | Tolerances Reduced/Machined |
| | 2.25 | .391"/.375" | 3.61 | 1.08 | |
|  | 4.50 | .391"/.391" | 3.06 | 1.17 | |
| | 4.50 | .391"/.391" | | | |
| | 4.50 | .375"/.375" | 3.33 | 1.51* | *End Rotation Restrained |
| | 4.50 | .375"/.375" | 5.44 | 1.65* | Section 2 |
|  | 4.50 | .391"/.375" | 3.14 | 1.46* | |
| | 4.50 | .391"/.375" | 5.37 | 1.40* | Section 2 |
| | 4.50 | .391"/.391" | 2.93 | 1.28 | |
| | | | | | |

Figure I-8. Web end section test results summary.

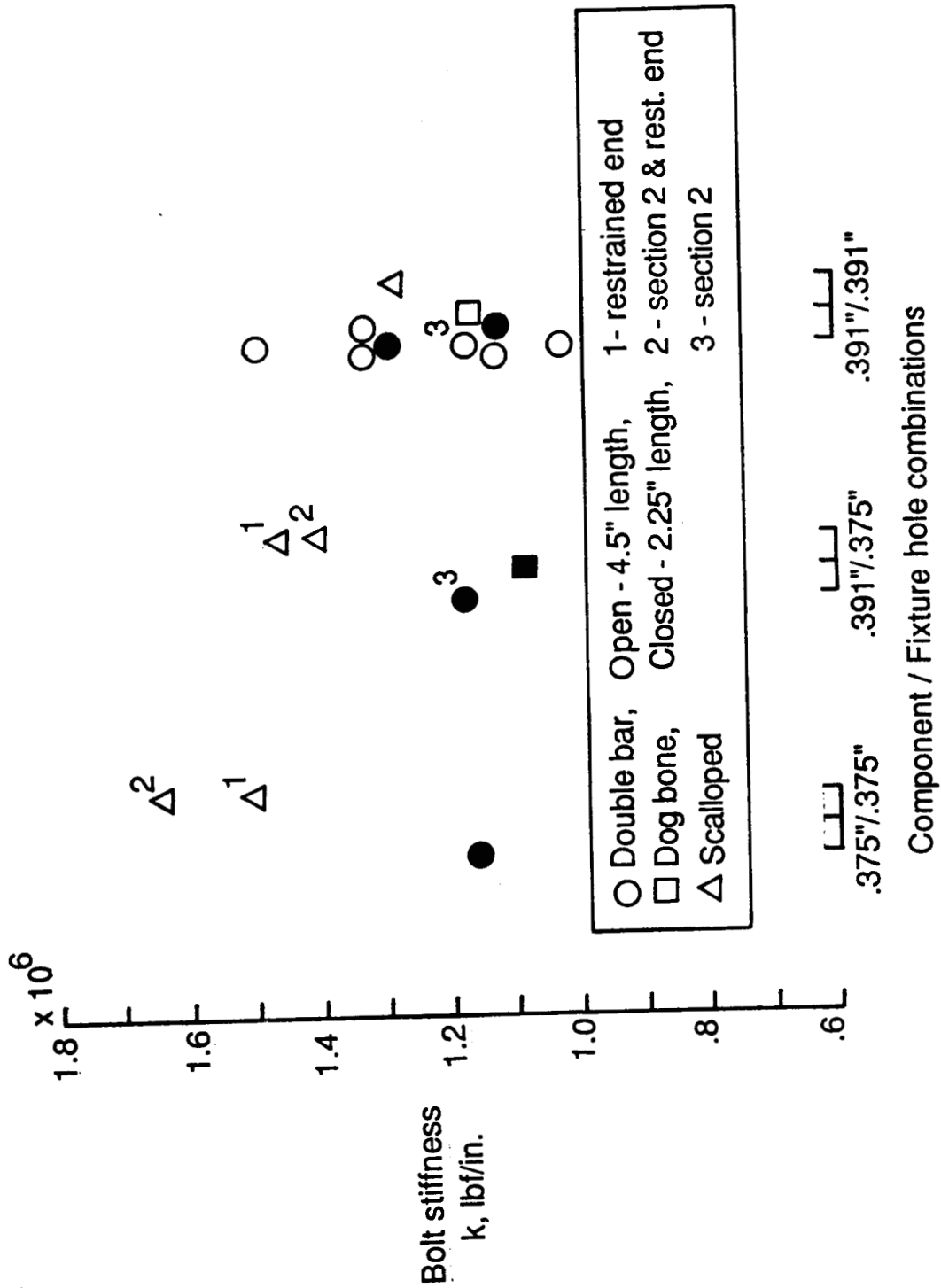


Figure I-9. 3/8-inch tang bolt stiffness for various component and fixture hole size combinations.

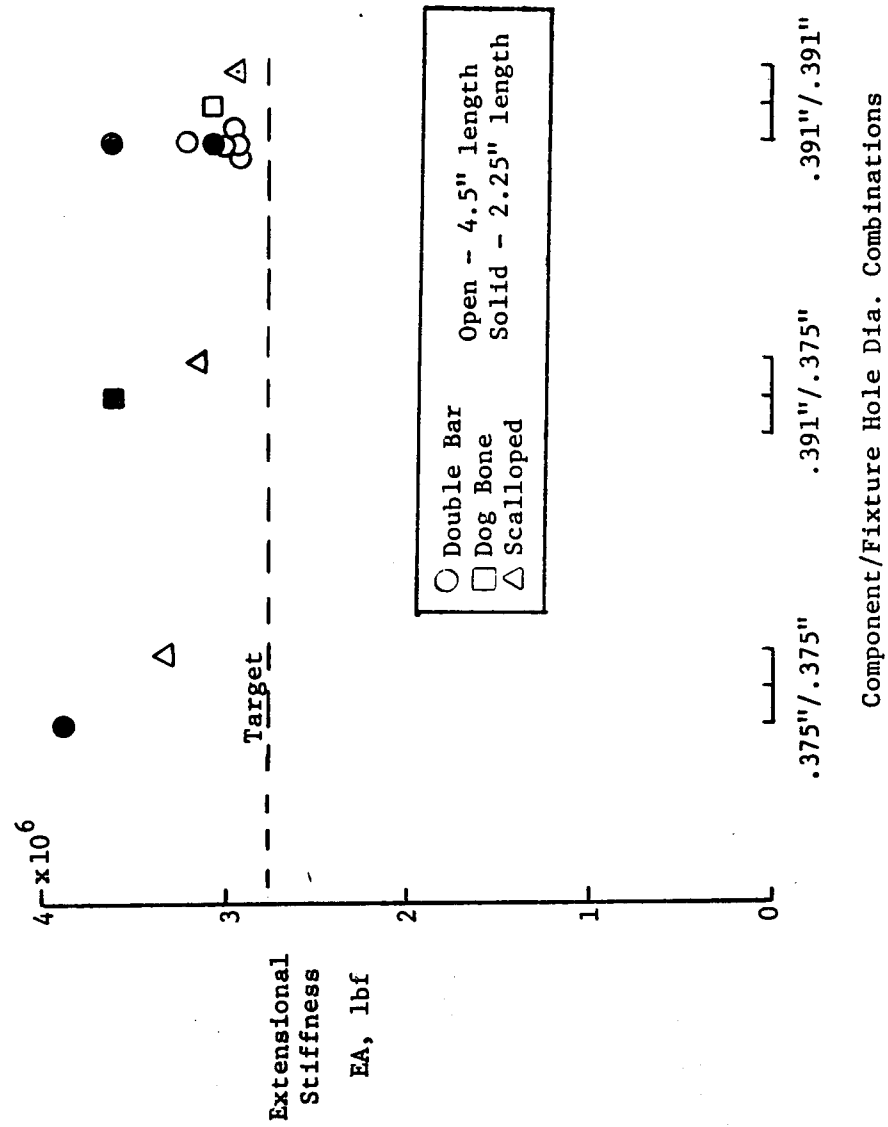
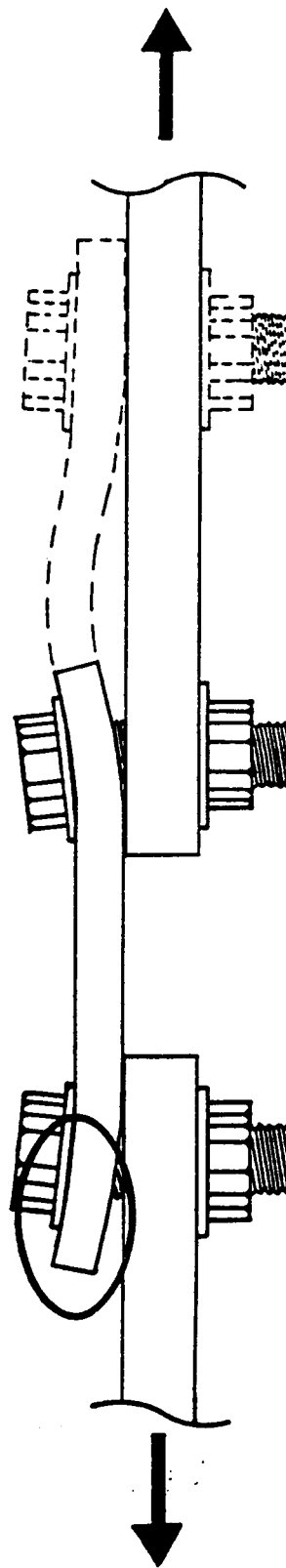
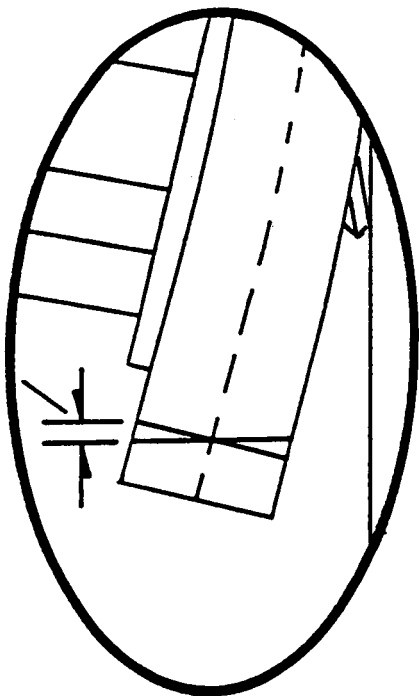


Figure I-10. Extensional stiffness of web section designs for various component and fixture hole combinations.

SINGLE SHEAR LOADING OF BOLTS CAUSES LOCAL BENDING OF WEB

— Difference in displacement from
 ϕ to outer surface



Test fixture center line

Figure I-11. Illustration of bending effects present in single shear bolt loading tests.

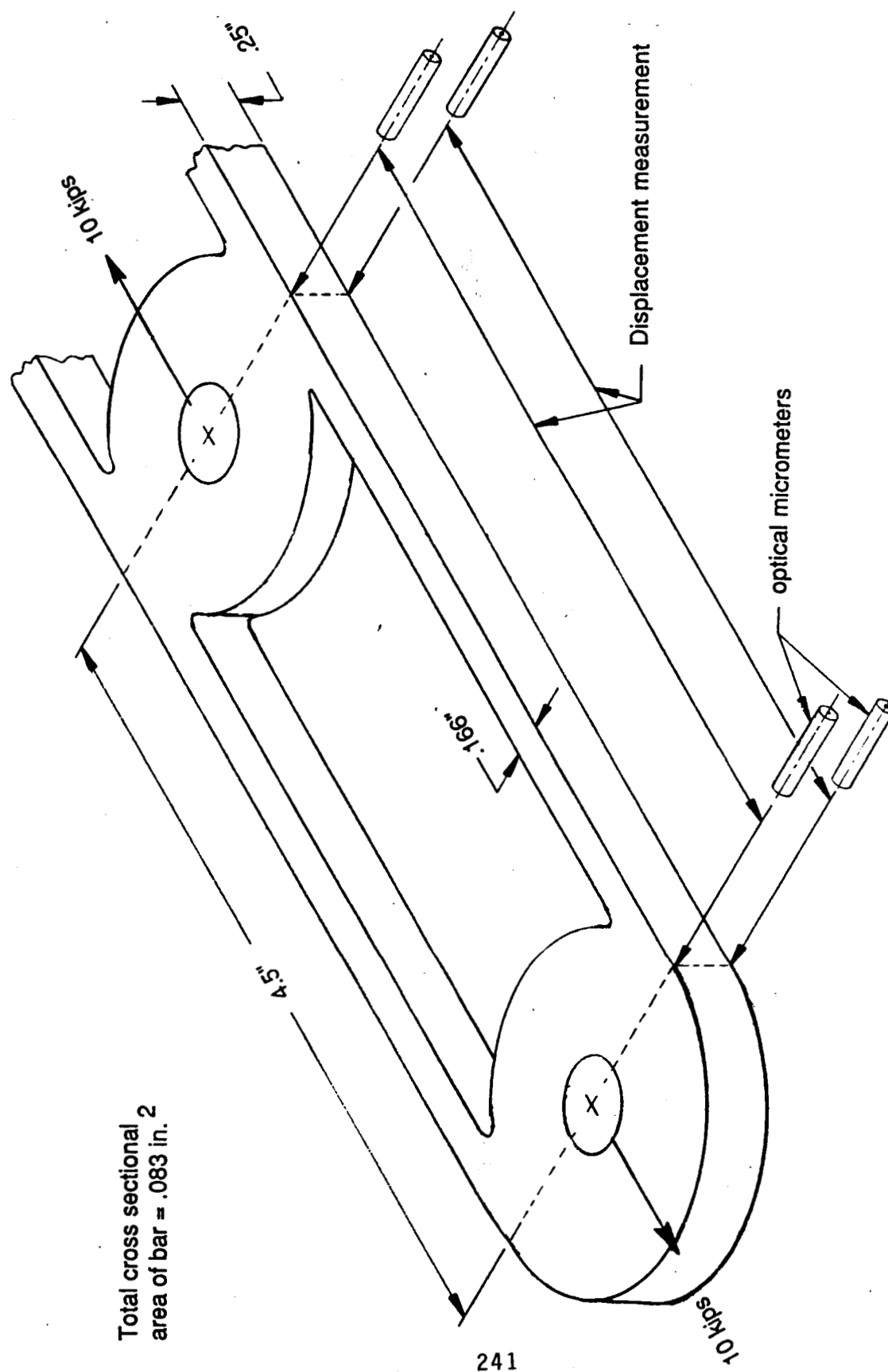
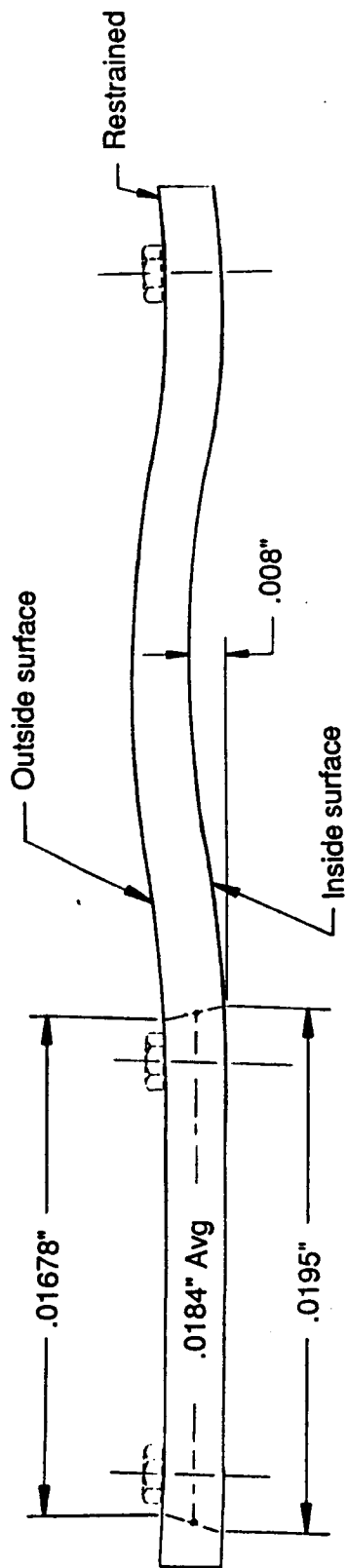


Figure I-12. Test component and optical measurement locations for quantifying bending effects.



Area = $.083$ in.

242

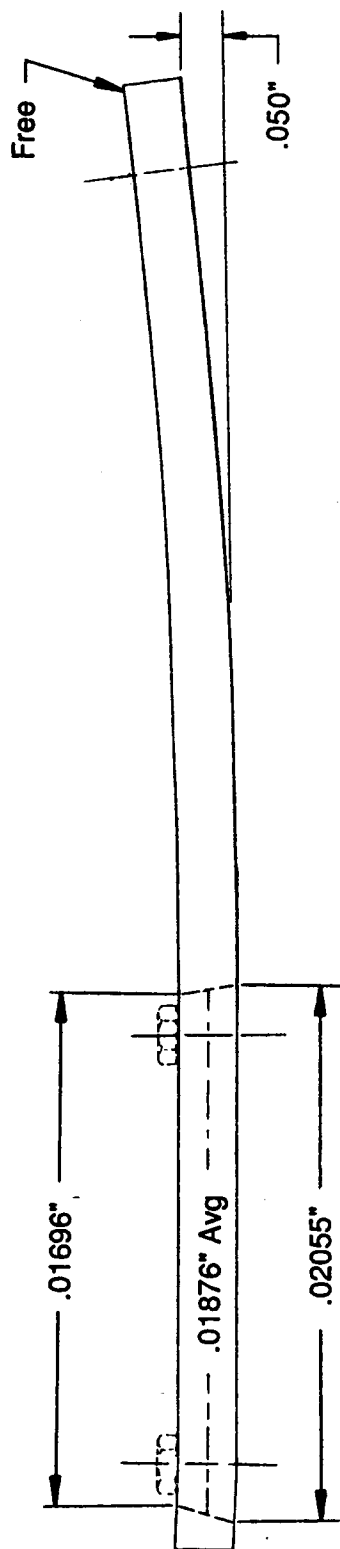


Figure I-13. Bending effect tests-optical measurement results.

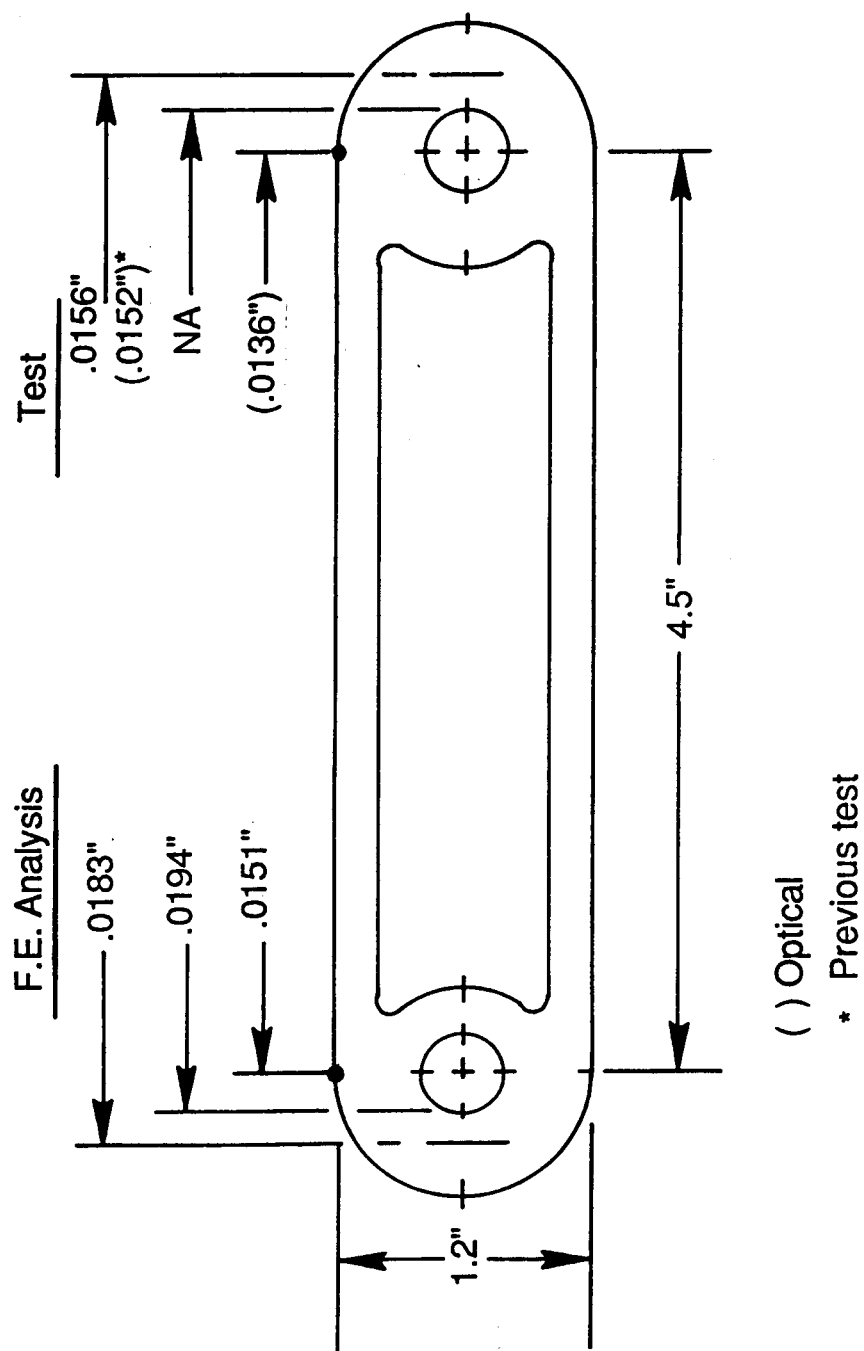


Figure I-14. Comparison of component finite element analysis and test results.

MATERIAL PROPERTY TESTS

- **3/8" TANG BOLTS - Ultimate Shear Strength = 17,500 lb
(5 tests @ 4 bolts/test)**
- **4130 STEEL - Young's Modulus = 29.8×10^6 lbf/in²
(5 tests)**

Figure I-15. Material property tests.

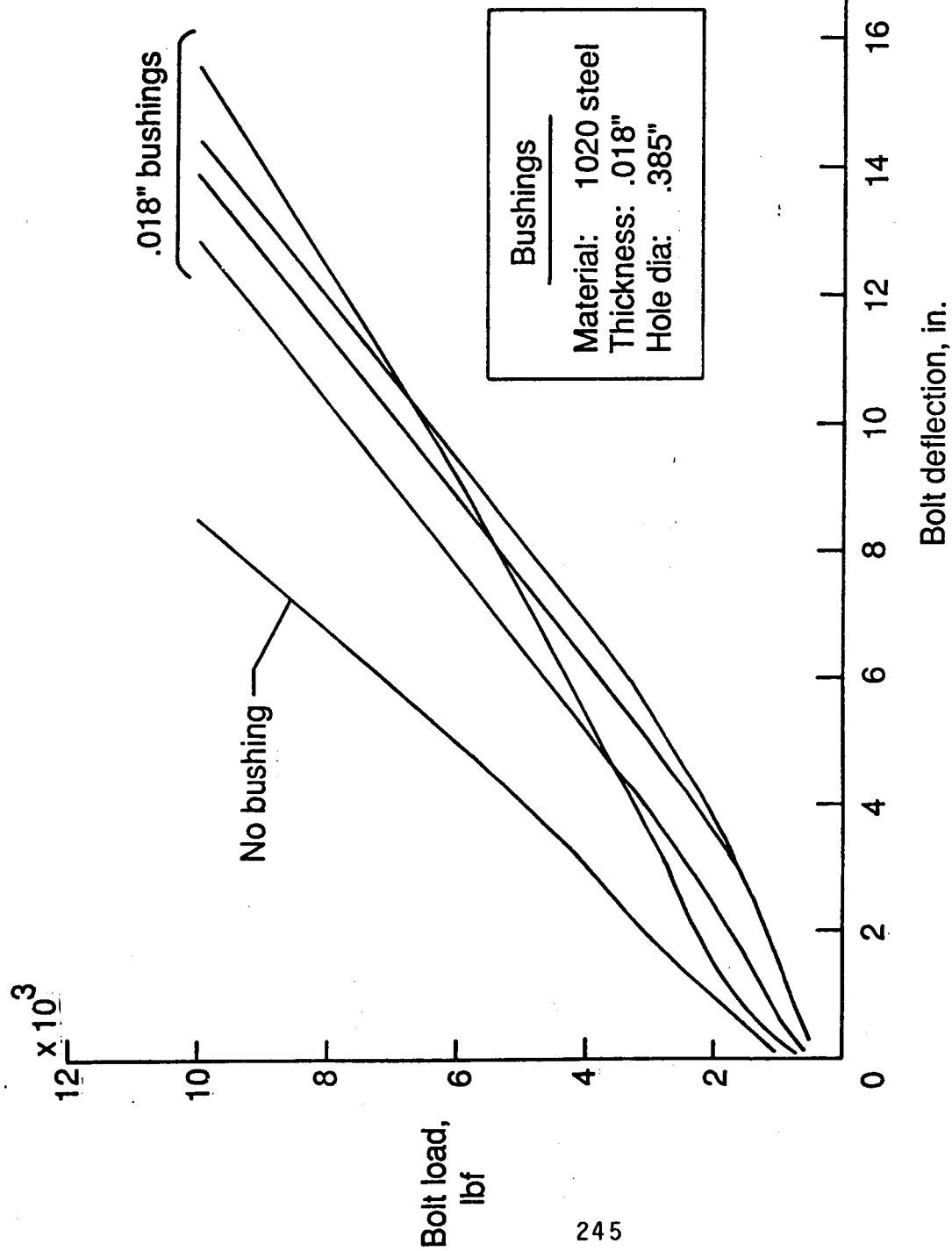


Figure I-16. 3/8-inch tang bolt load deflection response with 0.018-inch thick 1020 steel bushings.

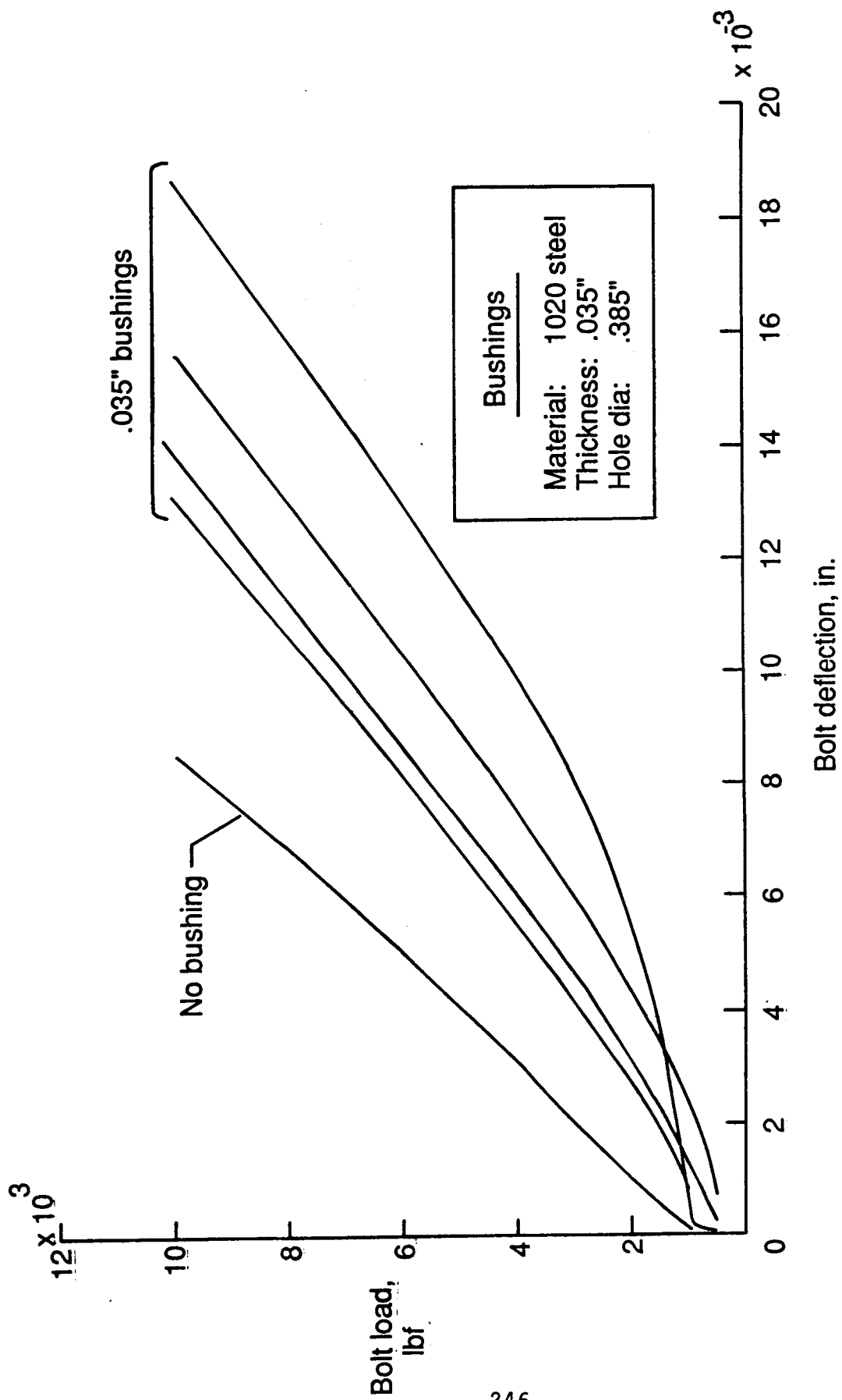


Figure I-17. 3/8-inch tang bolt load deflection response with 0.035-inch thick 1020 steel bushings.

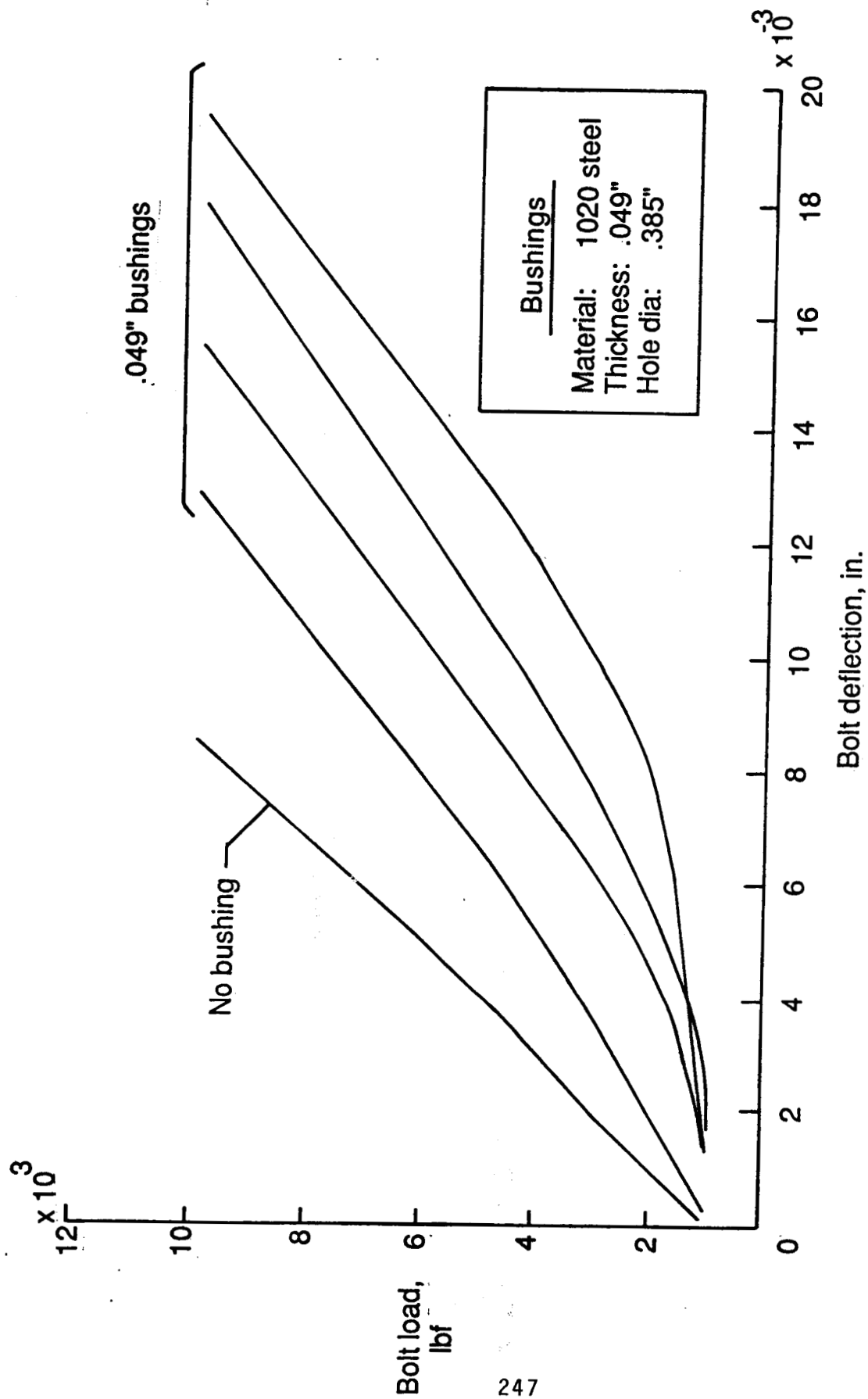


Figure I-18. 3/8-inch tang bolt load deflection response with 0.049-inch thick 1020 steel bushings.

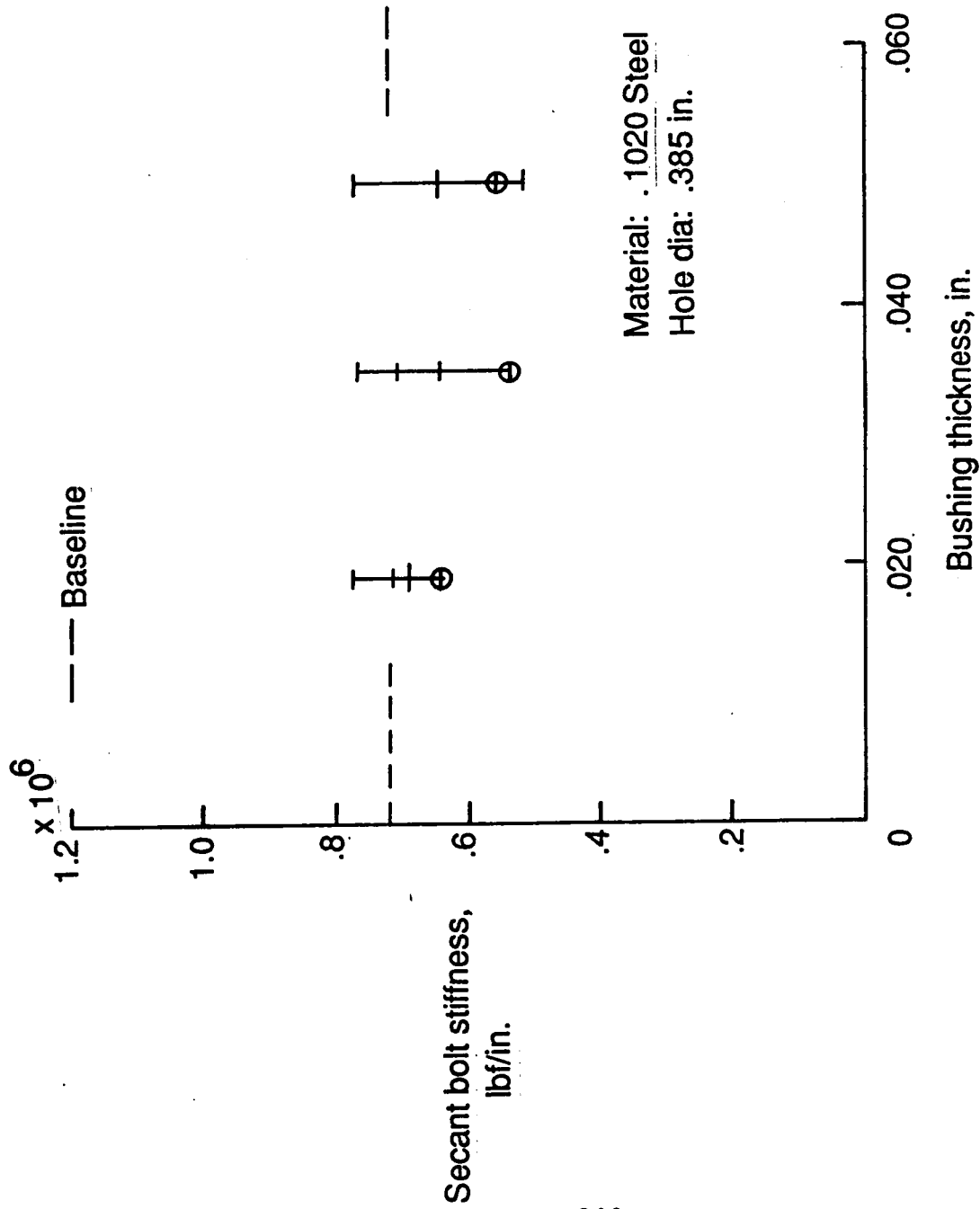
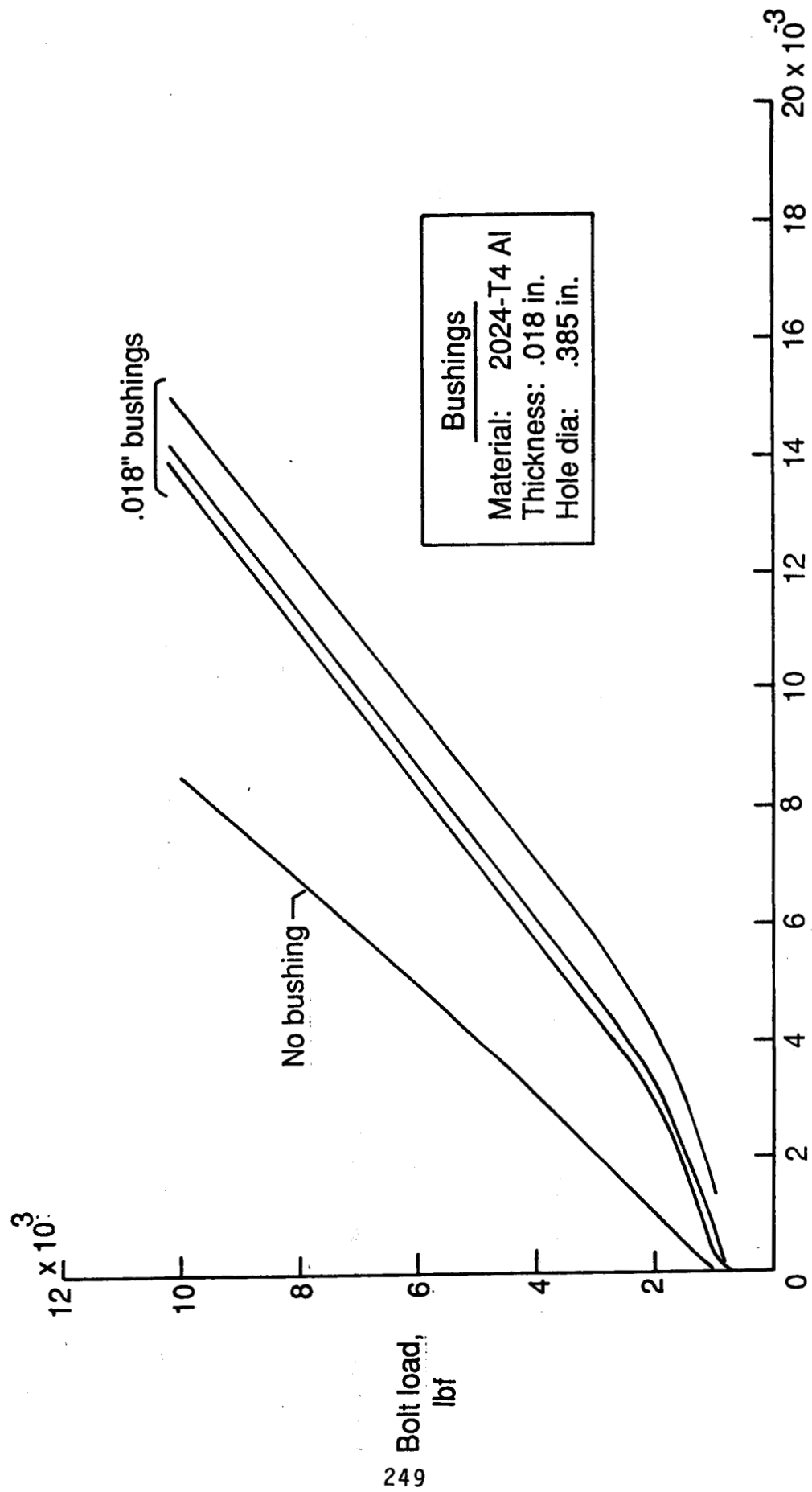
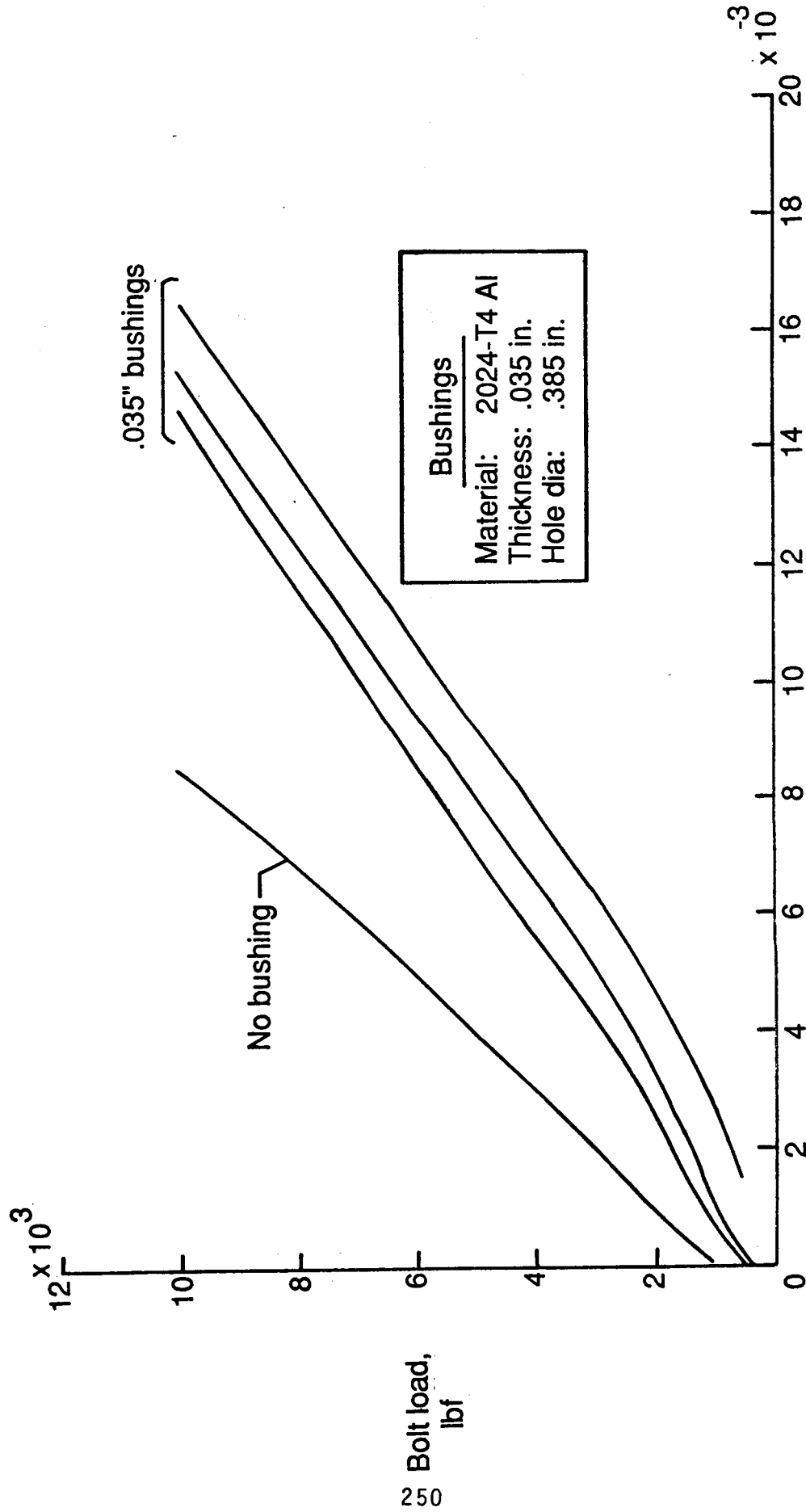


Figure I-19. Effective bolt stiffness of 3/8-inch tang bolts in conjunction with various thickness 1020 steel bushings.



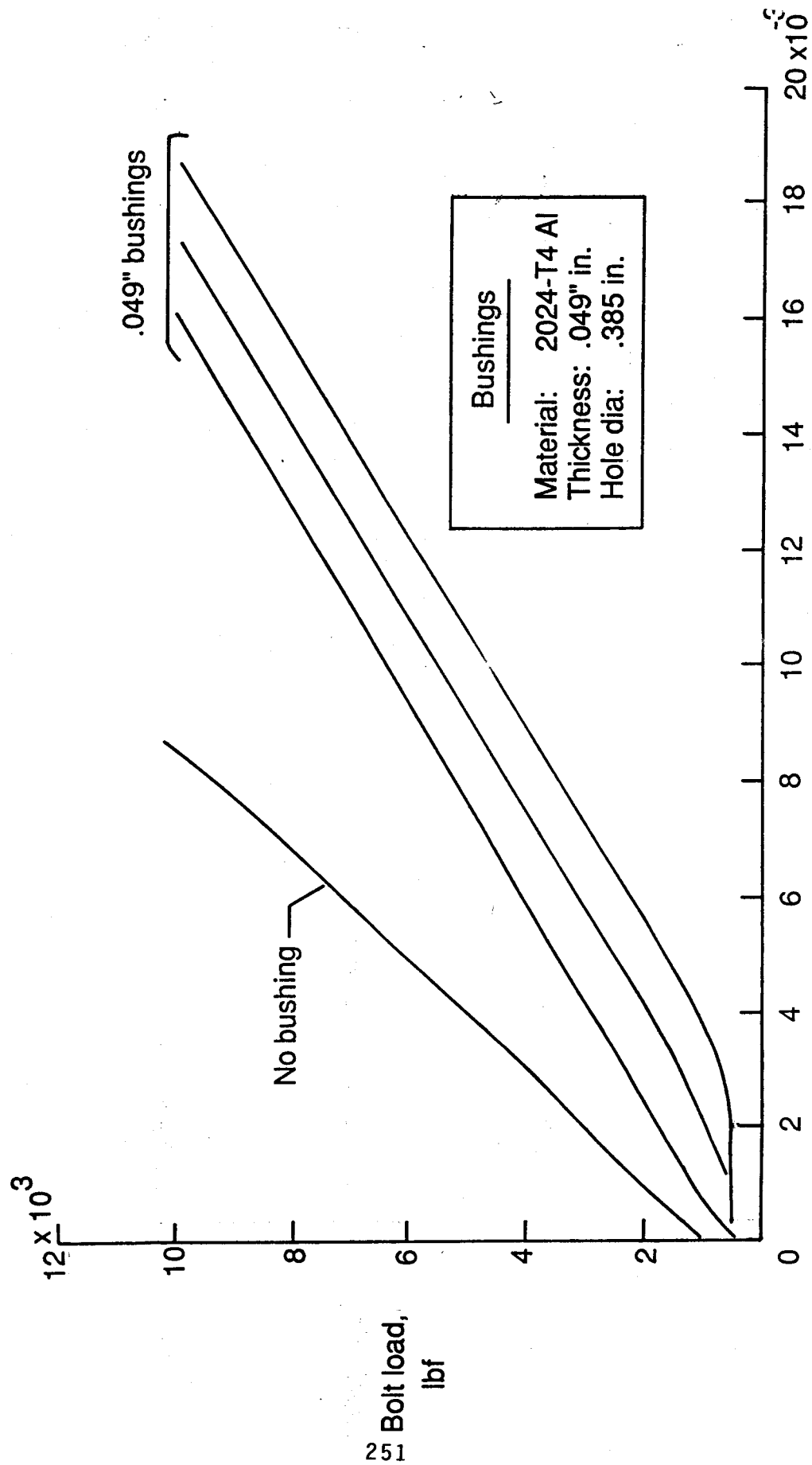
Bolt deflection, in.

Figure I-20. 3/8-inch tang bolt load deflection response with 0.018-inch thick 2024-T4 aluminum bushings.



Bolt deflection, in.

Figure I-21. 3/8-inch tang tang bolt load deflection response with 0.035-inch thick 2024-T4 aluminum bushings.



Bolt deflection, in.

Figure I-22. 3/8-inch tang bolt load deflection response with 0.049-inch thick 2024-T4 aluminum bushings.

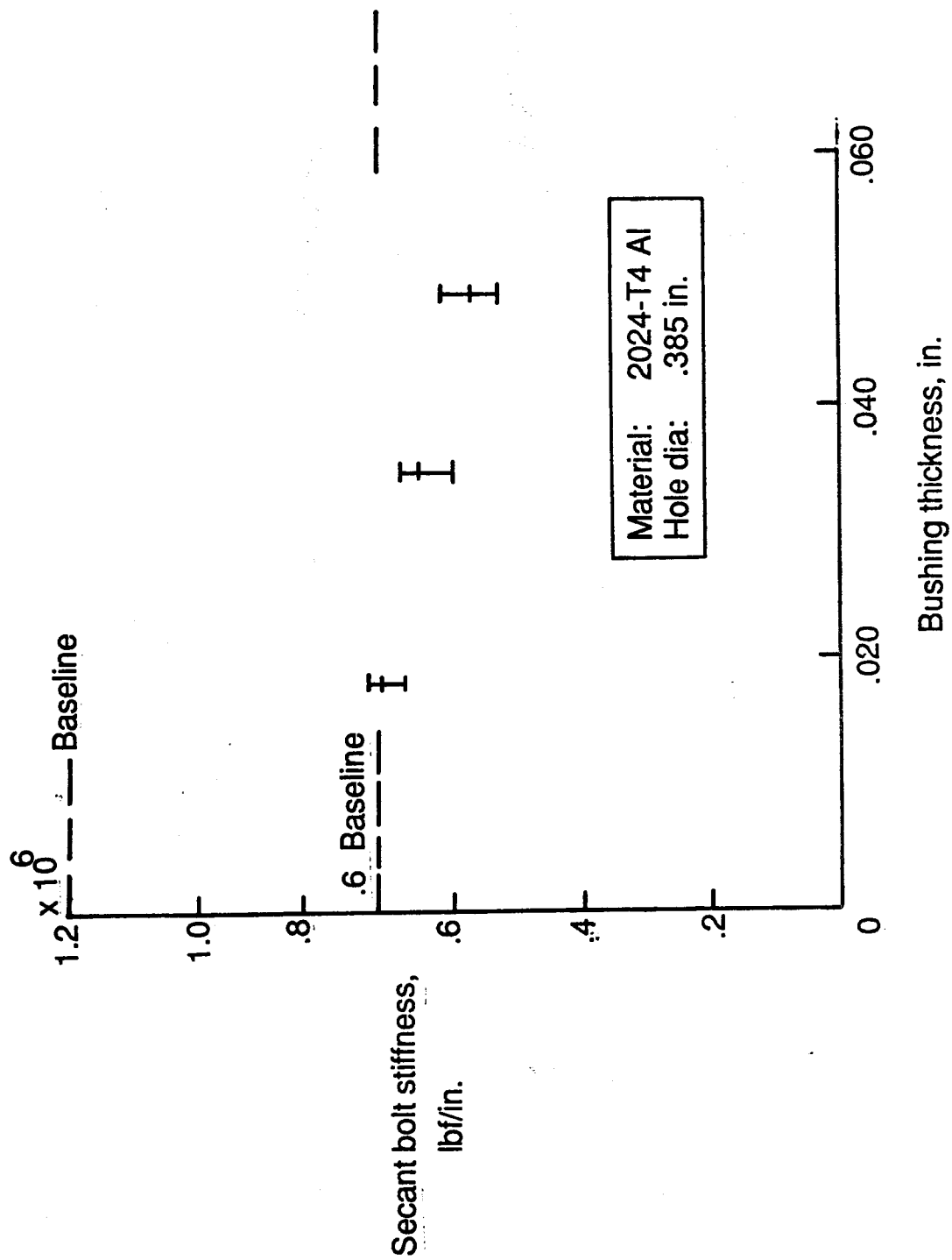


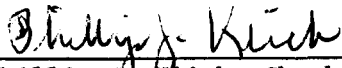
Figure I-23. Effective bolt stiffness of 3/8-inch tang bolts in conjunction with various thickness 2024-T4 aluminum bushings.

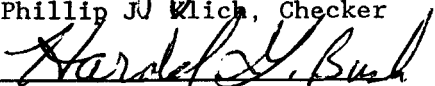
APPENDIX J


WEIGHT STATEMENT

by PRC Kentron
Aerospace Technologies Division
303 Butler Farm Road
Hampton, Virginia 23666
Phone (804) 865-1010

June 24, 1987


Phillip J. Klich, Checker


for Martin M. Mikulas, Jr., Project Engineer


David H. Butler, Project Manager

APPENDIX J

WEIGHT STATEMENT

A weight statement is presented in Table J-1. This table lists weights of the ring end pieces and weights of fasteners and splice plates for attaching the end pieces to the main part of the ring. Weights for the proposed concept parts are compared to weights of comparable parts of the existing ring component.

TABLE J-1.

WEIGHT COMPARISON BETWEEN MSFC AND L₀RC ET ATTACHMENT RING CONCEPT

| WEIGHTS (IN POUNDS) | | | | |
|--------------------------|--------|-------------------|--------|--|
| DESCRIPTION | MSFC | L ₀ RC | DELTA | |
| LONG END WEB/CAP (EACH) | 50.46 | 29.27 | -21.19 | |
| LONG END WEB/CAP (PAIR) | 100.92 | 58.54 | -42.38 | |
| LONG END SPLICE PLATES | N/A | 40.80 | +40.80 | |
| LONG END TOTAL | 100.92 | 99.34 | -1.60 | |
| SHORT END WEB/CAP (EACH) | 42.50 | 29.27 | -13.23 | |
| SHORT END WEB/CAP (PAIR) | 85.00 | 58.54 | -26.46 | |
| SHORT END SPLICE PLATES | N/A | 40.80 | +40.80 | |
| SHORT END TOTAL | 85.00 | 99.34 | +14.34 | |
| SYSTEMS TUNNEL | 81.13 | 102.93 | +21.80 | |
| COMBINED TOTALS | 267.05 | 301.61 | +34.56 | |

WEIGHTS BASED ON PRELIMINARY DATA AND SHOULD BE USED ACCORDINGLY.

| | | | | | |
|---|--|---|--|--|--|
| 1. Report No. NASA TM-100476 | | 2. Government Accession No. | | 3. Recipient's Catalog No. | |
| 4. Title and Subtitle Redesign of Solid Rocket Booster/External Tank Attachment Ring for the Space Transportation System | | | | 5. Report Date October 1987 | |
| | | | | 6. Performing Organization Code | |
| 7. Author(s) Harvey G. McComb, Jr., Compiler | | | | 8. Performing Organization Report No. | |
| | | | | 10. Work Unit No. 506-43-41-04 | |
| 9. Performing Organization Name and Address NASA Langley Research Center Hampton, VA 23665-5225 | | | | 11. Contract or Grant No. | |
| | | | | 13. Type of Report and Period Covered Technical Memorandum | |
| 12. Sponsoring Agency Name and Address National Aeronautics and Space Administration Washington, DC 20546-0001 | | | | 14. Sponsoring Agency Code | |
| | | | | | |
| 15. Supplementary Notes Appendices: (A) T. C. Jones; (B) J. T. Dorsey; (C) M. S. Lake & W. B. Fichter; (D), (E), & (F) O. H. Bradley; (G) L. D. Wall; (H) P. O. Brown & J. C. Newman; (I) H. G. Bush; (J) PRC Kentron Harvey G. McComb, Jr.: Analytical Services and Materials, Inc., Hampton, VA | | | | | |
| 16. Abstract An improved design concept is presented for the Space Shuttle solid rocket booster (SRB)/external tank (ET) attachment ring structural component. This component picks up three struts which attach the aft end of each SRB to the ET. The concept is a partial ring with carefully tapered ends to distribute fastener loads safely into the SRB. Extensive design studies and analyses were performed to arrive at the concept. Experiments on structural elements were performed to determine material strength and stiffness characteristics. Materials and fabrication studies were conducted to determine acceptable tolerances for the design concept. The text of the report provides an overview of the work, conclusions and major recommendations. Supporting technical details are contained in 10 appendices. | | | | | |
| 17. Key Words (Suggested by Author(s)) Space Shuttle Solid Rocket Booster External Tank Attachment Ring | | | | 18. Distribution Statement Unclassified - Unlimited Subject Category 18 | |
| 19. Security Classif. (of this report) Unclassified | | 20. Security Classif. (of this page) Unclassified | | 21. No. of pages 260 | |
| | | | | 22. Price A12 | |